



UNLIMITING THERMODYNAMIC CONSTRAINTS IN CONTINUOUS CATALYTIC TRANSFORMATION OF CARBON DIOXIDE AND METHANOL TOWARDS DIMETHYL CARBONATE

Dragos Constantin Stoian

ADVERTIMENT. L'accés als continguts d'aquesta tesi doctoral i la seva utilització ha de respectar els drets de la persona autora. Pot ser utilitzada per a consulta o estudi personal, així com en activitats o materials d'investigació i docència en els termes establerts a l'art. 32 del Text Refós de la Llei de Propietat Intel·lectual (RDL 1/1996). Per altres utilitzacions es requereix l'autorització prèvia i expressa de la persona autora. En qualsevol cas, en la utilització dels seus continguts caldrà indicar de forma clara el nom i cognoms de la persona autora i el títol de la tesi doctoral. No s'autoritza la seva reproducció o altres formes d'explotació efectuades amb finalitats de lucre ni la seva comunicació pública des d'un lloc aliè al servei TDX. Tampoc s'autoritza la presentació del seu contingut en una finestra o marc aliè a TDX (framing). Aquesta reserva de drets afecta tant als continguts de la tesi com als seus resums i índexs.

ADVERTENCIA. El acceso a los contenidos de esta tesis doctoral y su utilización debe respetar los derechos de la persona autora. Puede ser utilizada para consulta o estudio personal, así como en actividades o materiales de investigación y docencia en los términos establecidos en el art. 32 del Texto Refundido de la Ley de Propiedad Intelectual (RDL 1/1996). Para otros usos se requiere la autorización previa y expresa de la persona autora. En cualquier caso, en la utilización de sus contenidos se deberá indicar de forma clara el nombre y apellidos de la persona autora y el título de la tesis doctoral. No se autoriza su reproducción u otras formas de explotación efectuadas con fines lucrativos ni su comunicación pública desde un sitio ajeno al servicio TDR. Tampoco se autoriza la presentación de su contenido en una ventana o marco ajeno a TDR (framing). Esta reserva de derechos afecta tanto al contenido de la tesis como a sus resúmenes e índices.

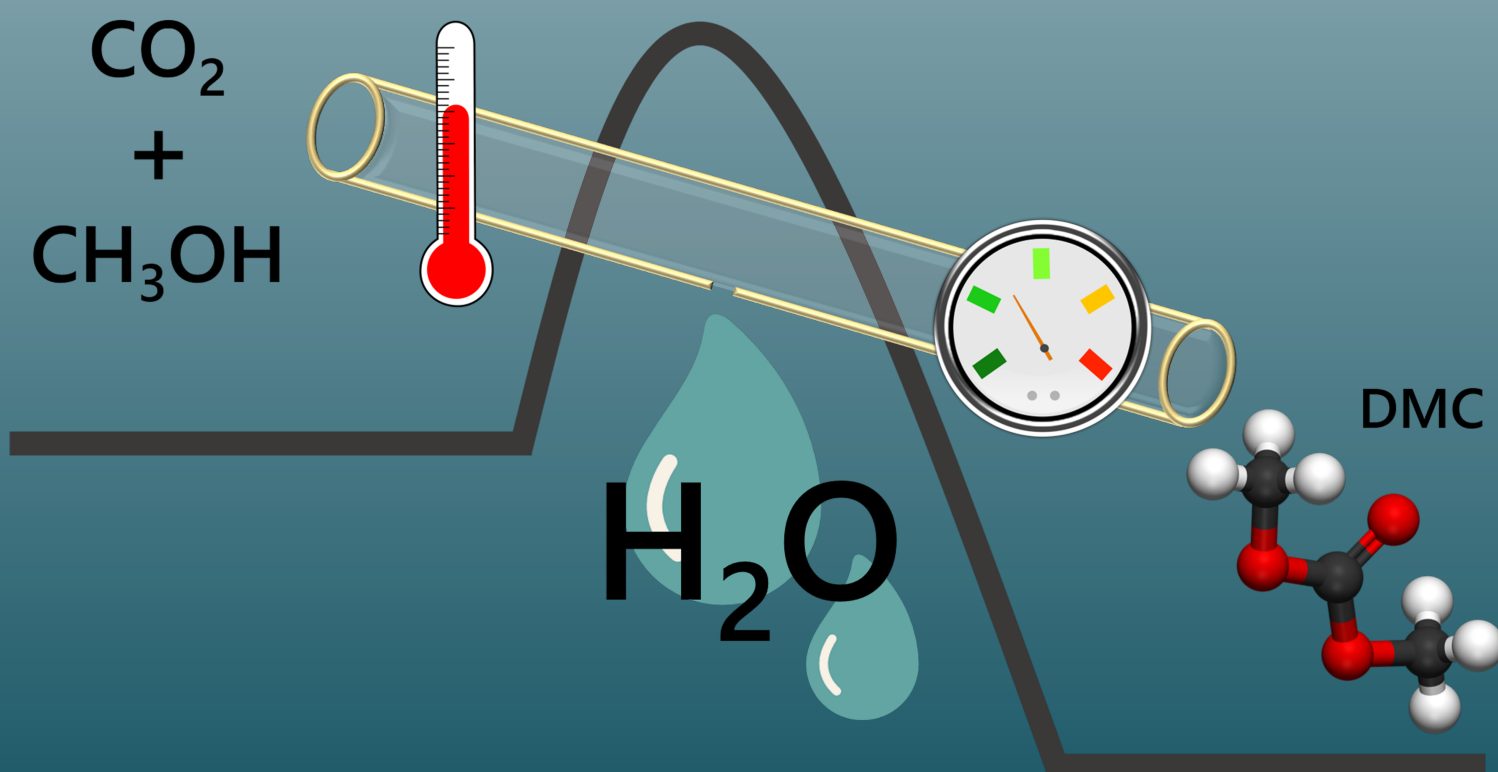
WARNING. Access to the contents of this doctoral thesis and its use must respect the rights of the author. It can be used for reference or private study, as well as research and learning activities or materials in the terms established by the 32nd article of the Spanish Consolidated Copyright Act (RDL 1/1996). Express and previous authorization of the author is required for any other uses. In any case, when using its content, full name of the author and title of the thesis must be clearly indicated. Reproduction or other forms of for profit use or public communication from outside TDX service is not allowed. Presentation of its content in a window or frame external to TDX (framing) is not authorized either. These rights affect both the content of the thesis and its abstracts and indexes.



UNIVERSITAT ROVIRA I VIRGILI

Unlimiting Thermodynamic Constraints in Continuous Catalytic Transformation of Carbon Dioxide and Methanol towards Dimethyl Carbonate

DRAGOȘ CONSTANTIN STOIAN



DOCTORAL THESIS

2016

DOCTORAL THESIS

Unlimiting Thermodynamic Constraints in
Continuous Catalytic Transformation of
Carbon Dioxide and Methanol towards Dimethyl Carbonate

Dragoș Constantin Stoian

Supervised by:

Prof. Dr. Francisco Medina and **Prof. Dr. Atsushi Urakawa**

URV – ICIQ



Tarragona

2016



UNIVERSITAT ROVIRA I VIRGILI
ESCOLA TÈCNICA SUPERIOR D'ENGINYERIA QUÍMICA
DEPARTAMENT D'ENGINYERIA QUÍMICA

Av. dels Països Catalans, 26
43007, Tarragona (Spain)
Tel. +34 977 55 96 03 / 04
Fax +34 977 55 96 21
E-mail: secdeq@etseq.urv.es
Web: <http://www.etseq.urv.es/DEQ/>



Prof. Dr. Francisco Medina Cabello and Prof. Dr. Atsushi Urakawa,

CERTIFY THAT:

The present study, entitled “Unlimiting Thermodynamic Constraints in Continuous Catalytic Transformation of Carbon Dioxide and Methanol towards Dimethyl Carbonate”, presented by Dragoș Constantin Stoian for the award of the degree of Doctor, has been carried out under my supervision at the Department of Chemical Engineering (DEQ) of University Rovira i Virgili and the Institute of Chemical Research of Catalonia (ICIQ), and that it fulfils all the requirements to obtain the degree of Doctor in Chemical, Environmental, and Process Engineering.

Tarragona, 2nd of November, 2016

Doctoral Thesis Supervisor

Prof. Dr. Francisco Medina Cabello

Prof. Dr. Atsushi Urakawa

ACKNOWLEDGEMENTS

It is uncanny, but after five years in Tarragona this introductory part seems to be the most difficult one. Somehow, the words are not coming out at the desired frequency. It is most likely related with a series of mixed feelings that are crossing my mind at increased velocity. I could write a book about my experience here and it would be having very promising prospects. I won't be doing it now though ...

First of all, I would like to express my profound gratitude towards my thesis supervisor, Dr. Atsushi Urakawa (from Institute of Chemical Research of Catalonia, ICIQ), for giving me a hand when I mostly needed it. Since the day we started to work together, he supported me without hesitation and he constantly offered me his expert guidance and endless motivation to continue fighting. He is the best professional I have ever met and I feel extremely fortunate to have been under his supervision during all this time. I am grateful to him for all the scientific and non-scientific discussions early in the morning or late at night, for all the things I learned from him during this period and, maybe most important, for his constant dose of optimism. For all these things and many others: THANK YOU, Atsushi!

I would like to thank Dr. Francisco Medina, my supervisor from "Rovira i Virgili" University (URV), for giving me the opportunity to start this amazingly challenging journey in his research group, CATHETER. I hope that I have finally managed to make you proud of our work.

I would like to express my sincere gratitude to all the scientific and non-scientific staff from URV and ICIQ that came across my path during these five years. All the help and cooperation that I received made my life much easier. Special thanks to Dr. Miguel González Hevia from Heterogeneous Catalysis Unit for all the time spent together, everlasting support and indications and for introducing me to all the characterization techniques in his lab. The help and assistance received from Dr. Marta Giménez Pedrós (Chemical Reaction Technologies Unit), Dr. Fernando Bozoglian (Spectroscopy and Reaction Kinetics Unit) and their staff is greatly appreciated. Thanks to Dr. Francesc Gispert i Guirado (from Servei de Recursos Científics i Tècnics, URV) for the advices on XRD analysis. Many thanks to José Luis León (Mechanical Workshop) and Xavier Asensio (Glass Blowing Workshop) for making

experiments happen. Your reliable work and great personal qualities are highly acknowledged. Marc and Jesús (Logistics) are not to be forgotten. Bringing joy and parcels to the lab P 2.11 since forever. Gracias! I also thank Aurora Càceres (ICIQ) and Núria Juanpere (URV) for the great administrative support (and not only) received throughout my stay in Tarragona. Gràcies! And speaking about administrative tasks and Spanish bureaucracy, I will never forget the help (in both personal and professional matters) given by Sandra Ramos and Vanessa Torné. Sharing experiences and kind words is the key for a better world.

My next thoughts go to the lab families. I was lucky as I had two of them. I would like to express my deepest appreciation to all the former/current members and visiting scientists of Urakawa research group and CATHETER. Words are not enough to describe how important can be to have a nice working environment, with enjoyable colleagues and friends. People that can change your mood on a rainy day. And I had many of those days. A big hug to all of you! Special thanks to Susana Dominguez (despite being a Real Madrid fan) for being a very special person and a great lab technician. With you, a beer is always a pleasure. Oscar Osegueda, Alex Miranda, Luis Iglesias and Abel Toscano are highly acknowledged for the great support and nice time spent together during my early stay in Tarragona. Thanks for the smooth incorporation, guys! I could never forget the pleasant coffee time and all the scientific and non-scientific talks with Mayra Garcia, Enrique Del Río Nieto (and their fluffy cats, Gibbs, King and Lola) and Anton Dafinov. It has been a pleasure and I owe you a lot for the help and kind words during harsh times. Special mention to Sven Reimann, for being there for me when I was completely lost and for sharing his vast scientific knowledge. I will never forget that! And thanks to all the other CATHETER (and related) members that I have ever crossed paths with (Iuliana Cota, María Alba, Ricardo Chimentão, Jesús Sueiras, Veronica Pinos, Sandra Contreras, Shailesh Sable, Pallavi Ghute, Sandra Toledo, Llorenç Gavilà, Ana Antolin, Silvia Jimenez, Barbara Miranda and many others).

When I started my ICIQ experience I got hit by a train. For the first time, I could witness things that worked smooth and it felt better. Big thumbs up for that to the three pioneers of the Urakawa research group, Antonio Bazzo, Atul Bansode and Jordi Ampurdanés, great colleagues and great friends. Thanks for listening me crying and helping me get over it, for sharing your knowledge and experience, for many synchrotron times

altogether, for Friday's night beer and many other things. Thanks Antonio for bringing a bliss to the lab, thanks Atul for being able to fix everything, and thanks Jordi for all the great talks we had and all the FCB-moments. I learned a lot from you guys! I cannot forget Dina Fakhrnasova, to whom I shared many thoughts at the beginning of my stay in Tarragona and throughout my ICIQ period.

A group's life is in a continuous change, and so I would like to express my sincere gratitude to Ta Corrales, Sergio Lima, Luis Bobadilla, Yi Zhang, Andrea Alvarez, Sergio Roso, Muralidhar Chourashiya, Damien Cornu, Rui Huang, Lingjun Hu, Reza Taheraslani, Joan Giner (and many others) for continuing making the lab a warm and fun place to stay and work, for all the assistance provided and many unforgettable moments. I sincerely hope that whoever is still around will keep the fame of this group where it belongs (no pressure!). That is the most important treasure we could own. A very special mention, from the bottom of my heart, goes to Rohit Gaikwad, Marta Borges (Visca Barça) and Juan José Corral. Thank you, guys, for all the time spent together! For all the dinners and parties, for all the beers, for sharing knowledge, fears, ideas, disappointments and a strong shoulder to rely on. All the mutual mocking, slang and jokes we made together represented the funniest part of our time together. It is profoundly and forever appreciated. I could not have forgotten our small Japanese community. Special thanks to Tsuyoshi Hyakutake, his wife Yoko and their adorable daughter Toyo for many beautiful moments shared together. Many thanks to Shunsaku Yasumura and Shintaro Hara for the good vibes and positive attitude they brought in the group.

My gratitude is also extended to Dr. Wouter van Beek, beamline scientist at ESRF (Grenoble, France). Thanks for the help and all the possible support showed during many hours (and long nights) of synchrotron measurements.

O sa ies puțin din sfera ICIQ-URV și o sa incep prin a mulțumi domnilor profesori Anca și George Marton și domnului Constantin Drăghici. Trei dintre persoanele care și-au pus amprenta asupra viitorului meu și căroră le mulțumesc din suflet pentru inalta ținută morală și nivelul ridicat al discuțiilor pe teme științifice și nu numai. O parte din această teză vă aparține in egală măsură!

Ma reintorc in Tarragona și vreau să le mulțumesc in primul rand Simonei și lui Dan Libotean (impună cu cei doi copii, Ana si Victor). Vă mulțumesc pentru tot ... pentru

pranzuri, cine, bere, sfaturi, meciuri la Nastic, concerte in Barcelona, Andorra, etc. A fost intodeauna o placere imensă să împărțim niște ore cu toții. Doresc să ii mulțumesc Georgianeii Stoica pentru numeroasele discuții pe teme extrem de diverse și pentru cuvintele frumoase venite in cele mai bune momente.

Imi e greu sa ii cuprind pe toți, dar doresc să le mulțumesc din tot sufletul tuturor prietenilor din Romania, mai vechi sau mai noi, mai tineri sau mai bătrani. Laurențiu, Dan, Iuliana, Claudiu, Vlad, Ciprian, Florin, Cătălin, Mădălin, Alin, Mihai, Marcel, Lăcrămioara. Sunt doar cateva nume înșirate pe o foaie si nu inseamna mare lucru ... cu siguranța vă știți voi mai bine. Mulțumiri familiei pentru suportul arătat de-a lungul timpului.

Nu aș fi ajuns persoana care sunt astăzi fără susținere necondiționata și increderea nețărmurită a părinților mei, Cecilia si Gelu Stoian. Vă mulțumesc din suflet pentru tot!

Te-am lăsat la urmă pentru că ocupi un loc special in inima mea. Iți multumesc cu toată puterea, Dana! Pentru că au fost cinci ani extrem de dificili și pentru că ai fost intotdeauna acolo. Pentru că impreuna am reusit sa trecem peste tot mai ușor. Pentru asta și pentru tot ce va urma, îți mulțumesc!

iconfinder.com, freepik.com and flaticon.com are acknowledged for the icons and inspiration that helped making this thesis more colorful.

“Rovira i Virgili” University, ICIQ foundation and Ministerio de Economía y Competitividad (MINECO) are greatly acknowledged for financial support, making this doctoral project possible.



UNIVERSITAT ROVIRA I VIRGILI



UNIVERSITAT ROVIRA I VIRGILI
UNLIMITING THERMODYNAMIC CONSTRAINTS IN CONTINUOUS CATALYTIC TRANSFORMATION OF CARBON DIOXIDE
AND METHANOL TOWARDS DIMETHYL CARBONATE
Dragos Constantin Stoian

UNIVERSITAT ROVIRA I VIRGILI
UNLIMITING THERMODYNAMIC CONSTRAINTS IN CONTINUOUS CATALYTIC TRANSFORMATION OF CARBON DIOXIDE
AND METHANOL TOWARDS DIMETHYL CARBONATE
Dragos Constantin Stoian

Table of Contents

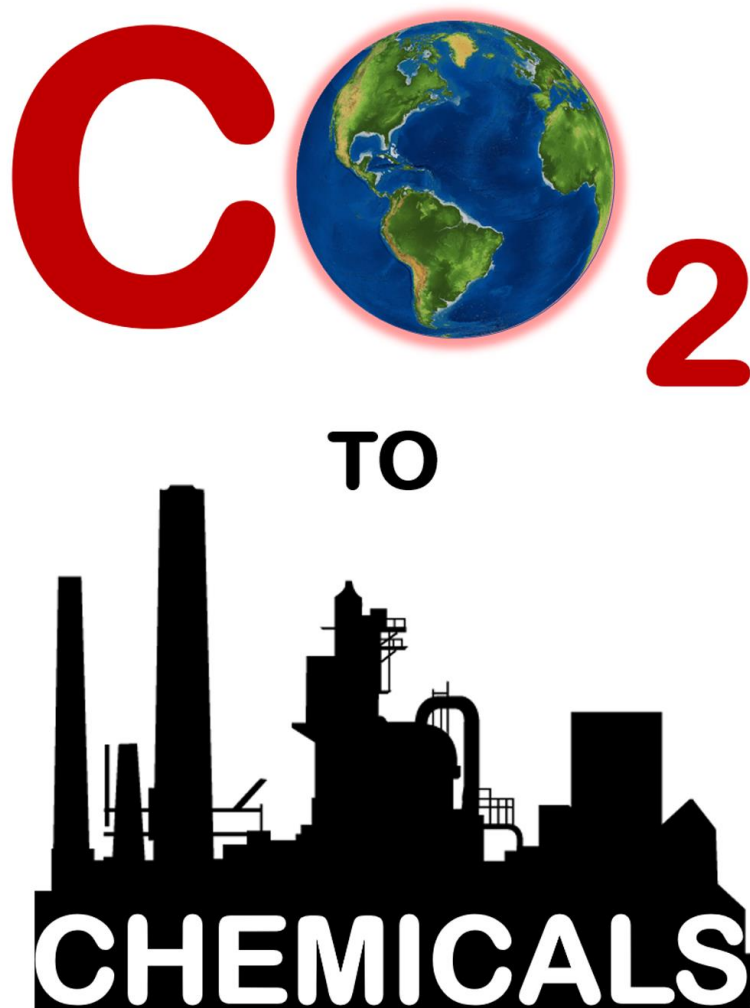
1	Introduction and overview	1
1.1	Carbon dioxide and related concerns.....	2
1.1.1	Actual context	2
1.1.2	A guided walk throughout the history	3
1.1.2.1	World energy demand and consumption statistics	3
1.1.2.2	Greenhouse gas generation.....	5
1.1.2.3	Global climate change	7
1.1.2.4	Climate change mitigation.....	8
1.1.2.5	CO ₂ mitigation strategies	11
1.2	Dimethyl carbonate: past and present. Future directions.....	14
1.2.1	Description and relevance of the topic. Organic carbonates.....	14
1.2.2	Dimethyl carbonate: fine chemical from CO ₂	16
1.2.2.1	Processes for DMC synthesis	20
1.2.2.2	Direct carboxylation reaction – DMC synthesis using CO ₂	23
1.3	Aim and overview of the thesis.....	37
	Bibliography	39
2	Materials and methods	43
2.1	Catalyst materials	44
2.2	Reaction setup for continuous production of DMC	46
2.2.1	Preliminary studies.....	47
2.2.1.1	Microactivity Reference catalytic system.....	47
2.2.1.2	Low pressure setup	48
2.2.1.3	AMTECH SPR16	49
2.2.2	High-pressure (50 bar) methanol carboxylation reactor setup.....	50
2.2.2.1	Reactor system.....	50
2.2.2.2	Separation system	53

2. 2. 2. 3	Reaction protocol.....	54
2. 2. 2. 4	Analytical system	55
2. 2. 2. 5	Maintenance and troubleshooting	56
2. 3	<i>In situ</i> studies.....	58
2. 3. 1	Synchrotron studies	59
2. 3. 2	<i>In situ</i> DRIFTS-MS and Raman-MS studies.....	63
2. 3. 3	Modulation excitation spectroscopy (MES) and multivariate curve resolution (MCR). Theory and applications.....	67
	Bibliography	72
3	Catalysis under microscope	73
3. 1	Introduction	74
3. 2	Experimental.....	76
3. 2. 1	Materials	76
3. 2. 2	Reaction system	76
3. 2. 3	Visual inspection and spectroscopic analysis.....	78
3. 3	Results and discussion	79
3. 3. 1	Verification of the fused quartz tubular reactor for the continuous DMC synthesis.....	79
3. 3. 2	Catalyst deactivation-reactivation studies assisted by visual inspection	81
3. 3. 3	Spectroscopic investigation of the origin of catalyst deactivation.....	85
3. 3. 4	<i>Operando</i> visual inspection.....	91
3. 4	Conclusions	92
	Bibliography	94
4	Effects of REM promoters	97
4. 1	Introduction	98
4. 2	Experimental.....	100
4. 2. 1	Materials	100
4. 2. 2	Reaction system	100
4. 2. 3	Characterization.....	101
4. 3	Results and discussion	102

4. 3. 1	Direct methanol carboxylation: Stability studies	102
4. 3. 2	Characterization of pristine and as-synthesized catalysts	107
4. 3. 3	Characterization of pristine and 1 wt% REM-CeO ₂ : before and after.....	119
4. 4	Conclusions	123
	Bibliography	125
5	Mechanistic insights	129
5. 1	Background and motivation.....	130
5. 2	Experimental.....	131
5. 3	Results and discussion	133
5. 4	Conclusions	138
	Bibliography	139
6	Conclusions and Outlook	143
6. 1	Summary of the thesis	144
6. 2	Open challenges and outlook.....	149
7	Appendices	153
	Appendix A Supplementary information Chapter 1.....	154
	Appendix B Supplementary information Chapter 2.....	155
	Appendix C Supplementary information Chapter 3	156
	Appendix D Supplementary information Chapter 4	158
	Appendix E Supplementary information Chapter 5.....	160
	Shorthand and glossary	163
	List of publications	169
	Curriculum Vitae	173

1

Introduction and overview



1 | Introduction and overview

1.1 Carbon dioxide and related concerns

1.1.1 Actual context

It is well-known that there is a continuously increasing trend in atmospheric carbon dioxide concentration when it comes to comparing the actual values with the ones recorded 50-60 years ago. In the summer of 2014 NASA (National Aeronautics and Space Administration) launched its first dedicated satellite for measurement of atmospheric carbon dioxide, a heat-trapping gas that represents the driving force for the well-known phenomenon of global warming. All the measurements are performed with the spacecraft named Orbiting Carbon Observatory-2, or OCO-2, which has as the main goal to locate Earth's sources of and storage places for atmospheric carbon dioxide [1]. The concentration of CO₂ in ppm across different regions can be seen from **Figure 1.1**. The continuous population growth, world energy demand and consumption in a tremendous change from year to year, a more and more modern lifestyle which requires people adapting to it, industrialization that led to a better living standard and countless discoveries over the centuries are all major contributors leading to increased carbon dioxide concentration.

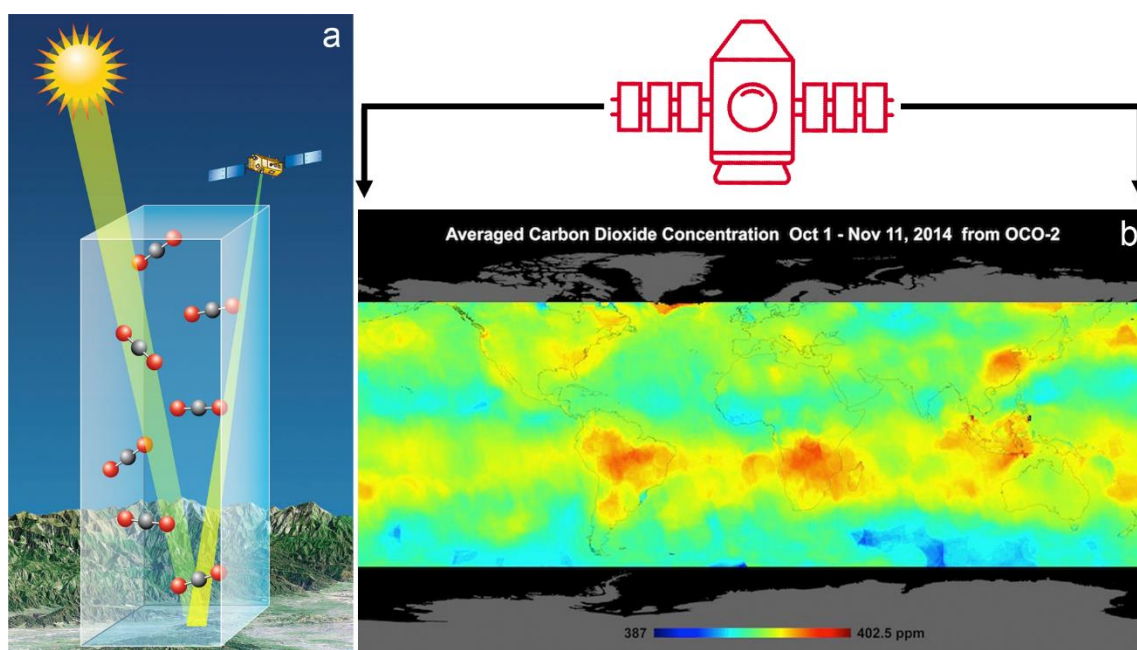


Figure 1.1 a. Artist rendition of the CO₂ column that OCO-2 sees, and b. NASA satellite's 1st CO₂ maps [1]

Why does carbon dioxide deserve a lot of attention? Carbon dioxide (CO₂) is the main greenhouse gas emitted through human activities. CO₂ occurs in the atmosphere as part of the Earth's carbon cycle (the natural motion of carbon among the atmosphere, oceans, soil, plants, and animals). Human activities are acting upon the carbon cycle - both by adding more CO₂ to the atmosphere and by influencing the ability of "natural sinks", e.g. forests (by

deforestation), to remove CO₂ from the atmosphere. While CO₂ emissions come from a variety of natural sources, human-related emissions are held responsible for the increase that has occurred in the atmosphere from the beginning of industrial revolution (end of 18th century – beginning of 19th century) onward.

1. 1. 2 A guided walk throughout the history

To be able to better understand the present and to predict the future of our society in a clearer manner, one needs to have a comprehensive view of the past and a realistic presentation on what is going on nowadays (**Figure 1.2**). There is strong evidence that climate change is occurring and that this is largely caused by human activities. We owe a better understanding of the whole process (natural and non-natural) and clear actions ought to be taken to reduce the energetic and environmental risks that hover over our lives, and more importantly over the future generations.

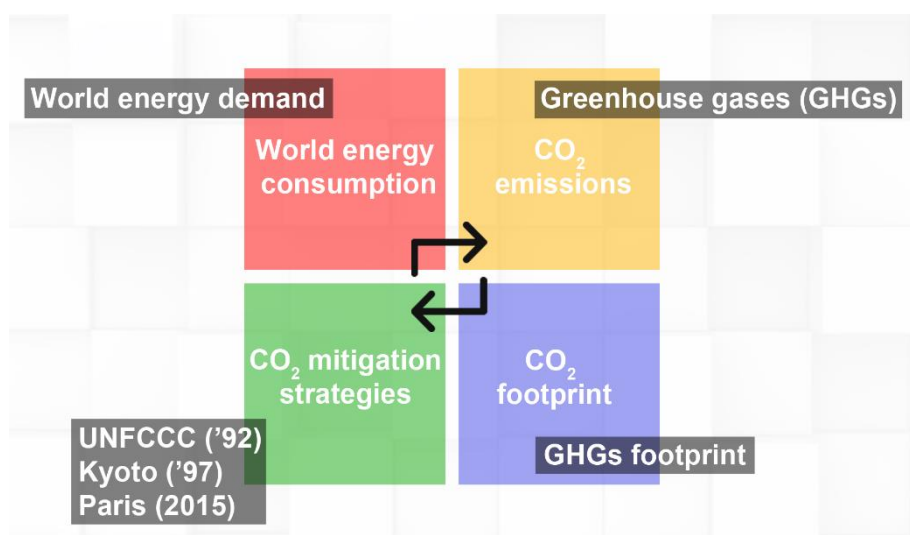


Figure 1.2 CO₂ problem – past and future

1. 1. 2. 1 World energy demand and consumption statistics

Life is all about energy. Life necessitates energy to survive and everything that happens around us is due to energy in all its forms. From the sun that gives light and heat energy, the cars that require gasoline or electricity to be powered to the food that we eat and which gives us the necessary amount of energy to perform our daily tasks, absolutely everything is centered on this sole term: energy. The world total primary energy supply (TPES) refers to the raw form of energy as it can be found in nature and that has never been subjected to any kind of transformation process. At a glance, the results presented in 2015 by the International Energy Agency (IEA) [2] – *Key world energy statistics* – indicate (**Figure 1.3**) that there are more energy resources in the world today than ever before. However, the major component of TPES is the fossil fuel, which forms more than 80% (in 2013) of the annual energy

1 | Introduction and overview

production. Basically, a share around 82% comes from oil (~ 31%), natural gas (~ 21%), and coal (~ 29%): distinctly old energy sources. The vital thing to emphasize from this data set is that our society is completely dependent on this finite and non-renewable energy source i.e. fossil fuel. The real meaning of this statement is that we rely on a source of energy that will end at some point and cannot be regenerated on human life time-scale.

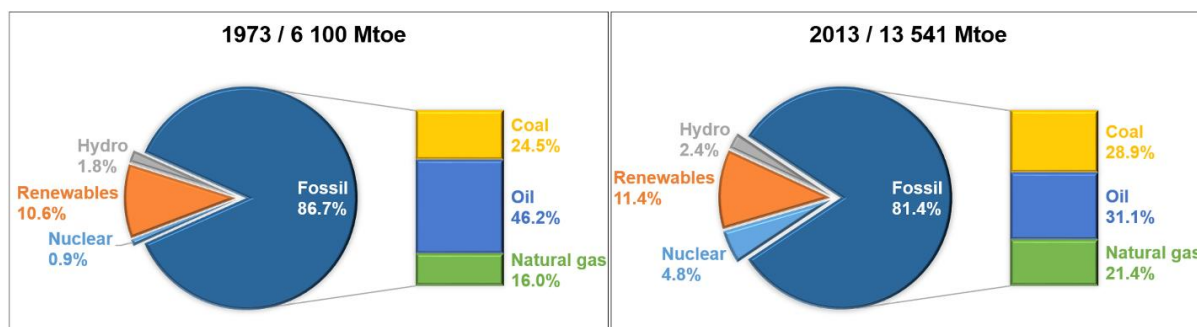


Figure 1.3 World total primary energy supply (TPES) by resource (in 1997 and 2013). The graphs include international aviation and international marine bunkers. Peat and oil shale are aggregated with coal, while geothermal, solar, wind, heat, etc. are aggregated to renewables. Data represented in million tons of oil equivalent (Mtoe) → 1 Mtoe = 11.63 TWh (terawatt-hours). Source: International Energy Agency (IEA) - Key world energy statistics from 2015

As mentioned above, there are three major forms of fossil fuels: coal, oil and natural gas. Basically, hydrocarbons that are all formed from the remains of dead plants and animals millions and millions of years ago and have carbon atom as main component (hence the name of the age they all were formed, Carboniferous Period). The data from IEA regarding total world energy consumption (**Figure 1.4**) is unequivocal [2]. The values presented are consistent with the supplies that are available and we rely on, and so, out of the total energy consumption the biggest share (of ca. 67%) is represented by fossil fuel. According to the reports generated by EIA - Energy Information Administration, Independent statistics and analysis bureau by the end of 2012 [3] more than 50% of the energy consumed worldwide belonged to the industrial sector. At rather large distance it comes, on the second place, transportation sector with a share around 27%. With shares of around 14% - residential sector and 8% - commercial sector are completing the tableau that highlights what was already known. These all are clear indications that our society continuously grows and, consequently, its desire for more energy grows. We aim at better and better living standards, we consume more so we require more, and we need more and more industry to “produce” all the assets necessary to fulfill, or at least to improve, our great journey through life.

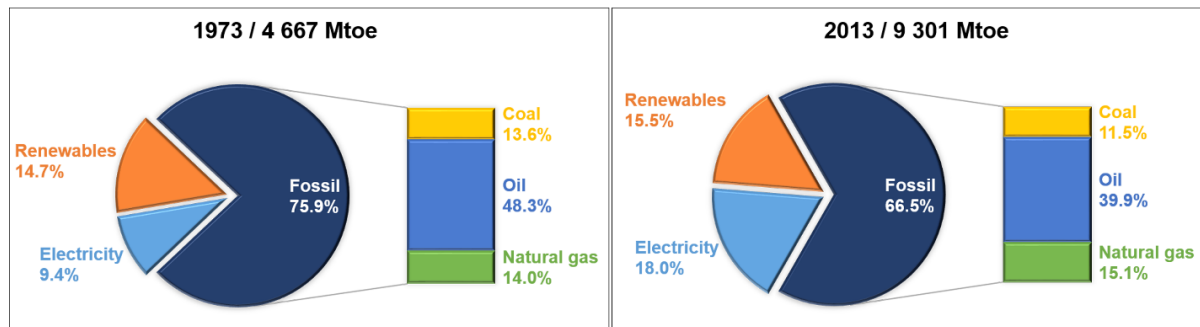


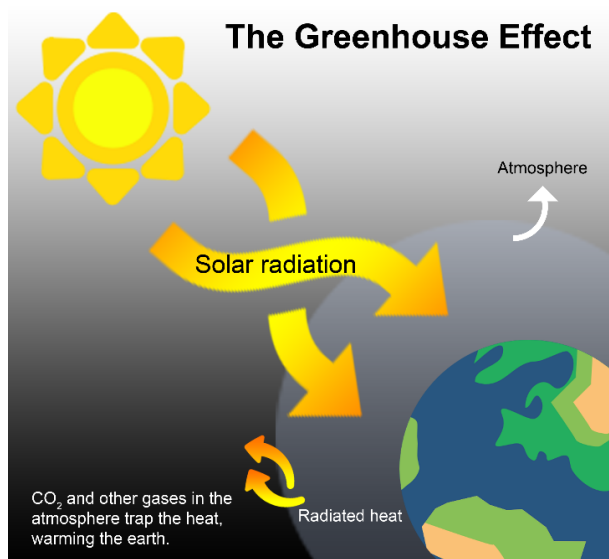
Figure 1.4 World total final energy consumption by resource (in 1997 and 2013). The graphs include international aviation and international marine bunkers. Peat and oil shale are aggregated with coal, while geothermal, solar, wind, heat, etc. are aggregated to renewables. The figures for renewables (biofuels and waste) final consumption have been estimated for a relevant number of countries. Data represented in million tons of oil equivalent (Mtoe) → 1 Mtoe = 11.63 TWh (terawatt-hours). Source: International Energy Agency (IEA) - Key world energy statistics from 2015

It is important to take a closer look at the World Energy Outlook Factsheet released in 2014 by the IEA to understand the actual trends in energy demand and its consumption [4]. IEA clearly states that the total world energy demand will increase with 37% by year 2040. Also, it is expected that the energy demand growth will decisively shift away from OECD countries (Organization for Economic Co-operation and Development), an international economic organization of 34 countries founded in 1961 to stimulate economic progress and to encourage world trade. Other important facts state that by the mid-2020s China will dominate this economic growth and soon after (given that China's population is leveling off) India will take over. Despite all the measures and policies aimed at promoting energy efficiency and fuel switching technologies, the coal, gas, and oil demand (fossil fuel) will still represent the major share of the market by 2040 (with an estimated value of around 55%).

1. 1. 2. 2 Greenhouse gas generation

Going back to the question regarding the implications of the large-scale consumption of fossil fuel and its decisive and irreversible touch on the world, it should be accentuated that upon consumption of fossils CO₂ is generated, the most abundant of the greenhouse gases (GHGs) that later “generate” radiative forcing (RF) and finally contribute to global warming (Figure 1.5).

1 | Introduction and overview



Greenhouse gases (GHGs) are gases that trap heat in the atmosphere. The primary greenhouse gases in the Earth's atmosphere are water vapor, carbon dioxide, methane, nitrous oxide, and fluorinated gases - sometimes found as high global warming potential gases.

Their **greenhouse potential** is quantified in carbon dioxide equivalents (e.g. the global warming potential for methane over 100 years is 21. This means that emissions of one million metric tons of methane is equivalent to emissions of 21 million metric tons of carbon dioxide).

Radiative forcing (RF) describes the change in energy in the atmosphere due to GHGs emissions, change that actually contributes to the global climate modification.

Figure 1.5 The greenhouse gas effect

The effect that GHGs have on the climate change is depending upon three major factors, i.e. the gas concentration in atmosphere, their lifetime, and their direct impact on the Earth's temperature, a measure given by the global warming potential. The basic rule is that the more energy they absorb, the more dangerous they are. The greenhouse gas footprint defines the amount of GHGs that are emitted during the manufacture of products or creation of services, whereas carbon footprint is the share that CO₂ emissions contributes to GHGs footprint. According to NOAA's - National Oceanic and Atmospheric Administration is a scientific agency within the United States Department of Commerce focused on the conditions of the oceans and the atmosphere - report on Annual Greenhouse Gas Index (AGGI) the following discussions have risen (from IPCC, Intergovernmental Panel on Climate Change – an international organism under the hood of United Nations) [5, 6]:

- The issue – increasing concentrations of greenhouse gases in Earth's atmosphere represent a long-term commitment by society to living in a changing climate and, ultimately, a warmer world (IPCC, 2014, Working Group I)
- The problem – climate change has disruptive and uncertain consequences for agriculture, water supply, transportation, coastal communities, the economy, energy, ecosystems, and ultimately national security (IPCC, 2014, Working Group II)
- The question – how much is the human influence on climate changing owing to continued emission of greenhouse gases?

The recent global level of CO₂ concentration is rising serious concerns about the direction we are heading to. With the last update done on the 5th of July (NOAA) 2016, it was find that in June 2016 the CO₂ global level was 406.81 ppm which is more than the value presented in

June 2015, 402.80 ppm. Even more, data from co2now.org indicates that the atmospheric CO₂ level for November 2014 was 397.13 ppm. The concentrations of CO₂ in the atmosphere are increasing at an accelerating rate from decade to decade. The latest atmospheric CO₂ data is consistent with a continuation of this long-standing trend (it is enough to have a look at the Keeling curve, a graph which plots the ongoing change in concentration of CO₂ in Earth's atmosphere since 1958, displaying an increasing trend in CO₂ levels since the beginning of the time **Appendix A, Figure 7.1**). Adding on top of this that the upper safety limit for atmospheric CO₂ is 350 ppm [7] and atmospheric CO₂ levels have stayed higher than 350 ppm since early 1988 one can get the full picture. We should act fast and it must be firm!

"The science is sobering—the global temperature in 2012 was among the hottest since records began in 1880. Make no mistake: without concerted action, the very future of our planet is in peril." Christine Lagarde, Managing Director - International Monetary Fund

An IEA report from 2012 states that the CO₂ share on the global forcing greenhouse gas emissions was more than 75%. Also, a recent study released by NOAA on CO₂ accumulation in the atmosphere from the burning of coal, oil, and natural gas (fossil fuels) over a two-year time period (2011-2012) indicates that the largest emitters are Eastern Asia, Western Europe, and the North East of North America - with a total accumulation of 9 to 10 ppm CO₂ (equal to 2.3% of increase in concentration) over the two-year period ([8], according to Open-source Data Inventory for Anthropogenic CO₂). Over a ten-year period, these emissions would be equivalent to 45 ppm of CO₂ or an increase of 11.5%.

1. 1. 2. 3 Global climate change

In 2010, the National Research Council concluded that "Climate change is occurring, is very likely caused by human activities, and poses significant risks for a broad range of human and natural systems" [9]. The climate change indicators are obvious and are presented worldwide: (average) temperatures are rising, snow and rainfall patterns are shifting (USA), four-season year (spring-summer-autumn-winter) became two-season year (winter-summer) in many of the European countries, along with a visible change in the precipitation patterns, more extreme climate events are taking place – record high temperatures, large flooding periods, heavy rainstorms or extended drought episodes, increased glacier melting, etc. Warming of the climate system is undeniable, and many of the observed changes are unprecedented over decades. The atmosphere and ocean have warmed, the amounts of snow and ice have diminished, sea level has risen, and the concentrations of greenhouse gases have increased.

From the Intergovernmental Panel on Climate Change (IPCC Climate Change 2013: The Physical Science Basis - IPCC Working Group I Contribution to AR5), the globally averaged

1 | Introduction and overview

combined land and ocean surface temperature data as calculated by a linear trend, shows a warming of 0.85 (0.65 to 1.06) °C, over the period 1880 to 2012. The projections are, depending on the future GHGs emissions and how the climate will respond to it, that the average global temperatures will increase worldwide by 1.1 to 6.4 °C by 2100. Warming is and will be greatest over land areas and higher latitudes. Natural processes such as changes in the sun's energy, shifts in ocean currents, and others affect Earth's climate. However, they do not explain the warming that we have observed over the last half-century. In their attempt to shed some light on the actual events more and more scientists are linking these changes in the global climate to the increased levels of CO₂ and other greenhouse gases in our atmosphere, which are caused by human activities. In the same report signed by IPCC it is mentioned that total radiative forcing is positive, and has led to an uptake of energy by the climate system. The largest impact to total radiative forcing is produced by the increase in the atmospheric concentration of CO₂ since 1750. What are the repercussions? Climate change has a direct impact on our lives, on our health (we are going to be exposed to more and more health risks), on the environment (e.g. water supply and water quality, soil properties), and economy (e.g. influence agricultural crop yields, or changes in forests). Ultimately it will affect humanity. We do have to learn how to adapt our life style to the changes that are expected to occur in the (near) future.

1. 1. 2. 4 Climate change mitigation

- United Nations Framework Convention on Climate Change (UNFCCC, signed in Rio de Janeiro in 1992, became effective in 1994)
- The Kyoto Protocol (signed in Kyoto in 1997, became effective in 2005)
- 2015 United Nations Climate Change Conference (Paris, France) - COP 21/CMP 11 meetings (effective after being signed in April, 2016 in New York. It came into force on 4th November, 2016)

Over the last century, global population and economic growth have been leading to increased emissions and concentrations of greenhouse gases. Although the impact of these increasing concentrations is not completely understood, concern is growing, and various means for reducing these emissions are being exploited. Advanced technology is an important component of any emissions reduction scheme, because it is potentially the key to lowering the costs of emissions reductions. It is of prime importance to mitigate the global climate change with long-lasting effects. Climate change mitigation defines the sum of actions necessary to limit the magnitude and (or) proportion of long-term climate change (B.S. Fisher *et al.* at [5]). Before the Industrial Revolution in the 19th century, global average CO₂ was about 280 ppm. During the last 800000 years, CO₂ fluctuated between about 180 and 280 ppm during ice ages and interglacial warm periods, respectively. Given that the CO₂ level is

above the maximum admitted level since 1988 and that today's rate of increase (**Figure 1.6**) is more than 100 times faster than the increase that occurred when the last ice age ended (NOAA media release dating from 2013), it comes as a natural consequence that actions have been taken.

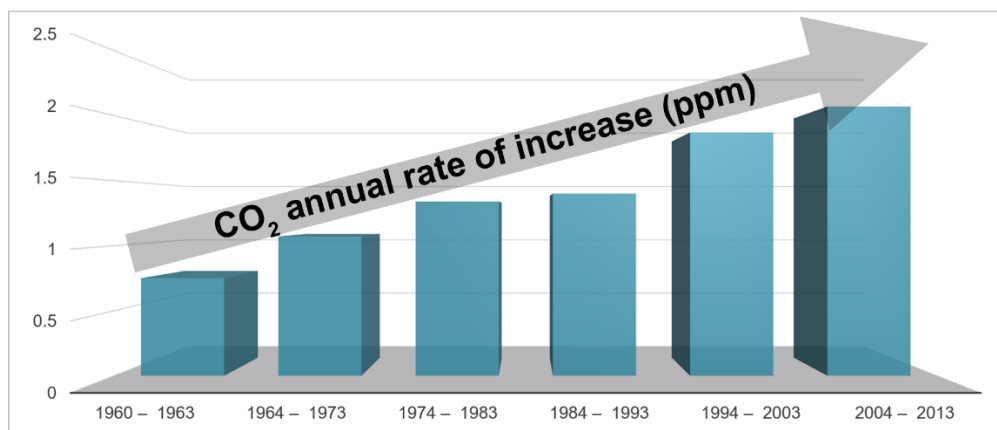


Figure 1.6 CO₂ annual rate of increase (in ppm) since 1960 until the present days

It started in 1992 (when the global CO₂ level was already 356.38 ppm), when the United Nations Framework Convention on Climate Change (UNFCCC) was signed at the United Nations Conference on Environment and Development (UNCED) held in Rio de Janeiro, Brazil. The agreement represents an environmental treaty having as a main objective to “stabilize greenhouse gas concentrations in the atmosphere at a level that would prevent dangerous anthropogenic interference with the climate system” (Article 2. The United Nations Framework Convention on Climate Change. Retrieved 15 November 2005). Later, in 1997 in Kyoto, Japan the treaty with the same name was signed (Kyoto Protocol) as an extension of the UNFCCC agreement. It had the same major objective – to reduce GHGs emissions – and it was based on two premises: global warming exists and is affecting our life, and the global warming phenomenon has been caused and accelerated by the man-made CO₂ emissions. 192 parties signed the protocol.

On 31 December 2012, the Protocol was expired. Negotiations were held in Paris in 2014 to agree on a post-Kyoto legal framework that would force all major polluters to pay for CO₂ emissions but China, India, and the United States have all gave clear indications that they would not agree any treaty that would commit them legally to reduce CO₂ emissions. It is difficult to judge to what extent Kyoto Protocol has been successful. The first remark to make is the GHGs emissions have showed no sign of slowing down. In that direction, only, the Kyoto protocol has been a failure. But the Kyoto Protocol was indubitably an important first step in terms of global climate diplomacy and awareness. In December, 2015 the United Nations Climate Change Conference (Paris, France) was held and substantial outcome is expected.

1 | Introduction and overview

The conference negotiated the Paris Agreement, nothing more than a global agreement on the reduction of climate change (196 parties attended). Everyone awaits that this treaty will represent a turning point into reaching our objective of finally reducing the global warming effect. As from the 4th of November, 2016 it has been officially ratified. **Table 1.1** presents a summary of the most important dates in the history of CO₂ levels.

Table 1.1 Important dates in CO₂ levels

Year	CO ₂ level (ppm)	Event
2015	401.85	Paris Agreement on the reduction of climate change
2009	387.37	Copenhagen Accord endorses the continuation of Kyoto Protocol
1997	363.71	Kyoto Protocol – extension for UNFCCC treaty
1992	356.38	Earth Summit in Rio de Janeiro – UNFCCC was signed
1987	349.16	The last year when the annual CO ₂ level was less than 350 ppm
1959	315.97	The first year with a full year of instrument data

One difficult question is risen: is it too late to do anything about the climate change? It comes out with a simple answer: it is not too late to have a substantial influence on future climate change and its effects on us, nor to get ready for the changes we already know they are coming. With suitable actions by governments, communities, individuals, and businesses, we can diminish the amount of greenhouse gas pollution we release and lower the risk of much greater warming and more severe consequences. Bringing CO₂ levels down will likely require a significant investment of money and resources (e.g. increasing transportation efficiency and transport conservation, building efficiency, or efficient electricity production). However, many of the actions that we can take to address climate change will later offer more important benefits, such as cleaner, healthier air, or fewer (human) tragedies caused by drastic climate changes.

While they are offering important estimation over the reality near us, the numbers presented in the “CO₂ and related concerns” aim at better understanding of the present and predicting the future. Having an exhaustive background on the energetic issues, fossil fuel, greenhouse gases, and global warming effect, it should be straightforward to understand why stabilizing the atmospheric CO₂ concentrations (and implicitly reducing the GHGs) is one of the major concerns and challenges for the humanity. Despite sounding like a cliché, it is up to all of us making it happen.

1. 1. 2. 5 CO₂ mitigation strategies

With the actual level of CO₂ on an increasing trend from decade to decade, finding the proper mitigation strategies is the key for a safer and sustainable environment. The easiest and the most effective way to reduce CO₂ emissions is, no doubt, to reduce fossil fuel consumption, situation which will have a direct impact on another big problem of the century represented by the fossil fuel depletion. Even though nature has its own way to substantially reduce CO₂ level in the atmosphere (via photosynthesis) this simply does not generate that level of CO₂ consumption at such a rate so that the required balance can be created. It simply does not happen fast enough. The “mitigative” approach of the CO₂ emissions generated from the use of fossil fuels gave rise to different strategies, technical solutions, and alternative options along with new questions, uncertainties, and doubts to tackle the problems:

- Improve energy efficiency (e.g. improving the conversion efficiencies of fossil fuels to electrical and thermal energy reduces CO₂ emissions; improving the insulation of buildings, traveling in more fuel-efficient vehicles, and using more efficient electrical appliances are all ways to diminish energy consumption, and thus CO₂ emissions)
- Energy conservation (e.g. reducing personal energy use by turning off lights and electronics when not in use reduces electricity demand; reducing distance traveled in vehicles reduces petroleum consumption)
- Fuel switching technologies (e.g. the substitution of natural gas and oil for coal reduces the CO₂ emissions)
- Removal, recovery, and disposal of CO₂ (e.g. CO₂ can be recovered from fossil-fuel-burning power plants and engines, captured, transported, and stored into deep underground rock formations)
- Utilization of CO₂ (the recovered CO₂ can be converted to materials of use to economy, including fuels, chemicals, and construction materials)
- Decarbonization of fossil fuels (e.g. extracting carbon from fossil fuels and utilizing only the hydrogen-rich fraction of fossil fuels can reduce CO₂ emissions significantly)
- Use of non-fossil energy sources (nuclear energy, solar energy, hydroelectric power, or geothermal energy. Renewable energy in all its forms)
- Reforestation (i.e. the planting of trees provides means of reducing atmospheric CO₂ through natural photosynthesis. Moreover, reforestation will improve the quality of human life by soaking up pollution and dust from the air)
- Utilization of biomass energy (the use of wood and other agricultural biomass, including aquatic plants such as algae, will diminish CO₂ emissions)

1 | Introduction and overview

It can be concluded that the actual CO₂ mitigation strategies are under the auspices of three leading pathways: CO₂ emissions reduction, Carbon Capture and Storage (sequestration), and Carbon Capture and Utilization (recycling). The focus will be given to carbon capture and utilization, which implements CO₂ use as a chemical feedstock. The use of CO₂ as a chemical feedstock has been under exhaustive studies for many, many years. However, most of the processes investigated are highly endothermic and so require large amounts of energy input for successful employment and use. This is rather easy to be imagined since it is well known that CO₂ molecule is quite an unreactive one (very stable) under normal conditions (20 °C and 1 atm).

Extensive research would be needed to transform CO₂ into an important feedstock for the chemical industry worldwide. Otherwise, we have a very abundant natural feedstock, CO₂, with huge potential and very offering at the same time, but difficult to activate for a chemical process. Nonetheless, over the time sustainable methods have been found to successfully transform CO₂ molecule into valuable chemicals. Most of them are involving the use of a catalyst – hence the name, catalytic conversion process. Catalysis, a term that was firstly introduced by the Swedish chemist Jöns Jacob Berzelius back in 1835 (**Figure 1.7**), represents the increase in the reaction rate of a chemical process upon addition of a catalyst that makes the reaction to take place more rapidly and with less amount of energy required.

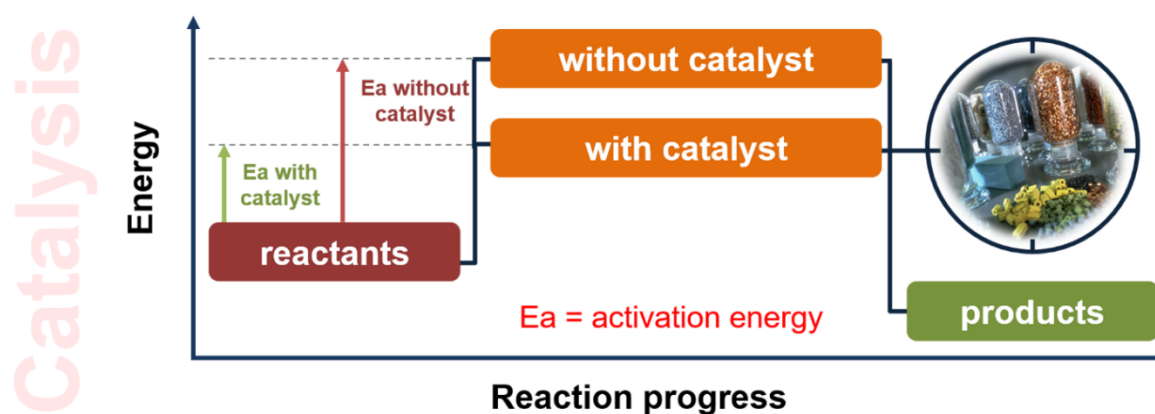


Figure 1.7 Basics of catalysis

One other important feature of catalysis is that the catalytic materials can be recycled and reused to obtain the desired products (thereby not being consumed in the reaction cycle). Among the most important chemical reactions that CO₂ undergoes (summarized in **Figure 1.8**) to produce valuable products it is worth mentioning the CO₂ reforming of methane to produce syngas (mixture of carbon monoxide and hydrogen), methanol formation by CO₂ hydrogenation reaction, ammonia reaction with CO₂ to produce ammonium carbamate in a

first step and then urea as a final product, propylene carbonate formation by the reaction of CO_2 with propylene glycol, cyclic carbonates synthesis from CO_2 and epoxides, etc.

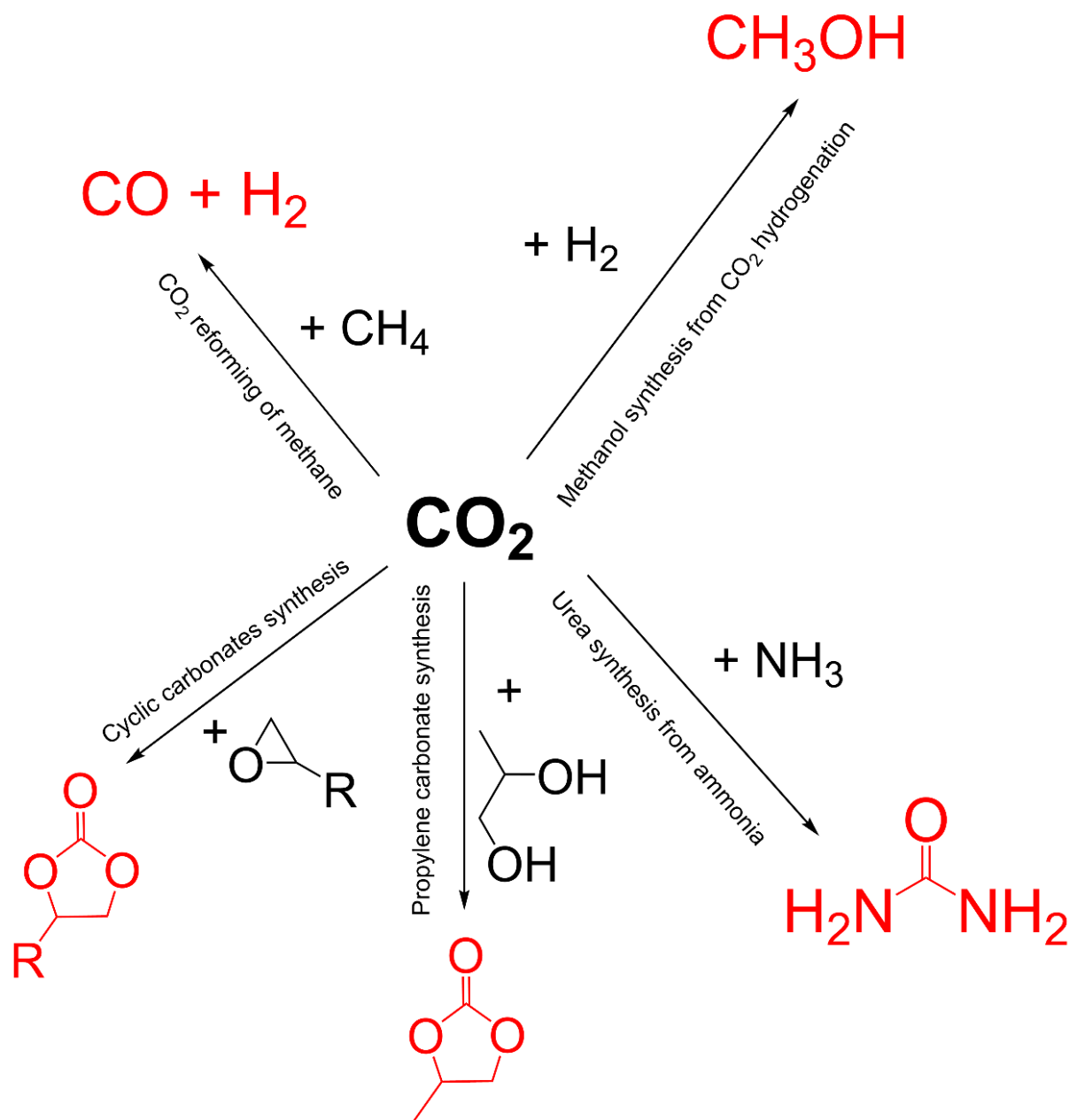


Figure 1.8 CO_2 – most relevant chemical reactions

1 | Introduction and overview

1.2 Dimethyl carbonate: past and present. Future directions

1.2.1 Description and relevance of the topic. Organic carbonates

Human activities have been influencing climate changes. A good example is the significant increase in the emissions of greenhouse gases (as it has already been discussed in the previous section), and CO₂ is the most important exponent of this situation. Emissions of CO₂ by human activities (anthropogenic emissions) are currently more than 130 times greater than the quantity emitted by volcanoes, amounting to about 27+ billion tons per year. Actually, according to Friedlingstein *et al.*, human activities are responsible for 35 billion metric tons (gigatons) of CO₂ emissions in 2010 [10], an amount that makes the CO₂ emissions of the world's degassing subaerial and submarine volcanoes seem petite [11].

Organic carbonates (also known as carbonate esters) are very important chemical compounds that can be classified in two main classes (**Figure 1.9**) linear carbonates and cyclic carbonates (such as dimethyl carbonate, diethyl carbonate, ethylene carbonate, propylene carbonate, and styrene carbonate – to mention only the simplest representatives).

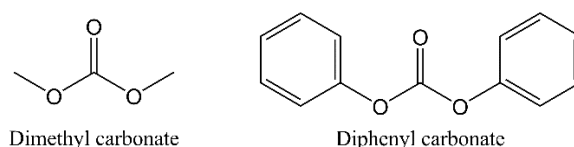
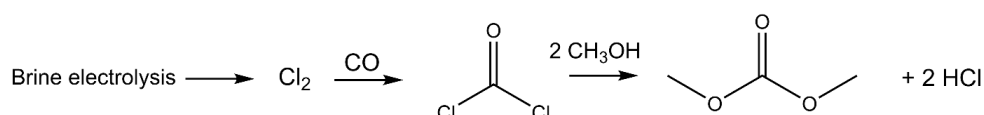


Figure 1.9 The simplest linear organic carbonate (dimethyl carbonate) and its cyclic correspondent (diphenyl carbonate)

Organic carbonates are widely used as solvents for a variety of applications (paints, coatings) due to their low toxicity and biodegradability, as monomers for the preparation of polymers, as intermediates for the pharmaceutical industry, as lubricants, as electrolytes for lithium-ion batteries, etc. In addition, they can be used in the energy sector as they lead to a better gasoline combustion reduction emissions [12]. One of the major synthesis routes (**Figure 1.10**) for the production of acyclic carbonates involves the use of phosgene (COCl₂) [13], whereas for the production of the cyclic carbonates the reaction between CO₂ and epoxides is intensively used at industrial level since mid-1950s. To highlight the foregoing statements, one of the most intense studied reactions in the last decades of the 20th century is the coupling reaction of CO₂ and epoxides to provide cyclic carbonates as final product. An entire series of catalytic systems [14-19] have been developed for the coupling of CO₂ and epoxides, such as alkali metal salts [20], alkali metal salts combined with crown ethers or quaternary ammonium salts [21], organoantimony halide [22], MgO [23] or Mg–Al mixed oxides [24], porphyrin [25], phenol- and organic-based or sodium iodide [26, 27], phthalocyanine [28], polyoxometalate [29], etc. Another interesting example is the direct

oxidative carboxylation of styrene to styrene carbonate (in both single step and multistep experiment) [30-33]. It is quite a laborious reaction since styrene oxide, in comparison with other epoxides such as propylene oxide and ethylene oxide, is more difficult to convert to styrene carbonate as it has a less reactive β -carbon atom. This necessitates harsher conditions, longer reaction time and higher reaction temperatures, and in most of the cases it involves the use of a solvent, a phase-transfer catalyst, an oxidant, and a catalyst for the CO_2 cycloaddition to the epoxide.

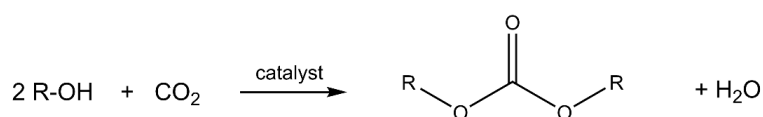
Chlorine cycle for DMC synthesis via phosgene route



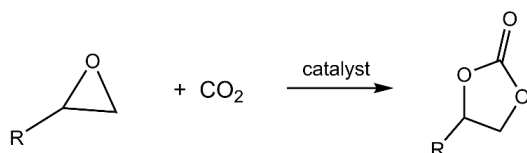
Oxidative carbonylation of alcohol



Linear carbonate synthesis in a phosgene-free technology



Cycloaddition reaction of epoxides and CO_2



One-pot synthesis of styrene carbonate from styrene and CO_2

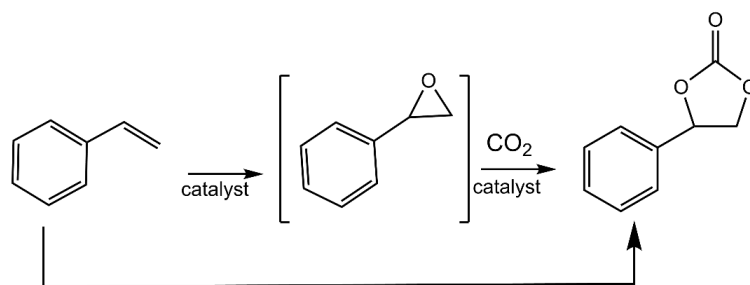


Figure 1.10 Several formation routes for various organic carbonates

The increased use of carbonates as monomers for polymers formation may grow even sooner, leading to a large increase of their demand on the global market. If we ponder upon the current synthetic technology that uses phosgene (a very toxic chemical compound already banned in many countries) as a building block, then we will surely understand why the

1 | Introduction and overview

development of new synthetic methodologies for organic carbonates is attracting much attention worldwide. The replacement of such toxic raw material with CO₂ (or urea, the more active form of CO₂) seems to be very challenging and interesting topic, answering at the same time to the “green chemistry” principles by using clean and safe technologies, and implementing the atom-economy strategy.

1.2.2 Dimethyl carbonate: fine chemical from CO₂

CO₂ emissions to the atmosphere can be reduced by chemical fixation in either organic or inorganic carbonates (giving rise to the so-called non-reductive CO₂ transformations). Many compounds can be commercially produced on an industrial scale using CO₂, thus allowing turning a waste gas into economic profit. Moreover, financial, legal, social and environmental factors promote the development of markets and technologies that make use of industrially CO₂ as a chemical feedstock. Since the 1990s increasing amounts of fuels, polymers and other organic and inorganic products have been produced using new alternative routes. Besides a small contribution to CO₂ emissions reduction such processes often have the benefit of higher energy efficiency, lower fossil fuel consumption, less pollution or the use of less toxic chemicals [34]. Different organic carbonates can be obtained from the CO₂ such as the alkyl carbonates - dimethyl carbonate (DMC) and diethyl carbonate (DEC), polycarbonates (PC) and others - primarily cyclic - organic carbonates. It is very important the role of homogeneous (one-phase system) or heterogeneous (multiple-phase system) catalyst in the carbonate(s) synthesis. One of the key points for large-scale (industrially relevant) process development is to find heterogeneous catalysts to replace homogeneous catalysts because of product separation and catalysts recovery thereby drastically reducing the final cost of the process [35].

Development of the direct carboxylation reaction of alcohols such as methanol for the synthesis of alkyl carbonates is very attractive in terms of CO₂ chemical fixation and green chemistry (not to mention the atom economy of the process), and this can also contribute to the substitution of phosgene with the harmless CO₂ molecule. In this context, it is worthwhile exploring new ways to valorize CO₂ by generation of fine chemicals such as carbonates. The dimethyl carbonate (DMC) is drawing attention as a safe, non-corrosive and environmentally acceptable alternative to methylating and carbonylating agents [36, 37]. Its extensive use worldwide in the last 20-25 years drove us into trying to find better options for its synthesis, mainly related on the “green chemistry” approach.

DMC is an extremely versatile compound (**Figure 1.11**) which represents an attractive eco-friendly alternative to both methyl halides (CH₃X) or dimethyl sulfate (DMS), and more important to phosgene (COCl₂), which are toxic and corrosive methylating or carbonylating

agents [38-40]. The DMC is also used in the synthesis of polycarbonates, polyurethane among others fine chemicals, and even as a solvent for replacing: methyl ethyl ketone – MEK (gums, resins), tert-butyl acetate - tBuAc (lacquers, inks, adhesives, thinners), para-chlorobenzotrifluoride - PCBTF (printing industry). Many of the properties of DMC make it a genuinely green reagent, particularly if compared with conventional alkylating agents. It has high octane number, low Reid vapor pressure (RVP), and low CO and NO_x emissions. Finally, DMC is classified as a flammable liquid, smells like methanol and does not have irritating or mutagenic effects either by contact or inhalation (therefore, it can be handled safely and without any special precautions) [41]. **Table 1.2** presents a concise summary of the most important properties of DMC.

Table 1.2 Some physical and thermodynamic properties of DMC [42]

Appearance	clear liquid	Flashing point (°C)	21.7
Molecular formula	C ₃ H ₆ O ₃	Dielectric constant (ε ²⁵)	3.087
Molecular weight	90.08 g/mol	Dipole moment (μ, D)	0.91
Melting point (°C)	4.6	ΔH ^{vap} (kcal/kg)	88.2
Boiling point (°C)	90.3	Solubility H ₂ O (g/100 g)	13.9
Density (D ²⁰ ₄)	1.07	Azeotropical mixtures	water, alcohols, hydrocarbons
Viscosity (μ ²⁰ , cps)	0.625		

Dimethyl carbonate uses

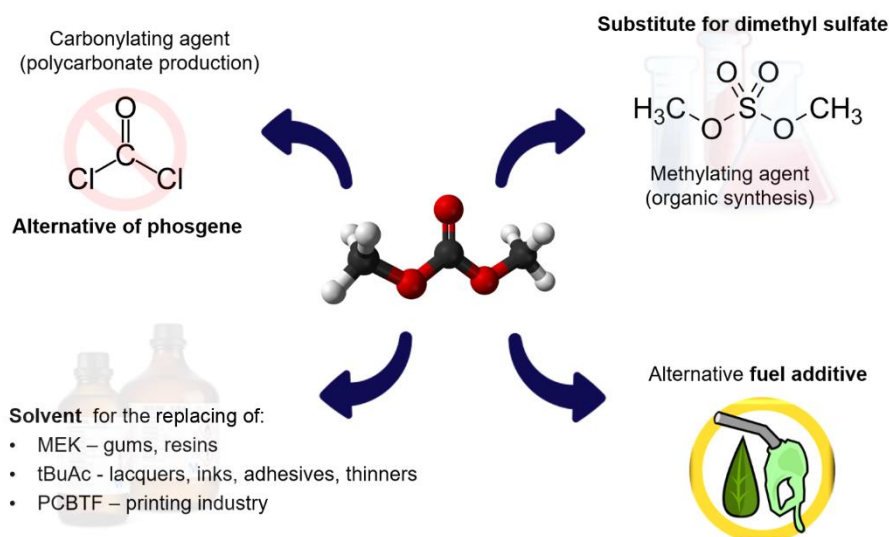
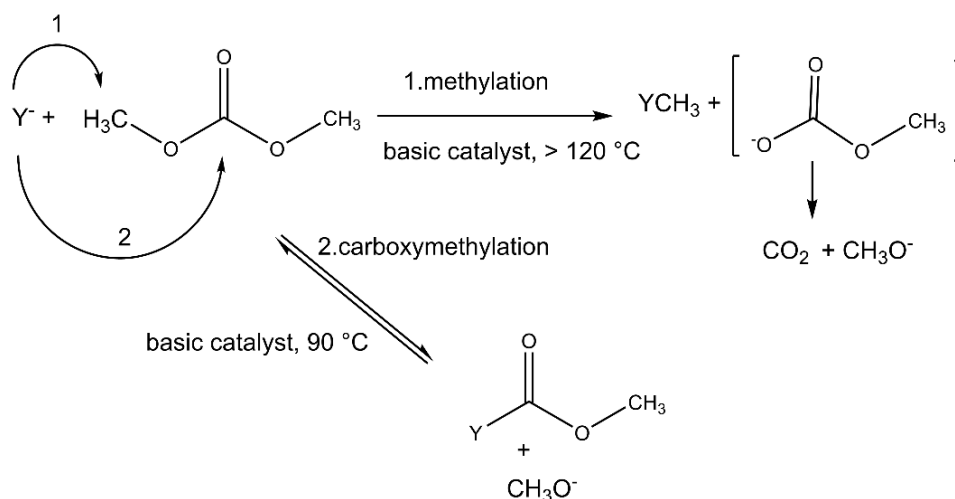


Figure 1.11 DMC – main uses

1 | Introduction and overview

DMC is known for exhibiting a versatile and tunable chemical reactivity, **Scheme 1.1**, such as a methoxy-carbonylating/carbonylating agent and methylating agent, depending on the experimental conditions (temperature, nucleophile (Y^-), catalyst, etc.). Both reactions can be conducted in the presence of catalytic amounts of base to avoid the formation of unwanted inorganic salts as by-product and the related disposal problems. On the other hand, the methylation with methyl halides or DMS, and carbonylation with phosgene generate stoichiometric amounts of inorganic salts. In addition, the methanol produced in this process can be recycled for the production of DMC [43].



Scheme 1.1 Nucleophilic substitution of DMC

Furthermore, DMC is also used as an oxygenate additive to diesel fuel because of its high oxygen content (around 53 wt% - three times the oxygen content of methyl tert-butyl ether, MTBE). The use of oxygenated fuels has the potential to reduce soot from diesel engines. Also, DMC has a good octane rating, it does not phase separate in a water stream like some alcohols do and it is both low in toxicity and quickly biodegradable. Diesel engine studies have shown that DMC addition to the fuel can significantly reduce smoke emissions [44-46].

All the current applications for DMC (**Figure 1.12**) would then yield a market volume of 2000 Mt (2000 megatonne = 2 billion metric tons) annually as anticipated by Bertilsson and co-workers [47] with a potential market of 30 Mt/yr for DMC use as gasoline additive [48]. Although exact numbers can hardly be given (for example several plants have been/are being built in China and the market is in a continuous expansion), current DMC production capacity can be estimated to be around 0.1–0.5 Mt/yr [49]. In 2005, the worldwide consumption of DMC was about 100000 tons, with production concentrated only in USA, Europe and Japan. Yet, nowadays DMC production is expanding rapidly in other countries, with China forecasting a production capacity in the range of 20000 tons (before 2005). In 2007, China produced 120000 tons of DMC, twice the output of 2006 [50]. By the end of 2009, China had 12 major

DMC producers, with a combined capacity of 267000 tons/yr (mostly produced by transesterification process) [50].

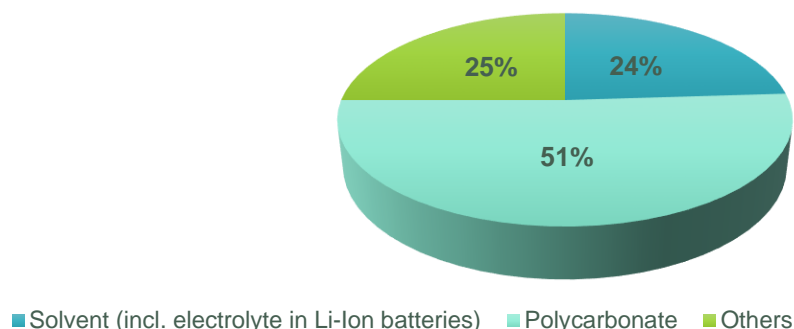
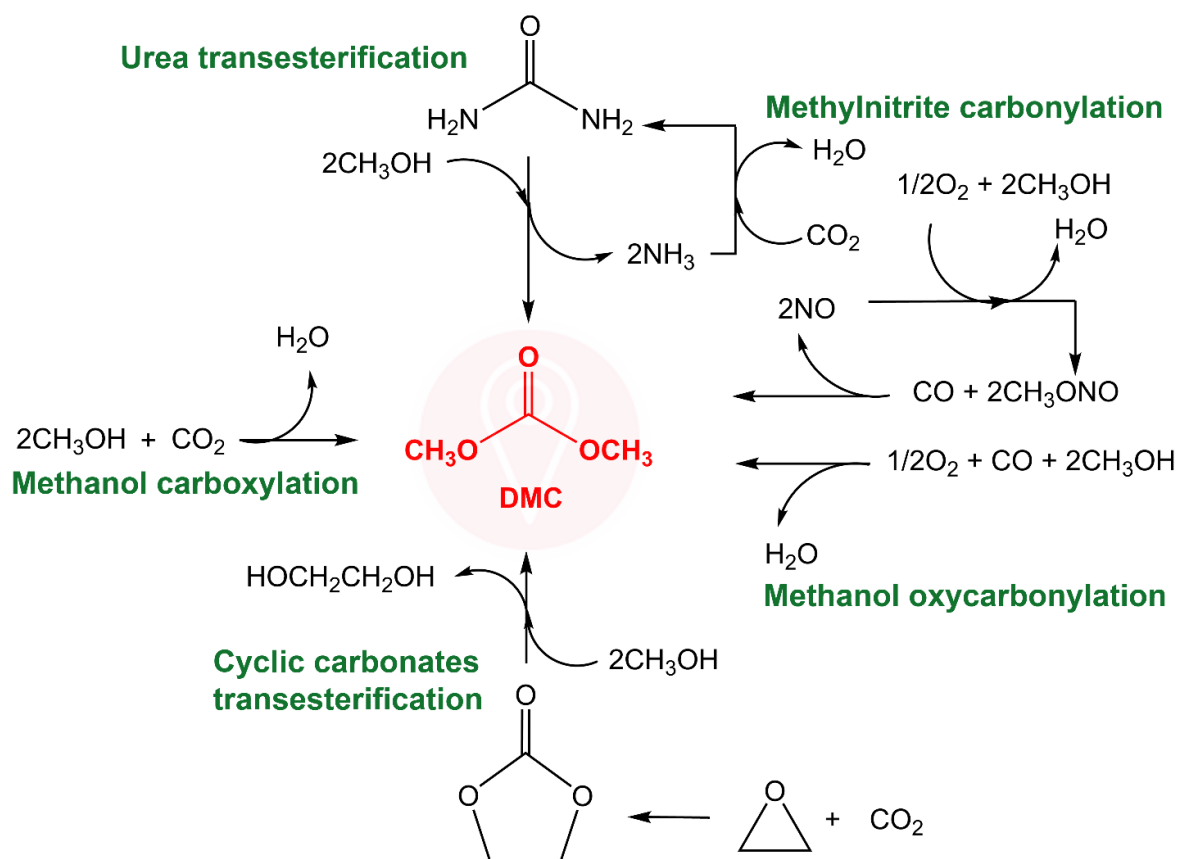


Figure 1.12 Global DMC consumption by end use

The current interest toward the development of DMC manufacturing processes and applications is witnessed not only by the increased demand for DMC but also by the growth of literature and patents references, mainly in the most recent years. The increasing demand of DMC has caused researchers to investigate new more sustainable and effective routes of synthesis avoiding the use of phosgene, briefly presented in the **Scheme 1.2**.



Scheme 1.2. Alternative synthetic routes for DMC preparation

1 | Introduction and overview

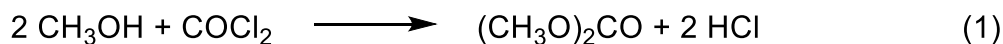
1. 2. 2. 1 Processes for DMC synthesis

Many of the current industrial synthesis of DMC with phosgene-free technologies are principally based on the oxidative carbonylation of methanol (i.e. Enichem and UBE processes). As per Chemsystems Perp Program on dimethyl carbonate (PERP 2012S12 from December 2012) the commercial routes to produce dimethyl carbonate that are currently in operation include:

- Liquid phase oxidative carbonylation (via cuprous methoxychloride intermediate) represented by Versalis (ENI group) and Lummus process (China and N.W. Europe)
- Vapor phase oxidative carbonylation (via methyl nitrate intermediate) as illustrated by the Bayer (China and N.W. Europe) and UBE processes
- Transesterification reaction of a carbonates with methanol, exemplified by the Asahi Kasei process using ethylene carbonate (early 2000s in China and later in N.W. Europe), and processes ran by several Chinese producers via propylene carbonate route
- Urea methanolysis, patented by Catalytic Distillation Technologies (China and N.W. Europe) and the Institute of Coal Chemistry (ICC, Chinese Academy of Science)

Stoichiometric reaction of methanol and phosgene – [Bayer AG and Group SNPE]

The traditional synthesis of DMC used to require dangerous, toxic phosgene as a reagent, (1). The phosgenation of methanol was the most important method to produce DMC till 1980s [51]. The reaction is accelerated using an acid scavenger such as a tertiary amine or an inorganic base, e.g. NaOH.

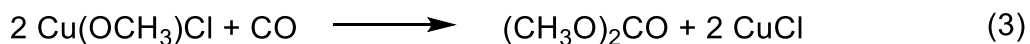


The major drawbacks of the phosgene processes are: i. the high toxicity of phosgene, which is controlled by the international treaty concerning chemical weapons, and ii. the disposal of the co-produced hydrogen chloride [52]. In order to achieve the principles of “Green Chemistry” that aims at the lowest impacts on human health and environment, other synthesis routes have been investigated [53].

Methanol oxycarbonylation – [Enichem and Dow process]

ENIChem’s process is the state of the art commercially proven process for DMC production. It is based on the oxidative carbonylation of methanol catalyzed by cuprous chloride (CuCl). The reaction is conducted in a slurry reactor or several slurry reactors in series at 120 °C and 27 atm [51]. Methanol and CO pass through the reactor or reactor train and are

only partially converted. The oxygen is the limiting reagent (4%) to avoid the potential explosion(s). The reaction proceeds in the next redox cycle of copper ions, (2) and (3) [53].

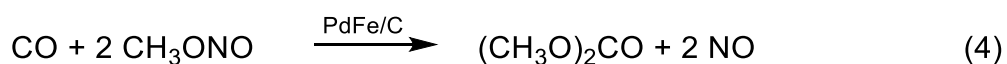


The CuCl catalyst was reported to be the best catalyst for this reaction. It provides excellent selectivity and very good reactions rates. However, the process has two principal problems: i. the low per-pass conversion (less than 20%) due to the catalyst deactivation, and ii. the difficult separation [54, 55].

On the other hand, Dow has patented a copper based catalyst, $[\text{Cu}(\text{OCH}_3)\text{Py}]\text{Cl}_2$ or CuCl_2 , like that used by Enichem, impregnated on a DARCO active carbon support. The best initial per-pass conversions are comparable to that obtained by Enichem system with a selectivity of 65%. Anyway, the supported copper catalysts deactivate quickly. Catalyst deactivation results from both a loss in copper surface area and the formation of paratacamite ($\text{Cu}_2(\text{OH})_3\text{Cl}$) as the only crystalline phase in the consumed catalyst. The activity of the catalyst could be partially regenerated by passing a 10% HCl in dry N_2 gas bringing the catalyst to a Cl/Cu ratio around 1.2 [56]. The pyridinal copper complex provides a higher productivity than the CuCl_2 . Both the Enichem and Dow catalysts are susceptible to deactivation by water.

Methylnitrite carbonylation – [UBE and Bayer AG process]

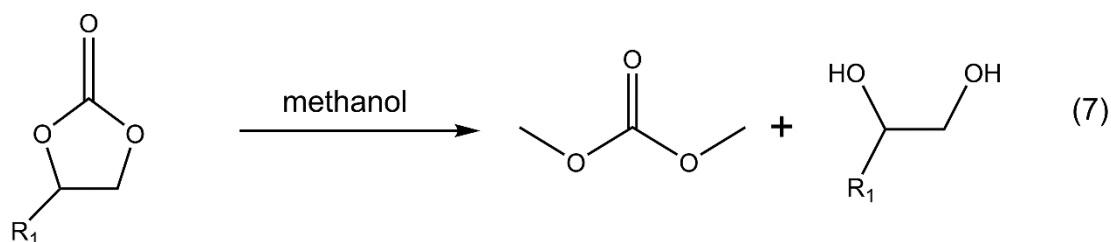
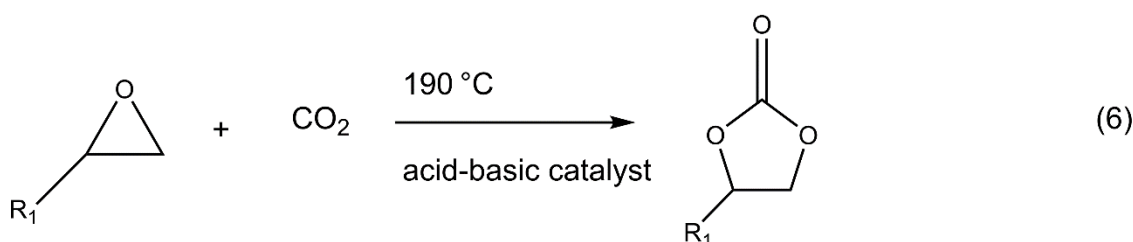
Ube Industries, Ltd. [57] developed an excellent DMC synthesis process using a PdCl_2 and a second metal chloride (Bi, Fe, or Cu) co-impregnated on an active carbon support catalyst together with an alkyl nitrite promoter at 100 °C and at 1 atm of CO, (4). The catalyst gives high selectivity towards DMC (>92%) formation with very high productivity (0.3 L of DMC/h) which is 3 times the activity of ENIChem's catalyst. High pressures favor the formation of the dimethyl oxalate (DMO) over the dimethyl carbonate (DMC). Under anhydrous conditions, the high catalytic activity is maintained for a longer time. In addition, the methyl nitrite used in the reaction is synthesized by the following reaction (5), which proceeds at room temperature without any catalyst [53].



1 | Introduction and overview

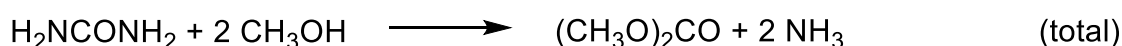
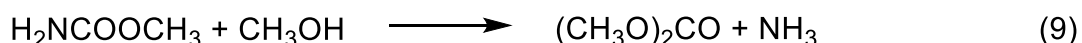
Trans-esterification between methanol and cyclic carbonates – [Texaco process]

Texaco (Texas Company) and others (e.g. Asahi Kasei) have developed DMC production by two-step synthesis from ethylene oxide. First, cyclic carbonate is synthesized (**6**) and via trans-esterification process it reacts with methanol to give a mole of ethylene glycol for every mole of DMC produced, (**7**). The final reaction is equilibrium-limited and has been the subject of several acid-base catalysts patents assigned to Texaco [58-62]. The catalysts are a wide variety of acidic and basic polymeric resins and metal-containing catalysts. However, this is the least likely process for the industry because of low productivity and the ethylene glycol's very strong market.



Trans-esterification between methanol and urea

Another possible route for DMC synthesis is the trans-esterification reaction between methanol and urea [37, 46]. It is a two-step process, which goes via a methyl carbamate intermediate, (**8**). In the second step, (**9**), the methyl carbamate intermediate reacts with methanol to give DMC and ammonia. The major shortcoming of this reaction is its high free enthalpy, resulting in a nonspontaneous (disfavored) chemical process.

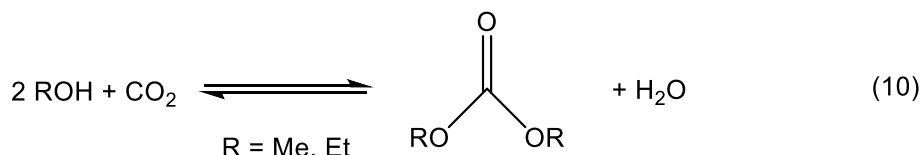


Based on this thorough analysis on the actual market and production premises (the potential demand for DMC could be much higher in the (near) future) one could easily conclude that more eco-efficient and economic pathways can and would be used instead of

the ones described above, including those based on the very abundant and easily affordable CO₂.

1. 2. 2. 2 Direct carboxylation reaction – DMC synthesis using CO₂

The development of the direct reaction between CO₂ and alcohols (methanol, MeOH and ethanol, EtOH) for the synthesis of carbonic acid diesters (DMC or diethyl carbonate, DEC) is very attractive in terms of CO₂ chemical fixation and green chemistry, and this can also contribute to the replacement of phosgene by CO₂ as carbonyl source [39], (10).



Although the carboxylation reaction using CO₂ is very clean and it has a high atom-efficiency (a measure of the conversion efficiency of a chemical process in terms of all atoms involved and the desired products obtained), the equilibrium for the formation of the linear carbonates from alcohols and CO₂ is located on the left side of the reaction, (10). The thermodynamic barrier causes extremely low yields (1-2%) at the equilibrium. To avoid this thermodynamic limitation, it is necessary to remove the water formed as a by-product using an adequate agent, or (e.g.) increasing the CO₂ concentration. The chemical water traps could be an option to displace the equilibrium to the right side of the reaction, (10). A well-known dehydrating agent is the molecular sieve. Unfortunately, it cannot be used at the carboxylation reaction temperature because of the formed surface –OH groups which are sufficiently acidic to protonate the carbonate and reverse the reaction. Organic water traps such as aldols, ketals and dicyclohexylcarbodiimide (DCC) are better suited to remove the water in the carboxylation reaction and favor the DMC formation. However, this approach is limited by the need of an efficient separation process [63].

The advantages of the direct carboxylation reaction of methanol with CO₂ (Figure 1.13, speaking in terms of material cost and synthetic strategy involved) in front of the current methodologies for the synthesis of DMC have attracted the attention of the scientific community all over the world and the industry as well.

1 | Introduction and overview

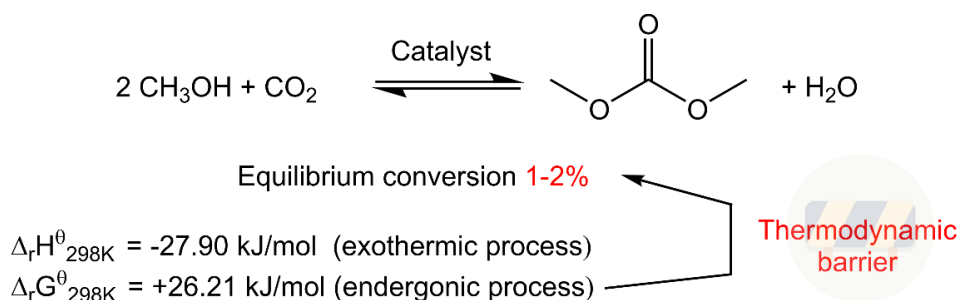


Figure 1.13 DMC synthesis from the carboxylation reaction of methanol and CO_2

In this context, several examples are present in the literature of both homogeneous and heterogeneous systems (batch and continuous operation) to study different catalysts for the direct synthesis of DMC, **Table 1.3**. The most important contributions will be briefly discussed in the following section, homogeneous and heterogeneous catalytic processes for DMC synthesis.

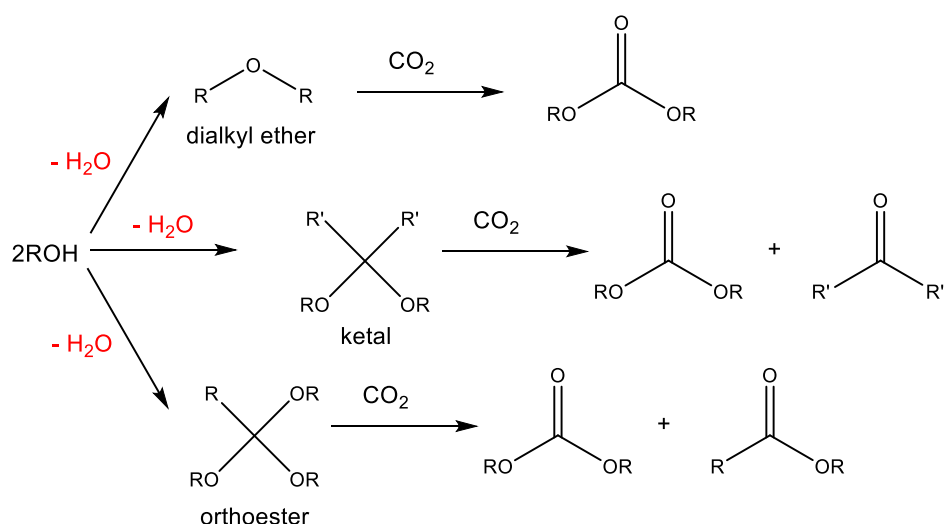
Table 1.3 Some examples of catalysts used in the direct synthesis of DMC

Homogeneous	Heterogeneous
Dialkoxydibutyltin	ZrO_2
Sn(IV) and Ti(IV) alkoxides	$\text{H}_3\text{PO}_4/\text{ZrO}_2$
Metal acetates	$\text{H}_3\text{PO}_4/\text{V}_2\text{O}_5$
Mg dialkoxide	$\text{CeO}_2\text{-ZrO}_2$
Observations and comments	
[-] Decompose with water	[-] Equilibrium reaction is not favored
[-] Use of expensive dehydrating agents	[-] Low conversion
[-] Difficult to recover and reuse	[+] Easy to recover and reuse
[+] High activity and high selectivity	[+] Economic

Homogeneous catalysis

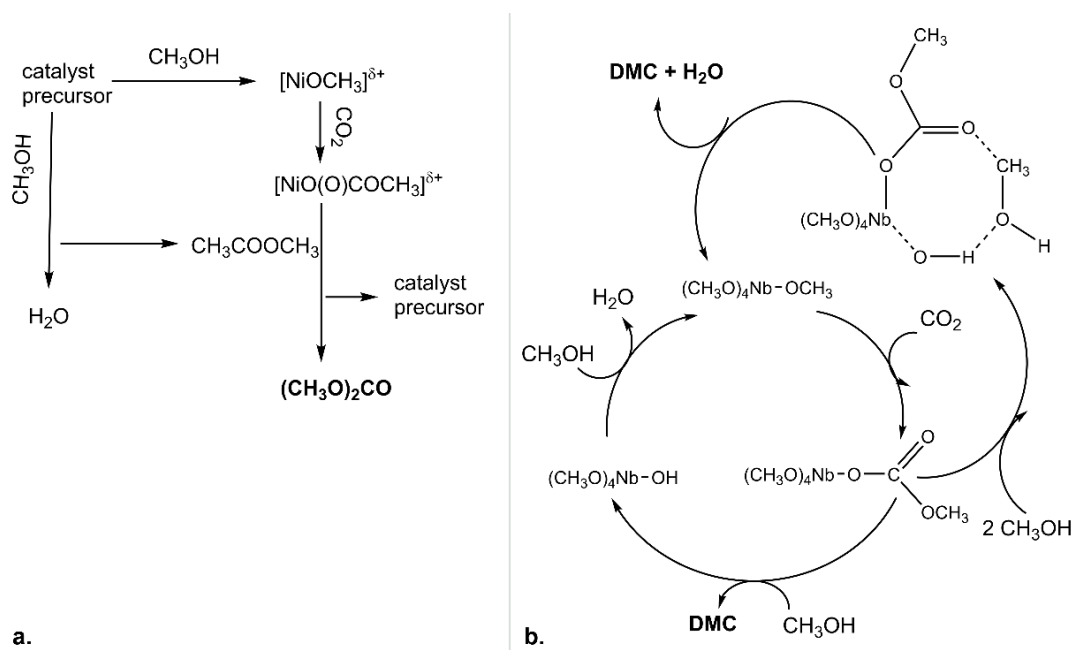
A considerable effort has already been devoted to the production of DMC from methanol and CO₂, and some of the reactions were catalyzed by a series of organo-tin compounds e.g. Bu₂SnX₂ where X = OMe, OEt, OBu, Cl Br, OPh, OOCMe, OOC(CH₂)₁₀Me) and X₂ = O, (OH, Cl) or Bu₂XSnOSnXBu₂ where X = Cl, Br, OOCMe, OBu, n-Bu. The possible organotin-catalyzed formation of DMC from CO₂ was first proposed by Japanese research groups [64, 65]. However, the catalytic activities obtained have been very low due to the decomposition of the catalysts by water, generating Bu₂SnO and methanol. The best catalyst materials were proved to be the tin alkoxides Bu₂Sn(OR)₂ (R = Me, Et, Bu) which gave the carbonate in up to 160 mole % yield (with respect to the tin compound) under suitable reaction conditions (low CO₂ pressure, 130 - 190 °C, 6 h). Higher yields for carbonate formation (reaching up to 150 - 330 mole %) have been obtained with the use of chemical water traps added to react with the water molecules formed during the reaction. It was also studied the synthesis of DMC from the carboxylation of methanol with CO₂ in the presence of metal alkoxides and metal carboxylates. The best results have been reached with Ti(IV) and Sn(IV) alkoxides which at temperatures from 130 to 180 °C and low CO₂ pressures resulted in a DMC yield of 30 to 100 mole % or 40 to 130 mole % with respect to the metal alkoxides, dependent upon the CO₂ (gaseous or solid one). The reaction yields can be further increased up to 70 - 190 mole % and 90 - 270 mole %, respectively, using chemical scavengers of the reaction water [66-68]. With the purpose of improving the efficiency of the homogeneous catalytic synthesis of DMC, Sakakura *et al.* proposed the dehydration of methanol before the reaction with CO₂ to produce DMC [69]. Typical dehydrated derivatives of methanol are trimethyl ortho ester, dimethyl ether and the dimethyl acetal (ketal), **Scheme 1.3**. The best results were obtained with trimethyl ortho ester as dehydrating agent, using the Bu₂Sn(OMe)₂ as catalyst at 180 °C and 300 atm, during 24 h of reaction (20% yield, 93% selectivity towards DMC). With the increasing of the CO₂ pressure to 2000 atm the yield reached 88% after 24 h [70]. Therefore, the yields in this reaction showed a highly dependence on the CO₂ pressure, attaining a maximum around the critical pressure of CO₂. The reaction of ortho esters and CO₂ is also promoted by several types of catalysts, including alkali metal halides and immobilized ammonium salts [71]. However, the principal considerations that this method brings along are: i. the ortho esters are relatively expensive as an industrial raw material, ii. co-production of esters, and iii. difficulty in regenerating ortho esters from esters.

1 | Introduction and overview



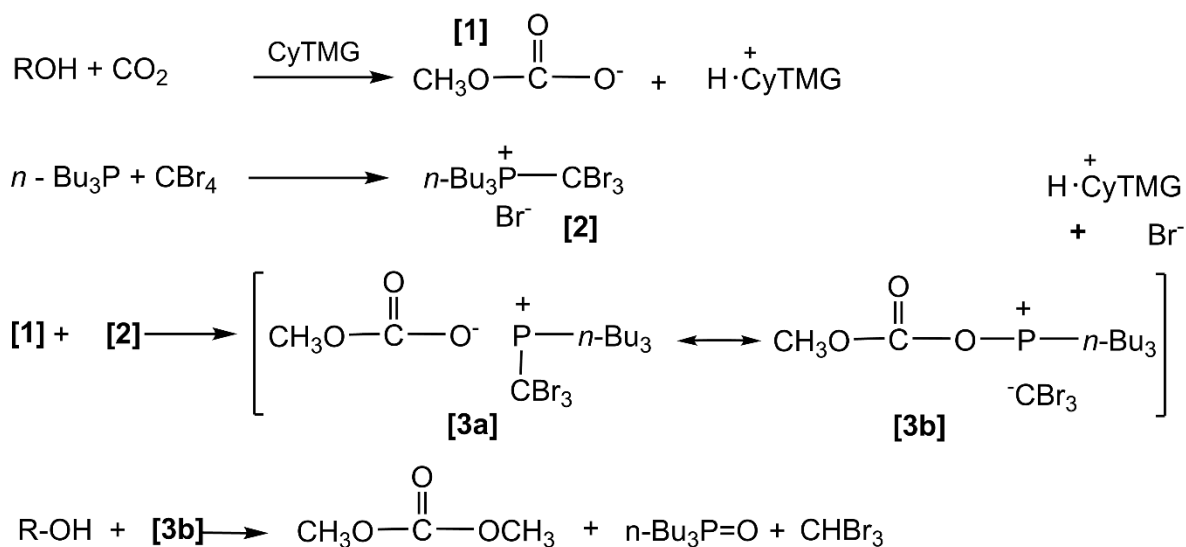
Scheme 1.3. DMC synthesis from CO₂ and the dehydrated derivatives of the corresponding alcohols

Other than tin compounds, combinations involving titanium alkoxides and polyether ligands (e.g., crown ethers or polyethylene glycols) show relatively high catalytic activities. Under study was also the reaction of CO₂ and methanol - investigated at near supercritical conditions using nickel acetate as a catalyst. DMC was synthesized as a unique product at a quite low temperature (around 32 °C) and the yield was twelve times higher than that obtained at non-supercritical conditions, a remarkable fact which proves once again (if necessary) that CO₂ pressure plays an important role for shifting the equilibrium toward product formation. The maximum yield for DMC synthesis was reached at the pressure of 9.3 MPa. The formation mechanism of DMC in supercritical phase was also proposed, [Scheme 1.4 a](#) [72]. Furthermore, niobium complexes showed good catalytic activity in the carboxylation of alcohols following the presented reaction scheme, [Scheme 1.4 b](#). [Nb(OR)₅]₂ compounds (R = Me, Et, allyl) can easily react with CO₂ to provide the corresponding monomers Nb(OR)₄[OC(O)OR]. Once the complex is formed, this represents the catalyst for DMC formation from CO₂ and methanol. Another study on direct carboxylation of alcohol to organic carbonates mediated by the group 5 element alkoxides revealed that the trend of reactivity among the series V, Nb, Ta follows the next sequence: Nb >> Ta > V [73, 74].



Scheme 1.4. DMC synthesis over **a.** Ni and **b.** Nb based catalysts

Kadokawa *et al.* [75] studied the direct condensation of CO₂ with alcohols such as methanol using the tributyl-phosphine-carbon tetrabromide-CyTMG system (where CyTMG= tetrabromide-2-cyclohexyl-1, 1, 3, 3-tetramethylguanidine) as a condensing agent, **Scheme 1.5**. The reaction of CO₂ with primary alcohols led to the corresponding carbonates in high or moderate yields (~87% of DMC) after 2 h of reaction (and using DMF as a solvent).

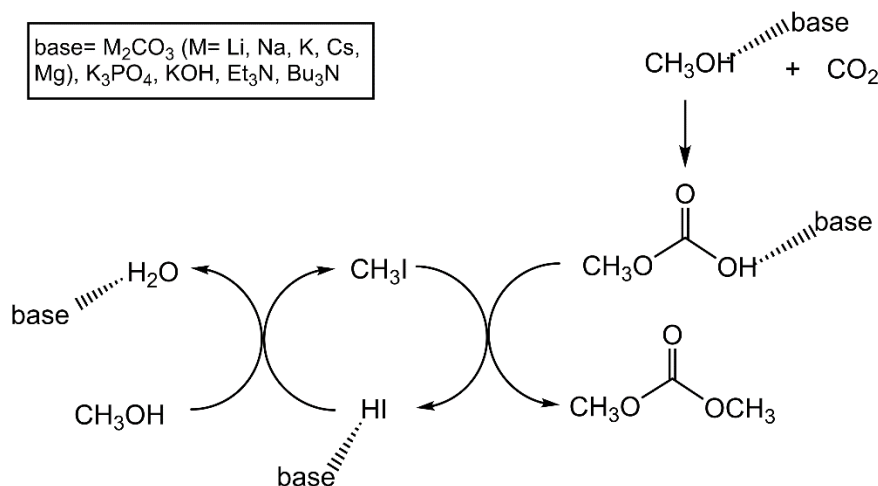


Scheme 1.5. DMC synthesis by direct condensation of CO₂ with alcohols

DMC synthesis by reacting CO₂ and methanol in the presence of methyl iodide as promoter plus a base has been proposed by Fujimoto *et al.* [76]. Reactions were run for 2 h at moderate temperature (80-100 °C) and the yield of DMC based on CH₃I consumption was

1 | Introduction and overview

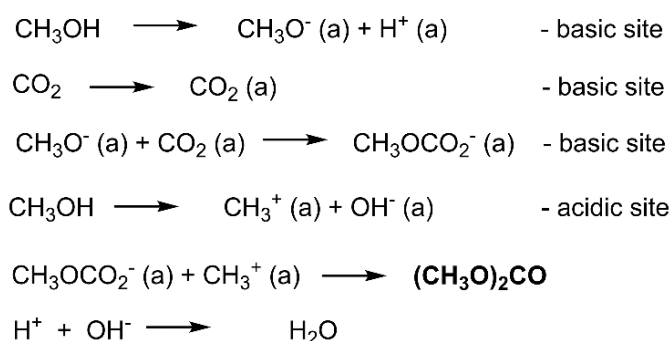
very large (up to 400% mole base). This means that methyl iodide is also involved in the catalytic cycle. It was shown that the crucial element of the reaction is represented using a base with an appropriate basicity, as for example K_2CO_3 and K_3PO_4 , which provided the best results. In the **Scheme 1.6**, a possible catalytic cycle is presented.



Scheme 1.6. DMC synthesis in the presence of methyl iodide as a promoter

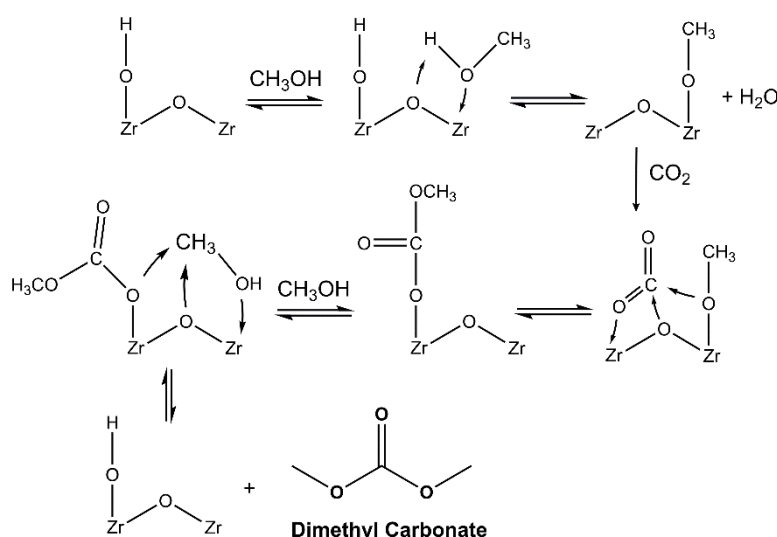
Heterogeneous catalysis

Solid acid-base catalysts such as zirconia (ZrO_2) catalyse DMC formation from methanol and CO_2 [77]. More precisely, this is one of the first heterogeneous catalysts displaying some activity for DMC production starting from CO_2 and methanol. Tomishige *et al.* have studied the use of zirconia materials as heterogeneous catalysts in the carboxylation of methanol [53, 77]. Although the selectivity of DMC over these catalyst materials is very high (ca. 100%), unfortunately, the methanol conversion is very low (less than 1%). The highest amount of DMC formation was obtained from zirconia synthesized by calcination of zirconium hydroxide at 400 °C - at a reaction temperature of 160 °C (for 2 h reaction time) and 5 MPa initial CO_2 pressure (at room temperature). It was also suggested that there is a direct correlation between the acid-base sites from the surface of the catalyst and the catalytic activity response (the key element is the ratio between the tetragonal and monoclinic zirconia from bulk/surface; the bulk of the zirconia had mainly tetragonal phase, while near the surface the monoclinic phase was dominant, with an important fraction of tetragonal phase). A reaction pathway was also proposed, **Scheme 1.7**, being among the first papers to support that DMC synthesis from CO_2 and methanol requires the presence of both acid and basic sites (bi-functional materials).



Scheme 1.7. Reaction mechanism for DMC synthesis over ZrO₂ materials

Using ZrO₂, the reaction mechanism has been investigated by Bell and co-workers via Raman and Infra-Red spectroscopy [78-82]. DMC (as concluded from IR data, **Scheme 1.8**) is produced through the following steps: i. dissociative adsorption of methanol to form methoxide species, ii. CO₂ insertion resulting in the formation of monomethyl carbonate (MMC), and iii. the transfer of a methyl group from previously adsorbed methanol to the monomethyl carbonate to form DMC. Every step proceeds more rapidly (twice as fast) on monoclinic zirconia compared with tetragonal zirconia (later studies). Consequently, DMC formation rate was dependent on the structure of ZrO₂. The catalytic activity is attributed to the higher Brønsted basicity of hydroxyl groups and Lewis acid/base pairs presented on the surface of zirconia.

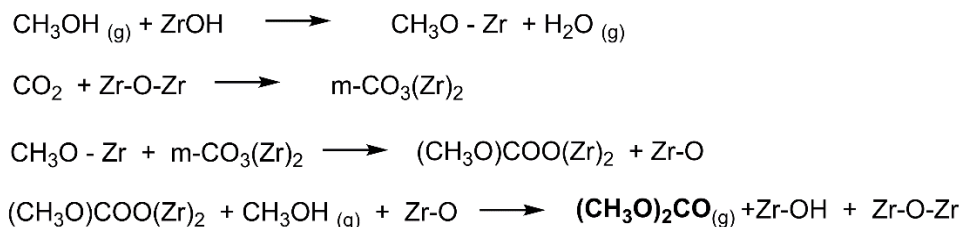


Scheme 1.8. Proposed mechanism for the formation of DMC from CO₂ and CH₃OH (from IR studies)

A similar study conducted via Raman spectroscopy confirmed the main steps shown in the previous papers. Reaction mechanism, **Scheme 1.9**, goes via i. methanol adsorption leading to the formation of adsorbed methoxide groups, ii. CO₂ adsorption leading to the formation of carbonate groups, and iii. formation of monomethyl carbonate species by the reaction of the

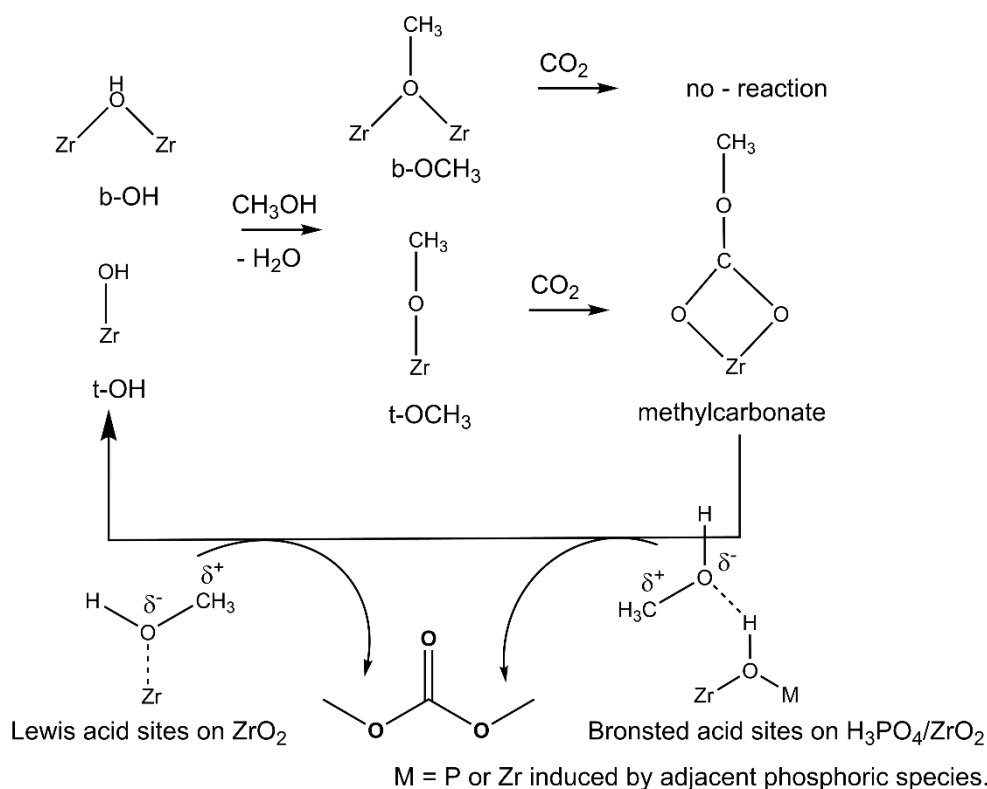
1 | Introduction and overview

pre-adsorbed methoxide groups i. and monodentate carbonate species ii.; lastly, iv. DMC formation results from the reaction of pre-adsorbed monomethyl carbonate and methanol. Interestingly enough, titania (TiO₂) did not display any catalytic activity for DMC production [83].



Scheme 1.9. Reaction mechanism (from Raman data) in DMC synthesis over ZrO₂

Modifying zirconia by acidic compounds such as phosphoric acid (H₃PO₄/ZrO₂) [84, 85] and ceria (CeO₂-ZrO₂) [86-88] promotes the catalytic activity. The modification of ZrO₂ catalysts with phosphoric acid was performed to boost the surface acidity of ZrO₂. It was found to be effective for the enhancement of the catalytic activity in DMC synthesis from methanol and CO₂. Also, by modifying the surface acidity, an important decrease in the reaction temperature as compared to the unmodified ZrO₂ was observed. Both ZrO₂ and H₃PO₄/ZrO₂ have Lewis acid sites, though only H₃PO₄/ZrO₂ has weak Brønsted acid sites. The optimum composition of H₃PO₄/ZrO₂ was reported at P/Zr ratio between 0.025-0.1. Using a P/Zr ratio of 0.025 and a temperature of 170 °C the equilibrium level was reached; decreasing the temperature to 150 °C afforded the formation of a DMC amount which is about four times larger as compared to that from ZrO₂. Finally, the same amount of DMC was reported when using H₃PO₄/ZrO₂ at 130 °C and ZrO₂ at 170 °C, while decreasing the temperature to 110 °C showed no catalytic activity for ZrO₂ whereas H₃PO₄/ZrO₂ led to (some) DMC formation. Tomishige *et al.* suggested that the presence of weak Brønsted acid sites (formed upon the direct interaction between Zr_{tetragonal} and P) in the modified-ZrO₂ could be more effective than the Lewis acid sites on ZrO₂ for the CH₃OH activation. And this fact was very important in the selective DMC synthesis since the expected by-product, dimethyl ether (DME), is easily formed on the rather strong acid site. It was also reported a model for the reaction mechanism, **Scheme 1.10**, which concluded that the presence of both acid and basic sites is required so that the direct carboxylation reaction of methanol to proceed towards DMC production. Moreover, the methyl-carbonate formation, which is the direct intermediate for DMC synthesis, proceeds via the terminal methoxy species (reacting further with CO₂) rather than bridged methoxy species which seem to give no reaction with CO₂.



Scheme 1.10. DMC synthesis over $\text{H}_3\text{PO}_4 / \text{ZrO}_2$ catalyst materials

In addition to zirconium-based catalysts, vanadium-based catalysts such as $\text{H}_3\text{PO}_4/\text{V}_2\text{O}_5$ and $\text{Cu-Ni}/\text{V}_2\text{O}_5\text{-SiO}_2$ have been tested in the gas-phase reaction [89, 90]. In the case of the modified vanadium-based catalyst ($\text{H}_3\text{PO}_4/\text{V}_2\text{O}_5$), the yield and selectivity of DMC, as well as the methanol conversion, increased with increasing H_3PO_4 content at low P/V ratios (the optimum ratio proved to be $P/V = 0.15\text{--}0.50$). The DMC yield and selectivity reached a maximum value at $P/V = 0.20$ (1.9% of yield at 140 °C) and then decreased with further increasing H_3PO_4 content. On the other hand, the direct interaction between V and P is essential for the formation of weak Brønsted acid sites. As in the case of zirconium, the Brønsted acid sites on $\text{H}_3\text{PO}_4/\text{V}_2\text{O}_5$ were more effective than Lewis acid sites on V_2O_5 for the CH_3OH activation [89]. Lu *et al.* also reported the use of $\text{Cu-Ni}/\text{VSO}$ ($\text{VSO} = \text{V}_2\text{O}_5\text{-SiO}_2$) as catalyst for direct DMC synthesis in gaseous phase using a continuous tubular fixed-bed micro-gaseous reactor. The optimal reaction conditions for both increased methanol conversion and good selectivity toward DMC production were found to be 140 °C and a pressure of 0.6 MPa [90].

The $\text{CeO}_2\text{-ZrO}_2$ (ratio $(\text{Ce}/\text{Ce} + \text{Zr}) = 0.2$) solid-catalyst has proved to be an even more effective catalyst (at lower temperature) for the direct DMC synthesis from CO_2 than ZrO_2 and $\text{H}_3\text{PO}_4/\text{ZrO}_2$. The catalyst showed a high selectivity towards DMC (ca. 100%) under the reaction conditions (110 °C, 2-16 h, 6/12/21 MPa CO_2 pressure, and with the catalyst pre-calcined at 1000 °C even though this results in a rather low surface area material). However,

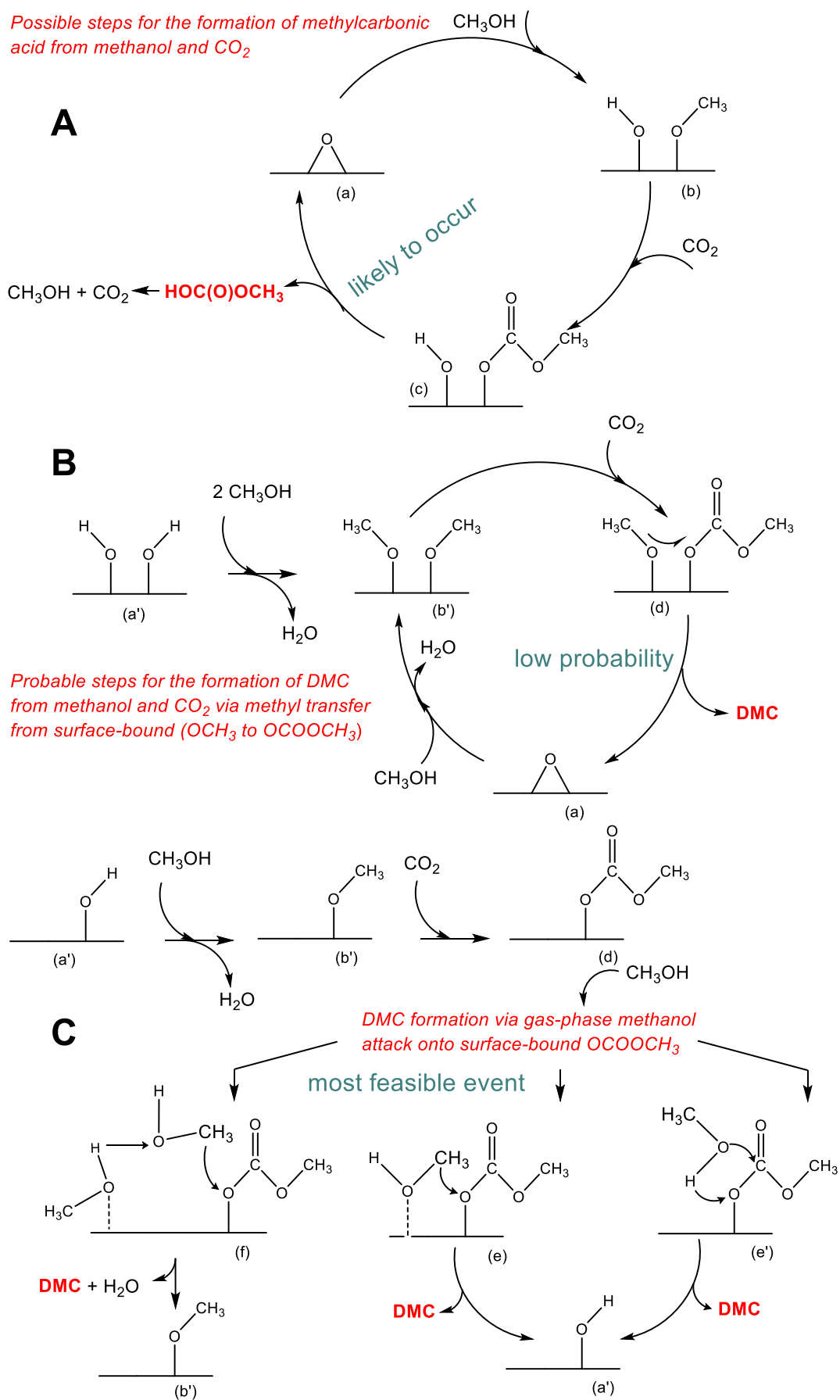
1 | Introduction and overview

the methanol conversion continues to be very low because of the reaction equilibrium (**Figure 1.13**). For the removal of H₂O from the reaction system it was studied the addition of the dehydrating agent, 2, 2-dimethoxy propane (DMP), to the carboxylation reaction system which was very effective for the increasing of the conversion. DMP addition enhances the DMC formation rate above the equilibrium level, while the reaction between DMP and water formed during the reaction takes place to produce methanol and acetone. This discovery opens a new path of a chemical water trap usage in the direct carboxylation reaction of methanol for the synthesis of DMC. However, the addition of larger amounts of DMP was not suitable due to the fact that it leads to a decrease of DMC formation rate and the by-production of the dimethyl ether (DME) [86, 87].

The catalytic properties of different CeO₂ materials were also investigated in the direct synthesis of DMC from methanol and CO₂. The various ceria catalysts calcined at 600 °C and above showed a proportional relation between surface area and the amount of DMC formation in the carboxylation reaction. Suggestions have been made that the active sites for this reaction are on a stable crystal surface such as (1 1 1) of CeO₂. The CeO₂-HS calcined at 600 °C exhibited the highest activity in the whole series of CeO₂ catalysts (0.71 mmol of DMC), whereas decreasing the calcination temperature to 400 °C led to a considerable amount of amorphous phase [91]. Aresta *et al.* have studied the cerium oxide modification by the addition of a hetero-atom for direct DMC synthesis in a batch reactor [92]. It is stated that the reduction of Ce (IV) to Ce (III) (as resulted from the XPS analysis performed on the catalysts before and after the reaction) associated with methanol oxidation towards other C1 molecules and some surface modifications (crystal conglomeration) are the reasons for the ceria catalyst deactivation. Al and Fe were loaded on ceria catalysts to check for changes in methanol conversion or DMC selectivity, and to seek for any improvement during the stability tests. All the catalysts were synthesized from the corresponding nitrate salts (or iron standard solution) by co-precipitation method. Al-loaded CeO₂ offered the most interesting results in terms of lifetime and activity with 3% Al/Ce mixed oxide (calcined for 3 h at 650 °C) leading to a methanol conversion around 0.4%, and a DMC production of 0.4 mmol DMC per mmol of catalyst used (under the reaction conditions: 3 h at 135 °C, and 5 MPa CO₂ pressure). Loading the catalyst with an Al content between 3 to 10% has a positive effect on CeO₂, stabilizing it and at the same time reducing or even cancelling the causes that lead to ceria deactivation. Later, in a more in depth study [93] of the methanol carboxylation reaction with Al/Ce mixed oxide it was found that the equilibrium conversion can be reached after ca. 8 h of reaction in the conditions above mentioned. A very comprehensive reaction mechanism was also presented, gathering together the new findings with the generally assumed mechanistic steps already presented in DMC synthesis. It was concluded that the DMC formation occurs via the

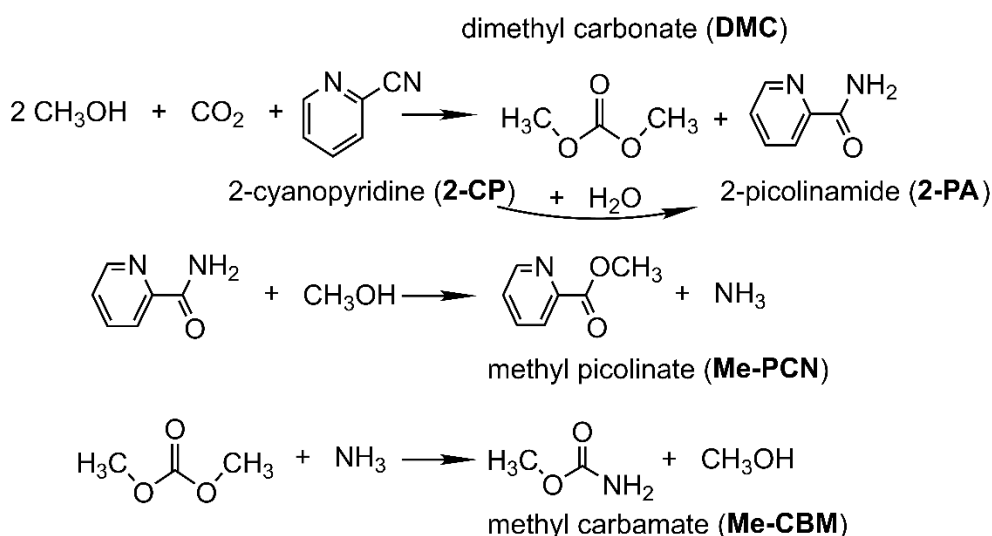
gas phase methanol attack onto the surface bound intermediate, monodentate methyl carbonate (MMC), **Scheme 1.11 C**. Looking for an improvement in the mixed ceria-zirconia catalysts for the carboxylation of methanol Lee and co-workers [94, 95] conducted a study on the acidity/basicity of such materials enriched by the addition of Ga_2O_3 (and other transition metal oxides, but the former proved to be the best one). First, mixed ceria-zirconia catalysts were synthesized by sol-gel method and second Ga_2O_3 on mixed ceria-zirconia catalysts was prepared using the incipient wetness impregnation method and a convenient salt precursor. They found that $\text{Ce}_{0.6}\text{Zr}_{0.4}\text{O}_2$ was the best support for Ga_2O_3 oxide. It was proven that all the catalysts impregnated with Ga_2O_3 ($x\text{Ga}_2\text{O}_3/\text{Ce}_{0.6}\text{Zr}_{0.4}\text{O}_2$ with x from 1 to 15 wt%) showed an enhanced catalytic activity as compared with pure ceria-zirconia catalysts. The activation of methanol toward methyl and methoxy species, plus the formation of methoxy carbonate anion intermediated by the reaction of CO_2 with methoxy species, was facilitated even more by the presence of Ga_2O_3 , which provides enhanced acid and basis sites for the reaction to take place. Finally, it was stated that the amount of DMC production was directly related with an increase in both acidity and basicity of the catalyst. The catalyst showing the highest amount of acid and basic sites (5 wt% Ga_2O_3) was the one providing the best catalytic results [94].

1 | Introduction and overview



Scheme 1.11. Possible steps in DMC synthesis from methanol and CO₂

Following the path of the ceria catalyst already identified as a working material for direct DMC synthesis, Tomishige and co-workers tried to use this material while taking advantage of a water scavenger, since it was already demonstrated that the water formed during the reaction is seriously shifting the equilibrium towards reactant formation (10). And they came out with some outstanding results, being able to find a new compound, 2-cyanopyridine (2-CP), which showed its great effectiveness for the direct DMC production from methanol and CO₂ under mild reaction conditions [96]. 2-CP (a nitrile) acts as a dehydrating agent and reacts with the water formed during the reaction (being already known that ceria is a very good catalyst for the nitrile hydrolysis) [97] to afford the corresponding amide, 2-picolinamide (2-PA). Under the optimized reaction conditions (12 h, 120 °C, and 5 MPa CO₂ pressure – with the catalyst pre-calcined at 600 °C) a 94% methanol based yield of DMC was obtained along with a 95% 2-CP based yield of 2-PA. Small amounts of methyl-picolinate (Me-PCN) and methyl-carbamate (Me-CBM) were detected and identified as by-products and were attributed to the following reactions: i. 2-PA (2-CP hydrolysis product) with the methanol, and ii. DMC with the residual NH₃ from (i). The complete reaction scheme is presented below, **Scheme 1.12**.

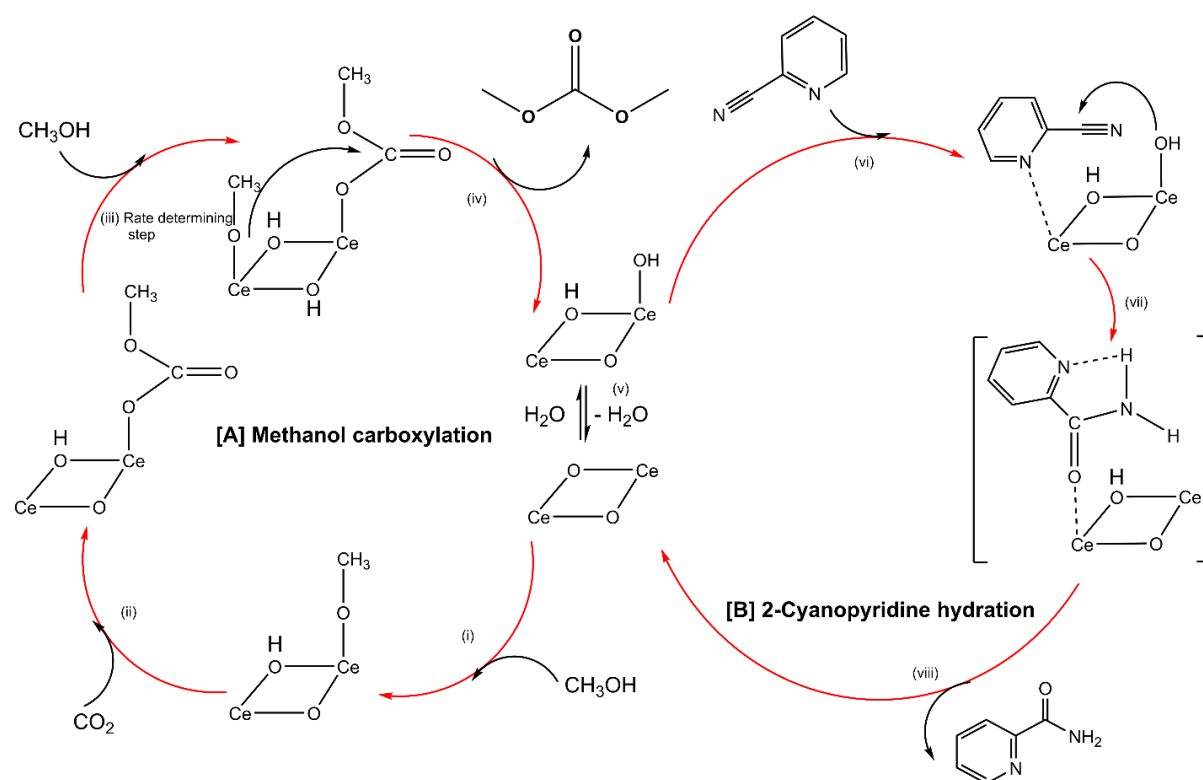


Scheme 1.12. DMC synthesis from CO₂ and methanol in the presence of a dehydrating agent, 2-CP

In addition, the recyclability of the dehydrating agent is confirmed by the dehydration of 2-PA back to 2-CP using a Na₂O/SiO₂ catalyst, which resulted in a conversion around 85% towards 2-CP, and a selectivity of almost 100% for the desired product. The same system (CeO₂ as an active catalyst and 2-CP as a dehydrating agent) has been proven effective for the synthesis of a wide variety of organic carbonates starting from alcohols and carbon dioxide [98] with high or very high alcohol - based yield. Also, direct cyclic carbonate synthesis from CO₂ and diols has been achieved with very good catalytic results [99]. This discovery stays as

1 | Introduction and overview

an extremely solid proof for Le Chatelier's principle (the equilibrium law), underlining the importance of removing the undesired side product(s) (e.g. water) from the reaction mixture to shift the equilibrium towards the formation of the product of interest (e.g. DMC). An in-depth investigation on the use of various nitriles as chemical water traps revealed that the most appropriate compound to be used is the one having a cyano (-CN) group at the 2-position relative to nitrogen (N) atom of the 6-membered ring hetero-aromatic compounds. Another important aspect is that due to an intramolecular hydrogen bonding - between the H atom in the amide group and N atom in the pyridine ring (that results in a reduction in the acidity of the amide, so weakening the adsorption forces to CeO₂ surface) - the amide can easily desorb from the surface and avoid the poisoning of the active sites. The proposed reaction mechanism for DMC synthesis [A] along with the nitrile hydrolysis [B] is carefully described in **Scheme 1.13** [98].



Scheme 1.13. Methanol carboxylation (A) and nitrile hydrolysis (B) over ceria based materials

Various metal oxide catalysts or acidic zeolites (SiO₂, Al₂O₃, TiO₂, H-ZSM5, H-USY, H-MOR, ZnO, MoO₃, and Bi₂O₃) have also been studied in the heterogeneous carboxylation reaction of methanol to produce DMC. In those cases, it was obtained only some dimethyl ether (DME) – for alumina, titania, and the acidic zeolites – and the DMC formation was not observed at all [53, 77]. Other oxides remained completely inactive: MgO, Y₂O₃, HfO₂, La₂O₃, Pr₂O₃, Ga₂O₃, GeO₂, In₂O₃, and Sb₂O₃ [77, 83]. Besides ZrO₂, CeO₂, and V₂O₅, only one metal oxide was reported to produce DMC from CO₂ and methanol namely the stannic oxide, SnO₂.

Nonetheless, the amount of carbonate formed by the latter is not comparable with the one obtained using ceria or zirconia [100, 101].

1.3 Aim and overview of the thesis

The aim of the present thesis is to bring the dimethyl carbonate (DMC) synthesis via methanol carboxylation reaction to a better level of knowledge and understanding. The principal objective of the project is to find a catalytic system capable to perform the DMC synthesis in a continuous manner by direct transformation of CO₂ over heterogeneous catalysts (which represent an eco-friendly and economic alternative to homogeneous counterparts), while taking advantage of the high-pressure approach. With this purpose, various acid-base bi-functional catalyst materials will be subjected to testing in reaction systems with different design (batch or continuous configuration). Ultimately, the goal is to be able to circumvent the thermodynamic limitations and to make the direct DMC synthesis more enticing and relevant for the chemical industry of today. Special emphasis will be given to study the stability / lifetime of the catalysts, and to the use of some *in situ* / *operando* spectroscopic characterization tools (e.g. IR, Raman, Xanes) to get a better grasp over the mechanistic aspects associated with the formation of DMC from CO₂ and methanol.

Chapter 2 describes in detail the materials, methods, and systems that have been used for the present research project. Remarkable attention is given to the high-pressure laboratory scale micro-reactor setup for the continuous catalytic CO₂ conversion to organic carbonates using an appropriate organic dehydrating agent, and the corresponding analytical system.

Chapter 3 presents some preliminary attempts for the DMC synthesis. Outstanding results were obtained once the appropriate dehydrating agent (2-cyanopyridine, 2-CP) was employed in the continuous DMC formation over CeO₂ materials. Further on, this chapter continues with unravelling the mechanism of catalyst de- and re-activation, study that was made possible by using an optically transparent fused quartz tubular reactor (allowing visual and spectroscopic investigation).

Chapter 4 deals with the impact of the rare-earth metal (La, Pr, Gd) promoters on CeO₂ in the long term continuous DMC synthesis from CO₂ and methanol in the presence of a dehydrating agent. Thorough investigation of the catalyst materials and their physical-chemical properties will provide good leads on how the acidity, basicity, and surface reducibility of CeO₂ materials affect the catalytic activity and long-term stability of CeO₂ based catalysts.

Chapter 5 shows some discoveries made from the *in situ* / *operando* spectroscopic studies (DRIFTS, Raman, Xanes, and MS) on DMC synthesis. The possible reduction of Ce in CeO₂, from 4+ to 3+ oxidation state, is discussed. Also, some mechanistic aspects (dealing with the

1 | Introduction and overview

possible existence of a transient species uncovered by using sensitivity enhancement and dynamic behavior analysis) will be addressed. The importance of multivariate curve resolution (MCR) as a very powerful blind source and spectral separation method will be highly acknowledged.

Chapter 6 concludes the thesis by summarizing the most relevant results and offering a brief outlook on the catalytic CO₂ conversion to organic carbonates.

Bibliography

- [1] <http://www.nasa.gov/>
- [2] International Energy Agency, *Key World Energy Statistics 2015*, (2015).
- [3] U.S. Energy Information Administration, *Annual Energy Outlook 2012 (with projections to 2035)*, (2012).
- [4] International Energy Agency, *WORLD ENERGY OUTLOOK 2014 FACTSHEET* (2014).
- [5] <http://www.ipcc.ch/>, (2014).
- [6] <http://www.climatechange2013.org/>, (2013).
- [7] J. Hansen, M. Sato, P. Kharecha, D. Beerling, R. Berner, V. Masson-Delmotte, M. Pagani, M. Raymo, D.L. Royer, J.C. Zachos, *TOASCJ*, 2 (2008) 217-231.
- [8] T. Oda, S. Maksyutov, *Atmos. Chem. Phys.*, 11 (2011) 543-556.
- [9] NRC, *America's Climate Choices: Final Report.*, The National Academies Press, Washington, DC, USA, 2011.
- [10] P. Friedlingstein, R.A. Houghton, G. Marland, J. Hackler, T.A. Boden, T.J. Conway, J.G. Canadell, M.R. Raupach, P. Ciais, C. Le Quéré, *Nat. Geosci.*, 3 (2010) 811–812.
- [11] T.M. Gerlach, *Eos, Trans. Amer. Geophys. Union*, 92 (2011) 201-202.
- [12] Kirk-Othmer – *Encyclopedia of Chemical Technology*, 4th ed., John Wiley and Sons, Inc. - vol.5, p.451995.
- [13] H. Babad, A.G. Zeiler, *Chem. Rev.*, 73 (1973) 75–91.
- [14] H.S. Kim, J.J. Kim, H.N. Kwon, M.J. Chung, B.G. Lee, H.G. Jang, *J. Catal.*, 205 (2002) 226–229.
- [15] H. Yasuda, L.-N. He, T. Sakakura, *J. Catal.*, 209 (2002) 547–550.
- [16] W.J. Kruper, D.V. Dellar, *J. Org. Chem.*, 60 (1995) 725-727.
- [17] X.-B. Lu, X.-J. Feng, R. He, *Appl. Catal. A-Gen.*, 234 (2002) 25–33.
- [18] M. Yoshida, M. Ihara, *Chem. Eur. J.*, 10 (2004) 2886-2893.
- [19] Y.M. Shen, W.L. Duan, M. Shi, *Eur. J. Org. Chem.*, (2004) 3080-3089.
- [20] N. Kihara, N. Hara, T. Endo, *J. Org. Chem.*, 58 (1993) 6198-6202.
- [21] G. Rokicki, W. Kuran, *B. Chem. Soc. Jpn.*, 57 (1984) 1662-1666.
- [22] R. Nomura, A. Ninagawa, H. Matsuda, *J. Org. Chem.*, 45 (1980) 3735-3738.
- [23] T. Yano, H. Matsui, T. Koike, H. Ishiguro, H. Rujihara, M. Yoshihara, T. Maeshima, *Chem. Commun.*, (1997) 1129-1130.
- [24] K. Yamaguchi, K. Ebitani, T. Yoshida, H. Yoshida, K. Kaneda, *J. Am. Chem. Soc.*, 121 (1999) 4526-4527.
- [25] T. Aida, S. Inoue, *J. Am. Chem. Soc.*, 105 (1983) 1304-1309.
- [26] Y.M. Shen, W.L. Duan, M. Shi, *Adv. Synth. Catal.*, 345 (2003) 337-340.

1 | Introduction and overview

- [27] Y.M. Shen, W.L. Duan, M. Shi, *J. Org. Chem.*, 68 (2003) 6705.
- [28] K. Kasuga, S. Nagao, T. Fukumoto, M. Handa, *Polyhedron*, 15 (1996) 69–72.
- [29] H. Yasuda, L. He, T. Sakakura, C. Hu, *J. Catal.*, 233 (2005) 119–122.
- [30] J.-L. Wang, J.-Q. Wang, L.-N. He, X.-Y. Dou, F. Wu, *Green Chem.*, 10 (2008) 1218–1223.
- [31] D. Xiang, X. Liu, J. Sun, F.-S. Xiao, J. Sun, *Catal. Today*, 148 (2009).
- [32] J. Sun, S.-i. Fujita, B.M. Bhanage, M. Arai, *Catal. Commun.*, 5 (2004) 83–87.
- [33] J. Sun, S.-i. Fujita, B.M. Bhanage, M. Arai, *Catal. Today*, 93–95 (2004) 383–388.
- [34] X. Xiaoding, J.A. Moulijn, *Energ. Fuel.*, 10 (1996) 305–325.
- [35] M. Aresta, I. Tommasi, *Energ. Convers. Manage.*, 38, Supplement (1997) S373–S378.
- [36] N. Keller, G. Rebmann, V. Keller, *J. Mol. Catal. A-Chem.*, 317 (2010) 1–18.
- [37] D. Delledonne, F. Rivetti, U. Romano, *Appl. Catal. A-Gen.*, 221 (2001) 241–251.
- [38] Y. Ono, *Appl. Catal. A-Gen.*, 155 (1997) 133–166.
- [39] M. Aresta, E. Quaranta, *ChemTech*, 27 (1997) 32–40.
- [40] A.-A.G. Shaikh, S. Sivaram, *Chem. Rev.*, 96 (1996) 951–976.
- [41] S. Budavari, *The Merck Index (Eleventh Edition)*, 11th. ed. 1989.
- [42] P. Tundo, M. Selva, *Accounts. Chem. Res.*, 35 (2002) 706–716.
- [43] D. Delledonne, F. Rivetti, U. Romano, *J. Organomet. Chem.*, 488 (1995) C15–C19.
- [44] N. Miyamoto, H. Ogawa, T. Arima, K. Miyakawa, Improvement of Diesel Combustion and Emissions with addition of various Oxygenated agents to Diesel fuels, (1996) SAE Paper No. 962115.
- [45] N. Miyamoto, H. Ogawa, N. Nurun, K. Obata, T. Arima, Smokeless, Low NO_x, High Thermal Efficiency, and Low Noise Diesel Combustion with Oxygenated Agents as Main Fuel, SAE, (1998) report SAE-980506.
- [46] M.A. Pacheco, C.L. Marshall, *Energ. Fuel.*, 11 (1997) 2–29.
- [47] F. Bertilsson, H.T. Karlsson, *Energ. Convers. Manage.*, 37 (1996) 1733–1739.
- [48] M. Aresta, A. Dibenedetto, *Catal. Today*, 98 (2004) 455–462.
- [49] R. Zevenhoven, S. Eloneva, S. Teir, *Catal. Today*, 115 (2006) 73–79.
- [50] <http://www.highbeam.com>, China's dimethyl carbonate industry enters a sustainable development track.(Fine and Specialty), China Chemical Reporter, China National Chemical Information Centre, 2010.
- [51] U. Romano, R. Tesel, M.M. Mauri, P. Rebora, *Ind. Eng. Chem. Prod. Rd.*, 19 (1980) 396–403.
- [52] T. Sakakura, J.-C. Choi, H. Yasuda, *Chem. Rev.*, 107 (2007) 2365–2387.
- [53] K. Tomishige, Y. Ikeda, T. Sakaihorii, K. Fujimoto, *J. Catal.*, 192 (2000) 355–362.
- [54] U. Romano, F. Rivetti, N.D. Muzio, Process for producing dimethylcarbonate, US4318862 A, Anic S.P.A. - EniChem, 1982.

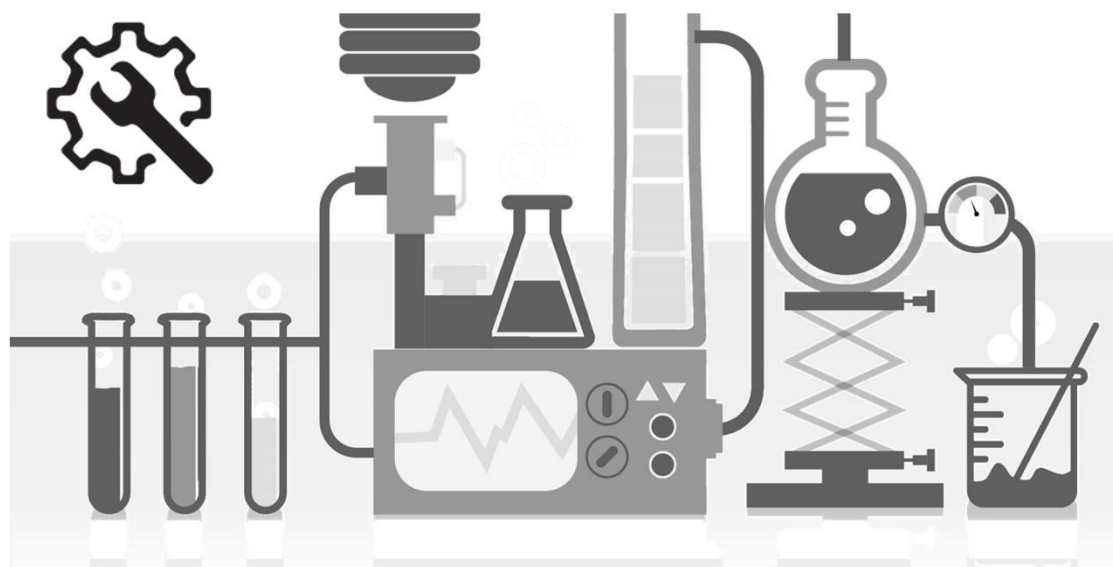
- [55] U. Romano, in: E.P. 365083 (Ed.), EniChem, 1989.
- [56] H.D. Myers, Integrated process for the production of dimethyl carbonate, in: US5183920 (Ed.), Dow Chemical Company, 1993.
- [57] T. Matsuzaki, A. Nakamura, *Catal. Surv. Asia*, 1 (1997) 77-88.
- [58] A.K. Bhattacharya, J.T. Nolan, Cupric methoxychloride catalyst, methanol, carbon monoxide, oxygen, US4636576 A, Texaco Inc., 1987.
- [59] A.K. Bhattacharya, J.T. Nolan, Preparation of organic carbonates, EP0217651 A3, Texaco Development Corporation, 1988.
- [60] A.K. Bhattacharya, Preparation of dimethyl carbonate, US4785130 A, Texaco Inc., 1988.
- [61] A.K. Bhattacharya, Reacting methanol, carbon monoxide and oxygen to produce dimethyl carbonate with a cupric methoxychloride-pyridine compound catalyst, US4761467 A, Texaco Inc., 1988.
- [62] A.K. Bhattacharya, Catalyst for preparation of dimethyl carbonate, US4879266 A, Texaco Inc., 1989.
- [63] M. Aresta, A. Dibenedetto, *Dalton. T.*, (2007) 2975-2992.
- [64] S. Sakai, T. Fujinami, T. Yamada, S. Furusawa, *Nippon Kagaku Kaishi*, 10 (1975) 1789-1794.
- [65] N. Yamazaki, S. Nakahama, F. Higashi, *Rep. Asahi Glass Found. Ind. Technol.*, 33 (1978) 31.
- [66] J. Kizlink, *Collect. Czech. Chem. C.*, 58 (1993) 1399-1402.
- [67] J. Kizlink, I. Pastucha, *Collect. Czech. Chem. C.*, 59 (1994) 2116-2118.
- [68] J. Kizlink, I. Pastucha, *Collect. Czech. Chem. C.*, 60 (1995) 687-692.
- [69] T. Sakakura, Y. Saito, M. Okano, J.-C. Choi, T. Sako, *J. Org. Chem.*, 63 (1998) 7095–7096.
- [70] T. Sakakura, J.-C. Choi, Y. Saito, T. Masuda, T. Sako, T. Oriyama, *J. Org. Chem.*, 64 (1999) 4506–4508.
- [71] G.H. Chu, J.B. Park, M. Cheong, *Inorg. Chim. Acta.*, 307 (2000) 131–133.
- [72] T. Zhao, Y. Han, Y. Sun, *Fuel Process. Technol.*, 62 (2000) 187–194.
- [73] A. Dibenedetto, C. Pastore, M. Aresta, *Catal. Today*, 115 (2006) 88–94.
- [74] M. Aresta, A. Dibenedetto, C. Pastore, I. Papai, G. Schubert, *Top. Catal.*, 40 (2006) 71-81.
- [75] J.-i. Kadokawa, H. Hideyuki, S. Fukamachi, M. Karasu, H. Tagaya, K. Chiba, *J. Chem. Soc. Perk. T. 1*, (1999) 2205-2208.
- [76] S. Fang, K. Fujimoto, *Appl. Catal. A-Gen.*, 142 (1996) L1–L3.
- [77] K. Tomishige, T. Sakaihorii, Y. Ikeda, K. Fujimoto, *Catal. Lett.*, 58 (1999) 225-229.
- [78] S. Xie, A.T. Bell, *Catal. Lett.*, 70 (2000) 137-143.

1 | Introduction and overview

- [79] K.T. Jung, A.T. Bell, *J. Catal.*, 204 (2001) 339–347.
- [80] K.T. Jung, A.T. Bell, *J. Mol. Catal. A-Chem.*, 163 (2000) 27–42.
- [81] K. Pokrovski, K.T. Jung, A.T. Bell, *Langmuir*, 17 (2001) 4297–4303.
- [82] K.T. Jung, A.T. Bell, *Top. Catal.*, 20 (2002) 97–105.
- [83] K. Tomishige, *Curr. Top. Catal.*, 3 (2002) 81 - 101.
- [84] Y. Ikeda, T. Sakai, K. Tomishige, K. Fujimoto, *Catal. Lett.*, 66 (2000) 59–62.
- [85] Y. Ikeda, M. Asadullah, K. Fujimoto, K. Tomishige, *J. Phys. Chem. B*, 105 (2001) 10653–10658.
- [86] K. Tomishige, Y. Furusawa, Y. Ikeda, M. Asadullah, K. Fujimoto, *Catal. Lett.*, 76 (2001) 71–74.
- [87] K. Tomishige, K. Kunimori, *Appl. Catal. A-Gen.*, 237 (2002) 103–109.
- [88] H.J. Hofmann, A. Brandner, P. Claus, *Chem. Eng. Technol.*, 35 (2012) 2140–2146.
- [89] X.L. Wu, M. Xiao, Y.Z. Meng, Y.X. Lu, *J. Mol. Catal. A-Chem.*, 238 (2005) 158–162.
- [90] X.L. Wu, Y.Z. Meng, M. Xiao, Y.X. Lu, *J. Mol. Catal. A-Chem.*, 249 (2006) 93–97.
- [91] Y. Yoshida, Y. Arai, S. Kado, K. Kunimori, K. Tomishige, *Catal. Today*, 115 (2006) 95–101.
- [92] M. Aresta, A. Dibenedetto, C. Pastore, C. Cuocci, B. Aresta, S. Cometa, E.D. Giglio, *Catal. Today*, 137 (2008) 125–131.
- [93] M. Aresta, A. Dibenedetto, C. Pastore, A. Angelini, B. Aresta, I. Pápai, *J. Catal.*, 269 (2010) 44–52.
- [94] H.J. Lee, S. Park, I.K. Song, J.C. Jung, *Catal. Lett.*, 141 (2011) 531–537.
- [95] H.J. Lee, W. Joe, I.K. Song, *Korean J. Chem. Eng.*, 29 (2012) 317–322.
- [96] M. Honda, M. Tamura, Y. Nakagawa, S. Sonehara, K. Suzuki, K.-i. Fujimoto, K. Tomishige, *ChemSusChem*, 6 (2013) 1341–1344.
- [97] M. Tamura, H. Wakasugi, K.-i. Shimizu, A. Satsuma, *Chem. Eur. J.*, 17 (2011) 11428–11431.
- [98] M. Honda, M. Tamura, Y. Nakagawa, K. Nakao, K. Suzuki, K. Tomishige, *J. Catal.*, 318 (2014) 95–107.
- [99] M. Honda, M. Tamura, K. Nakao, K. Suzuki, Y. Nakagawa, K. Tomishige, *ACS Catal.*, 4 (2014) 1893–1896.
- [100] D. Aymes, D. Ballivet-Tkatchenko, K. Jeyalakshmi, L. Saviot, S. Vasireddy, *Catal. Today*, 147 (2009) 62–67.
- [101] D. Ballivet-Tkatchenko, J.H.Z.d. Santos, K. Philippot, S. Vasireddy, *C. R. Chim.*, 14 (2011) 780–785.

2

Materials and methods



2 | Materials and methods

2.1 Catalyst materials

The goal of the preparation of catalytic materials that can be employed at an industrial scale is to obtain a final product with high activity, selectivity, stability and regenerability. In the first chapter (**Introduction**), it was shown that both acid and basic sites are required to activate carbon dioxide (weak acid) and methanol (that can dissociate into either methoxy CH_3O^- or methyl CH_3^+ species depending on the acidity/basicity of the environment) molecules towards dimethyl carbonate formation. The heterogeneous catalysts prepared and used/tested for the present research work are materials, typically oxides and mixed-oxides, displaying both acid-base properties (amphoteric materials). In most of the cases, these materials present Lewis acid-base pair, as for example ZrO_2 , where Zr^{+4} acts as a Lewis acid and can accept a pair of electrons, while O^{-2} is a Lewis base and can donate a pair of electrons. By properly tuning of a metallic oxide with a suitable reagent (e.g. H_3PO_4), the properties of the synthesized material can be easily enhanced and obtain, along with the Lewis acid-base pair, some Brønsted acid sites that are capable of donating protons [1]. As for the synthesis methods, two of the handiest procedures, namely coprecipitation and wetness impregnation have been chosen. For the obtaining of the metal oxide materials (i.e. CeO_2 , ZrO_2 , $\text{CeO}_2\text{-ZrO}_2$, etc.) or hydrotalcites (HTs) the first method has been elected. *N.B.* HTs, also known as layered double hydroxides (LDHs) - represent a family of natural and artificial minerals that have positively charged layers with compensating anions in the interlayer space; for this work some Mg:Al HT and Zn:Al HT with different metal to metal ratio have been synthesized. On the other hand, to prepare the metal supported materials (i.e. precious metals – PM: Rh, Ru, Pt, Pd – on Al_2O_3 , ZrO_2 , CeO_2 , SBA-15 or rare earth metals – REM: La, Gd, Pr – on CeO_2) the wetness impregnation method was preferred.

Coprecipitation (**Figure 2.1 a**) is a widespread synthesis method due to its ability of providing high chemical homogeneity catalyst materials and occurs when two or more solutions are mixed in a suitable, more intimate way. It consists of a simultaneous addition of an aqueous metal(s) solution and a base solution and it is usually done at constant pH, hence the role of the base incorporation. Both pH and the concentration of the mixed metal solution have a crucial effect on the chemical, structural and textural properties of the final catalyst material. Other critical parameters are represented by the temperature, mixing rate (rotation per minute, rpm), the order and rate of addition of one solution into the other, type of solvent used during coprecipitation and the chemical environment (e.g. use of inert atmosphere or not). The duration and type of ageing of the resulted gel (i.e. temperature, mixing rate, time) also present a very high importance. Finally, the as-synthesized solid material is filtered, washed, dried at appropriate temperature and lastly calcined to obtain the desired active phase component.

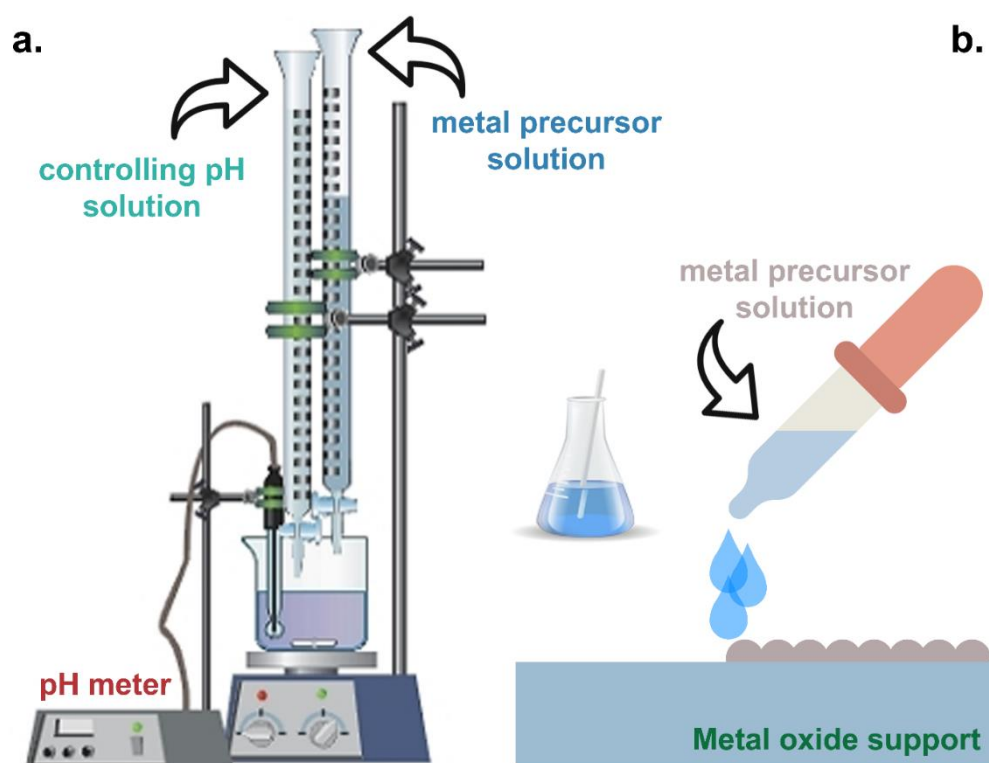


Figure 2.1 a. Schematic representation of coprecipitation method and b. incipient wetness impregnation method

Impregnation (Figure 2.1 b) is the most used preparation technique for the supported metal catalyst systems [2-4]. Many catalysts employed on an industrial scale consist of an active component (or components) deposited on a support (such as e.g. silica, alumina, active carbon). The role of the support may be to improve the properties (e.g. stability) of the active component(s), or to participate directly in the catalytic reaction (e.g. by providing more active sites). The principal catalyst-preparation protocol comprises of two stages. The first step consists of rendering a metal-salt component into a finely divided form on a support (followed by ageing and drying to remove excess solvent). Later, the conversion of the supported metal salt to a metallic or oxide state is reached via calcination or reduction protocols. Given that the impregnation is achieved by filling the pores of the support with a solution of the metal salt precursor, two different synthesis ways depending on the amount of solution used in the first step (dispersion) can be distinguished, namely the incipient wetness or dry impregnation because the volume of the solution containing the precursor does not exceed the pore volume of the support, and wet or soaking method, which involves the use of an excess of solution with respect to the pore volume of the support. Various factors such as type and concentration of precursor salt, solvent, temperature, type of support and contact time with support could be controlled to obtain optimum distribution of active species. The main advantages of the impregnation technique are that is fast and facile, simpler when compared to other more complicated synthesis methods (while it takes less time), and it offers good reproducibility of

2 | Materials and methods

the synthesized materials. Also, good metal dispersion is achieved while there is no loss of material within the support phases.

Commercially available high surface area CeO_2 powder ($>100 \text{ m}^2/\text{g}$) and $\text{CeO}_2\text{-ZrO}_2$ solid solutions (78-22, 50-50, and 25-75 wt%, respectively) were kindly supplied by Daiichi Kigenso Kagaku Kogyo Co. Ltd. (Japan) and used without any further treatment. High surface area ZrO_2 (1/8" pellets) was purchased from Alfa Aesar and used as received.

2.2 Reaction setup for continuous production of DMC

Heterogeneously catalyzed reactions are thoroughly studied under both batch (i.e. autoclaves) and continuous flow (i.e. stainless tube reactors) approaches. Nowadays, the use of continuously operated tubular reactors (and micro-reactors) has gained more and more interest owing to various advantages, such as the swift sample collection, better heat transfer capacities, smaller size (less space required) which leads to higher mixing rates, increased flexibility due to possibility of varying the space time yield. For most of the industry applications continuous flow operation saves time, energy and costs (if it is correctly and efficiently implemented).

For the initial catalyst screening and the assessment of reaction parameters, several systems (both batch and continuous configuration) have been tested in the direct DMC synthesis starting from CO_2 and methanol. Since the reaction is thermodynamically limited and the equilibrium conversion is lower than 1% even at high pressure conditions, thorough investigation of the important reaction parameters (i.e. type of material, amount of catalyst/particle size, temperature, pressure, space velocity, CO_2 to methanol ratio, etc.) is required to set better grounds and clear boundaries for the DMC process. Several different types of reaction setups were tested for this process and the main components of each reaction setup are briefly described in the following section with special emphasis given to the continuous – in-house built – high pressure setup.

2. 2. 1 Preliminary studies

2. 2. 1. 1 Microactivity Reference catalytic system

The **Microactivity-Reference** (PID Eng&Tech) unit is an automated and computer-controlled laboratory reactor for catalytic testing. A schematic of the reaction setup is presented in **Figure 2.2**. The reaction system consists of a tubular stainless steel (SS, internal diameter of 9 mm and length 305 mm) reactor (by Autoclave Engineers) equipped with a 2 μm porous plate where the catalyst is placed. The flow through the reactor is up-down, thereby the reactant mixture is fed through the upper part of the reactor and the reaction products are obtained at the lower part. The gas manifold allows the introduction of up to 6 different gases at a time (by means of a system of mass flow controllers from Bronkhorst). For the methanol carboxylation reaction, only the high pressure (max working pressure of 60 bar) CO_2 line was used. At the same time, one liquid component can be added to the system. It permitted to feed a known amount of methanol to the reactor. For this Microactivity setup the liquid delivery system was not dosed using a typical high pressure liquid pump (HPLC, GILSON, INC). Instead, the liquid was introduced by means of a MFC for liquids (properly calibrated for methanol) from Bronkhorst. This creates a certain disadvantage as it requires the use of a “pushing gas” (helium, high pressure) on one side and, on the other side, one carrier gas (helium, high pressure) to retrieve and carry the liquid once it comes out of the MFC. The problem here is that even when working at low methanol flows (e.g. 0 – 5 ml min^{-1}) it requires rather large values for the carrier gas (e.g. He carrier from 50 – 100 ml min^{-1}) to reach stable flows. Finally, this contributes to an increased total flow through the reactor (add CO_2 flow to the previous example). This implies certain limitations in the screening process risen from “imposed” values for the gas hourly space velocity ($\text{GHSV} = \text{reactant gas flow rate}/\text{reactor or catalyst volume}$, indicating how many reactor volumes of feed can be treated in a unit time).

Just before entering the reactor, the liquid methanol is passing through a controlled evaporator mixer (a mixing chamber for liquid and carrier gas with heat exchanger which ensures complete evaporation of the liquid). Further on, the liquid and gaseous flows are introduced into the hot box system (a temperature controlled closed space where the reactor is located – max temperatures of 160 $^\circ\text{C}$ to 180 $^\circ\text{C}$, to avoid possible condensation in the system). Once the gases have been preheated and liquids evaporated, these streams merge and flow to a 6-port valve, and later it can either go towards the reactor or by-passing it. At the outlet of the reactor a Peltier cell (cooling system \rightarrow liquid-gas separator) will ensure the proper separation of the liquid products from the gaseous ones. The gas phase products will move forward via the heated transfer line (ca. 150 $^\circ\text{C}$) until reaching the analytical system – gas chromatograph equipped with both flame ionic detector (FID) and thermal conductivity detector (TCD) for proper identification and analysis of the products. All the experiment

2 | Materials and methods

scheduling and analysis part is PC controlled via a very flexible and user-friendly graphical user interface (GUI).

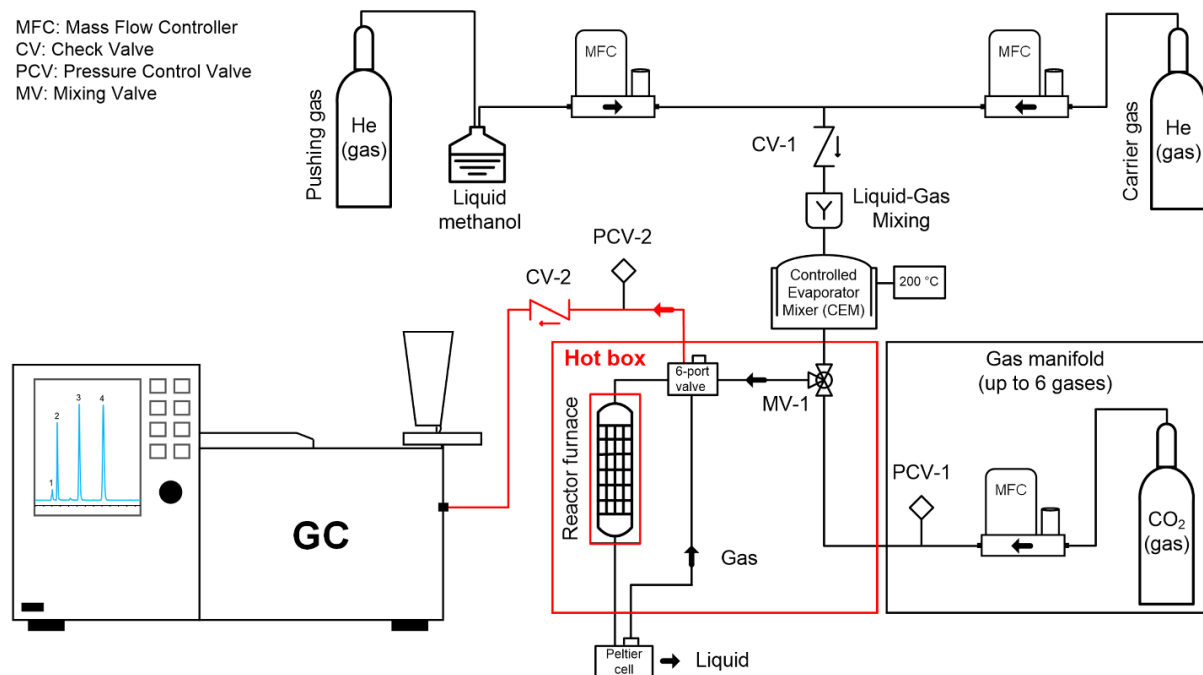


Figure 2.2 Schematics of high pressure Microactivity Reference reactor setup

2. 2. 1. 2 Low pressure setup

A simple **low-pressure** home-made continuous methanol carboxylation reactor system was designed and built (Figure 2.3). It consists of a quartz reactor (placed inside of a temperature controlled oven) having a 3 μm porous plate at the middle position of tube on which the catalyst was placed. The flow through the reactor is up-down, thereby the reactant mixture is fed through the upper part of the reactor and the reaction products are obtained through the lower part. The gas manifold allows the introduction of up to 3 different gases at a time (by means of a system of mass flow controllers from Alicat Scientific), namely CO_2 , an inert carrier gas (helium) that is passing through a glass saturator filled with liquid methanol (the inside of the saturator contains some glass Raschig rings for better interaction between liquid and gas or vapors), and air for catalyst pre-treatment (calcination) before the reaction. To control the methanol vapor pressure (thereby the amount of methanol added to the reaction) the glass saturator was placed in a cooling (liquid nitrogen based) / hot (oil) bath. The product identification and analysis was done using a gas chromatograph equipped with and FID detector and a mass spectrometer (if product identification is required).

Reaction setup for continuous production of DMC

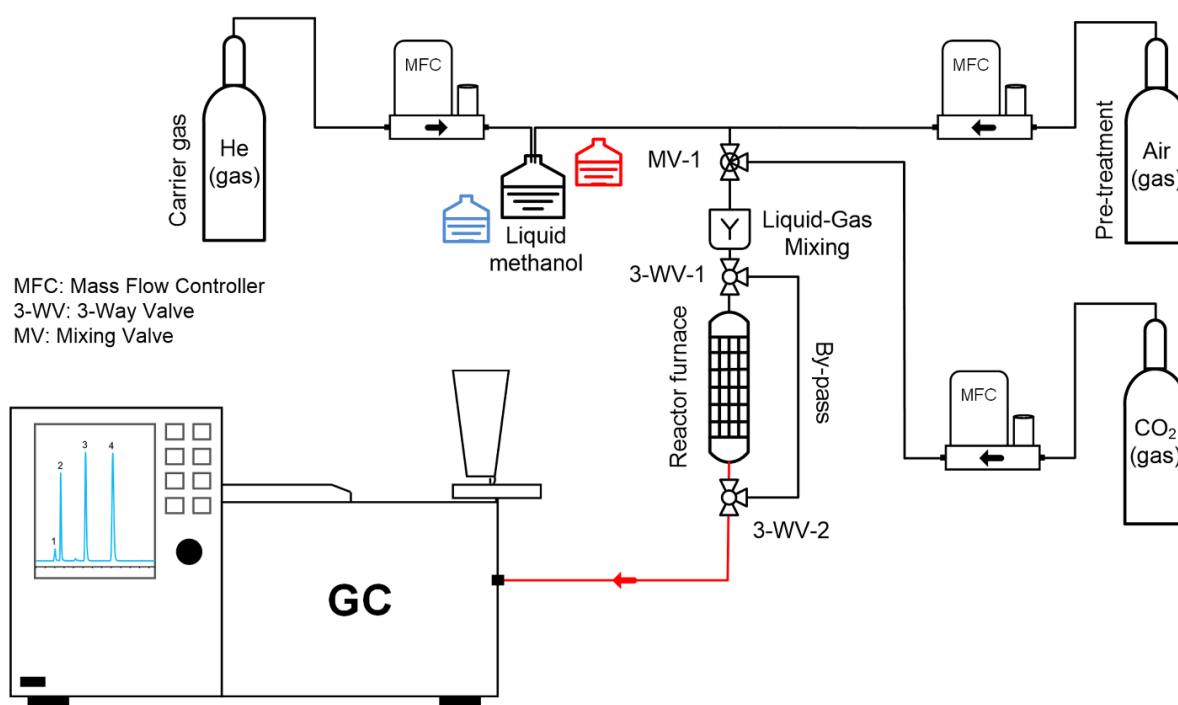


Figure 2.3 Representation of the low pressure (home-made) methanol carboxylation reaction system. Methanol concentration is changed by varying its vapor pressure (i.e. glass saturator temperature). Black = room temperature (ca. 25 °C), blue = ice-salt cold bath (0 °C), and red = oil bath (for higher temperature)

2. 2. 1. 3 AMTECH SPR16

Apart from the typical batch reactors (autoclaves), the automated slurry phase reactor system **AMTECH SPR16** (Advanced Machinery & Technology Chemnitz GmbH) was used for efficient screening of both catalytic materials and reaction conditions (i.e. rapid process optimization). The system comprised of 16 independently operable batch (stainless steel, 15 ml volume) reactors as shown in **Figure 2.4**. The process parameters such as, temperature (up to 220 °C), pressure (up to 150 bar) and stirrers (from 0 to 2000 rotations per minute, rpm) were individually adjustable. The SPR16 can be employed to investigate sixteen materials at common conditions or one material under sixteen different conditions.

In a typical experiment, the catalysts were placed in the respective autoclaves, the lines were purged with inert gas and the system was subjected to the pressure test. After successful pressure testing, the liquid methanol is injected at the top part of the reactor (aided by a transfer line) and the reaction can be started. A pressure sensor is used in combination with a MFC to supply CO₂ and to control the pressure inside the reactors. All the experiment scheduling and analysis part was PC controlled via a very flexible and user-friendly graphical user interface (GUI).

2 | Materials and methods



Figure 2.4 AMTECH SPR16 slurry phase reactor for high throughput experimentation

2. 2. 2 High-pressure (50 bar) methanol carboxylation reactor setup

2. 2. 2. 1 Reactor system

The schematic representation of the high-pressure reactor setup (aiming at following the chemistry presented in **Scheme 1.12**) constructed and used in this work for studying the direct DMC synthesis from CO_2 and methanol (up to 50 bar) is shown in **Figure 2.5**. A real-life representation of the reactor setup is shown in **Appendix B, Figure 7.2**. As depicted, a high pressure thermal mass flow controller (Bronkhorst) was used to flow high purity CO_2 (>99.9993%) gas (purchased from Abelló Linde, Spain). Just before the mass flow controller a stainless-steel container (extra volume 300 ml) was placed. The idea behind this extra volume was to prevent the small fluctuations, ensuring stable CO_2 flow. The liquid (methanol HPLC grade or methanol + 2-cyanopyridine mixture, both >99% purity, Sigma Aldrich, Spain) delivery system consists of a HPLC pump, model PU-2080 Plus (Jasco, Japan).

Reaction setup for continuous production of DMC

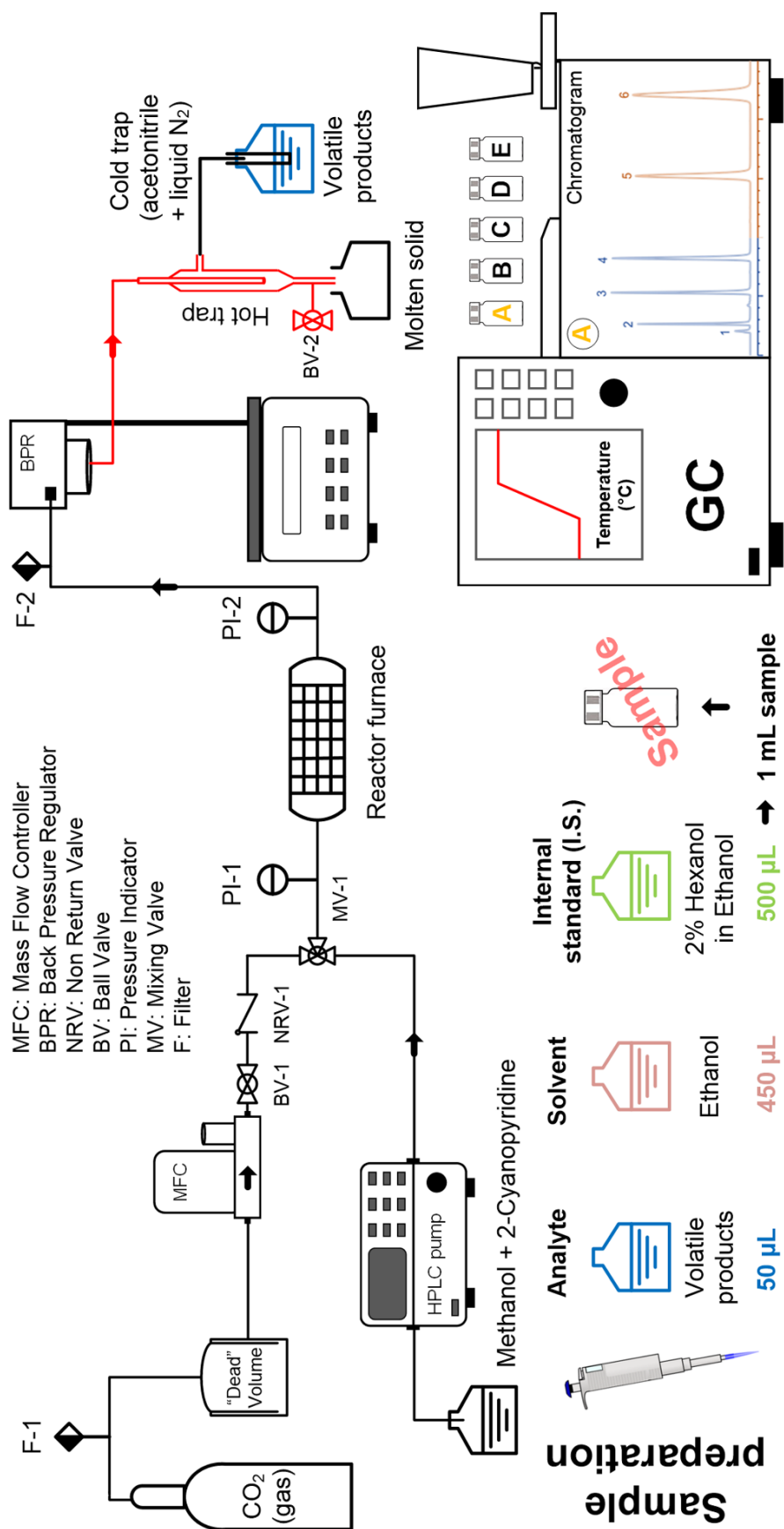


Figure 2.5 Schematic process flow diagram of the reaction system for the continuous production of DMC (lower panel: sample preparation and gas chromatograph)

2 | Materials and methods

A non-return valve was connected in between the CO₂ mass flow controller and the mixing valve (MV-1) to ensure one directional flow. The micro-reactor system consists of a 1/8" stainless steel tube (Swagelok) with an inner diameter (ID) of 1.75 mm and ca. 20 cm in length mounted horizontally, as shown in **Figure 2.6** together with the heating system. For the *in situ* / *operando* studies 3 mm fused quartz reactor (ID: 2 mm) was used (Technical Glass Products, Inc. USA). The heating system consists of two aluminium bodies having length of ca. 15 cm. A groove in the bottom of the aluminium body was machined to embed the reactor tube in it. Another L shaped groove, touching the reactor tube one was made for thermocouple (Type K, Watlow) embedment. Two resistive heating cartridge with capacity of 150 W were inserted into the bottom body. The temperature control was achieved by a PID controller from Jumo (Imago 500 Multichannel Process Controller and Program Controller). The heating assembly was covered with ceramic insulation material and the ceramic insulation was wrapped in aluminium foil.

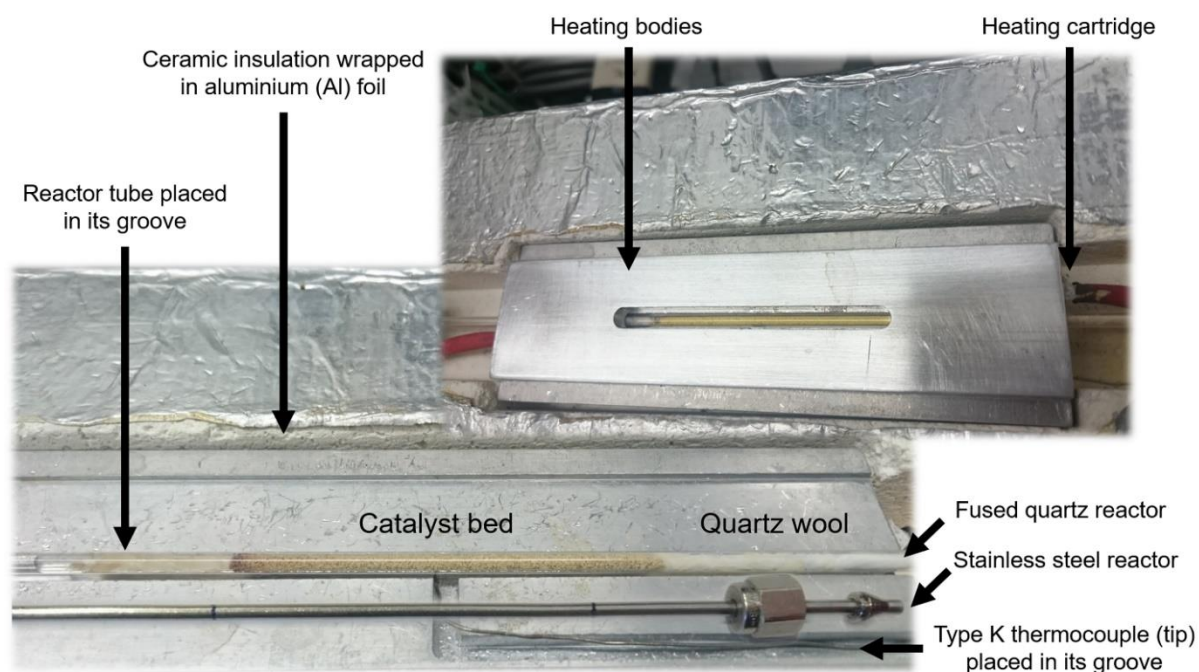


Figure 2.6 Reactor tube (both SS and fused quartz, for comparison purpose) with heating system and insulation

The pressure in the reactor system was maintained and controlled with a back-pressure regulator (BPR), model BP-2080 Plus (Jasco, Japan). One of its most important feature is very small dead volume (10 μ L or less). An inline 10 μ m filter frit F-2 was placed in the 1/8" fittings after the reactor tube to prevent the catalyst particles entering into back pressure regulator. Initially, all the transfer lines and components after the reactor were heated at 180 $^{\circ}$ C to avoid solid formation. Further on, the product stream coming out of the back-pressure regulator flows through the in-house built separation system. Moreover, given the very delicate and

challenging chemistry (**Scheme 1.12**), in this specific reactor system configuration the BPR was also used as a pressure measurement tool. This was achieved by removing the pressure indicator located at the inlet of the BPR and placing it at the inlet of the stainless-steel reactor (complete and detailed explanation in the following section, **Separation system**).

2.2.2.2 Separation system

Studies involving organic dehydrating agents have been performed in high pressure batch reactor setup. It is of great interest to implement the approach of using dehydrating agents in continuous flow processes due to obvious advantages. It is expected that the reaction time will be significantly reduced (as compared to a batch process), thereby avoiding (diminishing) the by-product formation that would reduce the desired product yield. Using the organic dehydrating agent (2-cyanopyridine, 2-CP) in a flow system was found to be a very challenging task due to the formation of high melting point products such as 2-picolinamide (2-PA). **Table 2.1** presents extended information about all the compounds involved in the process.

Table 2.1 Hot trap / cold trap separation system (r.t. = room temperature) [5]

Number	Compound	Melting point / °C	Boiling point / °C
Hot trap (2-cyanopyridine – [heavier] – derived products)			
1	2-Cyanopyridine	24-27	212-215
2	2-Picolinamide	110	284.1
Cold trap (methanol – [lighter] – derived products)			
3	Methanol	-98	64.7
4	Dimethyl carbonate	2-4	90
5	Methyl carbamate	56-58	176-177
6	Methyl picolinate	liquid / r.t.	95 / 1 mmHg
7	<i>Methyl nicotinate</i>	42-44	204
8	<i>Methyl isonicotinate</i>	8-8.5	207-209
9	<i>Ethyl-2-picolinate</i>	2	240-241
10	n-Octane	-57	125-127

2-PA is the hydrolysis product of 2-CP and is solid at room temperature and atmospheric pressure (**Table 2.1**). To avoid the clogging of reaction system due to the solid formation all the components after the reactor were heated at temperature high enough to melt the formed solid. The proper heating of the back-pressure regulator (for increased functionality) was of tremendous importance, and a modification to the BPR was made to allow sufficient heating

2 | Materials and methods

at the position where the fluid passed through. In consequence, the pressure sensor has been re-positioned as mentioned in the earlier section.

The reaction products (along with the reactants) for the continuous DMC production using 2-cyanopyridine as a dehydrating agent are divided into two categories (**Table 2.1**, entries 7-9 – presenting similar chemical structures – are shown as supporting information), namely the ones originating from 2-cyanopyridine (unreacted 2-cyanopyridine and 2-picolinamide) having high melting (2-picolinamide) and boiling points, and the methanol derived ones (unreacted methanol, dimethyl carbonate, methyl carbamate, and methyl picolinate) having lower melting and boiling points. Moreover, the significant difference in melting and boiling points of the reactants and products led to another major challenge, i.e. obtaining the reaction products in suitable and well separated forms, ready for the analytical system. Using our very innovative home-made hot trap – cold trap system, the separation of methanol derived products was achieved by maintaining the hot trap at 180 °C where high boiling compounds such as 2-cyanopyridine and 2-picolinamide were trapped (discharging of the heavy products is done by opening of the BV-2). Following the hot trap, the outlet stream (gas phase) was passed to a U-shaped glass condenser maintained at ca. -40 °C by means of an acetonitrile and liquid N₂ cooling bath. Later, the liquid is collected, filtered and stored in the freezer.

2.2.2.3 Reaction protocol

Prior to starting the reaction, the CO₂ mass flow controller was properly calibrated using a volumetric flow meter (e.g. Agilent ADM 2000). This operation was usually repeated once per month to ensure the proper functioning of the MFC. The dehydrating agent, 2-cyanopyridine, was dissolved in methanol at the desired molar ratio (most of the cases the stoichiometric molar ratio, 2-cyanopyridine to methanol = 1:2). The liquid mixture was always kept in the fridge to avoid any change in composition (unless in use). For catalytic activity tests, the catalyst was loaded inside a 1/8" tube having inner diameter of 1.75 mm (and outer diameter of 3.17 mm). Beforehand, the catalyst powder was pelletized with ca. 4-5 tons of pressure to form a pellet of 1.6 cm in diameter and 2-3 mm thickness (depending on the exact amount of powder catalyst and the type of material used). The pellet was then broken using mortar and pestle into smaller particles and sieved to particle size of 200-300 μm. As it depends a lot on its density, the required amount of catalyst was always carefully weighed. **Figure 2.7** depicts how the placement of the catalyst inside the reactor tube looks like. Before charging the catalyst into the reactor tube, a small piece of SS hollow tube having length of ca. 3-4 cm was inserted from the bottom of reactor tube. This tube acts as a support for catalyst inside the reactor tube and prevents the moving of catalyst bed caused by pressure / flow. This hollow tube was bent at different positions (against the reactor's walls), so that it was held inside the reactor under pressurized condition. A small portion of this tube was left outside of the reactor

to allow the easy withdrawal after the reaction. Above this support tube, quartz wool was inserted carefully to form a packed bed of length ca. 4-5 mm. The catalyst particles were then poured inside the tube while tapping the reactor tube to ensure uniform distribution of particles inside the tube. The catalyst bed length could be anywhere between 2-14 cm depending on the material and the studied space time. To ease the removal of the catalyst after the reaction, the reactor tube above the catalyst bed was kept empty. Afterwards, the reactor tube was placed inside the furnace and was connected to the system using 1/8" compression fittings.

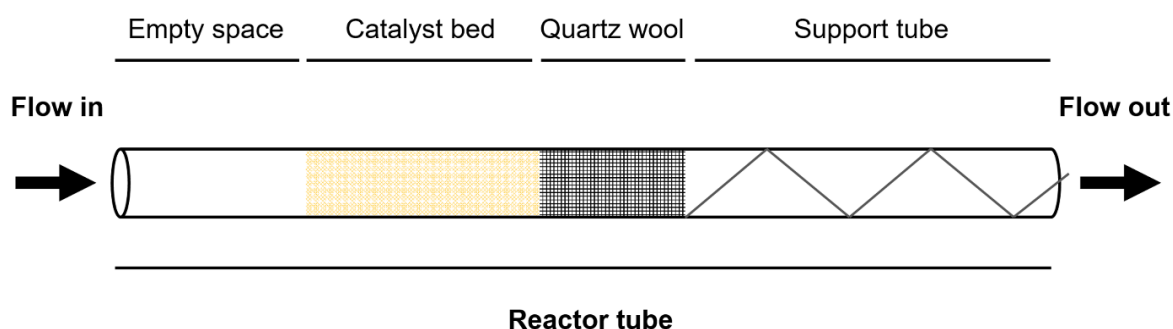


Figure 2.7 Catalyst placement inside the reactor tube

To begin with, the reactor was pressurized under CO₂ flow to the desired reaction pressure and then required flow rates of CO₂ and methanol+2-cyanopyridine mixture were passed over the catalyst bed. Feed stabilization takes ca. 2-2.5 h and it also represents the time required for the liquid stream to travel the whole system under reaction conditions. The moment that methanol was observed at the outlet of the hot trap coincides with the moment that the first sample is taken. The long time span to reach the system stabilization was attributed to the very low reactant flow rate at high pressure conditions. Unless mentioned otherwise, the time for collecting one sample was ca. 2 h.

2. 2. 2. 4 Analytical system

After the liquid sample was collected (2 h sampling time is long enough to collect the desired amount of liquid at the cold trap glass condenser) the product analysis and identification was performed by GC-MS (Scion 436-GC, Bruker) using ethanol as solvent and 1-hexanol as a GC internal standard. Additionally, n-octane was introduced in the reactant stream as an internal standard to minimize the errors in quantification of the products due to evaporation and condensation. **Figure 2.5** carefully describes the adequate sample preparation protocol used in the present work. 50 μ L liquid sample (analyte) from the glass condenser was mixed with 450 μ L ethanol (solvent) and 500 μ L 2% 1-hexanol in ethanol solution (1-hexanol was the internal standard). The as prepared sample (suitable for analysis, in 1.5 mL GC vial provided with septum) was then loaded into the GC-MS sample rack.

2 | Materials and methods

Injections were aided by the automated robotic arm (auto sampler) equipped with a 10 μL syringe for liquids (injection volume was 1 μL).

The GC-FID channel was equipped with an BR-Swax capillary column (length 30 m, ID 0.32 mm, film thickness 1.0 μm , Cat #: BR89346, Serial #: 1142258). Helium was used as a carrier gas. The injector of FID channel was operated in split mode with split ratio of 1:200. The column oven was kept at constant temperature of 45 $^{\circ}\text{C}$ for 3 min to allow better separation of the lighter components, followed by increasing the oven temperature to 200 $^{\circ}\text{C}$ at the rate of 10 $^{\circ}\text{C}/\text{min}$ and it was held 14 min to ensure complete removal of all the heavier components. The total analysis time was 32.50 min. For the data acquisition and analysis, MS Workstation 8 software was used. To determine the response factor and retention time in GC analysis, the following commercially available reagents from Sigma Aldrich were used: methanol (HPLC grade), dimethyl carbonate (99%), methyl picolinate (99%) and methyl carbamate (98%). The calibration of all detected components was carried out by using external standard method. Liquid mixtures of known composition were injected to generate a calibration curve (usually a 5-points calibration curve). Data treatment was performed using Microsoft Excel or OriginLab 9.0 software. As in the case of the reaction samples, for the calibration curves each injection was repeated at least three times for reproducibility purposes. Herein only the products directly or indirectly originated from methanol above the trace level were quantified and discussed; hence the product selectivity was calculated based on methanol.

2. 2. 2. 5 Maintenance and troubleshooting

Aside from offering numerous advantages, the high-pressure setup presented in the [section 2. 2. 2.](#) came with some major technical difficulties that we had to learn how to overcome. Mostly, back pressure regulator related problems were generated by the continuous usage under harsh reaction conditions (formation of very high melting and boiling point compounds led to implementation of the high-temperature hot trap, see [section 2. 2. 2. 2 Separation system](#)). Despite being a reliable and extremely precise laboratory equipment, the Jasco back pressure regulator is especially designed for being used with gases and/or supercritical fluids (for complete functionality, the BPR is equipped with a heating jacket that provides a maximum working temperature of 80 $^{\circ}\text{C}$). Long time exposure to high temperatures (> 180 $^{\circ}\text{C}$) and to a series of chemical compounds that do not comply with the equipment's compatibility led to the appearance of certain problems with a rigorous periodicity. [Figure 2.8](#) shows a typical cross section view of the back-pressure regulator used in this work. To control the pressure inside the system, a valve rod oscillates repeatedly to open and close the valve (the system is composed of: valve rod, needle valve **1**, seal **2** and seat **3**). The pressure is maintained by changing the time interval of needle oscillation. The common problems encountered while performing continuous DMC synthesis in the high-pressure setup relates

to the operation of above mentioned components. Thus, back pressure regulator might not be able to perform the important functions such as closing or opening the valve completely. To summarize, the major issues and the attempts to tackle them were represented by:

- Stainless steel needle valve (**1**). The needle was often getting contaminated/dirty when small dust/catalyst particles deposited on its polished surface. It was observed that the tip of needle may also get deformed (slightly bent) over the time. Attempts have been made to micro-polish the needle but, despite of re-gaining the initial aspect (visually), finally it had to be replaced.
- Teflon sealing (**2**) is by far the most delicate and malleable of all the spares. It was observed that with increasing the time of use the seal was clearly getting deformed and the needle hole became larger. Replacing it was the only workaround.
- Polyether ether ketone (PEEK) seat (**3**) was also prone to getting contaminated. The visible color change (seat is getting darker) could be removed by polishing it with very fine sand paper. Nevertheless, this did not provide proper functioning and the seat had to be replaced.
- Metallic valve rod is the part that holds the system together. Sometimes, due to long term use (thereby long time exposure to high temperatures), it was getting blocked, resulting in malfunctioning of the equipment. Therefore, it had to be completely taken out and thoroughly cleaned for proper functioning (e.g. small dust particles, hardened grease, etc.).

Other actions that helped us to keep the system in a proper shape for longer periods of time include: i) thorough washing with methanol in between the catalytic tests → to maintain the system clean (long-term flush with methanol at temperature from 30-150 °C with or without applying pressure), ii) the use of porous frit after the reactor (just before BPR inlet, to prevent the solid particles from going in) helped in certain cases, but it did not represent a critical point in the present case, and maybe the most important point iii) proper optimization of the hot-trap temperature is required (the lower the temperature, the better. Nevertheless, chemistry is dictating!). Since at the beginning the hot trap was constructed by simply wrapping it in heating wire, introducing the hot-trap in a home-made temperature-controlled oven helped to reduce the temperature @ BPR ^{inlet/outlet} (from 180-200 to 130-140 °C). This action had significant consequences over the back-pressure regulator lifetime, offering the possibility of working under proper conditions for longer time. Besides, a ventilation system (cooling) for the solenoid (i.e. controlling the movement of the needle valve) was added. However, when (if) something was too damaged to be re-used (after repairing attempt), it would likely be replaced by new spares.

2 | Materials and methods

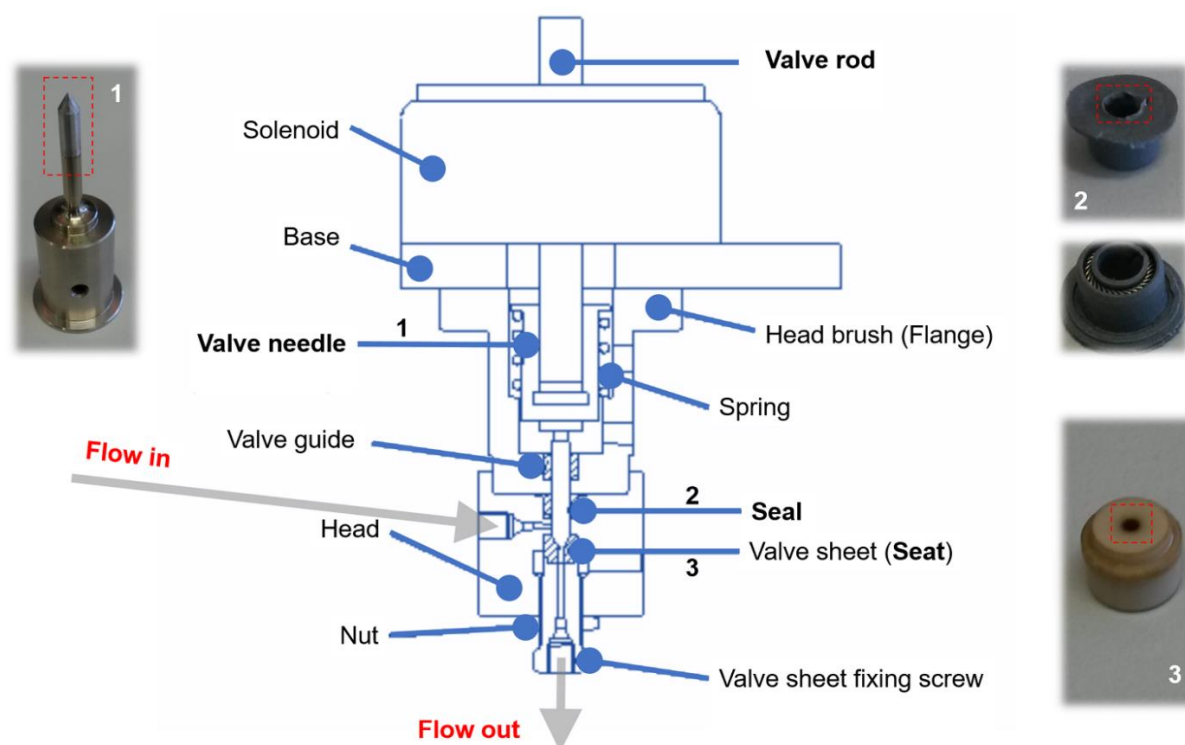


Figure 2.8 Cross section view of the Jasco back pressure regulator (BPR)

2.3 *In situ* studies

Better understanding of physical and chemical processes, with both fundamental and industrial relevance, represents one of the most challenging task in today's "research world". The use of *in situ* experimental techniques has gained more and more attention over the last couple of decades, providing a useful tool for studying heterogeneous catalysts and reaction mechanisms [6]. Gaining advantages of sophisticated techniques enabled the rational development of catalytic systems. It is of great importance to understand the significant steps of a heterogeneous catalyzed reaction. We can distinguish between fundamental catalytic processes that can occur extremely fast (e.g. nanosecond scale), like the formation of the reaction intermediates, or processes that can usually require a larger amount of time (e.g. from minutes to hours) like the different stages in a catalyst's lifetime, such as activation/deactivation/reactivation. By applying the appropriate characterization technique (e.g. X-ray absorption spectroscopy (XAS) for characterization of local geometry, electronic and structural properties of catalysts, X-ray diffraction techniques (XRD) for structural characterization of materials, microscopy and morphological studies, or techniques for studying the interaction of adsorbates with catalyst surfaces, such as infrared spectroscopy (IR), Raman spectroscopy, electron paramagnetic resonance (EPR), and X-ray photoelectron spectroscopy (XPS), etc.) or by properly integrating a several techniques as combined

approach it is possible to obtain the information about the material structure that can be correlated with the catalytic activity.

Along with the *in situ* approach, *operando* methodology (*in situ* spectroscopy and simultaneous activity measurements under technically relevant catalytic reaction conditions) has been extensively used over the last years for better understanding of catalytic materials and reaction mechanisms [7].

2.3.1 Synchrotron studies

A synchrotron is an extremely powerful source of X-rays and many of the techniques mentioned in the introductory part of this section can be implemented at a synchrotron facility. The X-rays are produced by high energy electrons moving in a circular path. The entire synchrotron world floats around this principle: when a moving electron changes direction, it emits energy. When the electron is moving fast enough, the emitted energy is at X-ray wavelength. Thereby, a synchrotron machine is used to accelerate electrons to very high energy level and then to make them change direction periodically. The major component parts of any synchrotron facility are briefly presented in the **Figure 2.9 b**. First, free electrons are produced (**1**, electron gun) which are accelerated in linear accelerator (**2**, LINAC). The LINAC feeds the electrons into the booster ring (**3**, pre-accelerator), an element that uses magnetic fields to force the electrons to travel in a circle. Following the booster ring, the electrons go into the storage ring (**4**, a giant donut) where they circle for hours at a velocity close to the speed of light. The tube is maintained at very low pressure (around 10^{-9} mbar). The X-ray beams emitted by the electrons are directed towards beamlines (**5**) that surround the storage ring in the experimental hall (**6**, application room serving for different type of research depending on the available techniques).

Among others, X-ray absorption fine structure (XAFS) is one of the most important spectroscopic techniques used to characterize heterogeneous catalysts [8, 9]. By analyzing the XAFS data, information can be acquired on the local structure and on the unoccupied local electronic states (e.g. coordination chemistry or oxidation states) [10]. X-ray absorption measurements are very straightforward, provided one has an intense and energy-tunable source of X-rays - which usually means a synchrotron facility. XAFS is element-specific, in that sense the x-rays are chosen to be at and above the binding energy of a core electronic level of an atomic species. XAFS spectra are divided into two regimes, namely XANES (X-ray Absorption Near-Edge Spectroscopy) and EXAFS (Extended X-ray Absorption Fine-Structure). XANES is the region of x-ray absorption spectrum within $\sim 50\text{eV}$ of the absorption edge and EXAFS contains related but slightly different information about an element's local coordination and chemical state. XANES is strongly sensitive to formal oxidation state and

2 | Materials and methods

coordination chemistry of the absorbing atom whereas EXAFS can be used to determine the distances, coordination number, and species of the neighbors of the absorbing atom. Since all atoms have core level electrons, XAFS spectra can be measured for essentially every element on the periodic table. More importantly, crystallinity is not required for XAFS measurements making it one of the few available techniques for non-crystalline and highly disordered materials. Since X-rays are fairly penetrating in matter, XAFS is not intrinsically a surface-sensitive technique though special measurement approaches can be applied to enhance its surface sensitivity.

Given the intense use of CeO₂ related materials in the present project, various synchrotron measurements have been performed to understand the role of catalyst in DMC synthesis starting from CO₂ and methanol. A priori: CeO₂ is a catalyst well-known for its acid-base properties (Ce⁺⁴ is a Lewis acid, while O⁻² is a Lewis base), but also very famous for its redox potential, being able to rapidly switch from Ce⁺⁴ to Ce⁺³ and vice versa, under the proper experimental conditions. To get better insights on the Ce oxidation state during DMC synthesis and to understand the extent of redox process (if any) in this process, synchrotron measurements have been performed. All the experiments were performed at European Synchrotron Radiation Facility (ESRF, Grenoble – France) at the Swiss Norwegian Beamline (SNBL). The workstation is equipped with two monochromators, a channel-cut (CC) monochromator for diffraction experiments and a double-crystal monochromator (DCM) for XAFS measurements. They can be easily and rapidly interchanged. Besides these two traditional synchrotron-based techniques, the experiments can also be followed by Raman scattering. The Raman instrument, a Renishaw RA100 – green laser at 532 nm and a red laser at 785 nm, is located outside the experimental hutch. More information about the optics, beamline layout, monochromators design, and Raman probe design can be found in [11] and [12].

XANES experiments targeting Ce L3 (5.7234 keV) and K (40.4430 keV) edges have been conducted in both gas and liquid phase. **Figure 2.9 a** briefly describes the experimental setup. The reaction cell (**7**) consisted of commercially available quartz capillary tubes as a transparent tubular reactor for continuous flow process and it is shown in **Figure 2.10**. The reactor tubes were purchased from Hilgenberg GmbH (Germany) with standard length of 80 mm and various outer diameter (OD of 0.7 and 1.0 mm, depending upon the experiment). The wall thickness of the capillary tube is very small, 0.01 mm, making it appropriate for the desired experiments. One end of the capillary was funnel-shaped to aid the catalyst loading, while the other one remain closed until the start of reaction. The closed end of tube was opened by using GC capillary column cutter once the system is mounted. The catalyst bed consists of CeO₂ particles sieved to the desired size (µm) and placed properly in between two layers of

quartz wool. Since all the experiments were run at atmospheric pressure, the main purpose of the quartz wool was to keep the catalyst bed at fixed position under the continuous flow or when changing from one flow to the other. The reactor tube is glued with two-component high temperature epoxy to a stainless-steel bracket equipped with 1/8" fittings which serves as holder as well as provides connections to flow the gases (**Figure 2.10**).

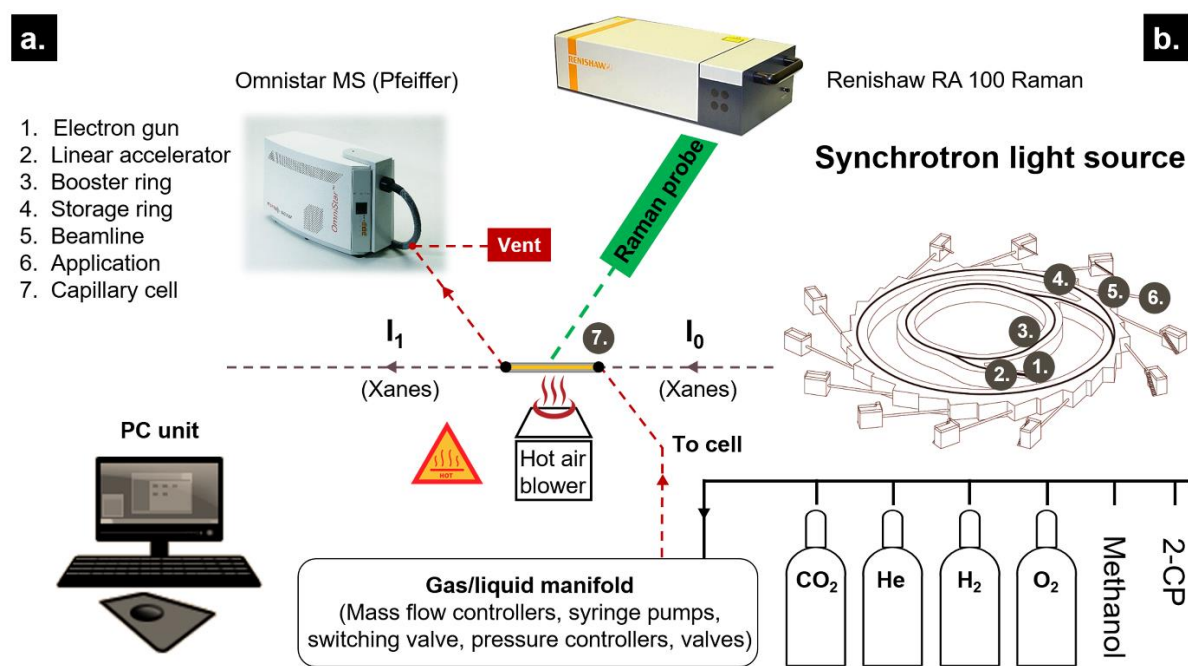


Figure 2.9 European Synchrotron Radiation Facility (ESRF), Swiss Norwegian Beamline (SNBL - Grenoble, France, Station B). **a.** Schematics of the experimental setup used to monitor the DMC synthesis using CeO₂ materials. Both gas and liquid phase experiments have been performed. Raman (green laser) and MS (Pfeiffer, Omnistar) were used to follow the surface species and gas phase products formation, respectively and **b.** Synchrotron light source – component parts

Two high precision slides ensure that the fittings remain perfectly coaxial and allows the easy alignment relative to the X-ray beam and to the hot air blower (properly controlling the reaction temperature) placed below the capillary.

2 | Materials and methods

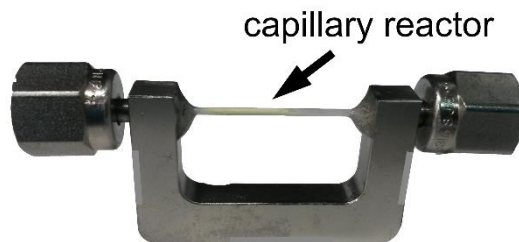


Figure 2.10 Capillary cell with stainless steel bracket equipped with 1/8" fittings. The tube is glued with two-component high temperature epoxy into the bracket frame. The catalyst is placed in between two quartz wool layers for increased stability under the reaction (flow) conditions

Gas flows were remotely controlled by mass flow controllers (Bronkhorst). To introduce methanol (gas) into the reaction cell, an inert gas (helium) was passed through a glass saturator (kept at room temperature) containing liquid methanol. Hydrogen and oxygen were used to perform the reduction and oxidation cycles. For experiments using liquid reactants (water and 2-cyanopyridine), two syringe pumps were used (Chemyx Fusion 100 and KDS Scientific 100, both equipped with glass syringe), combining precision with simplicity and reproducibility even at micro-flow rates. The syringe filled with 2-cyanopyridine (solid at normal conditions of 20 °C and 1 atm) was properly wrapped into heating wire and heated to 40-50 °C, to ensure its transformation into liquid and normal flow towards the reaction cell.

One of the main elements of the setup is the switching valve. The switching valve allowed rapid switching between two gas lines (e.g. H₂ and O₂). The pressure in both lines (sample and blank) was adjusted to 1.2 bar by back pressure controllers (Bronkhorst). Equalizing the pressure in both lines is very important as it enables a sharp and clean switching front between the gases. At the outlet of the capillary cell a quadrupole mass spectrometer (Pfeiffer, Omnistar) capable of separating fragments with molecular mass to charge ratio (m/e) up to 100 was connected to analyze the gas phase products coming out of the reactor. To avoid condensation of the liquid phase when introducing vapors into the capillary, the transfer line connecting the reactor with the MS was continuously heated at 150 °C. The outlet gases were analyzed by connecting the MS inlet to a 1/16" stainless steel tee (open to the atmosphere) on the exhaust tube.

All the instruments and equipment presented above (i.e. XANES data collection, MS and Raman spectrometer, temperature controller, MFCs and back pressure regulators, switching valve, etc.) are connected to a hub and further on they are remotely controlled using a powerful computer unit located in the analysis room near the experimental hutch.

2.3.2 *In situ* DRIFTS-MS and Raman-MS studies

Infra-red spectroscopy (vibrational spectroscopy) is one of the most sensitive, useful and important analytical techniques used for the investigation of the active species and sites in catalysis. All organic molecules absorb infra-red (IR) radiation at characteristic vibrational frequencies. The amount of absorbed radiation and the frequency at which the event occurs varies with the presence of various functional groups (e.g., OH, NH, C=O, COCl, C-C, C=C, etc). Basically, infrared spectroscopy is a technique entirely built on the vibrations of the atoms of a molecule. An infrared spectrum is commonly obtained by passing infrared radiation through a sample and determining what fraction of the incident radiation is absorbed at a certain energy level. Hence, any peak in an absorption spectrum appears at certain energy level and corresponds to the vibration frequency of a specific part of a molecule. Many times, the IR measurements are done in transmission mode, where samples should be prepared as thin films or diluted in non-absorbing matrices (to avoid strong absorption generated by most of the materials). On the other hand, reflectance techniques may be used for samples that are difficult to analyze by the conventional transmittance method as they require minimal sample preparation and provide reliable results. The reflectance methods include:

- Attenuated Total Reflectance (ATR) Spectroscopy (utilizing the phenomenon of total internal reflection)
- Specular Reflectance Spectroscopy (external reflectance; ideally for smooth surfaces)
- Diffuse Reflectance Spectroscopy (DRIFTS) (combining internal and external reflectance phenomena; ideally for rough surfaces)

DRIFTS is of high interest for the heterogeneous catalyzed gas phase reactions since spectra of powders presenting rough surfaces can be rapidly recorded by illuminating the catalyst surface and collecting enough scattered radiation. The valuable information such as mechanistic pathway or formation of active reaction intermediates can be obtained by using *in situ* DRIFTS experiments.

***In situ* DRIFTS setup (Figure 2.12):** all the experiments were performed using a BRUKER IR instrument (FTIR-Vertex 70V) equipped with a liquid-nitrogen-cooled mercury cadmium telluride (LN-MCT) detector with a home-made stainless steel cell mounted in a Praying Mantis (Harrick). The Praying Mantis accessory consists of an optical system equipped with a series of mirrors for redirection and collection of diffuse reflected light as well as minimizing the detection of specularly reflected light (Figure 2.11). Detailed description of the experimental setup is shown in Figure 2.12. The cell design included gas inlet-outlet ports as well as thermocouple entrance to measure the catalyst bed temperature. The temperature of the cell was controlled with a programmable PID temperature controller. In a typical experiment, the

2 | Materials and methods

catalyst in powder form or sieved to the desired particle size (μm) was placed in the cell (in the special designed notch) in between two quartz wool layers (sandwich structure like, horizontally placed). A flat zinc selenide (ZnSe) crystal serving as IR transparent window was placed on top of the catalyst bed. The graphite sheet was placed between the window and the main body for sealing purpose. The optical window was then covered with another layer of graphite sheet and a stainless-steel top lid which finally fixed to the cell body by using screws. The gases (i.e. carbon dioxide, helium) were fed to the reaction cell by the means of four calibrated ALICAT mass flow controllers. Methanol in gas phase was supplied using a liquid methanol saturator and helium as carrier gas. A 4-way switching valve (VICI, Valco Instruments) allowed rapid switching between two gases (e.g. CO_2 and methanol).

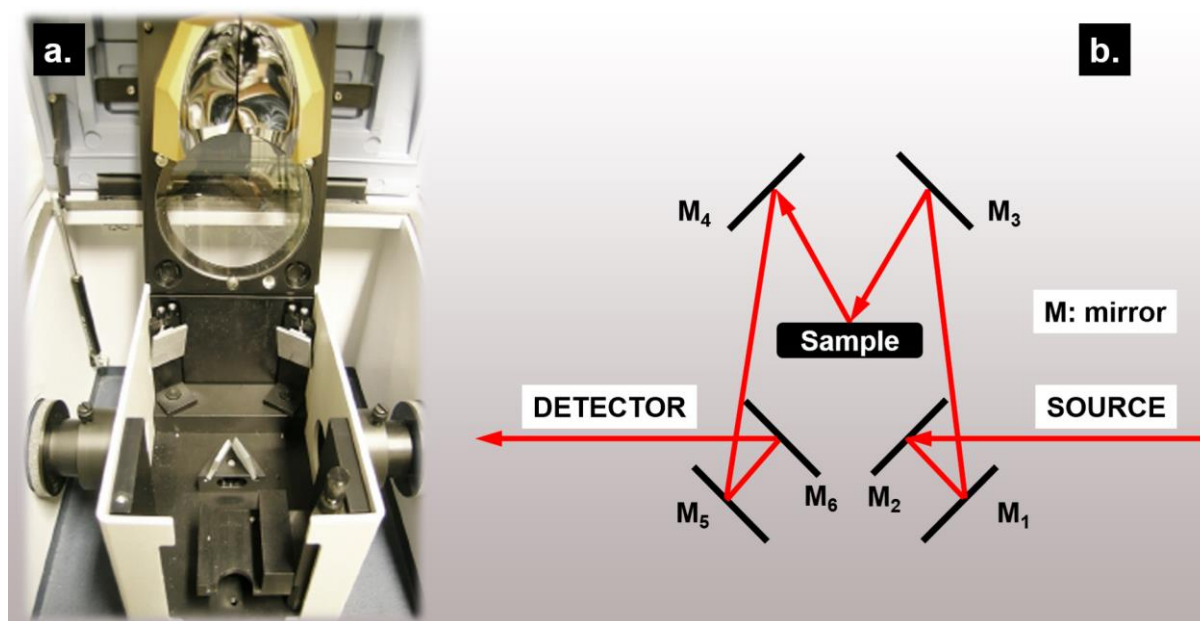


Figure 2.11 a. Photograph of a Praying Mantis (Harrick) and b. schematic diagram of the optical system

All the spectra were acquired with OPUS Spectroscopy Software package at a resolution of 4 cm^{-1} . The experiments were performed at various temperatures and atmospheric pressure, and all the gas phase effluents were analyzed online with the mass spectrometer equipment having the transfer line temperature set to $200\text{ }^\circ\text{C}$ to avoid condensation problems. Before starting the experiment, the whole system was purged with helium for at least half an hour or until complete stabilization was observed on the MS detector.

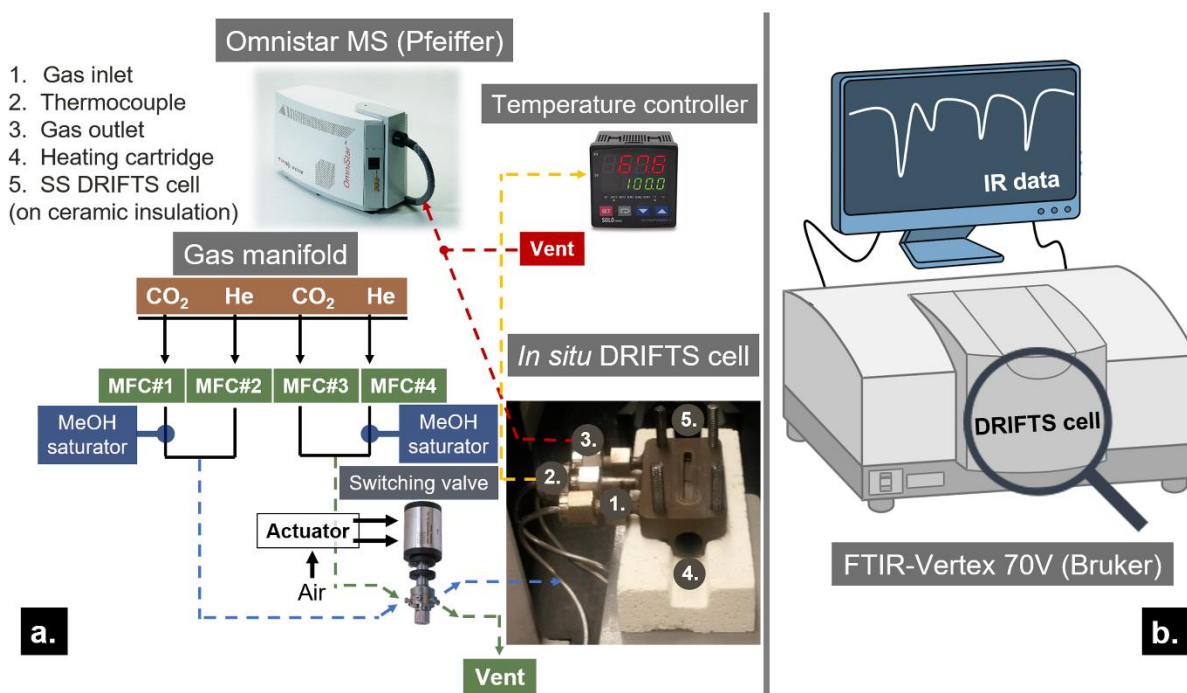


Figure 2.12 a. *In situ* DRIFTS-MS setup. The gas manifold allows feeding the reactants to the DRIFTS cell. IR measurements are done using **b.** Vertex 70V (Bruker) and the gas phase products are analyzed with Omnistar MS

Along with DRIFTS, Raman spectroscopy is among the most powerful and versatile analytical techniques used for chemical analysis and characterization of many different chemical species and reactions. Raman spectroscopy is a type of vibrational spectroscopy, pretty much alike infrared spectroscopy where IR bands arise from a change in the dipole moment (change in polarizability) of a molecule. Like the FT-IR, Raman spectroscopy is highly selective, which allows to identify and differentiate molecules and chemical species that are very similar. Nevertheless, certain vibrations that are allowed in Raman are forbidden in IR and vice versa, whereas other vibrations may be observed by both techniques although at significantly different intensities; thus, these two techniques can be often seen and referred as complementary ones.

The Raman effect was initially introduced by the famous Indian physicists C.V. Raman and K.S. Krishnan back in 1928 and it involves shining a monochromatic light source (i.e. laser) on a sample and detecting the scattered light. Most of the light that scatters off is unchanged in energy (also known as Rayleigh scattering), whereas a small portion of it has lost or gained energy (also known as Raman scattering). Depending on either the energy is lost (*) or gained (**), the process is called Stokes Raman scattering (*) or anti-Stokes Raman scattering (**).

In comparison to other vibrational spectroscopy methods, such as FT-IR and NIRS (near-infrared spectroscopy), Raman presents several major benefits. These advantages are consequences of the fact that the Raman effect manifests itself in the light scattered-off from

2 | Materials and methods

a sample as opposite to the light absorbed by a sample. Thus, Raman spectroscopy requires little to no sample preparation and is not sensitive to aqueous absorption bands (i.e. no special accessories are needed for measuring aqueous solutions). This property of Raman facilitates the measurement of samples that may come in the form of solids (particles, pellets, powders, films, fibers), liquids (gels, pastes), and gases not only directly, but also through transparent windows/reactors made from glass, quartz, and even plastic. This makes the Raman spectroscopy a very suitable and versatile technique for *in situ/operando* measurements which can be performed under high pressure and temperature conditions. In addition, CO₂ vapors are very weak scatterers and system purging is unnecessary.

***In situ* Raman setup:** a thorough description of the experimental setup used for the *in situ* Raman measurements is presented in **Figure 2.13**. All the experiments were carried out using a BWTEK dispersive i-Raman portable spectrometers equipped with 532 and or 785 nm excitation lasers and a TE-cooled linear array detector.

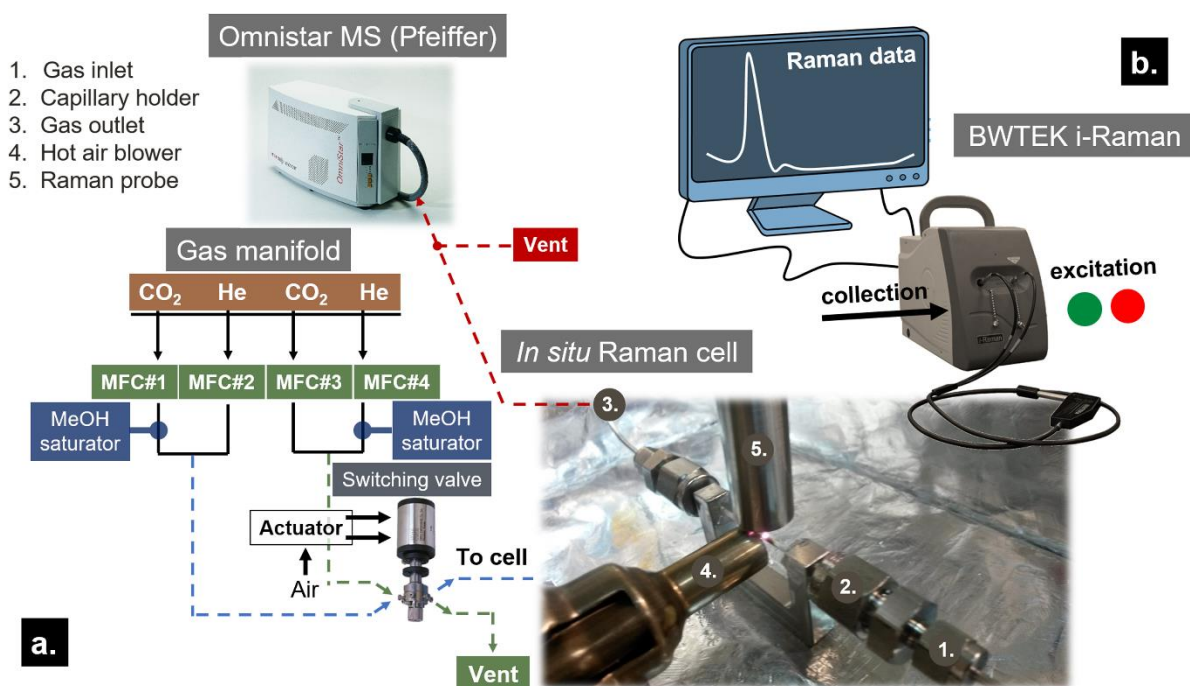


Figure 2.13 a. *In situ* Raman-MS setup. The gas manifold allows feeding the reactants to the Raman cell. Raman measurements are carried out using the **b.** BWTEK portable i-Raman. The gas phase products are analyzed with an Omnistar MS

The system is very like the one presented above (see ***in situ* DRIFTS setup**), relying on the same gas manifold to feed the reactants to the reaction cell. The major differences arise from the usage of a capillary reaction cell comparable to the one described in the section **2.3.1 Synchrotron studies** and a different heating system, based on a commercially available high

temperature (up to 500 °C) hot air gun. All the spectra were acquired with the BWSpec4.0 software and the gas phase effluents were analyzed online with a mass spectrometer, an Omnistar MS equipment having the transfer line temperature set to 200 °C to avoid any condensation issues.

2.3.3 Modulation excitation spectroscopy (MES) and multivariate curve resolution (MCR). Theory and applications

Given the increased complexity presented by a heterogeneous catalyzed reaction system (described in detail in **Figure 2.14**), involving liquid and gaseous reactants and products and a solid catalyst separated by a phase boundary, it is of high difficulty to properly understand how this surface process controls essential steps ongoing from reactants to product formation. There are physical transport phenomena of substrates and products to (and from) the active sites, reaction intermediates formation, and inactive species interfering with the reaction medium. It also presents high relevance to improve the control over all the reaction parameters that can significantly influence the overall reaction rate and process selectivity by suppressing the unwanted secondary reactions. To do this, we should own a complete understanding of the whole catalytic process. Finally, the objective will be attained by designing better catalyst materials able to overcome the transport limitations while providing enhanced activity and stability over time.

Although the power of *in situ/operando* spectroscopic techniques (part of which have been presented in the section **2.3 In situ studies**) is highly acknowledged, some important challenges stand still in the attempt to explain and correlate the signals originating from the catalytic interfaces with the activity and selectivity results. Among the most important problems encountered when dealing with *in situ* measurements it is worth to enumerate that the resulting spectra are often very crowded, bringing together information from reactants, products, reaction intermediates, solvents and even inactive species (spectators) that are not involved in the reaction directly. The main issue here is that the signals originating from spectators are frequently stronger than those of the active species, thus crucial information for the catalytic process may be hidden or lost.

2 | Materials and methods

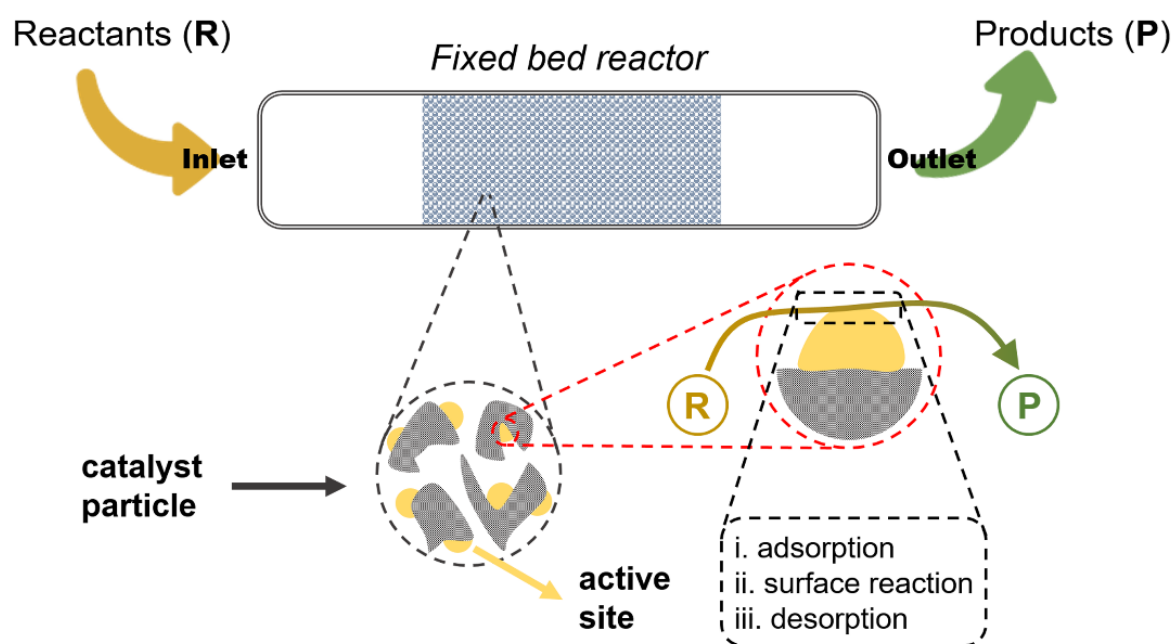


Figure 2.14 Schematic representation of the complex system represented by a heterogeneous catalyzed reaction taking place in a fixed bed reactor

Also, the highly dynamic nature of the reaction system under real working conditions (i.e. catalytic processes usually require high temperatures and/or pressures), the time-resolution (i.e. sensitivity and noise \rightarrow signal-to-noise ratio), and selectivity (i.e. being able to certainly assign that what we see is due to species actively involved in the reaction mechanism and not just spectators) are other factors that will have a huge impact in interpreting the data. To tackle these challenges, transient response techniques (e.g. temporal analysis of products, TAP and ultrafast laser spectroscopy, ULS) are widely applied in the analysis of reaction intermediates and active species or of reaction kinetics. Modulation excitation spectroscopy (MES) is another powerful and well-known tool that allows sensitive and selective detection and monitoring of the dynamic behavior of species directly involved in a chemical reaction [13, 14]. The basic principles of the modulation excitation spectroscopy are summarized in [Figure 2.15](#). Basically, when a system is perturbed by a periodic change of a parameter, such as concentration, pH, light flux, or temperature, this will selectively be reflected upon the species actively involved in the reaction and, in consequence, they will be offering a periodic response. Further on, this response can be sensitively monitored and the signal-to-noise ratio can be significantly enhanced by a phase-sensitive detection (PSD), a mathematical model used by MES to obtain better spectral separation of the signals. As illustrated in the [Figure 2.15](#), a realistic situation (i.) is pictured by an unclear and noisy image, where the active species and the spectators can barely be distinguished. A more desirable situation (ii.) can be achieved if an ideally sensitive technique has been used.

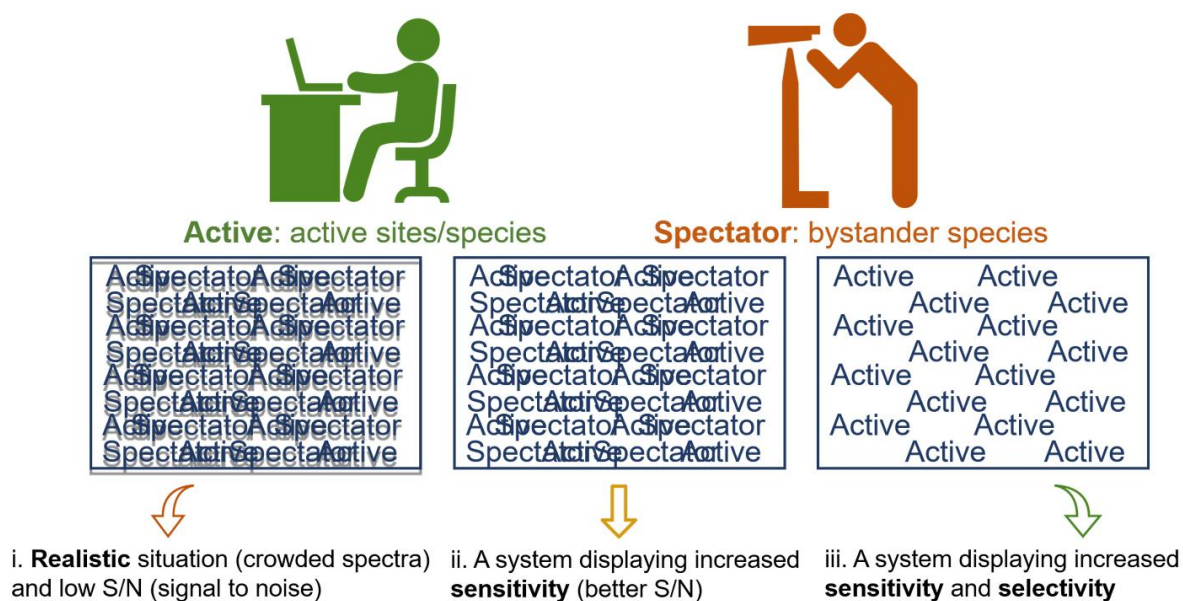


Figure 2.15 Modulation excitation spectroscopy (MES) – basic principles

Nevertheless, the signals of the active species are still largely interfering with the unwanted spectator signals. An ideal situation and the ultimate objective of applying such transient techniques (MES in the current case) is depicted in (iii.) and it shows that only the active species can be monitored with high temporal and spatial resolution so that its dynamic behavior can be closely observed. In a typical MES experiment two kinds of stimulation are generally used, namely sinusoidal- and square-wave stimulations. While sinusoidal-wave stimulation is simpler to treat theoretically for the quantitative analysis of the responses, the square-wave stimulation is easier to implement experimentally, precisely for the case of concentration stimulation, which is achieved by simply switching between two flows of different concentrations.

Alternatively, we combined the MES experiments with a chemometric method to realize better data processing and deconvolution of the complex spectra down to individual components. Chemometrics is a branch of the chemistry that employs mathematical and statistical methods to design or select optimal procedures and experiments, and to provide maximum chemical information by evaluating chemical data. As such, multivariate curve resolution (MCR) has become very popular in the last 40-50 years and has gained increased attention due to its improved ability to deliver the pure response profiles (e.g. spectra, pH profiles, time profiles, elution profiles) of the chemical constituents or species of an unresolved mixture when no previous information is available about the nature and composition of these mixtures [15]. Nowadays, MCR is heavily used as a blind-source separation method (without having any reference spectra *a priori*) to efficiently process large data sets coming from the *in situ* measurements performed in labs and at synchrotron facilities all over the world [16].

2 | Materials and methods

Herein, a brief description of the MCR-ALS (Multivariate Curve Resolution Alternating Least Square) method is presented. A more detailed description of the method and software used can be found in various literature reports and tutorials [17-25].

For MCR (**Figure 2.16**) analysis in a multicomponent system, two main requirements must be fulfilled, namely i) the experimental data should be structured as a two-way data matrix (or a multiset structure) and ii) this data set should be explained well enough by a bilinear model using a limited number of components. The MCR bilinear model is usually described by the equation $\mathbf{D} = \mathbf{CS}^T + \mathbf{E}$, where \mathbf{D} is the raw data set (initial spectroscopic data table; the rows of matrix \mathbf{D} are the spectra measured during the experiment), and \mathbf{S}^T (rows) and \mathbf{C} (columns) are the matrices corresponding to the pure spectra and the related concentration profiles, respectively, for each of the compounds encountered in the system (the superscript T denotes the transpose of matrix \mathbf{S}). \mathbf{E} is the matrix of residuals and ideally it should be close to the experimental error.

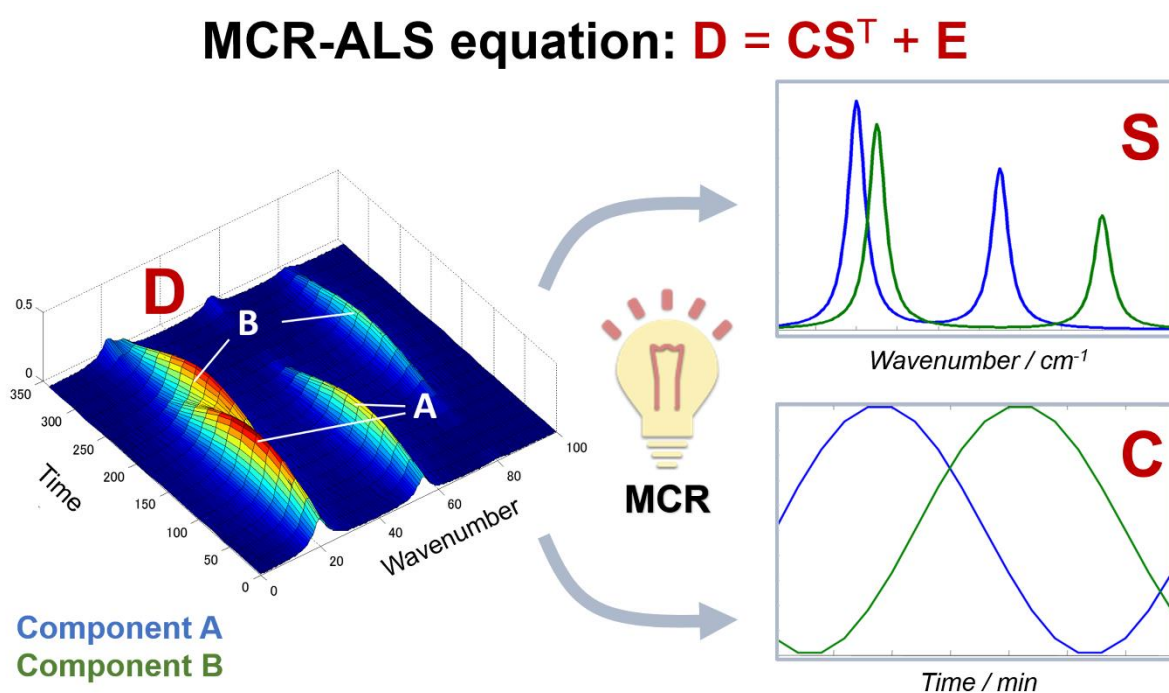


Figure 2.16 Multivariate curve resolution (MCR) – efficiently solving the mixture analysis problem (e.g. spectroscopic data set)

With the purpose of improving the data treatment and solve the MCR bilinear model and to realistically interpret and extract the profiles of \mathbf{C} and \mathbf{S}^T , a constrained Alternating Least Squares (ALS) algorithm is also implemented. MCR-ALS solves iteratively the equation presented in **Figure 2.16** by using the Alternating Least Squares algorithm which calculates the concentration and pure spectra matrices to optimally fit the experimental data matrix. To carry out the optimization procedure, a series of steps must be followed, namely i) estimation of the initial number of components in the system (can be done either manually or by using

single value decomposition algorithm), ii) preliminary estimation of both \mathbf{C} and \mathbf{S}^T (realized manually or by means of using the evolving factor analysis method or by a purest variable detection method), iii) the choice of constraints: several constraints can be applied to model the shapes of the \mathbf{C} and \mathbf{S}^T profiles (separately), such as non-negativity, unimodality, closure, trilinearity, selectivity or/and other shape or hard-modeling constraints, and iv) ALS optimization: convergence is achieved after a predefined number of iteration cycles or when there is no longer a visible difference in the standard deviations of the residuals between two consecutive iterative cycles.

In the end, the MCR-ALS algorithm is a very flexible mechanism which, by proper selection and application of the constraints that are fully fulfilled by the raw data set, can deal with huge amounts of datasets resulted from the most diverse situations. The final goal is to learn more about a certain chemical system behavior and to come up with meaningful results from both mathematical and chemical point of view.

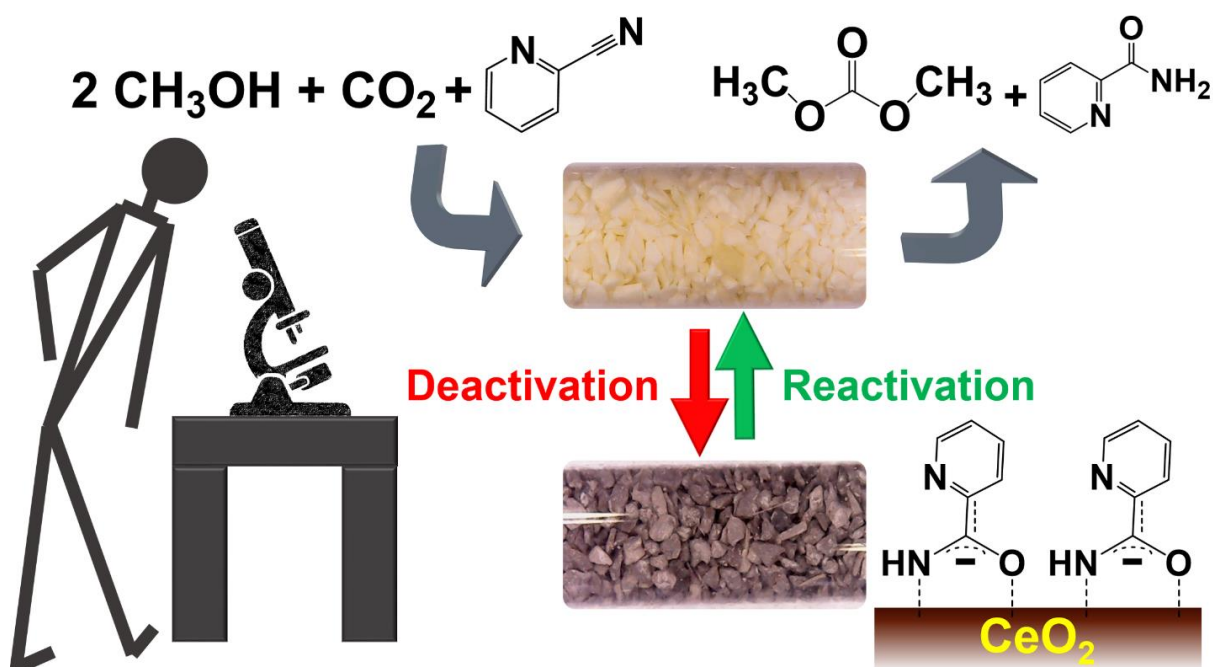
Bibliography

- [1] Y. Ikeda, M. Asadullah, K. Fujimoto, K. Tomishige, *J. Phys. Chem. B*, 105 (2001) 10653–10658.
- [2] F. Pinna, *Catal. Today*, 41 (1998) 129-137.
- [3] J. Haber, *Pure & Appl. Chem.*, 63 (1991) 1227-1246.
- [4] J.T. Richardson, *Principles of Catalysts Development. Fundamental and Applied Catalysis.*, Springer US, New York, 1989.
- [5] <http://www.sigmaaldrich.com/>, Sigma-Aldrich Co. LLC., 2015.
- [6] H. Topsøe, *J. Catal.*, 216 (2003) 155–164.
- [7] M.A. Bañares, *Catal. Today*, 100 (2005) 71-77.
- [8] R.S.v. Bordwehr, *Ann. Phys. Fr.*, 14 (1989) 377 - 465.
- [9] M. Newville, *Rev. Mineral. Geochem.*, 78 (2014) 33-74.
- [10] D.C.K. (Editor), R.P. (Editor), *X-Ray Absorption: Principles, Applications, Techniques of EXAFS, SEXAFS and XANES*, 1987.
- [11] <http://www.esrf.eu/>, 2016, pp. SNBL workstation.
- [12] W.v. Beek, O.V. Safonova, G. Wiker, H. Emerich, *Phase Transit.*, 84 (2011) 726–732.
- [13] A. Urakawa, T. Burgi, A. Baiker, *Chem. Phys.*, 324 (2006) 653–658.
- [14] A. Urakawa, T. Burgi, A. Baiker, *Chem. Eng. Sci.*, 63 (2008) 4902 – 4909.
- [15] A. Malik, A.d. Juan, R. Tauler, *40 Years of Chemometrics – From Bruce Kowalski to the Future*, ACS Symposium Series, pp. 95-128.
- [16] A. Voronov, A. Urakawa, W.v. Beek, N.E. Tsakoumis, H. Emerich, M. Rønning, *Anal. Chim. Acta*, 840 (2014) 20-27.
- [17] R. Tauler, A.K. Smilde, B.J. Kowalski, *J. Chemometr.*, 9 (1995) 31 – 58.
- [18] R. Tauler, *Chemometr. Intell. Lab.*, 30 (1995) 133 – 146.
- [19] R. Tauler, *J. Chemometr.*, 15 (2001) 627 – 646.
- [20] M. Amrhein, B. Srinivasan, D. Bonvin, M.M. Schumacher, *Chemometr. Intell. Lab.*, 33 (1996) 17 – 33.
- [21] J. Saurina, S. Hernandez-Cassou, R. Tauler, A. Izquierdo-Ridorsa, *J. Chemometr.*, 12 (1998) 183 – 203.
- [22] A.d. Juan, R. Tauler, *Anal. Chim. Acta*, 500 (2003) 195 – 210.
- [23] J. Jaumot, R. Gargallo, A.d. Juan, R. Tauler, *Chemometr. Intell. Lab.*, 76 (2005) 101 – 110.
- [24] A.d. Juan, J. Jaumot, R. Tauler, *Anal. Methods*, 6 (2014) 4964-4976.
- [25] J. Jaumot, A.d. Juan, R. Tauler, *Chemometr. Intell. Lab.*, 140 (2015) 1-12.

3

Catalysis under microscope

Unraveling the mechanism of catalyst de- and re-activation in the continuous dimethyl carbonate synthesis from CO₂ and methanol in the presence of a dehydrating agent



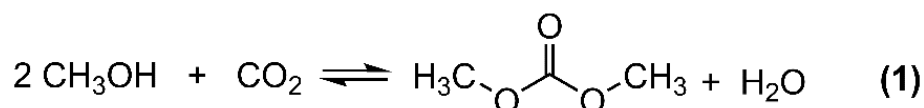
3 | Catalysis under microscope

3.1 Introduction

Human activities have been influencing climate changes by the significant increase in the emissions of greenhouse gases, among which carbon dioxide (CO₂) is the main exponent. According to a study by Friedlingstein *et al.*, human activities are responsible for 35 billion metric tons (gigatons) of CO₂ emission in 2010 [1], an amount that makes the CO₂ emissions from the world's degassing subaerial and submarine volcanoes seem rather small [2]. In this context, exploring new ways to valorize CO₂ in a form of chemicals such as fuel [3] and organic carbonates, has gained great attention. Among them, development of the direct carboxylation reaction of alcohols such as methanol and ethanol with CO₂ for the synthesis of alkyl carbonates is attractive in terms of CO₂ chemical fixation and green chemistry (organic carbonates are well known for their low toxicity, non-corrosivity and biodegradability) [4, 5]. Also, the reaction can contribute to the substitution of toxic phosgene by abundant and less harmful CO₂ molecule.

Dimethyl carbonate (DMC) has attracted much attention in the last few decades due to its unique chemical properties as a safe, non-corrosive and environmentally acceptable alternative to methylating and carbonylating agents (CH₃X, DMS, COCl₂) [4-8]. Also, DMC has been used in the synthesis of polycarbonates and polyurethane, and even as a solvent, replacing methyl ethyl ketone, butanone, or *tert*-butyl acetate [4, 9]. Moreover, due to its high oxygen content (around 53 wt%; three-times more oxygen-rich than methyl *tert*-butyl ether, i.e. MTBE), DMC has been employed as an oxygenate additive to diesel fuel, thus increasing the potential to reduce soot from diesel engines [10].

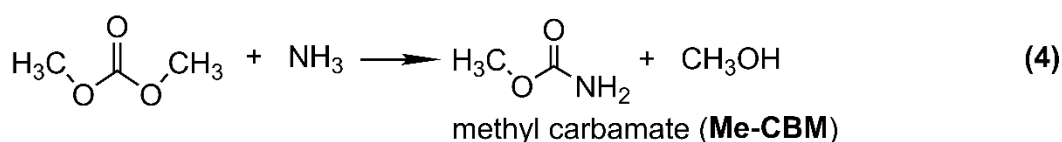
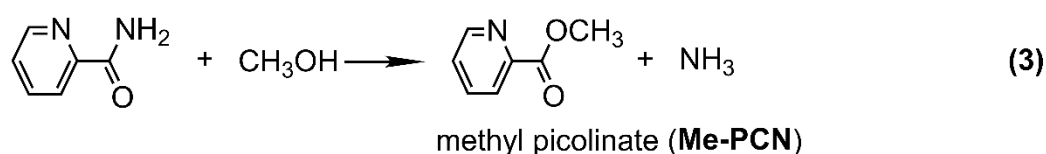
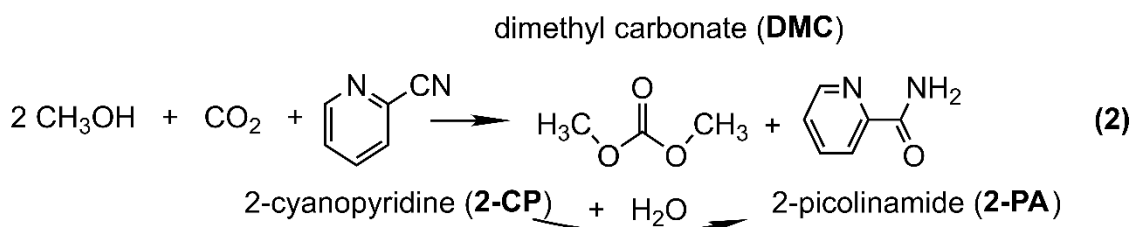
Both batch and continuous operations have been reported for the direct DMC synthesis using heterogeneous catalysts from carbon dioxide and methanol as a safer and cleaner way for DMC production, eliminating the use of the toxic phosgene or CO required for the conventional DMC synthesis. The reaction can, in principle, provide an extremely high atom efficiency (**Reaction 1**).



Zirconia and ceria are the catalyst materials widely reported for the methanol carboxylation reaction [11-20]. Even though the selectivity towards DMC (S_{DMC}) was very high (almost 100% in some cases), the methanol conversion (X_{MeOH}) was limited by the reaction equilibrium. Other attempts have been made with vanadium-based catalysts such as H₃PO₄/V₂O₅ and Cu-Ni/V₂O₅-SiO₂ [21, 22], without improving the methanol conversion and DMC yield to a large extent. Different oxides like SiO₂, Al₂O₃, TiO₂, H-ZSM5, H-USY, H-MOR, ZnO, MoO₃, and

Bi_2O_3 were tested in the reaction, but mainly dimethyl ether (DME) was produced instead of desired DMC [12].

Several researchers have examined different ways to improve the thermodynamically-limited equilibrium conversion to shift towards DMC formation, because DMC yield is <1% even at thermodynamically favorable high pressure conditions [23, 24]. The uses of high pressure conditions [25], both chemical or physical water traps (dehydrating agents) [16, 26], and catalytic membrane reactors (CMR) [27] did not show a great improvement for the direct carboxylation reaction of methanol. Recently, Tomishige *et al.* first reported the use of 2-cyanopyridine (2-CP) as a dehydrating agent in the direct DMC formation from methanol and carbon dioxide in a batch system, demonstrating outstanding results in terms of methanol conversion and DMC selectivity (**Reactions 2-4**) as well as recycling of 2-picolinamide (2-PA) by dehydration reaction to 2-CP [28, 29].



Inspired by the work of Tomishige, our group reported the direct DMC synthesis in a fixed bed reactor over ceria (CeO_2) catalysts in the presence of 2-CP with >90% methanol conversion and >95% DMC selectivity [25]. Excellent results were obtained, but at the same time a drop in methanol conversion by ca. 50% was observed after ca. 200 h of continuous operation and the origin of the deactivation remains unclarified.

Operando methodology (*in situ* spectroscopy and simultaneous activity measurements under technically relevant catalytic reaction conditions) has been increasingly used over the last years for better understanding of catalytic materials and reaction mechanisms [30]. The use of traditional tubular quartz reactors as spectroscopic cells [31-36] is an extremely powerful and efficient approach since a wide range of temperatures and pressures can be easily studied. On the other hand, visually inspecting catalysts in real time using such an

3 | Catalysis under microscope

optically transparent reactor can possibly offer new perspectives on catalytic reaction mechanism, catalyst functionality, and process optimization. There are several reports where visual observations were made on the basis of the use of capillary quartz reactors (or windows), such as working under high pressures (250 bar) and temperatures (500 °C) for biomass gasification [37], coke identification in the conversion of biomass in hot compressed water [38], assessment of the mixing behavior in a reformer prototype for hydrogen production [39], and evaluation of the temperature profile during the efficient reheating of a reverse-flow reformer [40].

The present study aims at first demonstrating the continuous DMC synthesis using CeO₂ as catalyst and 2-CP as dehydrating agent in a fused quartz reactor operated up to the optimum reaction pressure of 30 bar [25] and then at shedding light on critical parameters that can help better understand and improve the process by visual and spectroscopic inspections. Particularly, focuses are given to gain new insights into the origin of deactivation and its mechanism to propose effective conditions for catalyst reactivation. Furthermore, our first attempts to visualize the complexity of the catalytic interface consisting of three-phase boundaries (gas-liquid-solid) under operando conditions will be presented.

3. 2 Experimental

3. 2. 1 Materials

High surface area CeO₂ powder (>100 m²/g) was kindly supplied by Daiichi Kigenso Kagaku Kogyo Co. Ltd., Japan and used without any further treatment. Methanol (>99%) and 2-cyanopyridine (2-CP, 99%) were purchased from Sigma Aldrich. High purity CO₂ (>99.9993%) gas was purchased from Abelló Linde, Spain.

3. 2. 2 Reaction system

The details of the reaction set-up, protocols used, and analytical methods for the identification and quantification of reaction products were described in our previous work [25]. The reaction set-up used in this work is a simplified and improved version of the system [25]. The present system differs in product separation efficiency by means of an improved hot trap design. This was achieved by introducing the hot trap into a home-made metallic oven. The temperature of the oven was kept at 130-140 °C so that high separation efficiency between low and high boiling-point compounds could be assured. The temperature range is enough to reach the proper separation of compounds with low boiling-points, while minimizing the high boiling-point compounds traveling from the hot to the cold trap. The product analysis was performed by GC-MS (Scion 436-GC, Bruker) using ethanol as solvent and 1-hexanol as an internal standard. Additionally, n-octane was introduced in the reactant stream as an internal

standard to minimize the errors in quantification of the products due to evaporation and condensation.

In a typical experiment, 300 mg of the CeO_2 catalyst (pelletized, crushed, and sieved to 200-300 μm particle size) was loaded into the reactor tube (fused quartz reactor with ID: 2.0 mm, and OD: 3.0 mm, purchased from Technical Glass Products, Inc. USA), resulting in the catalyst bed length of ca. 6.0 cm (**Figure 3.1**).



Figure 3.1 Fused quartz reactor with regular compression fittings. Fresh CeO_2 catalyst is loaded inside the reactor

The flow of CO_2 was kept at 6 NmL/min while the HPLC pump was operated at constant flow rate of 10 $\mu\text{L}/\text{min}$ to pump the mixture of methanol and 2-CP at 2:1 molar ratio (see **Appendix C, Chapter 3** for the estimation of the space time [25]). The quartz reactor tube was connected to the reaction system using regular compression fittings, using the approach like that described to achieve the high-pressure sealing [41]. The compression fittings for quartz reactor included SS 316 nuts and Valcon polyimide ferrules (high temperature graphite-reinforced polyimide composite), purchased from Swagelok® and Valco (VICI® AG International) respectively.

For the study of pressure and temperature effects, the reaction system was first stabilized for 2.5 h before starting the sample collection. Pressure effects on the reaction performance were examined from 1 to 30 bar at two temperatures (70 and 120 $^{\circ}\text{C}$) by starting from 30 bar and step-by-step decreasing the pressure in the reactor. Temperature effects were investigated at 30 bar in the range of 80-160 $^{\circ}\text{C}$. The first sample was collected at the lowest examined temperature of 80 $^{\circ}\text{C}$ and then the reaction at higher temperatures were studied. For all the cases (after switching from the initial conditions) 30 min of system stabilization and subsequent 45 min of sample collection period were applied.

3 | Catalysis under microscope

3. 2. 3 Visual inspection and spectroscopic analysis

For the video recording of the catalyst under working conditions, the reactor furnace was modified by opening a channel of ca. 6 cm (long enough to see the whole catalyst bed) in the center of aluminum cover along the catalyst bed (**Figure 3.2**). This channel was covered by a glass window (above the aluminium cover) during the operation to minimize the heat loss while recording the catalyst under working conditions. The image/video recording was performed by two different video cameras: (i) a Panasonic Handy-Cam model SDR-S50 with a 78x enhanced optical zoom to record the overall picture of the furnace and quartz reactor and (ii) an USB digital microscope (800-1000x magnification) – to obtain zoom-in images and videos at the level of the catalyst particles.



Figure 3.2 Home-made Al cover plate for the reactor furnace with ca. 6 cm channeling to allow the recording of the experiments

In situ and *operando* Raman measurements were performed with BWTEK dispersive *i*-Raman spectrometers equipped with 532 and 785 nm excitation lasers and a TE-cooled linear array detector. *Ex situ* Raman measurements were carried out on a Thermo Scientific™ Nicolet™ iS™50 FT-IR Spectrometer equipped with the Raman module with a 1064 nm near-infrared laser. FT-IR measurements were performed at 2 cm⁻¹ resolution on a Bruker Alpha spectrometer equipped with a DTGS detector and a KBr beam splitter using a single-reflection ATR accessory with a diamond internal reflection element. Transmission FT-IR measurements were performed at 2 cm⁻¹ resolution on an Agilent Technologies Cary 630 FTIR spectrometer equipped with a DTGS detector and a DialPath accessory with ZnSe windows at the path length of 100 μm.

Band assignments of IR and Raman spectra were assisted by quantum chemical calculations of vibrational frequencies and intensities and normal mode analysis. They were performed with density functional theory (DFT) using B3PW91 functional [42, 43] with 6-311G(2d,2p) basis sets using Gaussian 09 [44] as an isolated molecule without solvent effects. The simulated IR and Raman spectra are shown as the sum of Lorentzian lines taking the calculated IR/Raman intensity of a normal mode as the height at each vibrational frequency. The vibrational frequencies were empirically scaled by 0.98.

3.3 Results and discussion

3.3.1 Verification of the fused quartz tubular reactor for the continuous DMC synthesis

To test the capabilities of the fused quartz tube as a truly operando reactor, catalytic tests were performed and the catalytic results were evaluated under different reaction conditions. **Figure 3.3** shows the effects of reaction pressure on methanol conversion and product selectivity at 70 °C. As expected from the low reaction temperature, a very low methanol conversion was observed. Still, the use of the highly efficient dehydrating agent (2-CP) afforded 8% methanol conversion at 1 bar, much higher than the value observed at higher temperature at 400 bar without dehydrating agent (ca. 1%) [25]. The level of methanol conversion increased from 8.3% at 5 bar up to 12.4% at 30 bar. The DMC selectivity remained very high in the range of 96.3% (30 bar) – 98.2% (1 bar). The formation of the undesired side products (Me-PCN and Me-CBM, **Reactions 3** and **4**) increased at higher pressures. In fact, Me-CBM formation was only observed under the most DMC-productive condition (70 °C and 30 bar). This is likely a consequence of the enhanced NH₃ formation by increased Me-PCN selectivity (**Reaction 3**) from 1.8% (at 1 bar) to 2.7% (at 30 bar) as well as the enhanced DMC yield (at 30 bar) since products are required for Me-CBM formation (**Reaction 4**).

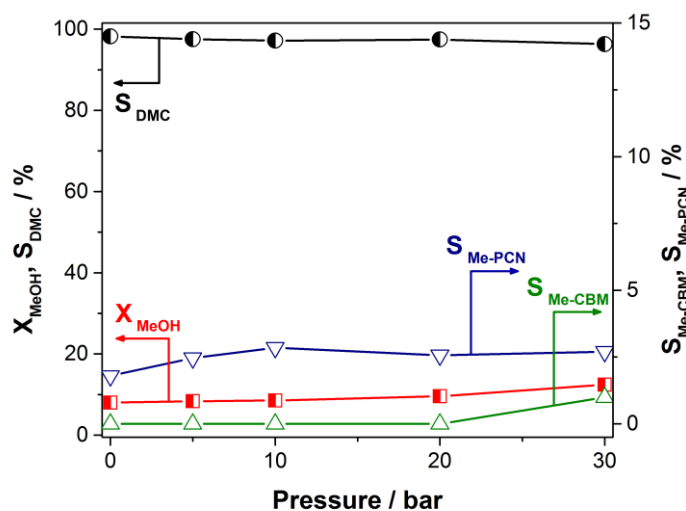


Figure 3.3 Effects of reaction pressure on methanol conversion (X_{MeOH}) and product selectivity (S_i ; $i = \text{DMC, Me-PCN, Me-CBM}$) at 70 °C

Figure 3.4 presents the effects of reaction pressure on methanol conversion and product selectivity at 120 °C. The methanol conversion follows the same profile as that reported in our previous study using a tubular reactor made of stainless steel [25]. The methanol conversion was strongly impacted by the increase in the reaction pressure. Even at 1 bar, 27.6% methanol

3 | Catalysis under microscope

conversion, more than three times higher compared to the value obtained at 70 °C, was observed. Increasing the pressure from 1 to 5 bar resulted in a drastic increase in methanol conversion (72.4%) and the prominent importance of 2-CP in the reaction was once again confirmed. Further increase in methanol conversion from 83.5% (10 bar), 88.6% (20 bar), to >92% (30 bar) was observed in good agreement with our previous work [25]. The increase in reaction pressure resulted in an increase in DMC selectivity by suppressing the formation of by-products. At 1 bar the selectivity towards DMC was 91.2% (with more than 7% Me-PCN selectivity, and ca. 1.5% Me-CBM selectivity), while at 30 bar DMC was produced with >99% selectivity with high methanol conversion (92%). The positive influence of higher reaction pressure is ascribed to the suppression of NH₃ formation which is likely preferred at lower pressure conditions. When NH₃ formation is suppressed, both Me-PCN and Me-CBM formation will be minimized (*vide supra*).

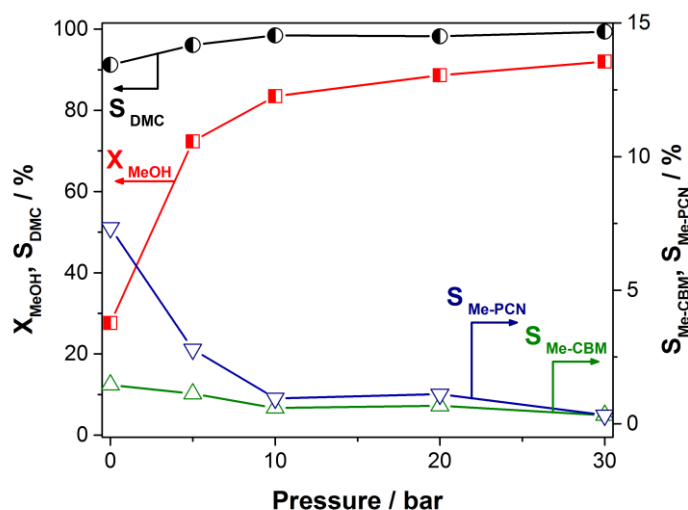


Figure 3.4 Effects of reaction pressure on methanol conversion (X_{MeOH}) and product selectivity (S_i : i = DMC, Me-PCN, Me-CBM) at 120 °C

Figure 3.5 depicts the effects of reaction temperature on methanol conversion and product selectivity at 30 bar. At 80 °C, methanol conversion was low (17.6%) whereas high DMC selectivity (98.7%) was observed. DMC selectivity became very high and reached the maximum (>99%) at 120 °C. Above the temperature, both methanol conversion and DMC selectivity went down. On the contrary, the selectivity towards Me-PCN (3.2% at 140 °C, and 11.4% at 160 °C) and Me-CBM (1.8% at 140 °C, and 6.1% at 160 °C) greatly increased. These results indicate that **Reaction 3** and consequent NH₃ formation become more favorable at higher temperatures. This is most likely related to phase change of the reactants, especially methanol, which become gaseous above the temperature and therefore the suppression effects by the higher-pressure conditions of **Reaction 3** as discussed above are less effective.

The above studies of the reaction temperature and pressure clearly assure that the catalytic reactor made of optically transparent fused quartz can be used as a routine laboratory reactor with the advantages of possible *operando* visual and spectroscopic inspections as described below.

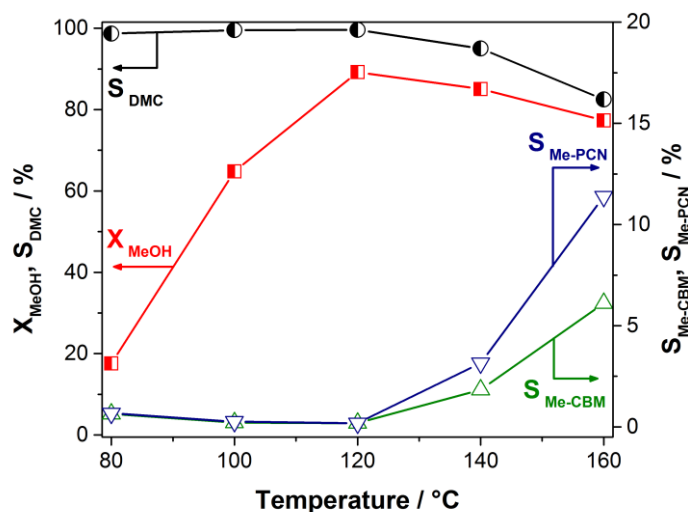


Figure 3.5 Effects of reaction temperature on methanol conversion (X_{MeOH}) and product selectivity (S_i : i = DMC, Me-PCN, Me-CBM) at 30 bar

3.3.2 Catalyst deactivation-reactivation studies assisted by visual inspection

While the advantages of the heterogeneous catalysts over the homogeneous ones are widely recognized (e.g. in terms of product separation, re-use and scale up), one of the major problems that heterogeneous catalysts confront with is catalyst deactivation which become serious when the reaction scale is large. Even though the issue has not been clearly reported when the DMC synthesis was operated in the batch system (the catalyst was regenerated for three consecutive runs by calcination at 550 °C [28]), catalyst deactivation was confirmed when the reaction was run continuously [25].

The first striking observation that has drawn our attention during the catalytic tests using the fused quartz reactor was the color change of the ceria catalyst (from original light yellow color to dark marron or even more blackened one) within the first hours of the reaction. **Figure 3.6** shows the catalysts after ca. 24 hours of reaction and subsequent drying in the furnace at 80 °C. Along with the color change, we could easily observe the formation of small crystallites that agglomerated and covered the surface of the catalyst.

3 | Catalysis under microscope



Figure 3.6 Photograph of the CeO₂ catalyst in the fused quartz reactor after 24 h of the reaction and subsequent drying

The presence of a color gradient along the axial direction of the catalyst bed should be noted as the color change was much more pronounced at the inlet of the reactor and less prominent towards the outlet. In addition, the color change was more accentuated under the condition where high methanol conversion was observed (**Figure 3.7**).

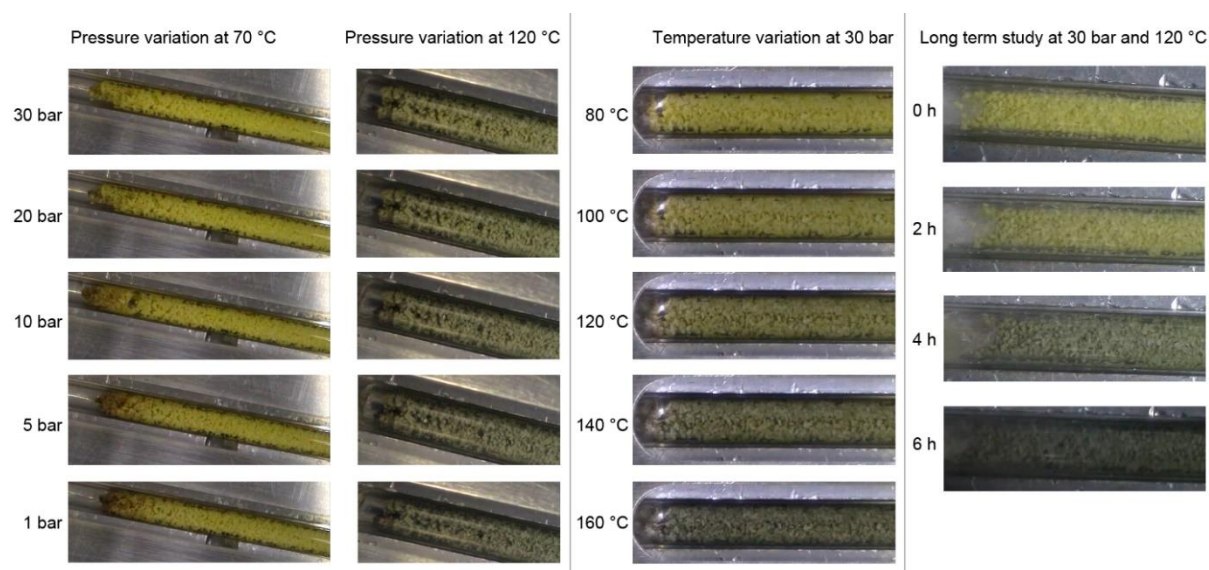


Figure 3.7 Color change of CeO₂ during the DMC synthesis. Snapshots of the catalyst bed close to the inlet of the reactor taken during the verification of the performance of the fused quartz reactors with the Panasonic handy-cam

We suspected that this color change of the catalyst and/or the formation of the substance (looks crystallites) covering the catalyst may be related to or cause the catalyst to deactivate over days of reaction. Hence, some attempts were made to identify the origin of the catalyst deactivation and an optimum condition for catalyst reactivation.

Our first attempt as a reactivation strategy was to wash the catalyst with the polar reactant, methanol. Initially, the washing was performed at room temperature under a small methanol flow at 0.1-0.3 mL/min. Visually no drastic change could be observed with this mild washing condition, resulting only in some surface cleaning of the accumulated crystallites (**Figure 3.8 b**). As the next attempt, methanol was passed through the reactor at a higher flow rate (1-3 mL/min) at 120 °C. This treatment lightened the color of the catalyst remarkably after 30-60 min (**Figure 3.8 c**).



Figure 3.8 Photograph of the CeO_2 catalyst at three different locations along the axial direction of the catalyst bed: **a.** before the reaction, **b.** after the DMC synthesis for 35 h and a short (5-10 s) methanol washing at room temperature to remove the crystallites (Figure 3.6), **c.** subsequent methanol washing at 120 °C for 1 h, and **d.** after calcination of (c) under the flow of air at 300 °C for 12 h

Encouraged by the great color change, catalytic tests were performed after methanol washing treatments at 120 °C and the catalytic activity expressed in terms of methanol conversion was compared with that without methanol washing (Figure 3.9). Without the methanol washing treatment, the activity dropped monotonously from 92.4% to ca. 70% in 70 h. To compare with this profile and check the influence of the washing treatment, the reaction was terminated after 20 h (Figure 3.9, run 1) and the catalyst was washed with methanol thoroughly for 4 h at 120 °C. Then the catalytic test was resumed for another 24 h (Figure 3.9, run 2). The catalytic activity was found to follow the trend of the unwashed catalyst. This procedure was repeated another time with increased washing time (40 h) and the reaction was tested for another 24 h (Figure 3.9, run 3). There was an apparent increase in methanol conversion after the second thorough washing but the increase was minor and followed the reaction profile of the unwashed catalyst. It is worth mentioning that the selectivity towards DMC was stably high (98-99%, not shown) during the catalytic tests after methanol-washing. On the other hand, in the catalytic test without methanol washing the DMC selectivity was slowly decreasing over 70 h of the reaction, reaching the final value around 90%. Even though

3 | Catalysis under microscope

the methanol washing protocol does help to improve the stability of DMC selectivity over time, it does not virtually improve the general aspect of the catalyst deactivation.

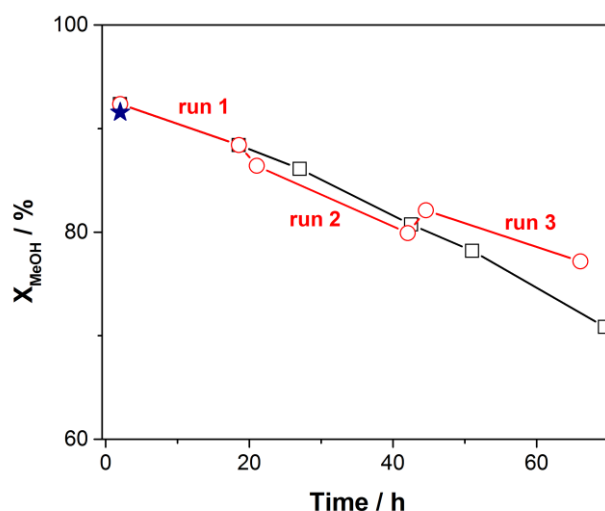


Figure 3.9 Deactivation-reativation study using CeO₂ at 120 °C and 30 bar. Methanol conversion profile **a.** during long-term catalytic test for 70 h (black line) and **b.** three consecutive catalytic runs (red lines) of ca. 20 h with methanol washing between the runs (4 h washing between runs 1 and 2 and 40 h washing between runs 2 and 3, both at 120 °C). The blue star symbol shows the methanol conversion value after calcination of the methanol-washed catalyst at 300 °C

Another strategy of catalyst reactivation by thermal treatment in air was evaluated since this is a general protocol for reactivation, especially to regain reactivity after coking. Thanks to the optically transparent fused quartz reactor, we monitored the color change during the thermal treatment (see video at the online version of the article [45]). The catalyst material got slightly brighter when the temperature of the reactor was raised from 120 to 200 °C under air flow (20 mL/min). Then the temperature was further increased to 300 °C. As soon as the temperature approached ca. 280 °C the color of the catalyst turned lighter into more and more orange. It was just a matter of few seconds (while going from 280 to 290 °C) for the material to turn to light orange. The thermal treatment at 300 °C was sufficient to observe the material completely turning back to the yellowish color close to that of the original material (**Figure 3.8 d**). Remarkably, the catalytic test of this material after the thermal treatment at 300 °C exhibited the identical performance as the original one (**Figure 3.9**) with methanol conversion (91.6%) and DMC selectivity (99.5%). This shows that the simple reactivation protocol under the relatively mild condition is sufficient for full recovery of the catalytic activity.

The textural properties (**Table 3.1**) of i) the catalyst before the reaction, ii) catalysts after the reaction and washing, and iii) after the thermal treatment at 300 °C are in very good agreement with the visual observations and catalytic performance. The material after reaction

and washing showed a drastic decrease in the BET surface area and pore volume, while they were recovered after the thermal treatment.

Table 3.1 BET surface area and pore volume of the CeO₂ catalyst i) before the reaction, ii) after the reaction and washing, and iii) after calcination. Two different batches/experiments are presented for comparison purposes

Property / material	CeO ₂ (initial)	after reaction and washing (batch 1)	after reaction and washing (batch 2)	after calcination (batch 1)	after calcination (batch 2)
S _{BET} (m ² /g)	150	108	119	141	130
Pore volume (cc/g)	0.197	0.135	0.148	0.146	0.156

3.3.3 Spectroscopic investigation of the origin of catalyst deactivation

The use of optically transparent fused quartz reactor is ideal to perform spectroscopic studies, e.g. Raman and UV-Vis spectroscopy for which optical fiber-based spectrometer systems can be conveniently used. Therefore, besides visual inspection of the catalytic reactor, we have performed *operando* Raman study; however, it failed because of the compatibility of the excitation lasers of our mobile Raman systems (532 and 785 nm). Under the reaction conditions, strong fluorescence was observed likely due to the products originating from 2-CP. This was the case also after the thorough methanol washing. Therefore, we have investigated the catalyst materials in the reactor under different conditions (before/after the reaction, after methanol washing, and after air calcination) but *ex situ* using the Raman system equipped with a 1064 nm laser, with which the sample did not show fluorescence.

Figure 3.10 a shows the Raman spectrum of the CeO₂ catalyst after the methanol washing. The spectral features are clearly defined, indicating that the species residing on the catalyst surface is not coke but a more well-defined molecular entity. Also, the intensity due to the surface species increased towards the inlet of the catalyst bed, showing a larger accumulation of the surface species towards the front position as indicated by the darker color (**Figure 3.8 c**). After comparing with Raman spectra of different molecular species, we identified that the Raman spectrum resembles that of 2-PA (**Figure 3.10 b**). The band assignments of 2-PA were made based on the previous reports for the molecule [46-50], the characteristic vibrational frequencies of the carboxamide group [47] and the DFT calculation (**Figure 3.10 c** and normal mode analysis). **Table 3.2** summarizes the observed Raman bands as well as the proposed assignments.

3 | Catalysis under microscope

Table 3.2 Raman band assignments of 2-picolinamide (solid reference), surface species on ceria after the reaction and methanol washing (after subtracting pristine ceria spectrum), and theoretical (DFT) vibrational frequencies of 2-picolinamide. * v - stretching, δ - in-plane bending, γ - out-of-plane bending, ρ - rocking, sh. – shoulder, ~ – hardly identifiable. The notion of assignments is in accordance with Otero *et al.* from J. Colloid. Interf. Sci., 396 (2013) 95

2-PA solid	Surface species on CeO ₂ after methanol washing	2-PA (DFT)	Assignments*
1656	1658 (~)	1750	Amide I
1587	1589	1611 (sh.1593)	8a; ν_{ring}
1569	1574 (~)	1557	8b; ν_{ring}
1470	1479	1478	19a; ν_{ring}
1447	1444	1445	19b; ν_{ring}
1399	1390	1363	Amide III
1289	1295	1299	3; $\delta(\text{CH})$
1254	1245	1280	14; ν_{ring}
1167	1172	1160	13; $\nu(\text{C-X})$
1142	1148	1143	9a; $\delta(\text{CH})$
1099	1102 (~)	1092 (?)	15; $\delta(\text{CH})$
1081	1091	1073	$\rho(\text{NH}_2)$
1043	1048	1045	18a; $\delta(\text{CH})$
998	1008	1000	12; δ_{ring}
824	-	826	10a; $\gamma(\text{CH})$
782	847	767	1; ν_{ring}
750	715 (~)	753 (sh.)	10b; $\gamma(\text{CH})$
642	634 (~)	628	6b; δ_{ring}

The 600–1800 cm^{-1} region of the Raman spectrum of 2-PA (**Figure 3.10 b**) is dominated by the two very strong bands at 998 and 1587 cm^{-1} assigned to δ_{ring} and ν_{ring} modes, respectively. Three significant bands observed at 782, 1167 and 1399 cm^{-1} are assigned to ν_{ring} , $\nu(\text{C}_{\text{ring}}-\text{C}_{\text{amide group}})$, and Amide III (mainly $\nu(\text{C-N})$) vibrations, respectively. The theoretical spectrum of 2-PA (**Figure 3.10 c**) resembles the features of the experimental Raman spectrum of 2-PA with a few exceptions, e.g. the band at 1750 cm^{-1} (theory) corresponding to Amide I (mostly C=O stretching) which appears ca. 95 cm^{-1} red-shifted (experiment), the band at 1611 cm^{-1} (theory, corresponding to ν_{ring}) which appears ca. 25 cm^{-1} red-shifted (experiment), and the band at 1363 cm^{-1} (theory, corresponding to Amide III) which appears ca. 35 cm^{-1} blue-shifted (experiment). These bands are mainly related to the vibrations of the amide functional group in 2-PA and they are likely shifted in the experimental spectrum because 2-PA molecules are packed in a form of crystallites within the sample via inter-molecular interactions via the amide group.

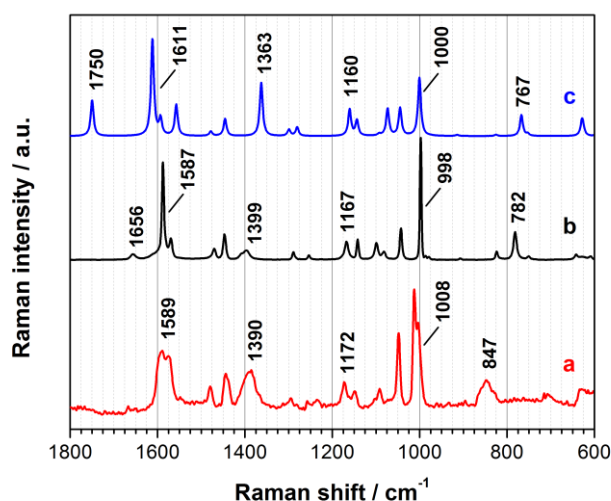
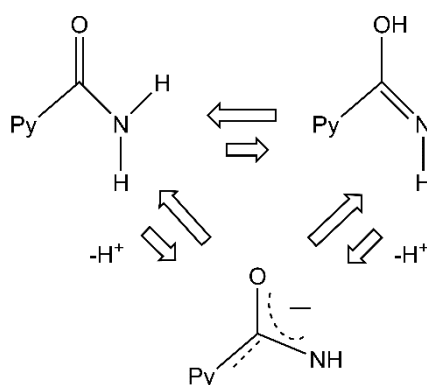


Figure 3.10 Raman spectra of **a.** the CeO₂ catalyst after the reaction and after the methanol-washing treatment (Figure 3.8 c) and after subtracting spectral contribution of CeO₂, **b.** 2-PA powder, and **c.** 2-PA calculated by the DFT method

The Raman spectrum of the surface species over the methanol-washed CeO₂ after the reaction (**Figure 3.10 a**) can be easily correlated with the bands of 2-PA (**Figure 3.10 b** and **3.10 c**) with a few notable differences. The band at 847 cm⁻¹ of the surface species appeared much more broadened and blue-shifted by 65 cm⁻¹ compared to the band at 782 cm⁻¹ of 2-PA. The band is assigned to the vibration involving a combined contribution of δ_{ring} and $\nu(\text{C}_{\text{ring}}-\text{C}_{\text{amide group}})$ [49]. Remarkably, the band corresponding to Amide I is hardly observable or red-shifted to the extent that merged with the band at ca. 1590 cm⁻¹. The great band shifts of the two bands indicate that 2-PA is adsorbed on the surface via the amide group.

A very similar shift of the first band (combined δ_{ring} and $\nu(\text{C}_{\text{ring}}-\text{C}_{\text{amide group}})$) was observed in the SERS spectra of benzamide [51, 52] and 2-PA [46, 50], undergoing a blue-shift of the same magnitude with respect to the Raman band of the solids of the respective molecule (53 and 48 cm⁻¹, respectively). The observed blue-shift has been attributed by Otero and co-workers [50, 52] to the adsorption of benzamide or 2-PA molecule on the metal surface in its azanion (Ar-CONH⁻/Py-CONH⁻; Ar = aryl and Py = pyridyl ring) form, that is, with the carboxamide group partially deprotonated. While the formation of the azanion goes via deprotonation of the tautomeric carboxamide and carboximidic forms of the corresponding amides (**Scheme 3.1**), the high stability of the deprotonated amide could be due to electron delocalization along the π -system of the functional group and the pyridyl ring.

3 | Catalysis under microscope



Scheme 3.1 Formation of the azanion by deprotonation of the tautomeric carboxamide and carboximide forms of 2-PA [50]

Furthermore, **Figure 3.11** shows a similar study by IR spectroscopy. For the IR study, the 2-PA spectrum was measured in transmission mode in a diluted manner in an apolar solvent (toluene) to minimize the intermolecular interactions which were observed for the solid sample (not shown). The IR spectrum of the catalyst after the methanol washing was recorded by removing the sample from the reactor and in the ATR sampling configuration to minimize light absorption by CeO_2 and to maximize signals from surface species. The band assignments of 2-PA are based on those previously proposed for this molecule [48, 49, 53, 54] as well as by the DFT calculation. **Table 3.3** summarizes the observed IR bands as well as the proposed assignments.

The 600–1800 cm^{-1} region of the IR spectrum of 2-PA (**Figure 3.11 b**) is dominated by four important features at 750, 1368, 1557, and 1700 cm^{-1} assigned to δ_{ring} , $\nu(\text{C-N})$, $\delta(\text{NH}_2)$, and $\nu(\text{C=O})$ modes, respectively. The theoretical IR spectrum of 2-PA (**Figure 3.11 c**) is in good agreement with the experimental one (**Figure 3.11 b**) except the band at 1750 cm^{-1} which corresponds to $\nu(\text{C=O})$, indicating that the vibrational mode is still, upon dilution in toluene, mildly interacting intermolecularly via the N-H group of the amide group.

Table 3.3 IR bands assignments for 2-picolinamide (0.1 M in toluene), surface species on ceria after the reaction and methanol washing (after subtracting pristine ceria spectrum), and theoretical (DFT) vibrational frequencies of 2-picolinamide. * ν - stretching, δ - in-plane bending, γ - out-of-plane bending

2-PA liquid	2-PA on CeO ₂	2-PA (DFT)	Assignments*
1700	–	1750	$\nu(\text{C=O})$ – Amide I
1590	1597	1612	ν_{ring}
1569	1582	1593	ν_{ring}
1557	1562	1557	$\delta(\text{NH}_2)$ – Amide II
–	1476	1478	$\nu_{\text{ring}} + \delta(\text{CH})$
–	1443	1445	ν_{ring}
1386, 1368	1393	1363	$\nu(\text{C-N})$ – Amide III
1289	1293	1299	$\delta(\text{CH})$
1250	1254	1280	ν_{ring}
1160	1170	1160	ν_{ring}
1042	1046	1044	δ_{ring}
998	1007	1001	δ_{ring}
820	849	825	$\gamma(\text{C=O})$
750	750	753	δ_{ring}
705	700	711	$\gamma(\text{CH})$

The IR spectrum of the surface species on CeO₂ after the reaction (**Figure 3.11 a**) can be again correlated with the characteristic bands of 2-PA (**Figure 3.11 b** and **3.11 c**). The notable difference is the absence or rather likely a significant red-shift of the $\nu(\text{C=O})$ mode. Furthermore, two broad bands at ca. 1393 and ca. 1562 cm⁻¹ are observed. The broadness of the bands as well as the suspected large red-shift of $\nu(\text{C=O})$ bands indicate that the surface species (likely 2-PA) interact with the heterogeneous structure of the CeO₂ surface via the amide group in a flexible manner or via various configurations of adsorption. According to literature, the existence of the CON functional group and the formation of 2-PA monoanion (Py-CONH⁻) on CeO₂ surface can be suggested [55-61]. Moreover, no trace of nitrile group ($-\text{CN}$, characteristic absorption around 2200-2300 cm⁻¹) was observed on the IR spectrum of CeO₂ after the reaction and washing. This clearly indicates that not 2-CP but 2-PA-like species are responsible for poisoning the catalyst by strongly binding over the active sites of the CeO₂ surface.

3 | Catalysis under microscope

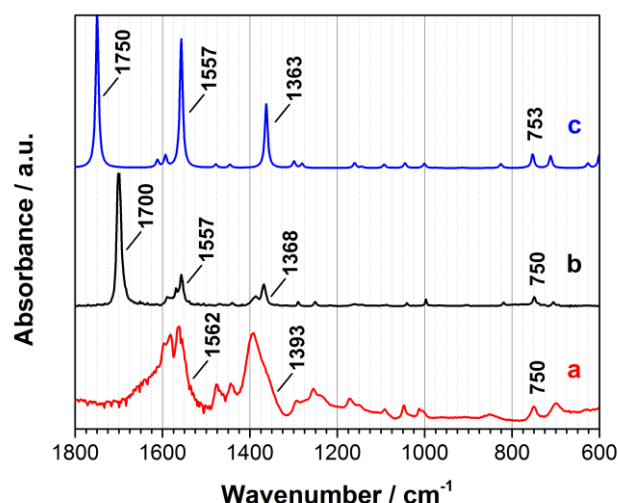
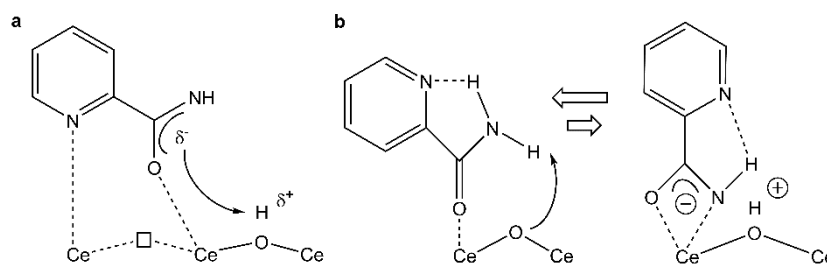


Figure 3.11 IR spectra of **a.** the CeO₂ catalyst after the reaction and after the methanol-washing treatment (Figure 3.8 c) and after subtracting spectral contribution of CeO₂, **b.** 0.1 M 2-PA in toluene (toluene contribution subtracted), and **c.** 2-PA calculated by the DFT method

In the direct DMC synthesis from CO₂ and methanol in the presence of 2-CP in a batch system, Tomishige *et al.* reported that the presence of an effective nitrile will lead, upon hydration, to amides that can weakly adsorb on CeO₂ surface via intramolecular H bonding and that they can easily desorb from the surface, thereby not causing catalyst poisoning [28, 29]. At the same time, mechanistic studies of the nitriles hydration to amides over CeO₂ catalysts confirm the presence of an amide anion intermediate (**Scheme 3.2**) [29] which was resulted via the interaction of both N and O atoms of this ionized amide group with the surface Ce atom as the key step of the reaction [60]. This intermediate is similar to the species indicated by the Raman and IR studies and likely causing deactivation.



Scheme 3.2 a. A proposed mechanism for nitrile hydration on CeO₂ going via the amide anion intermediate (adapted from [61] with permission from The Royal Society of Chemistry) and **b.** the suggested adsorption state of 2-PA in direct DMC synthesis from CO₂ and methanol (batch system) in the presence of 2-CP (adapted from [29] with permission from Elsevier)

The visual inspection (**Figure 3.8**) and catalyst reactivation study (**Figure 3.9**) indicated that the reactivation takes place, judging from the color change, in the temperature interval

between 280-290 °C and completes below 300 °C. Very interestingly, this temperature matches with the boiling point of 2-PA (284.1 °C at 760 mmHg; see [Section 2.2.2.2 Separation system](#) for complete data). Taking the Raman and IR spectroscopic results into account, we attribute that 2-PA is adsorbed via the amide group over CeO₂ and it causes the catalyst to deactivate.

3.3.4 Operando visual inspection

Using the fused quartz reactor, we have finally attempted to shed light on the catalyst surface under operando conditions where gas (CO₂ and methanol) and liquid (2-CP and 2-PA) are mixed over the catalyst surface at the optimum temperature (120 °C). According to our previous study, the residence time of the reactants was roughly estimated to be ca. 20 s at 30 bar [25]. It is of great interest and importance to understand how the catalytic interface of the three-phase boundary looks like to gain insights into the mass transfer and key factors enabling the high methanol conversion and DMC selectivity within such a short residence time in comparison to the batch reaction cases (in the order of hours).

Occasional traveling of liquid droplets through the catalyst bed could be observed at 70 °C (not shown), but this was not the case at 120 °C. Although at first glance the catalyst under the optimum condition (30 bar, 120 °C) looked dry, a closer look at the magnified level of the catalyst particle clarified that the surface of the catalyst was constantly wet. This indicates that 2-CP, 2-PA and possibly methanol cover CeO₂ catalyst as liquid and CO₂ gets dissolved into the liquid to get in contact with the reactants as well as the catalyst surface for the reaction to take place. Also, there was a formation of white islands (likely the crystallites of 2-PA) growing with time over the catalyst surface. The color of the islands and coating changed darker upon drying and this was the coating removed by hot-methanol washing as described above. Apparently, the surface become more dry at lower pressure conditions ([Figure 3.12](#)) probably due to the higher actual flow rate of gas phase CO₂ and methanol at lower pressures, which facilitated the removal of the liquid phase coating over the catalyst surface. This could have positively impacted on the reaction performance by improving the contact of CO₂ with the reactants and with the catalyst surface, but it was not the case and higher pressure condition (where the catalyst surface was more wet) was favorable for the catalytic performance ([Figure 3.4](#)). Longer residence time at higher pressure conditions may also contribute to the enhanced catalytic performance.

The catalyst deactivated but not completely after some days of the reaction. This implies that the active sites of the catalyst are still accessible when the catalyst surface is covered by coating of some crystallites. The visual inspection has elucidated the accessibility of the bulk region of the catalyst particle. The video (see online version of the article [45]) shows that

3 | Catalysis under microscope

when liquid droplets (mainly products and 2-PA) travels back through the reactor upon a sudden set-pressure decrease, the whole catalyst particle gets soaked by the droplets as evidenced by the color change. This clearly indicates the accessibility of catalytic sites in the bulk, thus maintaining the catalytic activity over some days of operation without full deactivation by the surface coating with the crystallites.



Figure 3.12 *Operando* visualization of the CeO₂ catalyst during the DMC synthesis from CO₂ and methanol in the presence of 2-CP. The experiment was started under the optimized reaction condition (30 bar, 120 °C) and the reaction pressure was lowered. The darker color at lower pressures is caused by the time-sequence of the experiment

3. 4 Conclusions

The present study shows a successful demonstration on how one can employ fused quartz reactors to gain unique insights into the continuous dimethyl carbonate (DMC) synthesis from carbon dioxide and methanol over CeO₂ catalysts in the presence of a dehydrating agent (2-cyanopyridine). The catalytic performance was identical to that using a conventional stainless steel reactor. The fused quartz reactor can offer new perspectives on the catalytic process and design by the verified idea that a picture is worth a thousand words (or numerous experiments without seeing inside). It allowed the visual inspection of the catalyst under working conditions and it was possible to observe the drastic color change of the ceria materials (from light yellow to dark maroon) even within the first few hours of reaction. These observations were correlated with the methanol conversion drop. Based on the Raman and IR studies, it was identified that 2-picolinamide (and not coke formation) is the main source of catalyst deactivation by strongly binding to and thus poisoning the catalyst surface. The *ex situ* space resolved spectroscopic studies along the catalyst bed revealed the existence of a gradient reflecting how much the catalyst was poisoned (more intense towards the inlet and less intense towards the outlet of the reactor) in good agreement with the color gradient visually observed. Complete catalyst reactivation was achieved under mild conditions, just by using in situ methanol washing coupled with a moderate thermal treatment at the temperature slightly above the boiling point of 2-picolinamide. Moreover, the use of quartz reactors afforded the observation of the complete synergy between the solid catalyst, the liquid methanol and 2-cyanopyridine mixture, and gaseous CO₂. The reaction is taking place in both bulk and surface of CeO₂ catalyst. This study opens new opportunities in heterogeneous catalysis on

how to investigate continuous processes with involved deactivation processes at three-phase boundaries and how to take advantage of the visual observations for better understanding and optimization of heterogeneously catalyzed reactions.

Bibliography

- [1] P. Friedlingstein, R.A. Houghton, G. Marland, J. Hackler, T.A. Boden, T.J. Conway, J.G. Canadell, M.R. Raupach, P. Ciais, C. Le Quéré, *Nat. Geosci.*, 3 (2010) 811–812.
- [2] T.M. Gerlach, *Eos, Trans. Amer. Geophys. Union*, 92 (2011) 201-202.
- [3] A. Bansode, A. Urakawa, *J. Catal.*, 309 (2014) 66–70.
- [4] Y. Ono, *Appl. Catal. A-Gen.*, 155 (1997) 133–166.
- [5] A.-A.G. Shaikh, S. Sivaram, *Chem. Rev.*, 96 (1996) 951–976.
- [6] N. Keller, G. Rebmann, V. Keller, *J. Mol. Catal. A-Chem.*, 317 (2010) 1-18.
- [7] D. Delledonne, F. Rivetti, U. Romano, *Appl. Catal. A-Gen.*, 221 (2001) 241–251.
- [8] M. Aresta, E. Quaranta, *ChemTech*, 27 (1997) 32-40.
- [9] T. Sakakura, J.-C. Choi, H. Yasuda, *Chem. Rev.*, 107 (2007) 2365–2387.
- [10] M.A. Pacheco, C.L. Marshall, *Energ. Fuel.*, 11 (1997) 2–29.
- [11] K. Tomishige, T. Sakaihorii, Y. Ikeda, K. Fujimoto, *Catal. Lett.*, 58 (1999) 225-229.
- [12] K. Tomishige, Y. Ikeda, T. Sakaihorii, K. Fujimoto, *J. Catal.*, 192 (2000) 355–362.
- [13] Y. Ikeda, T. Sakaihorii, K. Tomishige, K. Fujimoto, *Catal. Lett.*, 66 (2000) 59-62.
- [14] Y. Ikeda, M. Asadullah, K. Fujimoto, K. Tomishige, *J. Phys. Chem. B*, 105 (2001) 10653–10658.
- [15] K. Tomishige, Y. Furusawa, Y. Ikeda, M. Asadullah, K. Fujimoto, *Catal. Lett.*, 76 (2001) 71-74.
- [16] K. Tomishige, K. Kunimori, *Appl. Catal. A-Gen.*, 237 (2002) 103–109.
- [17] H.J. Hofmann, A. Brandner, P. Claus, *Chem. Eng. Technol.*, 35 (2012) 2140–2146.
- [18] Y. Yoshida, Y. Arai, S. Kado, K. Kunimori, K. Tomishige, *Catal. Today*, 115 (2006) 95–101.
- [19] M. Aresta, A. Dibenedetto, C. Pastore, C. Cuocci, B. Aresta, S. Cometa, E.D. Giglio, *Catal. Today*, 137 (2008) 125–131.
- [20] M. Aresta, A. Dibenedetto, C. Pastore, A. Angelini, B. Aresta, I. Pápai, *J. Catal.*, 269 (2010) 44–52.
- [21] X.L. Wu, M. Xiao, Y.Z. Meng, Y.X. Lu, *J. Mol. Catal. A-Chem.*, 238 (2005) 158–162.
- [22] X.L. Wu, Y.Z. Meng, M. Xiao, Y.X. Lu, *J. Mol. Catal. A-Chem.*, 249 (2006) 93–97.
- [23] B.A.V. Santos, V.M.T.M. Silva, J.M. Loureiro, D. Barbosa, A.E. Rodrigues, *Fluid Phase Equilib.*, 336 (2012) 41–51.
- [24] B.A.V. Santos, C.S.M. Pereira, V.M.T.M. Silva, J.M. Loureiro, A.E. Rodrigues, *Appl. Catal. A-Gen.*, 455 (2013) 219–226.
- [25] A. Bansode, A. Urakawa, *ACS Catal.*, 4 (2014) 3877–3880.

- [26] B.A.V. Santos, V.M.T.M. Silva, J.M. Loureiro, A.E. Rodrigues, *Ind. Eng. Chem. Res.*, 53 (2014) 2473–2483.
- [27] C.-F. Li, S.-H. Zhong, *Catal. Today*, 82 (2003) 83–90.
- [28] M. Honda, M. Tamura, Y. Nakagawa, S. Sonehara, K. Suzuki, K.-i. Fujimoto, K. Tomishige, *ChemSusChem*, 6 (2013) 1341–1344.
- [29] M. Honda, M. Tamura, Y. Nakagawa, K. Nakao, K. Suzuki, K. Tomishige, *J. Catal.*, 318 (2014) 95–107.
- [30] M.A. Bañares, *Catal. Today*, 100 (2005) 71–77.
- [31] S.J. Tinnemans, J.G. Mesu, K. Kervinen, T. Visser, T.A. Nijhuis, A.M. Beale, D.E. Keller, A.M.J.v.d. Eerden, B.M. Weckhuysen, *Catal. Today*, 113 (2006) 3–15.
- [32] T.A.X. Nijhuis, S.J. Tinnemans, T. Visser, B.M. Weckhuysen, *Phys. Chem. Chem. Phys.*, 5 (2003) 4361–4365.
- [33] J.W. Couves, J.M. Thomas, D. Waller, R.H. Jones, A.J. Dent, G.E. Derbyshire, G.N. Greaves, *Nature*, 354 (1991) 465–468.
- [34] A.M. Beale, A.M.J.v.d. Eerden, K. Kervinen, M.A. Newton, B.M. Weckhuysen, *Chem. Commun.*, (2005) 3015–3017.
- [35] A. Brückner, E. Kondratenko, *Catal. Today*, 113 (2006) 16–24.
- [36] M.G. O'Brien, A.M. Beale, S.D.M. Jacques, M.D. Michiel, B.M. Weckhuysen, *ChemCatChem Catalysis*, 1 (2009) 99 – 102.
- [37] B. Potic, S.R.A. Kersten, M. Ye, M.A.v.d. Hoef, J.A.M. Kuipers, W.P.M.v. Swaaij, *Chem. Eng. Sci.*, 60 (2005) 5982 – 5990.
- [38] B. Potic, S.R.A. Kersten, W. Prins, W.P.M.v. Swaaij, *Ind. Eng. Chem. Res.*, 43 (2004) 4580–4584.
- [39] C. Tellaeche, B. Glöckler, G. Kolios, U. Nieken, *Chem. Eng. Technol.*, 32 (2009) 1348–1357.
- [40] B. Glöckler, H. Dieter, G. Eigenberger, U. Nieken, *Chem. Eng. Sci.*, 62 (2007) 5638 – 5643.
- [41] A. Bansode, G. Guilera, V. Cuartero, L. Simonelli, M. Avila, A. Urakawa, *Rev. Sci. Instrum.*, 85 (2014) 084105
- [42] A.D. Becke, *J. Chem. Phys.*, 98 (1993) 5648–5652.
- [43] J.P. Perdew, Y. Wang, *Phys. Rev. B*, 45 (1992) 13244–13249.
- [44] M.J. Frisch, G.W. Trucks, H.B. Schlegel, G.E. Scuseria, M.A. Robb, J.R. Cheeseman, G. Scalmani, V. Barone, B. Mennucci, G.A. Petersson, H. Nakatsuji, M. Caricato, X. Li, H.P. Hratchian, A.F. Izmaylov, J. Bloino, G. Zheng, J.L. Sonnenberg, M. Hada, M. Ehara, K. Toyota, R. Fukuda, J. Hasegawa, M. Ishida, T. Nakajima, Y. Honda, O. Kitao, H. Nakai, T. Vreven, J. Montgomery, J. A., J.E. Peralta, F. Ogliaro, M. Bearpark, J.J. Heyd, E. Brothers, K.N. Kudin, V.N. Staroverov, R. Kobayashi, J. Normand, K.

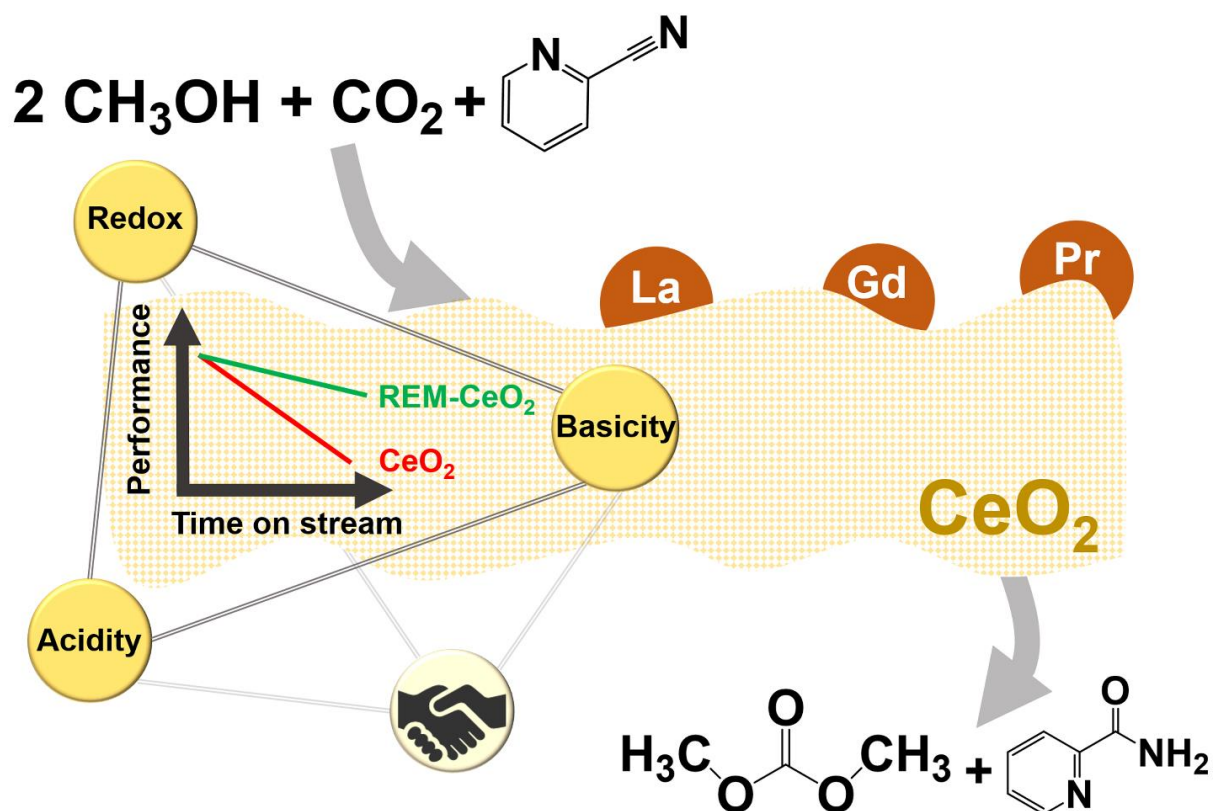
3 | Catalysis under microscope

- Raghavachari, A. Rendell, J.C. Burant, S.S. Iyengar, J. Tomasi, M. Cossi, N. Rega, J.M. Millam, M. Klene, J.E. Knox, J.B. Cross, V. Bakken, C. Adamo, J. Jaramillo, R. Gomperts, R.E. Stratmann, O. Yazyev, A.J. Austin, R. Cammi, C. Pomelli, J.W. Ochterski, R.L. Martin, K. Morokuma, V.G. Zakrzewski, G.A. Voth, P. Salvador, J.J. Dannenberg, S. Dapprich, A.D. Daniels, O. Farkas, J.B. Foresman, J.V. Ortiz, J. Cioslowski, D.J. Fox, Gaussian 09, Revision A.02, Gaussian, Inc., Wallingford CT, 2009.
- [45] D. Stoian, A. Bansode, F. Medina, A. Urakawa, *Catal. Today*, (2016) <http://dx.doi.org/10.1016/j.cattod.2016.1003.1038>.
- [46] J.F. Arenas, M.A. Montanez, J.C. Otero, J.I. Marcos, *J. Mol. Struct.*, 293 (1993) 341-344.
- [47] N.P.G. Roeges, *A Guide to the Complete Interpretation of Infrared Spectral of Organic Structures*, Wiley 1994.
- [48] E. Akalin, S. Akyuz, *Vib. Spectrosc.*, 42 (2006) 333–340.
- [49] M. Bakiler, O. Bolukbasi, A. Yilmaz, *J. Mol. Struct.*, 826 (2007) 6-16.
- [50] J.L. Castro, J.F. Arenas, M.R. Lopez-Ramirez, J. Soto, J.C. Otero, *J. Colloid. Interf. Sci.*, 396 (2013) 95–100.
- [51] J.F. Arenas, J.L. Castro, J.C. Otero, J.I. Marcos, *J. Raman Spectrosc.*, 23 (1992) 249-252.
- [52] J.L. Castro, M.R. Lopez-Ramirez, J.F. Arenas, J. Soto, J.C. Otero, *Langmuir*, 28 (2012) 8926–8932.
- [53] S. Akyuz, T. Akyuz, *Vib. Spectrosc.*, 42 (2006) 387–391.
- [54] A. Borba, A. Gomez-Zavaglia, R. Fausto, *J. Phys. Chem. A*, 112 (2008) 45-57.
- [55] H. Krietenbrink, H. Knözinger, *Z. Phys. Chem.*, 102 (1976) 43-56.
- [56] D.K. Paul, S.D. Worley, *J. Phys. Chem.*, 94 (1990) 8956–8959.
- [57] A. Aboulayt, C. Binet, J.-C. Lavalley, *J. Chem. Soc., Faraday Trans.*, 91 (1995) 2913-2920.
- [58] W.-C. Wu, L.-F. Liao, C.-C. Chuang, J.-L. Lin, *J. Catal.*, 195 (2000) 416–419.
- [59] C.-C. Chuang, W.-C. Wu, M.-X. Leea, J.-L. Lin, *Phys. Chem. Chem. Phys.*, 2 (2000) 3877-3882.
- [60] L.-F. Liao, C.-F. Lien, D.-L. Shieh, F.-C. Chen, J.-L. Lin, *Phys. Chem. Chem. Phys.*, 4 (2002) 4584–4589.
- [61] M. Tamura, A. Satsuma, K.-i. Shimizu, *Catal. Sci. Technol.*, 3 (2013) 1386-1393.

4

Effects of REM promoters

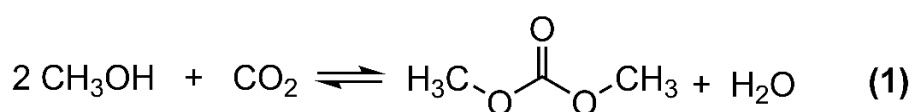
Improving the stability of CeO_2 catalyst in the continuous dimethyl carbonate synthesis from CO_2 and methanol with 2-cyanopyridine



4 | Effects of REM promoters

4.1 Introduction

One of the major global challenges urged by the climate change and the desired paradigm shift from the fossil-fuels dependent society to a more sustainable one is the carbon management, i.e. how to efficiently utilize carbon dioxide (CO₂) being emitted and accumulated in the atmosphere. Catalytic transformation of CO₂ into useful chemicals such as organic and inorganic carbonates via non-reductive CO₂ transformations has been widely investigated for that aim [1-3]. Among others, the synthesis of alkyl carbonates through direct carboxylation reaction of alcohols like methanol (**Reaction 1**, synthesis of dimethyl carbonate (DMC)) is very attractive in terms of atom economy [1, 4].

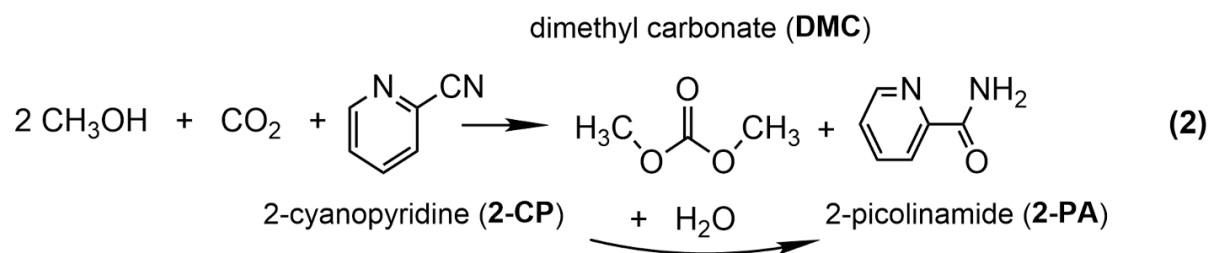


DMC is a versatile chemical and represents an ecologically benign alternative to toxic and corrosive methylating or carbonylating agents such as methyl halides (CH₃X), dimethyl sulfate (DMS), and phosgene (COCl₂) [1, 4-7]. DMC is used in the synthesis of polycarbonates and polyurethanes, as solvent replacing methyl ethyl ketone, butanone, and *tert*-butyl acetate, and as electrolyte in lithium ion batteries [1, 2, 4]. Furthermore, DMC has gained wide attention as an oxygenate fuel additive due to its high oxygen content, thus increasing combustion performance [8].

In the methanol carboxylation reaction with CO₂, many heterogeneous catalysts have been investigated to date. ZrO₂, SiO₂, Al₂O₃, TiO₂, H-ZSM5, H-USY, H-MOR, ZnO, MoO₃, Bi₂O₃, MgO, Y₂O₃, HfO₂, La₂O₃, Pr₆O₁₁, Ga₂O₃, GeO₂, In₂O₃, Sb₂O₃, and hybrid ones (e.g. H₃PO₄/V₂O₅ and Cu-Ni/V₂O₅-SiO₂) have been tested, but without or with very low activity (e.g. 0.3 mmol DMC g_{cat}⁻¹ h⁻¹ for zirconia (ZrO₂) materials) [9-13]. Occasionally, dimethyl ether (DME) instead of DMC was produced via dehydration reaction of methanol, which is commonly catalyzed by acidic sites, especially at high temperatures (>150 °C). According to previous studies, ZrO₂ and ceria (CeO₂) are the unique materials effectively catalyzing the DMC formation [9, 10, 14-21]. However, the major challenge is associated with the thermodynamics of **Reaction 1**, which is generally unfavorable due to equilibrium limitation. Even under thermodynamically favorable high-pressure conditions (>150 bar), DMC yield is ca. 1% in accordance with the thermodynamic expectation [22-24]. Therefore, it is imperative to employ an effective mean to shift the equilibrium to the product side for potential commercialization of DMC synthesis from CO₂ and methanol. It is well known that water removal can shift the equilibrium improving DMC yield. Chemical (e.g. 2,2-dimethoxy propane (DMP)) or physical

water traps [17, 25] and catalytic membrane reactors [26] have been employed for this purpose but the improvement had been relatively minor.

In 2013, Tomishige *et al.* described the DMC synthesis over CeO₂ in a batch reactor using a nitrile (2-cyanopyridine, 2-CP) as an organic dehydrating agent and reported an exceptionally high DMC yield of 94%. In the reaction, CeO₂ functioned as an effective catalyst for both DMC synthesis and nitrile hydrolysis, with 2-CP forming the corresponding amide (2-picolinamide, 2-PA, **Reaction 2**) [27, 28].



They also verified the recyclability of 2-PA by dehydrating 2-PA back to 2-CP with Na₂O/SiO₂ as catalyst. Together with the formation of DMC and 2-PA, very small amounts of methyl picolinate (Me-PCN) and methyl carbamate (Me-CBM) were found as byproducts. Me-PCN is co-produced with NH₃ because of the reaction between 2-PA and methanol, while Me-CBM originates from the reaction between DMC and NH₃ (**3.1 Introduction Reaction 3 and 4**).

Inspired by the work of Tomishige *et al.*, our group reported continuous DMC synthesis over CeO₂ in a fixed-bed reactor in the presence of 2-CP under low-to-high pressure conditions (up to 300 bar) [24]. Although striking DMC yields >90% were achieved during the continuous operation above 30 bar, a severe catalyst deactivation was noticed, resulting in more than 50% drop in methanol conversion in 10 days with a small loss (8-9%) in DMC selectivity. Our following investigation unravelling the cause of the catalyst deactivation by visual and spectroscopic inspections using an optically transparent fused quartz reactor. Most importantly, results showed molecularly adsorbed 2-PA over the deactivated CeO₂ catalyst. However, the catalyst could be reactivated when the adsorbed 2-PA was removed from the surface by a simple thermal treatment in air at 300 °C [29].

Motivated by the previous results and the superior DMC yield in the presence of 2-CP in comparison to other dehydrating agents [17, 30, 31] using CeO₂ as catalyst, the present study seeks for stable and active CeO₂-based catalysts in the reaction under continuous operation as well as to understand the material factors influencing the catalytic performance. The uniquely high catalytic activity of CeO₂ in this reaction may originate from the redox capabilities of the cerium oxide in conjunction with its acid-base properties [32-36]. Therefore, in this work

4 | Effects of REM promoters

common strategies to modify the chemical properties of CeO₂ such as the addition of metal and metal oxides to CeO₂ to influence the oxygen storage capacity, defect stability, and mobility of oxygen atoms were examined and their impacts on catalyst stability were thoroughly investigated. Specifically, Zr⁴⁺ [37, 38], La³⁺ [37, 39, 40], Gd³⁺ [41, 42], and Pr^{4+/3+} [43-46] promoters were chosen to influence the oxygen defects/mobility of CeO₂ based materials and Rh [47, 48], Ru [49-52], and Pd [53, 54] promoters were chosen to enhance the catalytic activity by the strong interaction with CeO₂. Besides the use of an ordinary stainless-steel tubular reactor, an optically transparent fused-quartz tubular reactor was employed in order to visually assess the deactivating state of the catalysts under the optimized reaction conditions (30 bar and 120 °C) [29]. Subsequently, the catalysts before and after the reactions were characterized by several techniques to identify critical material factors determining the catalytic activity and stability of the materials.

4. 2 Experimental

4. 2. 1 Materials

High surface area powders of CeO₂ and CeO₂-ZrO₂ solid solutions (78-22, 50-50, and 25-75 wt%) were kindly supplied by Daiichi Kigenso Kagaku Kogyo Co. Ltd., Japan and used without any further treatment. High surface area ZrO₂ (1/8" pellets) was purchased from Alfa Aesar and used as received. Precious metals (1 wt% Ru, Rh, Pd) and rare earth metals (REM) promoted ceria materials (**x** wt% **M** on CeO₂, where **x** = 0.25, 1, and 5 and **M** = La, Gd, and Pr) were synthesized by the incipient wetness impregnation of the pristine CeO₂ with an aqueous solution of the metal precursor (chloride precursors for the precious metals and lanthanum (III) nitrate hexahydrate, gadolinium (III) nitrate hydrate, and praseodymium (III) nitrate hydrate, respectively for REM). The metal nitrates and chlorides (99.9% purity) were purchased from Alfa Aesar. The impregnated materials were dried overnight at 80-90 °C in an oven and calcined at 400 °C for 4 h in a static air after a temperature ramp of 2 °C min⁻¹. Methanol (≥99.9%, HPLC grade) and 2-cyanopyridine (2-CP, 99%) were purchased from Sigma Aldrich. High purity CO₂ gas (>99.9993%) was purchased from Abelló Linde, Spain.

4. 2. 2 Reaction system

The details of the reaction set-up and analytical method for the identification and quantification of reaction products were described in our previous works [24, 29]. In a typical experiment, 300 mg of the catalyst (pelletized, crushed, and sieved to 200-300 μm particle size) was loaded into the reactor tube (a stainless-steel tube with ID: 1.74 mm and OD: 3.17 mm). For the visual inspection experiments, a fused quartz reactor (ID: 2.0 mm and OD: 3.0 mm) was used [29]. The CO₂ flow rate was kept at 6 NmL min⁻¹. The mixture of methanol and

2-CP at 2:1 molar ratio (methanol:CO₂ = 1:2.5, molar ratio) was passed to the reactor at 10 μL min⁻¹ by means of an HPLC pump (Jasco, PU-2080 Plus).

All catalytic tests were performed under optimized reaction conditions where the DMC yield is high while the reaction pressure is relatively mild (30 bar and 120 °C) [29]. We aimed to perform the reaction for over 100 h, but occasionally the reaction had to be stopped before due to the sealing issue of back pressure regulator (Jasco, BP-2080 Plus) caused by the high-temperature kept at the regulator and the clogging or damage of the sealing materials [29]. Nevertheless, the reaction was performed more than 48 h to observe a clear trend in catalytic activity, evaluate catalyst deactivation, and calculate its rate.

4. 2. 3 Characterization

X-ray diffraction (XRD) measurements were made using a Siemens D5000 diffractometer (Bragg-Brentano parafocusing geometry and vertical θ - θ goniometer) fitted with a curved graphite diffracted-beam monochromator, incident and diffracted-beam Soller slits, a 0.06° receiving slit and scintillation counter as a detector. The angular 2 θ diffraction range was between 5 and 70°. The data were collected with an angular step of 0.05° at 9 s per step (which resulted in a scan rate of 1°/3 min) and sample rotation with Cu-K α radiation at 40 kV and 30 mA.

Temperature programmed desorption (TPD) experiments were performed using a Thermo Scientific™ TPDR 1100 Advanced Catalyst Characterization System equipped with a flow-through quartz reactor and a thermal conductivity detector with a tungsten filament. In a typical experiment a catalyst material (100-150 mg) was firstly subjected to the following pretreatments, (i) drying / thermal treatment under He at 400 / 600 °C for 1 h, (ii) CO₂ (4% CO₂ in He) / NH₃ (5% NH₃ in He) saturation at 80 °C for 30 min, and (iii) flushing under He at 80 °C for 30 min. A TPD experiment consisted of ramping the temperature from room temperature to 800 °C at a ramp of 10 °C min⁻¹ under He flow at 20 mL min⁻¹. The effluent gases were analyzed by a mass spectrometer (Pfeiffer Omnistar GSD 301 C). An anhydrous magnesium perchlorate (Mg(ClO₄)₂) trap was used for CO₂-TPD experiments to absorb mainly H₂O, whereas no trap was used for NH₃-TPD experiments.

Temperature programmed reduction experiments with hydrogen (H₂-TPR), were performed using the same apparatus as in the TPD experiments. 50-70 mg of a sample was first pretreated at 100 °C for 1 h under N₂ stream and subsequently heated from 50 to 800 °C at the ramp rate of 5 °C min⁻¹ under the flow of 5% H₂ in N₂ at 20 ml min⁻¹. A soda lime (CaO + Na₂O) trap was used to remove H₂O and CO₂.

4 | Effects of REM promoters

The textural properties (BET surface area and BJH pore size distribution) of the materials were determined by N₂ physisorption experiments using Quantachrome Instruments, AUTOSORB iQ. The material (100-150 mg) was firstly outgassed at 150 °C at 4 mbar to clean the sample surface and pores prior to the measurements.

Ex situ Raman measurements were carried out on a Thermo Scientific™ Nicolet™ iS™50 FT-IR spectrometer equipped with 1064 nm near-infrared excitation laser. The instrument was preferably used to avoid the strong fluorescence shown by the samples after the catalytic test with 532/785 nm laser [29].

FT-IR measurements of the samples before and after the reaction were performed on a Bruker Alpha spectrometer equipped with a DTGS detector at 2 cm⁻¹ resolution in an ATR sampling configuration with a diamond internal reflection element.

Thermogravimetric analysis (TGA) of the samples before and after the reaction was performed on a Mettler Toledo TGA/SDTA 851 equipment. In a typical experiment, 3-5 mg of a catalyst placed in an alumina crucible were subjected to heating from 25 to 800 °C at a ramp rate of 5 °C min⁻¹ under a flow of synthetic air at 50 mL min⁻¹.

4. 3 Results and discussion

4. 3. 1 Direct methanol carboxylation: Stability studies

Various catalyst materials and approaches (e.g. reactor design and operation mode) have been reported for the direct DMC synthesis from CO₂ and methanol [9, 12, 13, 17, 24-26]. Nevertheless, the combination of CeO₂ as catalyst and 2-CP as dehydrating agent is the only one that proved to be the highly effective in terms of methanol conversion and DMC selectivity under both batch and continuous operations [24, 27, 29]. Despite the superb catalytic performance, a significant catalyst deactivation has been observed during the continuous operation on the time-scale of days. Herein, we examine the effect of the acidity, basicity, and reducibility of the CeO₂ materials on DMC yield and especially on the catalyst stability by surface modification (precious metal or REM addition) or bulk modification (ZrO₂ addition as a solid solution with CeO₂).

Effect of Zr and precious metal (PM)

Figure 4.1 a shows the catalytic performance in terms of methanol conversion (X_{MeOH}) and DMC selectivity (S_{DMC}) during the initial phase (0-2 h) and at 24-26 h of the DMC synthesis using CeO_2 , ZrO_2 and CeO_2 - ZrO_2 solid solutions. The reaction time, more precisely time on stream, is shown as 2 h interval due to the residence time of the liquid solution in the reaction system. The liquid sample was analyzed every 2 h when enough liquid product (ca. 1 mL) was collected (when one number is shown for the reaction time, the initial value of the interval is taken). Although the addition of Zr to CeO_2 has been reported to positively affect the catalytic activity [16-18, 55, 56] for the reaction, in this work negative effects of Zr incorporation were obvious. Regarding the initial activity (0-2 h), the decrease in X_{MeOH} became consistently more prominent at higher Zr content, decreasing from 92.4%, 88.4%, 72.9% to 37.3% for 0, 22, 50, and 75 wt% ZrO_2 amount in the solid solution, respectively. Moreover, the use of high surface area ZrO_2 gave only a trace amount of DMC. After 24 h, catalyst deactivation was observed for all catalysts and it was more pronounced for Ce-Zr [50/50] (ca. 21% activity drop compared to 6-8% drops of the other samples). On the other hand, the drop in catalytic activity did not affect S_{DMC} significantly, showing >95% with the formation of small amounts of Me-PCN (from 1.0 to 4.3%) and Me-CBM (0.4 to 1.6%). Interestingly, at higher ZrO_2 content in the solid solutions, the decrease in S_{DMC} was smaller over 24 h (ca. 5% S_{DMC} decrease for Ce-Zr [100/0], while only ca. 1% decrease for Ce-Zr [25/75]), indicating positive influences of Zr promotion on the catalyst stability in terms of DMC selectivity.

Figure 4.1 b presents the catalytic performance using CeO_2 -supported Ru, Rh and Pd catalysts. Clearly, these results indicate strongly negative influences of the PMs on the performance. For 1 wt% Pd- CeO_2 and 1 wt% Rh- CeO_2 , ca. 63% X_{MeOH} was initially observed, while the addition of 1 wt% Ru resulted in much lower activity of 34% X_{MeOH} . Regarding the catalyst stability, it is very striking to note that both 1 wt% Rh- CeO_2 and 1 wt% Ru- CeO_2 catalysts showed a tremendous loss in activity after 24 h (X_{MeOH} of ca. 7 and 12%, respectively). In contrast, a slight increase in X_{MeOH} (from 63 to 70%) was detected for 1 wt% Pd- CeO_2 . The incorporation of the PMs consistently impacted negatively on DMC selectivity, showing ca. 75-80% S_{DMC} for the three catalysts. Interestingly, unlike CeO_2 and CeO_2 - ZrO_2 solid solutions, all ceria-supported PM catalysts displayed an increase in S_{DMC} by ca. 10% after 24 h of the reaction. Still, S_{DMC} values were considerably lower compared to that observed for CeO_2 and the by-products were 1.6-20.4% Me-PCN and 1.1-5.4% Me-CBM. The high selectivity to Me-PCN indicates that 2-PA is formed via the hydration reaction of 2-CP and that the reaction between 2-PA and methanol (**3.1 Introduction Reaction 3 and 4**) is promoted by the PMs or by the sites created by the specific interactions between CeO_2 with the PMs. The reaction is similar to urea methanolysis where $-\text{NH}_2$ group is replaced by $-\text{OCH}_3$ group

4 | Effects of REM promoters

and both acidic and basic catalysts are known to catalyze the reaction [57, 58]. CeO₂-based materials are known to be active in the reaction [59, 60], and it is implied that promotion of CeO₂ by the PMs can be highly effective for methanolysis reactions.

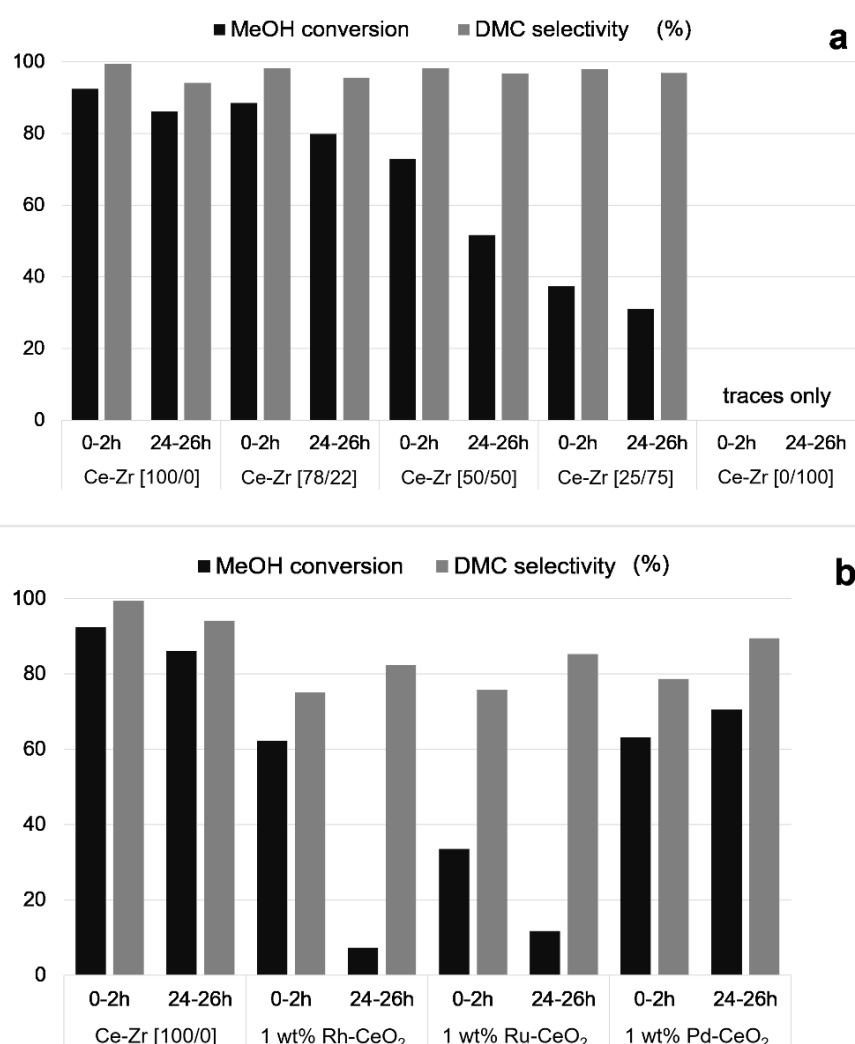


Figure 4.1 Methanol conversion and DMC selectivity during the continuous DMC synthesis at 120 °C, 30 bar at time on stream of 0-2 and 24-26 h using **a.** Ce-Zr mixed oxides and **b.** precious metal-CeO₂ as catalyst. Black and grey columns represent methanol conversion and DMC selectivity, respectively

Generally, both Zr and PMs incorporation showed negative influences on the catalytic performance, especially on the reactivity (X_{MeOH}). The lower reactivity of the catalysts at higher Zr contents implies that the reactivity originates from CeO₂ and its surface. In case of PMs addition, the impacts on the reactivity was drastic despite the relatively low amount of the PMs (1 wt%) with respect to CeO₂. Considering the much lower initial reactivity and the very low catalytic stability of Rh-CeO₂ and Ru-CeO₂ compared to CeO₂, it can be concluded that the PMs alter the chemical surface properties (e.g. acid-base, redox) completely, as confirmed later. Nonetheless, the effects of incorporating both Zr and PMs in CeO₂ were found negative for the activity and stability in the reaction.

Effect of rare earth metal (REM)

Figure 4.2 a depicts the effects of La addition to CeO₂ (0.25, 1, and 5 wt% La) on the long-term stability of the catalytic activity (X_{MeOH} and S_{DMC}) in the continuous DMC synthesis. Initially, slightly lower X_{MeOH} values (ca. 88%) were detected for all La-promoted CeO₂ materials as compared to that of the bare CeO₂ (92.5%). However, all La-containing catalysts performed better than CeO₂ after 60 h. About 74% X_{MeOH} was observed for 0.25 wt% La-CeO₂ at 71 h and 5 wt% La-CeO₂ showed ca. 75% X_{MeOH} at 86 h of the reaction. Remarkably, the most stable catalyst in La-series was 1 wt% La-CeO₂ which maintained a high activity (>80% of X_{MeOH}) even at 120 h, in contrast to ca. 60% X_{MeOH} with CeO₂ at the same time on stream. The La addition also impacted on the DMC selectivity. Initially, the higher the La loading, the poorer the S_{DMC} (>99% for bare CeO₂ and ca. 85% for the 5 wt% sample). The S_{DMC} values leveled off with time to ca. 92-93% and the most stable sample, 1 wt% La-CeO₂, displayed 94% S_{DMC} at 120 h of reaction.

The effects of Gd addition (0.25, 1, and 5 wt% Gd) to CeO₂ on the long-term reactivity are compared in **Figure 4.2 b**. 0.25 and 1 wt% Gd catalysts exhibited a higher level of initial X_{MeOH} compared to the La-promoted catalysts and at the same level as that of CeO₂. However, further increase of Gd loading to 5 wt% lowered the initial X_{MeOH} to 87%. Importantly, all the Gd-containing catalysts displayed better long-term stability than CeO₂. 81-82% X_{MeOH} was observed for 0.25 and 5 wt% Gd-CeO₂ at 68 and 50 h of the reaction, respectively. Similarly to the case of the La-promoted CeO₂, the most stable catalyst was 1 wt% Gd-CeO₂ which maintained a very high activity (84% X_{MeOH}) even at 100 h of the reaction, which is significant considering 63% X_{MeOH} using CeO₂ at 100 h. Furthermore, Gd addition resulted in high and stable S_{DMC} (mostly >98%) at all loadings over the reaction time tested. Based on the superior stability in catalytic activity at high S_{DMC} , 1 wt% was found to be the optimal Gd loading for the DMC synthesis.

4 | Effects of REM promoters

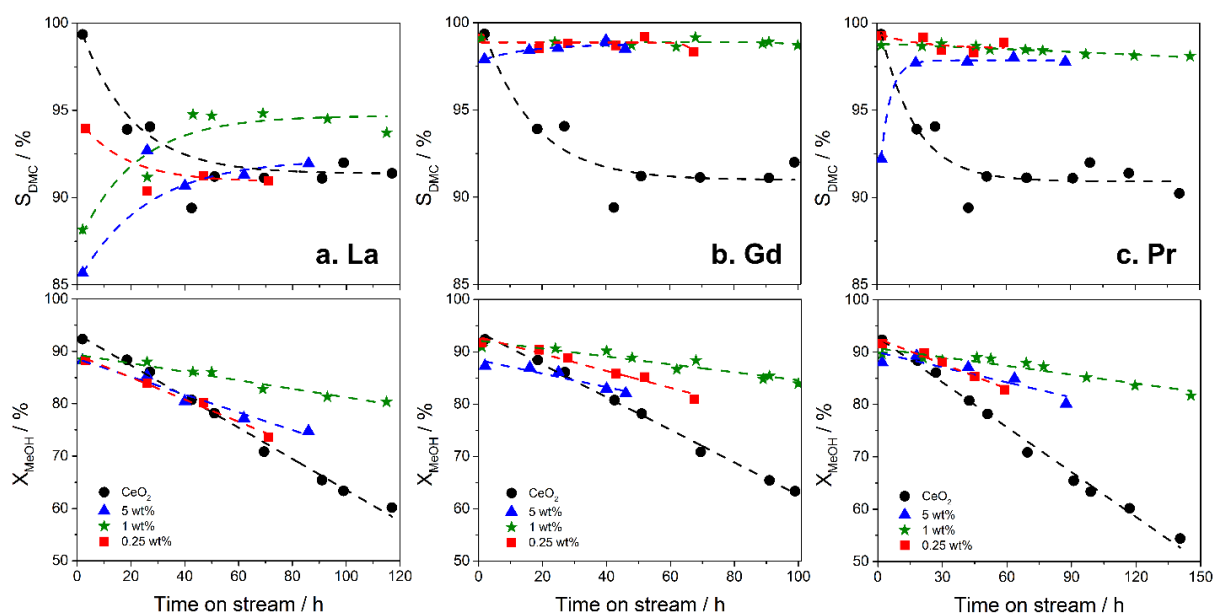


Figure 4.2 Effects of REM promoters on the stability of methanol conversion (X_{MeOH} , lower panels) and DMC selectivity (S_{DMC} , upper panels) in the DMC synthesis from CO_2 and methanol in the presence of 2-CP at 120 °C, 30 bar for **a.** La- CeO_2 (left panels), **b.** Gd- CeO_2 (middle panels), and **c.** Pr- CeO_2 (right panels). Different symbols are used to distinguish the data points of catalyst materials as follows: black circles - bare CeO_2 , red squares – 0.25 wt% REM, green stars – 1 wt% REM, and blue triangles – 5 wt% REM. The dashed lines represent the trend lines to guide eyes for S_{DMC} and to calculate deactivation rates of X_{MeOH} (**Figure 4.3**) with a linear fitting

Furthermore, the effect of Pr addition (0.25, 1, and 5 wt% Pr) to CeO_2 on the reactivity was investigated (**Figure 4.2 c**). The initial X_{MeOH} slightly decreased more notably at increased Pr loading, i.e. 92% (0.25 wt%), 90% (1 wt%), and 88% (5 wt%). However, similar to Gd-promoted catalysts, X_{MeOH} for all Pr-promoted catalysts became higher than that of CeO_2 after ca. 30 h due to the higher long-term stability. 83% X_{MeOH} was observed for 0.25 wt% Pr- CeO_2 at 60 h, while 5 wt% Pr- CeO_2 showed 80% X_{MeOH} at 88 h. As in the case of the other REM addition, the most stable catalyst was once again confirmed to be the one with 1 wt% loading. The catalyst could maintain remarkable 82% X_{MeOH} in comparison to 50% observed for CeO_2 at ca. 150 h. Moreover, Pr addition showed similarly stable S_{DMC} as observed for the Gd-promoted catalysts. 0.25 and 1 wt% Pr catalysts were highly selective to DMC (>98% at ca. 150 h of the reaction for the 1 wt% sample), whereas 5 wt% Pr catalyst showed comparably lower S_{DMC} , especially during the initial phase.

The above study of REM (La, Gd, Pr) promotion to CeO_2 clearly shows the positive impacts, leading to higher stability in both activity (X_{MeOH}) and DMC selectivity, thus significantly improving the overall performance. When 1 wt% Pr- CeO_2 and CeO_2 are compared, an increase of around 35% in the DMC yield for the Pr-promoted catalyst was obtained at ca. 150 h, which is significant and of high relevance in practice.

Figure 4.3 summarizes the results on catalyst stability in terms of deactivation rate, expressed by the drop in X_{MeOH} (%) per hour. Since the deactivation was reasonably linear for all REM-promoted samples (**Figure 4.2**), the slope was calculated with the least squares method assuming a linear trend line of X_{MeOH} . Obviously, the incorporation of REM was positive in terms of long-term catalytic activity and the positive effects were more evident for Gd- and Pr-CeO₂. As noted above, the best materials were 1 wt% REM catalysts, showing the lowest rate of deactivation (0.080, 0.075, and 0.055 % h⁻¹ for La-, Gd-, and Pr-CeO₂ respectively) in comparison to 0.253 % h⁻¹ of CeO₂. In addition, it should be reminded that 1 wt% Gd- and Pr-promoted catalysts were also the best ones in terms of long term stability in S_{DMC}.

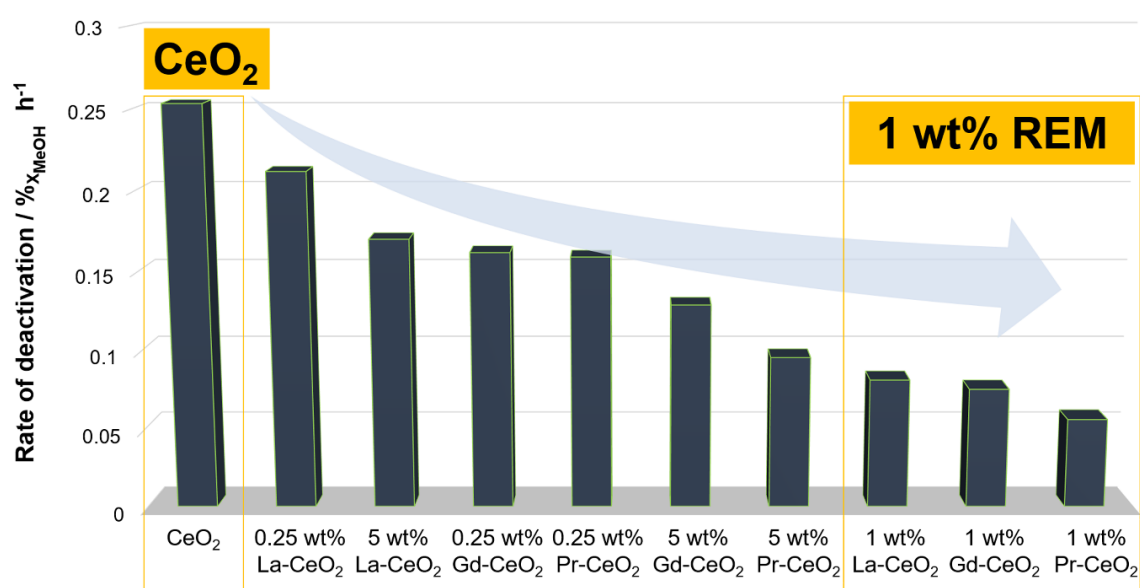


Figure 4.3 Rate of deactivation during the DMC synthesis (120 °C, 30 bar) expressed by the drop in X_{MeOH} (%) per hour for pristine CeO₂ and REM-promoted CeO₂ materials

4. 3. 2 Characterization of pristine and as-synthesized catalysts

The stability studies presented in 4.3.1 showed the positive effects of REM as promoter of CeO₂ in the DMC synthesis in the presence of 2-CP, especially at 1 wt% loading. To identify the origin of the enhanced stability of the REM-promoted catalysts, the chemical and structural properties of the pristine and as-synthesized catalysts as well as spent catalysts were investigated in detail.

4 | Effects of REM promoters

Structural and textural properties

The XRD patterns of the pristine CeO_2 , $\text{CeO}_2\text{-ZrO}_2$ solid solutions, and ZrO_2 are presented in **Figure 4.4**. The results for as-synthesized materials incorporating PM and REM are shown in **Appendix D, Figure 7.3**. CeO_2 showed the peaks corresponding to (111), (200), (220), and (311) planes of cubic fluorite phase, while ZrO_2 exhibited the peaks for a monoclinic phase with a small amount of a tetragonal phase. $\text{CeO}_2\text{-ZrO}_2$ solid solutions preserved a single cubic fluorite phase characteristic of CeO_2 without a detectable monoclinic/tetragonal phase characteristic of ZrO_2 . It should be noted that the characteristic XRD peaks of $\text{CeO}_2\text{-ZrO}_2$ solid solutions slightly shifted to higher angles compared to the peaks for cubic fluorite phase of CeO_2 . This can be explained by the insertion of zirconium atoms in the CeO_2 cubic matrix with the shrinkage of its unit cell (Ce^{4+} ionic radius is 0.97 Å, whereas Zr^{4+} ionic radius is 0.82 Å [61]) and by the deformation of the cubic phase to be transformed into the tetragonal phase for higher zirconium loading [61]. The materials with PM and REM showed negligible structural changes, indicating that metal promoters were finely dispersed on the surface of the support. This is consistent with other studies reporting materials synthesized by impregnation of an active metal over various supports (e.g. Al_2O_3 , $\text{CeO}_2\text{-ZrO}_2$ solid solution, ZnO-CeO_2) [55, 56, 60].

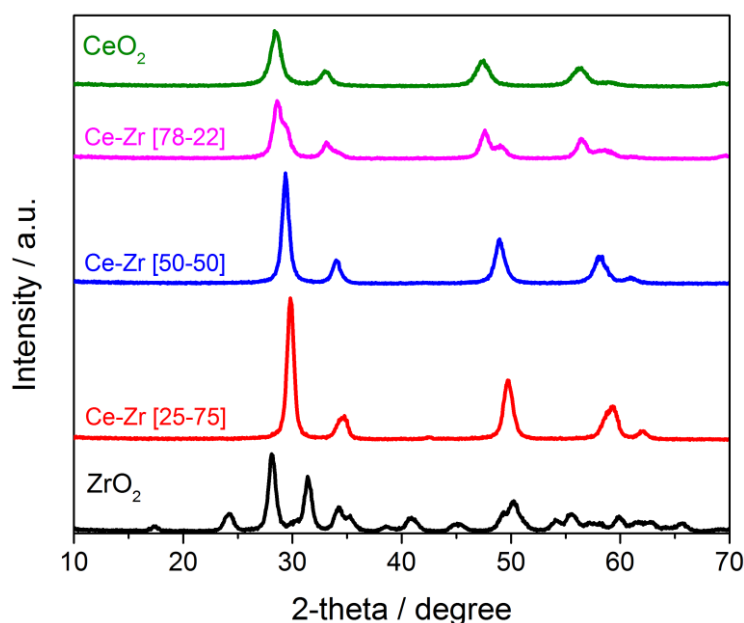


Figure 4.4 X-ray diffraction (XRD) patterns of the pristine CeO_2 , $\text{CeO}_2\text{-ZrO}_2$ solid solutions, and ZrO_2

The BET surface area and pore volume of all materials are presented in **Table 4.1**. Higher amount of incorporated Zr or REM to CeO_2 consistently decreased the surface area, although there was no clear trend in the pore volume with the type and loading of REM. In case of the PM-loaded materials, the surface area was also reduced and it was most pronounced for Pd-

CeO₂. The pore volume of the three PM-CeO₂ samples were similarly reduced by ca. 10%. Importantly, the changes in the textural properties and bulk structure of the materials are not correlated with the catalytic activity and stability.

Table 4.1 The BET surface area (m² g⁻¹) and pore volume (cm³ g⁻¹) of the pristine CeO₂, CeO₂-ZrO₂ solid solutions, ZrO₂ and as-synthesized materials incorporating precious metal and rare earth metal promoters

Material type	BET surface area (m ² g ⁻¹)	Pore volume (cm ³ g ⁻¹)
CeO ₂ -ZrO ₂ solid solutions	CeO ₂	160
	CeO ₂ -ZrO ₂ [78-22]	75
	CeO ₂ -ZrO ₂ [50-50]	59
	CeO ₂ -ZrO ₂ [25-75]	58
	ZrO ₂	97
Precious metals (PM) – CeO ₂	1 wt% Rh-CeO ₂	141
	1 wt% Ru-CeO ₂	147
	1 wt% Pd-CeO ₂	123
Rare earth metals (REM) – CeO ₂	0.25 wt% La-CeO ₂	149
	1 wt% La-CeO ₂	135
	5 wt% La-CeO ₂	122
	0.25 wt% Gd-CeO ₂	156
	1 wt% Gd-CeO ₂	146
	5 wt% Gd-CeO ₂	123
	0.25 wt% Pr-CeO ₂	152
	1 wt% Pr-CeO ₂	139
	5 wt% Pr-CeO ₂	126

Basicity and acidity of the catalysts

As mentioned in [4.1 Introduction](#), several acid-base heterogeneous catalysts have been tested in the direct carboxylation of methanol with CO₂. While the basic sites are required to activate CO₂ molecule, both acidic and basic sites are generally reported to be mandatory for methanol activation (CH₃O⁻ and CH₃⁺ formation). It has been widely reported that ZrO₂, CeO₂, and CeO₂-ZrO₂ solid solution show both acidic and basic characters [62]. CeO₂ possesses both Lewis acidic (Ce⁴⁺) and basic (O²⁻) sites and the material may have exactly the right acidity-basicity balance to catalyze the reaction, more precisely the two reactions of DMC synthesis and hydration reaction of 2-CP [27, 28]. Besides the acid-base property, the unique feature of the CeO₂ material compared to many other oxides is the reducibility of the catalyst and lattice/surface oxygen mobility. It is not yet clear but the latter features may play pivotal roles in DMC synthesis and related to the catalyst stability. Similarly, it has been previously suggested that addition of Cu in low amount (0.1 to 0.5 wt%) may work cooperatively with CeO₂ catalysts to accelerate the partial reduction of Ce⁴⁺ sites to Ce³⁺, enhancing the DMC yield by 20-60% [63]. For these reasons, acidity and basicity characterization by NH₃- and

4 | Effects of REM promoters

CO₂-TPD and material reducibility by H₂-TPR were performed to evaluate possible correlations between material properties and catalytic performance.

According to Hutter *et al.* [64] who investigated the adsorption mechanism of CO₂ on CeO₂ (111) by DFT calculations, three stable configurations of CO₂ on the CeO₂ surface have been identified: (i) monodentate carbonate, (ii) bidentate carbonate, and (iii) linearly adsorbed species. Among these three configurations, the linear species are represented as physically adsorbed CO₂ (no hybridization of the CO₂ gas phase orbitals) and the monodentate species are the most stably adsorbed ones. On the other hand, both mono- and bi-dentate carbonate species are represented by bent CO₂ configurations having the C atom chemically bonded to O atom on the surface. The stronger the interaction of CO₂ with the CeO₂ surface, the higher its desorption temperature, i.e. the low (20-200 °C), medium (200-450 °C), and high temperature (>450 °C) desorption peaks are assigned to linear, bidentate and monodentate carbonates, respectively [65]. In the same manner, the low (20-200 °C), medium (200-450 °C), and high temperature (>450 °C) desorption peaks in NH₃-TPD measurements will be attributed to the weak, medium, and strong acid sites, respectively.

CO₂- and NH₃-TPD profiles of all catalysts are presented in **Figure 4.5** (CeO₂-ZrO₂ solid solutions and PM-CeO₂) and **Figure 4.6** (REM-CeO₂) and the amounts of adsorbed-desorbed CO₂ and NH₃ are summarized in **Table 4.2**, respectively. Generally, the addition of a foreign atom on/in the CeO₂ structure reduced the amount of adsorbed CO₂/NH₃, thus the total number of acidic and basic sites. In other words, the bare CeO₂ material is more acidic and more basic compared to the doped/promoted CeO₂ materials, judging from the number of the sites. The exceptions were CeO₂-ZrO₂ solid solutions and ZrO₂ for which the weak acidity was greatly enhanced when the ZrO₂ content was >50 wt% due to more pronounced influence of highly acidic ZrO₂ [66-69] in the solid solutions (**Figure 4.5**). Zr-addition to CeO₂ resulted in weakening of the strong acidity/basicity as indicated by the small amount of adsorbed NH₃/CO₂, respectively, at temperature above ca. 500 °C.

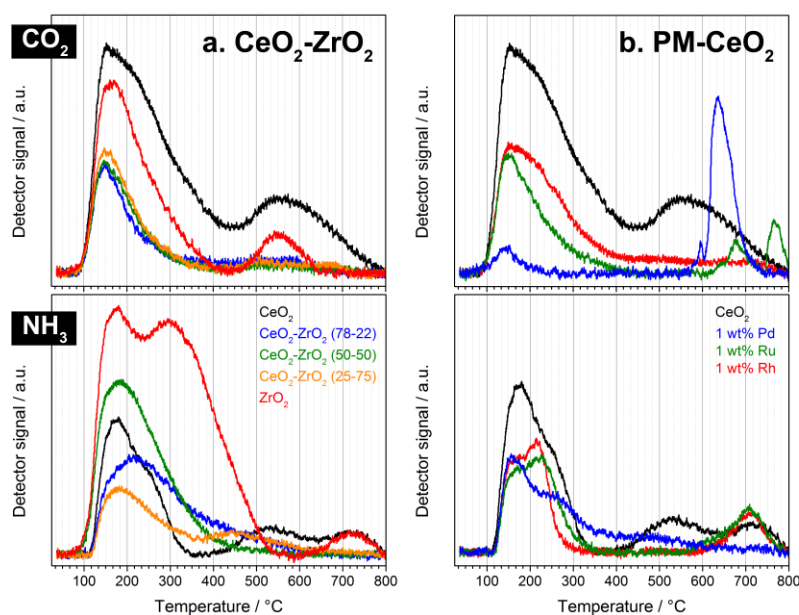


Figure 4.5 Temperature programmed desorption (TPD) profiles of the $\text{CeO}_2\text{-ZrO}_2$ solid solutions and precious metals (PM) promoted CeO_2 materials. Upper panels correspond to those of CO_2 -TPD, whereas the lower ones to those of NH_3 -TPD

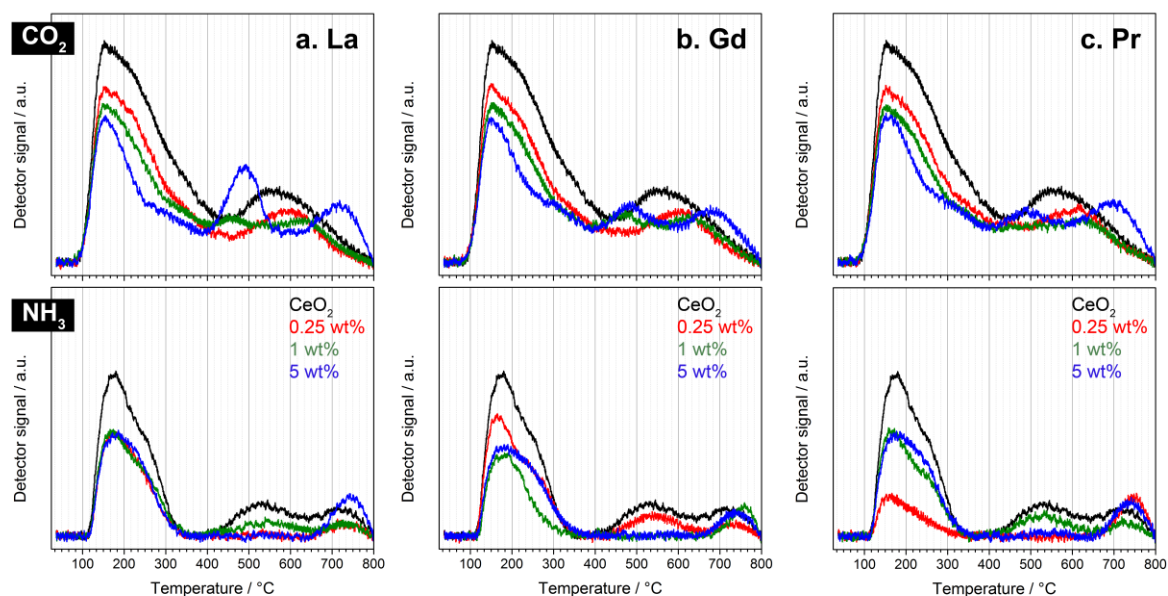


Figure 4.6 Temperature programmed desorption (TPD) profiles of the rare-earth metals (REM) promoted CeO_2 materials. Upper panels correspond to those of CO_2 -TPD, whereas the lower ones to those of NH_3 -TPD

On the other hand, PM addition to CeO_2 induced remarkable changes in the acidity/basicity of the material (**Figure 4.5**). Upon Rh and Ru addition to CeO_2 , weak and moderate acidic sites were decreased, but mildly strong acidic sites (desorption at ca. 520 °C) became less and, in contrast, highly strong acidity (desorption at ca. 700 °C) was enhanced. For Rh- and

4 | Effects of REM promoters

Ru-CeO₂, the number of strong basic sites were reduced significantly, although the formation of stronger basic sites characterized by the desorption peaks at 680 and 760 °C was observed for Ru-CeO₂. Pd addition resulted in very different changes in both acidity and basicity from those of Rh and Ru addition. Notably, the weak-moderate basicity of CeO₂, characterized by the broad CO₂ desorption peaks in the range of 100-450 °C, was largely suppressed and, instead, strong basic sites (desorption at ca. 640 °C) were formed. The similarity of acid-base properties of Rh- and Ru-CeO₂ in comparison to Pd-CeO₂ was consistently reflected in the catalytic activity and stability trend (**Figure 4.1 b**). This implies that acid-base properties are playing roles in the DMC synthesis from CO₂ and methanol in the presence of 2-CP.

Table 4.2 The amounts of adsorbed-desorbed CO₂ and NH₃ expressed in μmol g_{cat.}⁻¹ (a measure of the basicity and acidity of the materials) tested in the long-term studies of DMC synthesis

Material type		μmol CO ₂ g _{cat.} ⁻¹	μmol NH ₃ g _{cat.} ⁻¹
CeO ₂ -ZrO ₂ solid solutions	CeO ₂	520.8	396.2
	CeO ₂ -ZrO ₂ [78-22]	140.1	511.2
	CeO ₂ -ZrO ₂ [50-50]	137.7	710.0
	CeO ₂ -ZrO ₂ [25-75]	149.0	316.3
	ZrO ₂	313.6	1410.8
Precious metal (PM) – CeO ₂	1 wt% Rh-CeO ₂	259.6	255.8
	1 wt% Ru-CeO ₂	176.8	299.5
	1 wt% Pd-CeO ₂	118.1	360.1
Rare earth metal (REM) – CeO ₂	0.25 wt% La-CeO ₂	411.7	259.3
	1 wt% La-CeO ₂	380.3	317.9
	5 wt% La-CeO ₂	399.0	308.7
	0.25 wt% Gd-CeO ₂	410.8	364.3
	1 wt% Gd-CeO ₂	377.1	243.0
	5 wt% Gd-CeO ₂	386.2	286.1
	0.25 wt% Pr-CeO ₂	414.5	213.8
	1 wt% Pr-CeO ₂	374.4	317.6
	5 wt% Pr-CeO ₂	400.6	293.4

There were clear and consistent trends in the changes of acidity and basicity by the addition of REM to CeO₂ (**Figure 4.6**). In all cases, the total number of acidic and basic sites became smaller, and the degree of the decrease was less at lower REM loading without affecting the characteristics of the strength of acidity and basicity, as evident from the similar desorption profiles of CO₂- and NH₃-TPD for the 0.25 wt% REM-CeO₂ to those of CeO₂. Upon increasing the REM loading to 1 and 5 wt%, there were notable changes in the nature of the strong acidic and basic sites with the formation of two types of strong basic sites (desorption at ca. 500 and 700 °C). For acidic sites, mildly strong sites (desorption at ca. 500 °C) were reduced but strong sites (at ca. 750 °C) were enhanced. Thus, it can be concluded that higher loading of REM reduces the number of weak-moderate acidic/ basic sites but increases that of strong acidic/basic sites.

With the aim to identify the role of acidity, basicity and their synergy in the reaction, we evaluated the relations between acidity, basicity, or a unifying parameter (basicity/acidity ratio calculated from the total amount of the adsorbed probe molecules) of the examined materials and their catalytic performance and stability. The reactivity represented by DMC yield showed a reasonable trend with the ratio of basicity/acidity (**Figure 4.7**). When the ratio is larger than 1 (i.e. more basic catalysts; CeO₂ and REM-promoted CeO₂), the materials display good catalytic activity at the initial phase of the reaction (0-2 h). In contrast, at the basicity/acidity ratio <1 (i.e. more acidic) the materials such as CeO₂-ZrO₂ solid solutions, ZrO₂ and PM-CeO₂ series exhibited lower activity with one exception of Ce-Zr [78/22] likely due to the high CeO₂ content and negligible influence of Zr. It should be noted, however, that Ce-Zr [78/22] exhibited a remarkable decrease (ca. 10%) in X_{MeOH} after only 24 h of the reaction despite its high initial DMC yield. This implies that both the catalyst stability and reactivity cannot be properly correlated with the basicity/acidity ratio.

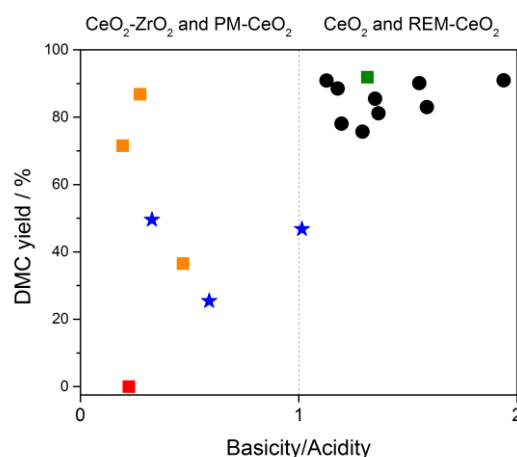


Figure 4.7 Initial DMC yield against basicity/acidity ratio for all examined materials of this study at 120 °C, 30 bar. Different symbols are used to distinguish the data points of catalyst materials as follows: squares for pure CeO₂ (green), pure ZrO₂ (red), and CeO₂-ZrO₂ solid solutions (orange), blue stars for PM-CeO₂, and the black circles for REM-CeO₂

It is widely reported that DMC synthesis from CO₂ and methanol requires the presence of both acidic and basic sites [10]. This study comes as a confirmation to that statement as well as an indication of the importance of a proper balance between acidity and basicity of catalyst material. Weak acidity is important in the selective DMC synthesis since the formation of common by-product, dimethyl ether (DME), is more easily catalyzed over strong acid sites, especially at higher temperatures [70]. Moreover, 2-PA (weak base) adsorption over the acidic sites of CeO₂ leads to a severe catalyst deactivation [29]. Importantly, basicity seems to be playing more important roles by activating the CO₂ molecule and formation of CH₃O⁻ species and monodentate methyl carbonate (MMC, CH₃OCOO-metal atom) as possible reaction

4 | Effects of REM promoters

intermediates [9, 19, 71]. The relatively high basicity of CeO_2 against its acidity (**Figure 4.7**) is negligibly influenced by the addition of REM unlike the materials with comparably lower basicity when Zr and PM are added (**Table 4.2**). This basicity/acidity ratio is thus a good indicator to evaluate the activation capability of catalyst for the reaction and it should be higher than the threshold (in our case >1 , **Figure 4.7**).

Furthermore, possible correlations of the rate of deactivation with the parameters related to acidity or basicity were sought for, especially for the promising REM-promoted materials. **Figure 4.8** presents the rate of deactivation for CeO_2 and REM- CeO_2 as a function of the basicity and acidity expressed by the total number of sites determined by the CO_2 - and NH_3 -TPD experiments. Albeit no clear correlation was found for the deactivation rate with acidity, the influence of the basicity on the deactivation was consistent; the lower the basicity, the lower the rate of deactivation. This implies that basicity induces the surface poisoning and thus deactivation, which is rather non-intuitive due to the expected stronger interaction of 2-PA with acidic sites. This point will be discussed in more detail later with the identification and quantitative analysis of surface adsorbed species during the reaction.

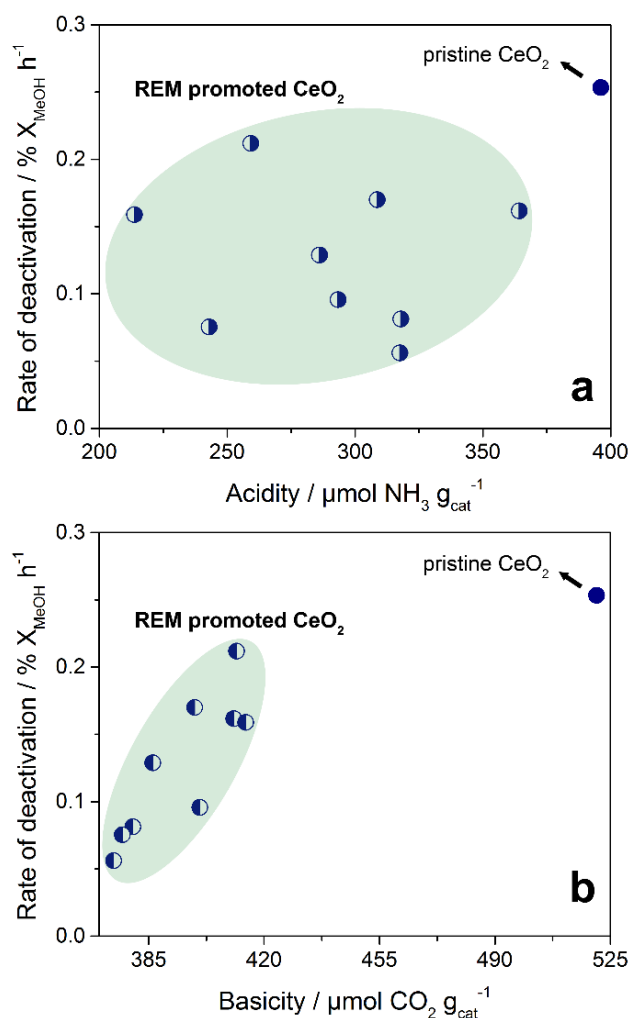


Figure 4.8 Rate of deactivation in the DMC synthesis plotted against **a.** acidity and **b.** basicity of CeO₂ and REM-CeO₂ materials. Filled circles are for pristine CeO₂, while the half-empty circles correspond to the REM promoted CeO₂

Reducibility of the catalysts

The reducibility of the CeO₂-based catalysts reflected by the oxygen mobility [72-74] was studied by H₂-TPR. The H₂-TPR profiles are presented in **Figure 4.9** for pristine CeO₂, in **Figure 4.10** and **4.11** for the Zr and PM incorporated catalysts, and in **4.12** and for the REM-promoted catalysts. **Table 4.3** summarizes the H₂ uptake of all the samples investigated.

The reduction of CeO₂ is known to proceed in two steps; the first one at ca. 500 °C, corresponding to the reduction of surface Ce (IV) atoms more relevant for the catalytic processes, and the second one at ca. 800 °C, corresponding to the bulk reduction of the material (elimination of O²⁻ from the lattice and formation of Ce₂O₃) [34, 74, 75]. The reducibility of ceria is known to be strongly dependent on the CeO₂ crystallite size [33, 76]. The CeO₂ used in this study has a high surface area with a crystallite size of ca. 10 nm (as calculated from the Scherrer equation using the (111) reflection peak) and it presents clearly the two

4 | Effects of REM promoters

major peaks assignable to surface reduction (peak at 487 °C) and bulk reduction (peak at 816 °C) processes (**Figure 4.9**).

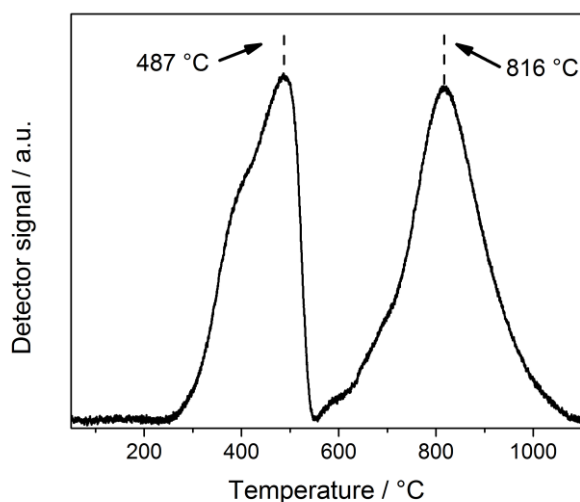


Figure 4.9 H₂-TPR profiles of the high surface area CeO₂ used throughout this study. Both surface (low temperature) and bulk (high temperature) reduction peaks can be clearly identified

As well known, Zr addition to CeO₂ induced drastic changes in the reducibility of CeO₂ [77-79] (**Figure 4.10**). The TPR profiles of the CeO₂-ZrO₂ solid solutions displayed only one main broad reduction peak in the region between 500–580 °C at different peak positions (507, 543, and 576 °C for CeO₂-ZrO₂ [78-22], [50-50], and [25-75], respectively). In contrast, the high surface area ZrO₂ used in the present study showed no reduction peaks under the condition investigated (**Figure 4.10**). Although the overall reducibility of CeO₂-ZrO₂ is enhanced by facilitating the bulk reduction compared to CeO₂, it should be noted that the reduction of surface Ce atoms is more facile for CeO₂ than CeO₂-ZrO₂ at lower temperatures (<400 °C, **Figure 4.10**). The catalytic tests clearly showed that CeO₂ and not ZrO₂ is responsible for activation of CO₂ and methanol (**Figure 4.1**), and this indicates that the reducibility of surface Ce may play important role in the reaction mechanisms besides the balance between basic/acidic sites. The importance of redox sites in the catalytic cycle have been investigated by operando spectroscopic means and will be communicated separately.

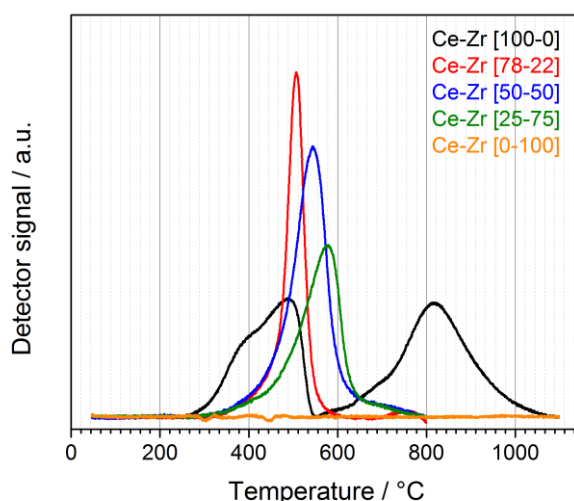


Figure 4.10 H₂-TPR profiles of the CeO₂-ZrO₂ solid solutions (black for pure CeO₂ and orange for pure ZrO₂)

PM addition to CeO₂ resulted in totally different TPR profiles (**Figure 4.11**). The three catalysts are characterized by the appearance of a new large peak in the TPR profiles at very low temperatures around 100-180 °C, characteristic of Ru, Rh, and Pd oxides reduction. The peak corresponding to the CeO₂ surface reduction was reduced drastically for the three PM-CeO₂ materials. As in the cases of the catalytic activity (**Figure 4.1**) and TPD results (**Figure 4.5**), the reducibility of Ru- and Rh-CeO₂ presented some similarities, showing the reduction peak at ca. 100 °C, while a higher reduction peak ca. 180 °C was observed for Pd-CeO₂. This indicates possible correlations among catalyst reducibility, acidity-basicity, and catalytic performance. Based on the H₂-TPR profiles of PM-CeO₂, the H₂ consumption is high at low temperatures below 200 °C considering that it is the reduction of 1 wt% PM. This observation together with lowered reduction peak at ca. 500 °C imply the promoted reduction of surface Ce by the catalytic function of PM, facilitating the reactivity of surface oxygen of CeO₂. Nevertheless, this high reducibility of surface CeO₂ did not positively affect the catalytic performance of PM-CeO₂ (**Figure 4.1**) and further investigation is required to elucidate the PM effects on the reactivity and product selectivity.

4 | Effects of REM promoters

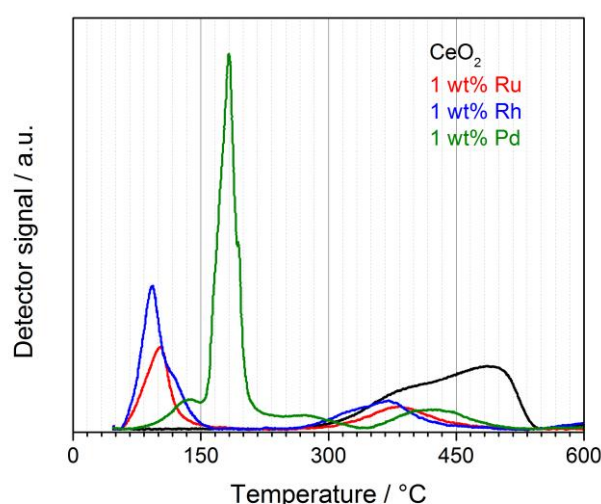


Figure 4.11 H₂-TPR profiles of the precious metals (PM) promoted CeO₂ materials (surface reduction region)

On the other hand, clear and more consistent changes in the material reducibility were observed for the REM promoted CeO₂ materials (**Figure 4.12**). At 0.25 wt% REM loading, the changes in reducibility were not pronounced. At 1 and 5 wt% REM loading, the appearance of highly reducible features of the materials was evident with a new shoulder-peak at ca. 310-380 °C for all REM types (5 wt% La displayed two shoulders). Interestingly, the presence of such a shoulder-peak near the low temperature CeO₂ reduction has been attributed to the existence of Ce⁴⁺ located in different chemical environment, such as the subsurface region [77, 80, 81]. Even more importantly, in the case of the catalysts with high stability during the reaction (i.e. 1 wt% REM loading) the surface reduction peak was shifted to slightly lower temperatures as compared to CeO₂. Precisely, the low temperature peak which started to rise at 235 °C for CeO₂ shifted to lower reduction-onset temperature of 210, 170, and 220 °C for 1 wt% La-, Gd-, and Pr-CeO₂, respectively. Among 5 wt% REM-CeO₂ materials, only the La-CeO₂ showed the same behavior reducing the onset temperature of surface reduction at ca. 160 °C, whereas for Gd- and Pr-CeO₂ showed higher onset temperature compared to the corresponding 1 wt% REM-CeO₂. Also, it is worth noting that 0.25 and 1 wt% REM loading did not affect considerably the shape of the surface reduction peak, while at 5 wt% REM loading, the materials displayed a small decrease of the latter. This is in a good agreement with the textural properties where increasing the REM loading to 5 wt% resulted in a decrease of ca. 25% in the S_{BET}, indicating less CeO₂ available on the surface. In summary, the reducibility of CeO₂ is enhanced at 1 wt% REM loading while retaining the good reducibility of surface CeO₂ which may be responsible for the catalysis as discussed above. The relation between the reducibility and catalyst stability will be discussed further in the next section.

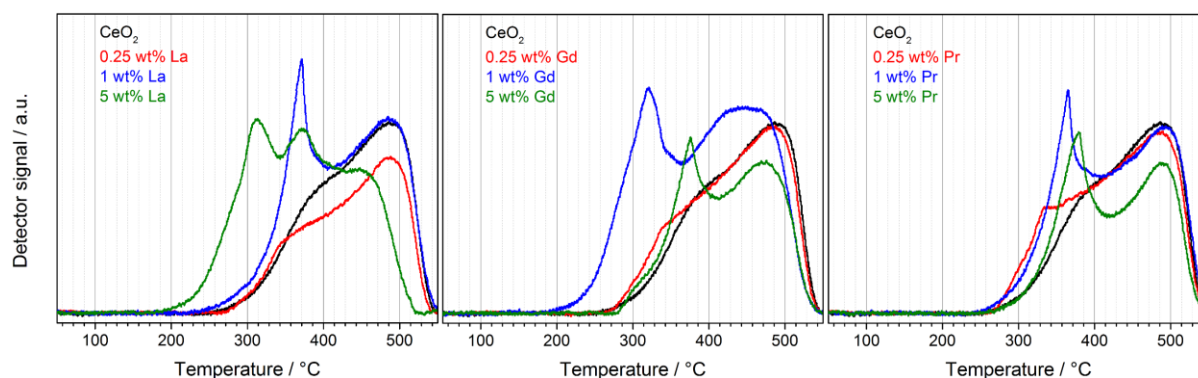


Figure 4.12 H₂-TPR profiles (corresponding to the surface reduction region) for CeO₂ and REM-CeO₂ materials

Table 4.3 H₂ uptake ($\mu\text{mol g}_{\text{cat.}}^{-1}$) of the CeO₂-ZrO₂ solid solutions, precious metals (PM) promoted CeO₂, and rare earth metals (REM) promoted CeO₂ catalysts used in long-term DMC synthesis. For the PM and REM promoted materials only the surface reduction has been included

Material type		H ₂ consumption in $\mu\text{mol g}_{\text{cat.}}^{-1}$
CeO ₂ -ZrO ₂ solid solutions	CeO ₂	376 (surface + bulk = 733)
	CeO ₂ -ZrO ₂ [78-22]	401
	CeO ₂ -ZrO ₂ [50-50]	532
	CeO ₂ -ZrO ₂ [25-75]	408
	ZrO ₂	no reduction
Precious metals (PM) – CeO ₂	1 wt% Rh-CeO ₂	355
	1 wt% Ru-CeO ₂	274
	1 wt% Pd-CeO ₂	533
Rare earth metals (REM) – CeO ₂	0.25 wt% La-CeO ₂	372
	1 wt% La-CeO ₂	434
	5 wt% La-CeO ₂	472
	0.25 wt% Gd-CeO ₂	406
	1 wt% Gd-CeO ₂	479
	5 wt% Gd-CeO ₂	369
	0.25 wt% Pr-CeO ₂	404
	1 wt% Pr-CeO ₂	420
5 wt% Pr-CeO ₂	371	

4. 3. 3 Characterization of pristine and 1 wt% REM-CeO₂ before and after the reaction

The long-term stability of CeO₂ catalyst in the direct DMC synthesis in the presence of 2-CP was markedly improved using REM promoters (i.e. La, Gd, and Pr), but there was still a gradual and substantial deactivation of the catalyst materials over more than 100 h of reaction. To better understand and explain the effects of the REM promoters and their functions during the reaction, bare CeO₂ and 1 wt% REM-CeO₂ after the reaction were characterized by visual, spectroscopic and thermal analyses. The reactions (120 °C, 30 bar, for 30 h) were performed in a fused quartz reactor to enable visual inspection and Raman spectroscopy of the materials within the reactor. Prior to the analyses, the catalysts were thoroughly washed with methanol

4 | Effects of REM promoters

at 120 °C at 3 mL min⁻¹ for 15 min in the reactor to remove some crystallites of 2-PA deposited over the catalyst surface, accordingly to our previous study [29]. This washing procedure is necessary to identify strongly adsorbed surface molecular species causing catalyst deactivation by Raman and ATR-IR spectroscopic studies [29].

Visual inspection and spectroscopic investigation

Figure 4.13 shows the photographs of the catalysts before and after the reaction with subsequent hot methanol washing. Initially, all materials displayed a light-yellow color characteristic of pristine CeO₂ except Pr-CeO₂ in a reddish tint. After the reaction, all the materials turned darker and there seems to be a correlation between the degree of catalyst deactivation and the degree of the color change. This tendency is the most noticeable for CeO₂ turning into dark maroon and less color change was observed for 1 wt% La-CeO₂. Even less change in color was observed for 1 wt% Gd-CeO₂. 1 wt% Pr-CeO₂ changed its color to brick-red due to the reddish color of the as-synthesized material. Interestingly, the degree of the color changes was in good agreement with the changes in the surface area (S_{BET}) and pore volume of the materials after the reaction (**Table 4.4**). 32.5% S_{BET} loss was observed for CeO₂, while La, Gd, and Pr promoted samples showed ca. 29% (La and Gd) and 24% (Pr) S_{BET} loss. On the other hand, the decrease in the pore volume of the materials was perfectly in accordance with the rate of deactivation (**Figure 4.3**); CeO₂ losing 31.5% of its pore volume and La, Gd, and Pr samples losing 18.3%, 12.1%, and 9.2%, respectively. No structural change in the crystallinity of the materials was detected by XRD after 30 h of the reaction (**Appendix D, Figure 7.4**).

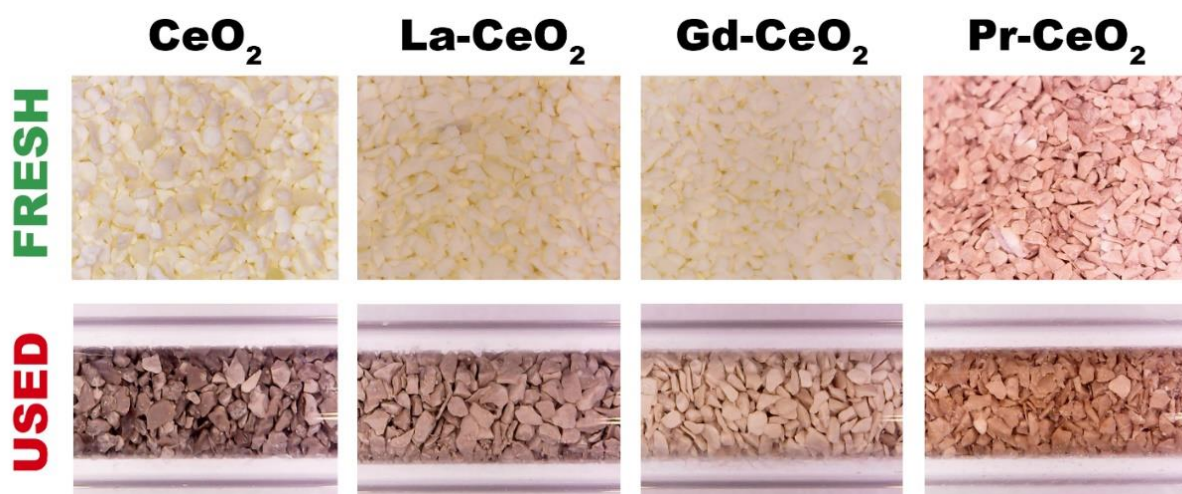


Figure 4.13 Photographs of CeO₂ and REM-CeO₂ materials before (top) and after (below) the reaction at 120 °C, 30 bar for 30 h and a subsequent hot methanol washing for 15 min

Table 4.4 BET surface area and pore volume of CeO₂ and REM-CeO₂ before and after the reaction (120 °C, 30bar, for 30 h) and subsequent hot methanol washing

Material	Surface area (m ² g ⁻¹)		Decrease (%)	Pore volume (cm ³ g ⁻¹)		Decrease (%)
	Before	After		Before	After	
Pristine CeO ₂	160	108	32.5	0.197	0.135	31.5
1 wt% La-CeO ₂	135	97	28.1	0.186	0.152	18.3
1 wt% Gd-CeO ₂	146	104	28.8	0.199	0.175	12.1
1 wt % Pr-CeO ₂	139	106	23.7	0.184	0.167	9.2

Ex situ Raman and ATR-IR measurements have been performed to clarify the cause of the catalyst deactivation by identifying the surface adsorbed species (**Figure 4.14**). Both Raman and IR studies indicate that 2-PA-like species (more precisely 2-PA monoanion, Py-CONH⁻) are adsorbed on the surfaces in accordance with our previous study of bare CeO₂ [29], implying that the REM promoters do not influence the adsorption mode and origin of deactivation. Based on the intensity of the Raman bands, the amount of 2-PA adsorbed on the surface of the pristine CeO₂ was suggested to be higher than that on the surface of REM-CeO₂ materials. This is in good agreement with the catalytic activity studies; catalyst deactivation is more pronounced when surface is more poisoned by the larger amount of adsorbed 2-PA. It is important to mention that the four materials re-gained their initial color and catalytic activity as demonstrated for CeO₂ upon mild calcination treatment at 300 °C in air [29].

4 | Effects of REM promoters

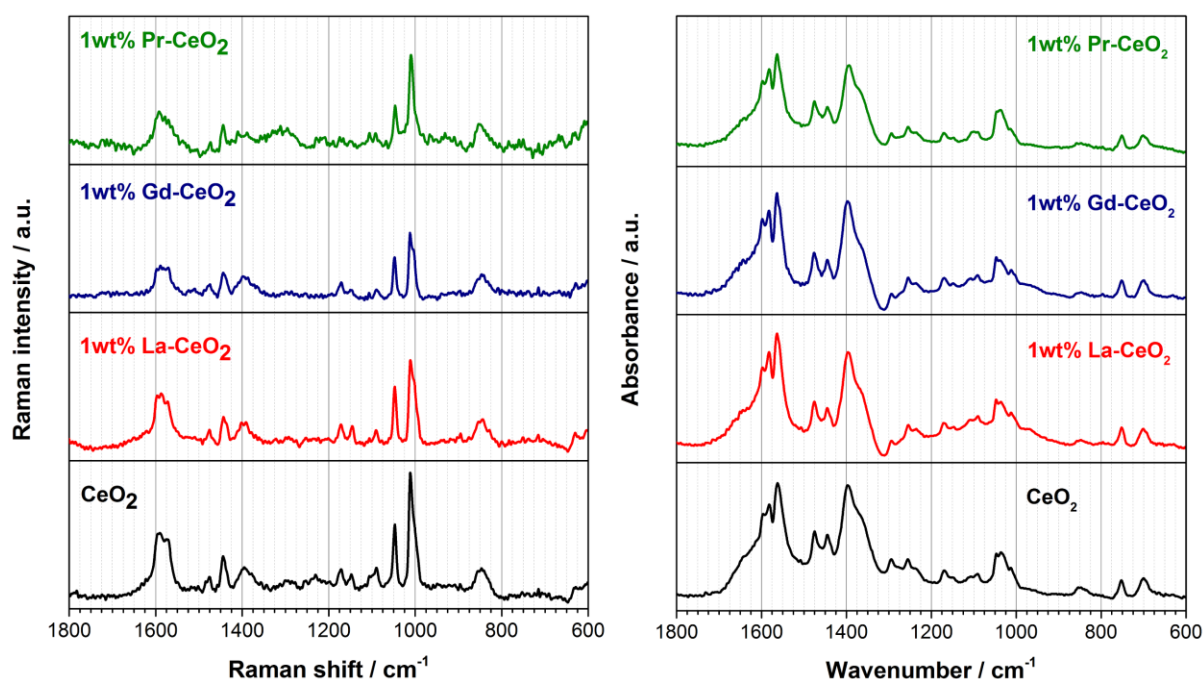


Figure 4.14 Raman (left) and ATR-IR (right) studies of the catalysts after the reaction and methanol washing. The spectral contribution due to CeO_2 has been subtracted and the Raman spectra have been normalized with respect to CeO_2 F_{2g} mode at ca. 460 cm^{-1}

TGA

Moreover, thermogravimetric analysis (TGA) was performed for the catalyst materials before and after the reaction and the results are summarized in [Table 4.5](#) (TGA profiles are shown in [Appendix D, Figure 7.5](#)). All the materials before the reaction showed only one desorption peak, assigned to the removal of surface impurities (i.e. physically adsorbed water). On the other hand, an additional feature of a peak slightly below $300 \text{ }^\circ\text{C}$ was observed for the materials after the reaction. This peak corresponds to the 2-PA elimination from the CeO_2 surface as the boiling point of 2-PA is $284.1 \text{ }^\circ\text{C}$. It is interesting to note that the peak slightly shifts towards lower temperatures (ca. $270 \text{ }^\circ\text{C}$) for 1 wt% REM- CeO_2 promoted materials as compared that of pristine CeO_2 (ca. $280 \text{ }^\circ\text{C}$), as determined by peak calculation taking the 1st derivative of the weight loss curve. This is a good indication of weaker interaction between the 2-PA and the catalyst surface when CeO_2 is promoted with 1 wt% REM. The lower amount of 2-PA adsorption indicated by the Raman study ([Figure 4.14](#)) was also confirmed by TGA ([Table 4.5](#)) where the REM promotion clearly reduced the degree of weight loss for the catalysts after the reaction. These results agree with the changes of surface area and pore volume; the less 2-PA adsorbed, the less changes in the surface area and pore volume. REM promotion at the effective amount (1 wt%) leads to the reduction in basicity ([Figure 4.8](#)) and decreases the interaction between 2-PA and the catalyst surface. This results in reducing the rate of poisoning by 2-PA, thus enhancing the catalyst stability when 2-CP is used as

dehydrating agent. When the basicity is sufficiently high compared to the acidity (Figure 4.7), the activity of the catalyst is also enhanced and become ideal for this reaction.

Table 4.5 Summary of TGA for the materials (CeO₂ and 1 wt% REM) before and after the reaction

Material	Peak no.	Before reaction		After reaction	
		Weight loss / %	Peak max / °C	Weight loss / %	Peak max / °C
CeO ₂	1	7.23	50.8	2.83	31.5
	2	-	-	5.21	277.5
1 wt% La-CeO ₂	1	5.34	41	2.01	30.5
	2	-	-	4.64	272.9
1 wt% Gd-CeO ₂	1	5.77	38.9	2.83	30.5
	2	-	-	3.59	268.5
1 wt% Pr-CeO ₂	1	5.49	41.7	3.02	39.3
	2	-	-	3.39	268.5

Another important factor influencing the catalyst stability is the reducibility of the catalyst surface, which was promoted by REM, especially at 1 wt% for all REM types as discussed above. Redox properties change the charge state of atoms and this can consequently modulate the acid-base properties. When the reducibility is enhanced while retaining the active CeO₂ sites by REM (presumably those characterized by the H₂-TPR peak <500 °C), it is possible that the catalyst surface poisoned by 2-PA may change its redox state (Ce⁴⁺ ⇌ Ce³⁺) flexibly under the reaction condition and create an environment facilitating 2-PA desorption from the surface. This would be naturally positive for the catalyst stability and it is speculated that 1 wt% Gd or Pr promotion is particularly effective in inducing such a function while retaining the active catalytic sites of CeO₂.

4. 4 Conclusions

Effects of three types of promoters, namely Zr, precious metals (PM; Rh, Ru, Pd), and rare earth metals (REM; La, Gd, Pr), to CeO₂ on the long-term behavior of catalytic performance in continuous DMC synthesis from CO₂ and methanol in the presence of a dehydrating agent (2-CP) were evaluated. Among these, 1 wt% REM-promoted catalysts, especially Gd-CeO₂ and Pr-CeO₂, exhibited outstanding catalyst stability while retaining the high catalytic performance of CeO₂. The visual, spectroscopic (IR and Raman) and TGA investigations clarified that the surface adsorption of 2-PA produced by the hydration reaction of 2-CP is the cause of the catalyst deactivation and there was a clear relation between the amount of 2-PA adsorbed and the degree of catalyst deactivation. The origins of the promoter effects were studied in detail by characterizing the textural properties, acidity-basicity, and reducibility of the catalyst materials. The right balance in basicity and acidity, especially sufficiently high

4 | Effects of REM promoters

basicity/acidity ratio thus more basic nature, is found necessary to achieve excellent catalytic activity. The pure CeO_2 has the right acidity-basicity balance and it is retained for REM-promoted CeO_2 materials, while Zr and PM incorporation induced the reduction in basicity and this resulted in lower catalytic performance of these materials. On the other hand, it was indicated that the catalyst deactivation is correlated with the basicity as well as the reducibility of catalyst materials. When the basicity is lower and the catalyst reducibility is higher (i.e. easier to create surface defects), there was a clear improvement in the catalyst stability. The enhanced surface redox properties of the REM-promoted catalysts, especially at 1 wt% Gd/Pr, may have resulted in reduced basicity and assist facile desorption of 2-PA, thus improving the long-term stability. Remarkably, compared to CeO_2 , 1 wt% Pr- CeO_2 and 1 wt% Gd- CeO_2 exhibited 35% higher DMC yield after 150 h and 25% higher DMC yield after 100 h of time on stream, respectively. This greatly enhanced catalyst stability by the REM promoters in the light of the previously found reactivation strategy (calcination at 300 °C in air) render the process more attractive in practice to produce DMC from CO_2 and methanol.

Bibliography

- [1] A.-A.G. Shaikh, S. Sivaram, *Chem. Rev.*, 96 (1996) 951–976.
- [2] T. Sakakura, J.-C. Choi, H. Yasuda, *Chem. Rev.*, 107 (2007) 2365–2387.
- [3] T. Sakakura, K. Kohno, *Chem. Commun.*, (2009) 1312–1330.
- [4] Y. Ono, *Appl. Catal. A-Gen.*, 155 (1997) 133–166.
- [5] M. Aresta, E. Quaranta, *ChemTech*, 27 (1997) 32–40.
- [6] N. Keller, G. Rebmann, V. Keller, *J. Mol. Catal. A-Chem.*, 317 (2010) 1–18.
- [7] D. Delledonne, F. Rivetti, U. Romano, *Appl. Catal. A-Gen.*, 221 (2001) 241–251.
- [8] M.A. Pacheco, C.L. Marshall, *Energ. Fuel.*, 11 (1997) 2–29.
- [9] K. Tomishige, Y. Ikeda, T. Sakaihorii, K. Fujimoto, *J. Catal.*, 192 (2000) 355–362.
- [10] K. Tomishige, T. Sakaihorii, Y. Ikeda, K. Fujimoto, *Catal. Lett.*, 58 (1999) 225–229.
- [11] K. Tomishige, *Curr. Top. Catal.*, 3 (2002) 81 - 101.
- [12] X.L. Wu, M. Xiao, Y.Z. Meng, Y.X. Lu, *J. Mol. Catal. A-Chem.*, 238 (2005) 158–162.
- [13] X.L. Wu, Y.Z. Meng, M. Xiao, Y.X. Lu, *J. Mol. Catal. A-Chem.*, 249 (2006) 93–97.
- [14] Y. Ikeda, T. Sakaihorii, K. Tomishige, K. Fujimoto, *Catal. Lett.*, 66 (2000) 59–62.
- [15] Y. Ikeda, M. Asadullah, K. Fujimoto, K. Tomishige, *J. Phys. Chem. B*, 105 (2001) 10653–10658.
- [16] K. Tomishige, Y. Furusawa, Y. Ikeda, M. Asadullah, K. Fujimoto, *Catal. Lett.*, 76 (2001) 71–74.
- [17] K. Tomishige, K. Kunimori, *Appl. Catal. A-Gen.*, 237 (2002) 103–109.
- [18] H.J. Hofmann, A. Brandner, P. Claus, *Chem. Eng. Technol.*, 35 (2012) 2140–2146.
- [19] Y. Yoshida, Y. Arai, S. Kado, K. Kunimori, K. Tomishige, *Catal. Today*, 115 (2006) 95–101.
- [20] M. Aresta, A. Dibenedetto, C. Pastore, C. Cuocci, B. Aresta, S. Cometa, E.D. Giglio, *Catal. Today*, 137 (2008) 125–131.
- [21] M. Aresta, A. Dibenedetto, C. Pastore, A. Angelini, B. Aresta, I. Pápai, *J. Catal.*, 269 (2010) 44–52.
- [22] B.A.V. Santos, V.M.T.M. Silva, J.M. Loureiro, D. Barbosa, A.E. Rodrigues, *Fluid Phase Equilib.*, 336 (2012) 41–51.
- [23] B.A.V. Santos, C.S.M. Pereira, V.M.T.M. Silva, J.M. Loureiro, A.E. Rodrigues, *Appl. Catal. A-Gen.*, 455 (2013) 219–226.
- [24] A. Bansode, A. Urakawa, *ACS Catal.*, 4 (2014) 3877–3880.
- [25] B.A.V. Santos, V.M.T.M. Silva, J.M. Loureiro, A.E. Rodrigues, *Ind. Eng. Chem. Res.*, 53 (2014) 2473–2483.
- [26] C.-F. Li, S.-H. Zhong, *Catal. Today*, 82 (2003) 83–90.

4 | Effects of REM promoters

- [27] M. Honda, M. Tamura, Y. Nakagawa, S. Sonehara, K. Suzuki, K.-i. Fujimoto, K. Tomishige, *ChemSusChem*, 6 (2013) 1341–1344.
- [28] M. Honda, M. Tamura, Y. Nakagawa, K. Nakao, K. Suzuki, K. Tomishige, *J. Catal.*, 318 (2014) 95–107.
- [29] D. Stoian, A. Bansode, F. Medina, A. Urakawa, *Catal. Today*, (2016) <http://dx.doi.org/10.1016/j.cattod.2016.1003.1038>.
- [30] V. Eta, P. Maki-Arvela, A.-R. Leino, K. Kordas, T. Salmi, D.Y. Murzin, J.-P. Mikkola, *Ind. Eng. Chem. Res.*, 49 (2010) 9609–9617.
- [31] Z.-F. Zhang, Z.-W. Liu, J. Lu, Z.-T. Liu, *Ind. Eng. Chem. Res.*, 50 (2011) 1981–1988.
- [32] A. Trovarelli, *Catalysis by Ceria and Related Materials*, Imperial College Press 2002.
- [33] A. Trovarelli, *Catal. Rev.*, 38 (1996) 439-520.
- [34] A. Trovarelli, *Comment. Inorg. Chem.*, 20 (1999) 263-284.
- [35] R.J. Gorte, *AIChE J.*, 56 (2010) 1126–1135.
- [36] B.C.H. Steele, A. Heinzl, *Nature*, 414 (2001) 345-352.
- [37] B.M. Reddy, L. Katta, G. Thrimurthulu, *Chem. Mater.*, 22 (2010) 467–475.
- [38] T. Masui, T. Ozaki, K.-i. Machida, G.-y. Adachi, *J Alloy. Compd.*, 303-304 (2000) 49–55.
- [39] J.S. Moura, J.d.S.L. Fonseca, N. Bion, F. Epron, T.d.F. Silva, C.G. Maciel, J.M. Assaf, M.d.C. Rangel, *Catal. Today*, 228 (2014) 40–50.
- [40] T. Miki, T. Ogawa, M. Haneda, N. Kakuta, A. Ueno, S. Tateishi, S. Matsuura, M. Sato, *J. Phys. Chem.*, 94 (1990) 6464–6467.
- [41] B.K. Cho, *J. Catal.*, 131 (1991) 74-87.
- [42] J.G. Lee, J.H. Park, Y.G. Shul, *Nat. Commun.*, 5:4045 (2014).
- [43] A. Martínez-Arias, A.B. Hungría, M. Fernández-García, A. Iglesias-Juez, J. Soria, J.C. Conesa, J.A. Anderson, G. Munuera, *Phys. Chem. Chem. Phys.*, 14 (2012) 2144-2151.
- [44] B.M. Reddy, G. Thrimurthulu, L. Katta, *Catal. Lett.*, 141 (2011) 572-581.
- [45] Y. Tang, H. Zhang, L. Cui, C. Ouyang, S. Shi, W. Tang, H. Li, J.-S. Lee, L. Chen, *Phys. Rev. B*, 82 (2010) 125104
- [46] K. Ahn, D.S. Yoo, D.H. Prasad, H.-W. Lee, Y.-C. Chung, J.-H. Lee, *Chem. Mater.*, 24 (2012) 4261–4267.
- [47] V. Rico-Pérez, A. Bueno-López, *Appl. Sci.*, 4 (2014) 468-481.
- [48] A.M.d. Silva, K.R.d. Souza, G. Jacobs, U.M. Graham, B.H. Davis, L.V. Mattos, F.B. Noronha, *Appl. Catal. B-Environ.*, 102 (2011) 94–109.
- [49] H. Miura, K. Wada, S. Hosokawa, M. Sai, T. Kondo, M. Inoue, *Chem. Commun.*, (2009) 4112-4114.
- [50] P.d.C. Zonetti, R. Landers, A.J.G. Cobo, *Appl. Surf. Sci.*, 254 (2008) 6849–6853.

- [51] F. Wang, S. He, H. Chen, B. Wang, L. Zheng, M. Wei, D.G. Evans, X. Duan, *J. Am. Chem. Soc.*, 138 (2016) 6298–6305.
- [52] S. Hosokawa, S. Nogawa, M. Taniguchi, K. Utani, H. Kanai, S. Imamura, *Appl. Catal. A-Gen.*, 288 (2005) 67–73.
- [53] G. Li, L. Li, D. Jiang, *J. Phys. Chem. C*, 119 (2015) 12502–12507.
- [54] M.-F. Luo, Z.-Y. Hou, X.-X. Yuan, X.-M. Zheng, *Catal. Lett.*, 50 (1998) 205-209.
- [55] H.J. Lee, S. Park, I.K. Song, J.C. Jung, *Catal. Lett.*, 141 (2011) 531-537.
- [56] H.J. Lee, W. Joe, I.K. Song, *Korean J. Chem. Eng.*, 29 (2012) 317-322.
- [57] M. Wang, H. Wang, N. Zhao, W. Wei, Y. Sun, *Catal. Commun.*, 7 (2006) 6–10.
- [58] M. Wang, N. Zhao, W. Wei, Y. Sun, *Ind. Eng. Chem. Res.*, 44 (2005) 7596–7599.
- [59] W. Joe, H.J. Lee, U.G. Hong, Y.S. Ahn, C.J. Song, B.J. Kwon, I.K. Song, *J. Ind. Eng. Chem.*, 18 (2012) 1018–1022.
- [60] W. Joe, H.J. Lee, U.G. Hong, Y.S. Ahn, C.J. Song, B.J. Kwon, I.K. Song, *J. Ind. Eng. Chem.*, 18 (2012) 1730–1735.
- [61] N. Sergent, J.-F. Lamonier, A. Aboukaïs, *Chem. Mater.*, 12 (2000) 3830–3835.
- [62] M.G. Cutrufello, I. Ferino, V. Solinas, A. Primavera, A. Trovarelli, A. Auroux, C. Picciau, *Phys. Chem. Chem. Phys.*, 1 (1999) 3369-3375.
- [63] S. Wada, K. Oka, K. Watanabe, Y. Izumi, *Front. Chem.*, 1 (2013) 1-8.
- [64] K.R. Hahn, M. Iannuzzi, A.P. Seitsonen, J. Hutter, *J. Phys. Chem. C*, 117 (2013) 1701–1711.
- [65] V.R. Choudhary, V.H. Rane, *J. Catal.*, 130 (1991) 411-422.
- [66] K. Tanabe, *Mater. Chem. Phys.*, 13 (1985) 347-364.
- [67] T. Yamaguchi, *Sekiyu Gakkaishi*, 36 (1993) 250-267.
- [68] K. Tanabe, T. Yamaguchi, *Catal. Today*, 20 (1994) 185-197.
- [69] W. Khaodee, B. Jongsomjit, S. Assabumrungrat, P. Praserthdama, S. Goto, *Catal. Commun.*, 8 (2007) 548–556.
- [70] Y. Ikeda, Y. Furusawa, K. Tomishige, K. Fujimoto, *ACS Symp. Ser.*, 809 (2002) 71–84.
- [71] K.T. Jung, A.T. Bell, *J. Catal.*, 204 (2001) 339–347.
- [72] A. Migani, G.N. Vayssilov, S.T. Bromley, F. Illas, K.M. Neyman, *J. Mater. Chem.*, 20 (2010) 10535-10546.
- [73] N. Sutradhar, A. Sinhamahapatra, S. Pahari, M. Jayachandran, B. Subramanian, H.C. Bajaj, A.B. Panda, *J. Phys. Chem. C*, 115 (2011) 7628–7637.
- [74] S.K. Meher, G.R. Rao, *ACS Catal.*, 2 (2012) 2795–2809.
- [75] H.C. Yao, Y.F.Y. Yao, *J. Catal.*, 86 (1984) 254-265.
- [76] F. Giordano, A. Trovarelli, C.d. Leitenburg, M. Giona, *J. Catal.*, 193 (2000) 273–282.

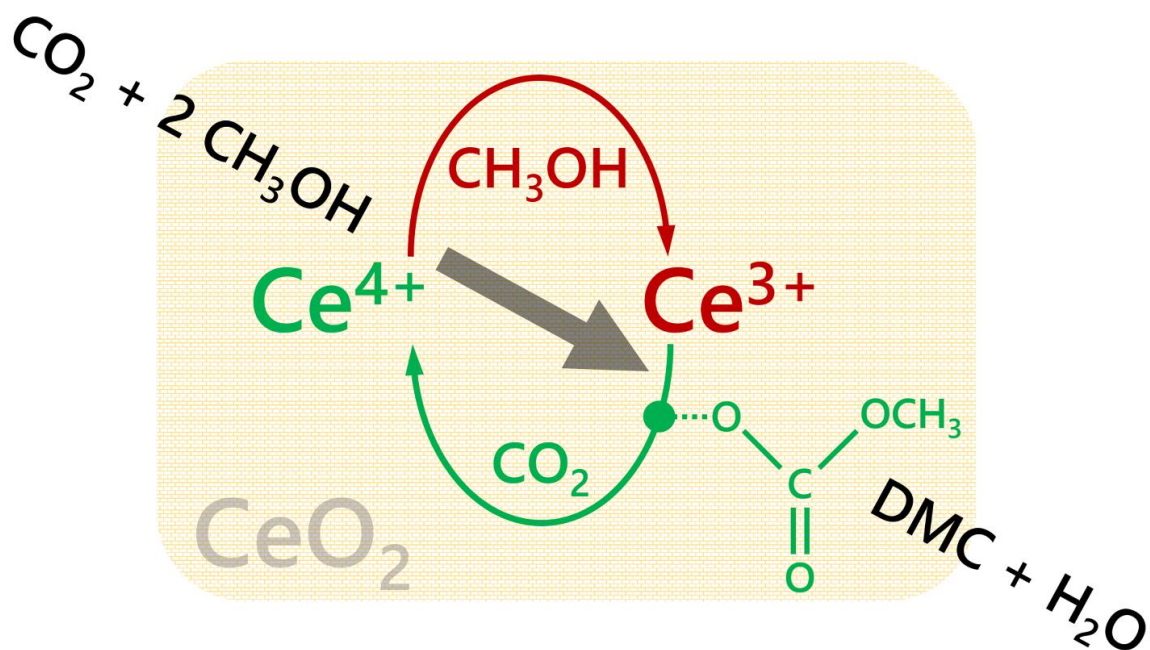
4 | Effects of REM promoters

- [77] I. Prymak, V.N. Kalevaru, S. Wohlrab, A. Martin, *Catal. Sci. Technol.*, 5 (2015) 2322-2331.
- [78] P. Fornasiero, R. Dimonte, G.R. Rao, J. Kaspar, S. Meriani, A. Trovarelli, M. Graziani, *J. Catal.*, 151 (1995) 168-177.
- [79] T. Murota, T. Hasegawa, S. Aozasa, H. Matsui, M. Motoyama, *J Alloy. Compd.*, 193 (1993) 298-299.
- [80] C. Pojanavaraphan, A. Luengnaruemitchai, E. Gulari, *Int. J. Hydrogen Energ.*, 38 (2013) 1348–1362.
- [81] Dobrosz-Gómez, M.Á. Gómez-García, J.M. Rynkowski, *Kinet. Catal.*, 51 (2010) 823–827.

5

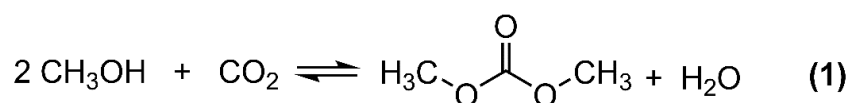
Mechanistic insights

Catching the surface intermediate and elucidating the redox contribution of CeO_2 during dimethyl carbonate synthesis from CO_2 and methanol



5.1 Background and motivation

The increasing interest in dimethyl carbonate (DMC) has been witnessed in the last decades for its usefulness: polar solvent for paints and coatings, methylating and carbonylating agent in organic synthesis, electrolytes in Li-ion batteries, and an appropriate substitute for methyl tert-butyl ether (MTBE) as a fuel additive owing to its high oxygen content [1-7]. While one of the major synthesis path of DMC is via the reaction between phosgene and methanol, nowadays the industrially recognized processes involve either oxidative carbonylation reactions using CO (Enichem, Ube and Bayer AG), transesterification reactions of organic carbonates with methanol (Asahi Kasei), or a two-step urea methanolysis method developed by Catalytic Distillation Technologies, Inc [8]. Despite the improvements, it can be easily understood why a safer, more eco-efficient and economic pathway for DMC synthesis is desired. Urged by the concerns on the global warming, the development of the direct reaction between CO₂ and short chain alcohols, particularly methanol (MeOH) and ethanol (EtOH), for the synthesis of organic carbonates such as DMC or diethyl carbonate (DEC) (**Reaction 1**, DMC synthesis) has drawn great attention in the light of CO₂ chemical fixation, green chemistry (high atom efficiency), and safety by replacing phosgene which is a toxic and corrosive reagent with CO₂ as carbonyl source.



In the last 20 years, various homogeneous and heterogeneous catalysts were reported for the direct carboxylation reaction of methanol using CO₂. Heterogeneous catalysts are more widely investigated and different materials have been tested under both batch and continuous operation. Among them, zirconia (ZrO₂), ceria (CeO₂), and ZrO₂-CeO₂ solid solutions [9-11] have been reported as the most effective catalysts in DMC synthesis, while other materials afforded no or very little formation of DMC [12]. Generally, the presence of both acidic and basic sites is required for the activation of both CO₂ and the methanol molecules. This is in good agreement with the reports supporting that ZrO₂, CeO₂ and CeO₂-ZrO₂ solid solutions present both the acidic and basic properties [13]. In practice, the reaction is highly thermodynamically limited and the DMC yield can be enhanced only up to about 1% even under thermodynamically favorable high-pressure conditions (ca. 400 bar) [14]. Recently, a drastic improvement in DMC yield (>90%) was reported by Tomishige *et al.* by *in situ* dehydration using 2-cyanopyridine (2-CP) as organic dehydrating agent over CeO₂ to remove the water byproduct (**Reaction 1**). CeO₂ functions as catalyst for both DMC synthesis and dehydration reaction optimally at ca. 120 °C. This strategy has been demonstrated for batch as well as continuous operation [14-17]. It is noteworthy that the reaction mechanism is

unaltered by the presence of 2-CP and understanding the simpler system without dehydrating agent can lead to the understanding of more complex yet practically relevant system in the presence of the dehydrating agent [16].

The unique catalytic performance of CeO₂ in this reaction may originate from the outstanding synergy between its acid-base properties together with its redox capabilities which include high lattice and surface oxygen mobility. Izumi *et al.* studied the reducibility of Cu (0.1 to 0.5 wt%)-promoted CeO₂ by X-ray absorption spectroscopy (XAS) by high temperature reduction treatment (400 °C) and subsequent CO₂ adsorption. They suggested that the partial reduction of Ce⁴⁺ sites to Ce³⁺ may be beneficial for DMC formation [18]. Also, Aresta *et al.* correlated by *ex situ* XPS the origin of catalyst deactivation, thus the activity, with the oxidation state of Ce [19, 20]. Despite of these indications, the contribution and importance of the redox properties of CeO₂ in the reaction has not been proven under working reaction (*operando*) conditions. Particularly, the reaction is commonly performed at relatively low temperatures (100-150 °C) where the reduction of surface and bulk CeO₂ is unlikely to occur according to temperature programmed reduction studies [21-23]. Furthermore, no *operando* spectroscopic investigation has been reported bridging the type of surface species present under reaction conditions with DMC formation by simultaneous detection of the product concentration.

Following the background, in this work we aim at capturing the surface intermediate species leading to DMC by diffuse reflectance infrared Fourier transform spectroscopy (DRIFTS) and also at elucidating the contribution of redox properties by XAS and Raman spectroscopy under working, *operando*, conditions. Transient techniques by periodical concentration perturbation were utilized to highlight the signals due to reactive species and the change in the oxidation state. These were later correlated with the product concentrations which was measured by mass spectrometry (MS). Importantly, multivariate analysis (here multivariate curve resolution (MCR) [24-26] was used) on the sets of large, complex spectroscopic data was employed to facilitate the spectral analysis by detecting subtle spectral changes in a blind-source manner without the necessity of reference spectra.

5.2 Experimental

High surface area CeO₂ powder (>100 m²/g) was kindly supplied by Daiichi Kigenso Kagaku Kogyo Co. Ltd., Japan and used without any further treatment. Methanol (>99%, HPLC grade) was purchased from Sigma Aldrich. High purity He (>99.999%) and CO₂ (>99.9993%, purchased from Abelló Linde) gas was used. A reaction setup similar to that already presented in the literature was employed for the *in situ/operando* XAS/Raman/MS measurements [25]. Synchrotron experiments were performed at the Swiss Norwegian Beam Line (SNBL) at the European Synchrotron Radiation Facility (ESRF) in Grenoble, France.

5 | Mechanistic insights

More information about the optics, beamline layout, monochromators design, and Raman probe design can be found in literature [27, 28]. Gaseous CO₂ and He were passed to the cell by means of mass flow controllers. The He flow was saturated with methanol and thus about 16.5 vol% of methanol was contained in the flow.

Operando DRIFTS-MS setup: all experiments were performed on a Bruker Vertex 70V IR spectrometer equipped with a liquid-nitrogen-cooled mercury cadmium telluride (LN-MCT) detector with a home-made temperature controlled stainless steel cell mounted in a Praying Mantis optical accessory (Harrick). The DRIFTS cell mimics the action of plug flow and the design is described elsewhere [29]. The measurement was performed at the center of the catalyst bed consisting of CeO₂. The Praying Mantis accessory consists of an optical system equipped with a series of mirrors for redirection and collection of diffuse reflected light as well as minimizing the detection of specularly reflected light. Spectra were collected at 4 cm⁻¹ resolution.

Operando Raman-MS experiments were carried out using Renishaw inVia spectrometer with 532 nm excitation laser (at SNBL, ESRF) as well as a BWTEK dispersive i-Raman portable spectrometers equipped with 532 and 785 nm excitation lasers and a TE-cooled linear array detector. A gas manifold was used to feed the reactants to the reaction cell (quartz capillary reactor, (Hilgenberg GmbH) with 0.7 mm OD and 10 μm wall thickness) and the heating system consisted of a commercially available high temperature (up to 500 °C) hot air gun.

A more detailed description of all the setups employed in the present study together with an exhaustive presentation of the multivariate curve resolution (MCR) technique can be found in [Chapter 2 \(Materials and methods\)](#).

Theoretical IR spectra calculation: band assignments of IR spectra were assisted by quantum chemical calculations of vibrational frequencies and intensities and normal mode analysis. They were calculated with density functional theory (DFT) using B3PW91 functional [30, 31] with 6-311++G(2d,2p) basis sets using Gaussian 09 [32] as an isolated molecule without solvent effects. The simulated IR spectra are shown as the sum of Lorentzian lines taking the calculated IR intensity of a normal mode as the height at each vibrational frequency.

5.3 Results and discussion

Figure 5.1 presents time-resolved *operando* DRIFT spectra and DMC concentration profile under a periodic concentration change of methanol (16.5 vol% in He, the first half period of 128 s) and CO₂ (the second half period of 128 s) performed at 120 °C and averaged over 8 periods to improve S/N. According to the MS signal (**Figure 5.1**, left), DMC was formed under the studied condition. The production level of DMC increased upon switching from CO₂ to methanol, reaching a constant level after ca. 40 s. Interestingly, the DMC production was boosted by ca. 5 times upon switching to CO₂ and then gradually ceased with time almost completely under the flow of CO₂. The differential DRIFT spectra (**Figure 5.1**, right; the last spectrum of the period, i.e. at the end of the CO₂ period, was used as the background) shows the characteristic C-O stretching vibrations of bridged and terminal methoxy species appearing at ca. 1060 and 1120 cm⁻¹, respectively, [10] as positive bands (in red) when the atmosphere was switched to methanol. At the same time, several negative bands characteristic of carbonates/bicarbonates were prominently observed in the region from 1150-1800 cm⁻¹ under the flow of CO₂. According to literature, these bands likely originate from carboxylate and protonated carboxylate species on the surface of the catalyst (at 1695 cm⁻¹), bridged (bi)carbonates (1235 and 1645 cm⁻¹), and monodentate and bidentate carbonates (1336, 1458 cm⁻¹ and 1282, 1548 cm⁻¹, respectively) [10, 33-36]. These results clearly indicate that carbonates/bicarbonates formed under CO₂ atmosphere were replaced (thus the bands appear negative) by methoxy under methanol atmosphere and vice versa under CO₂ atmosphere. At first glance, the DRIFT spectra do not show clear signatures of transient surface species whose concentration is similar to that of DMC, except a few slightly positive signals at ca. 1310 and 1630 cm⁻¹ appearing upon switching to CO₂. This sort of ambiguousness in spectral analysis is often encountered and arises from overlapping peaks and also impossibility to deconvolute the spectral contributions of different chemical species due to the unavailability of proper reference spectra of the chemical species that are only present/detected under reaction conditions and/or under transient conditions.

5 | Mechanistic insights

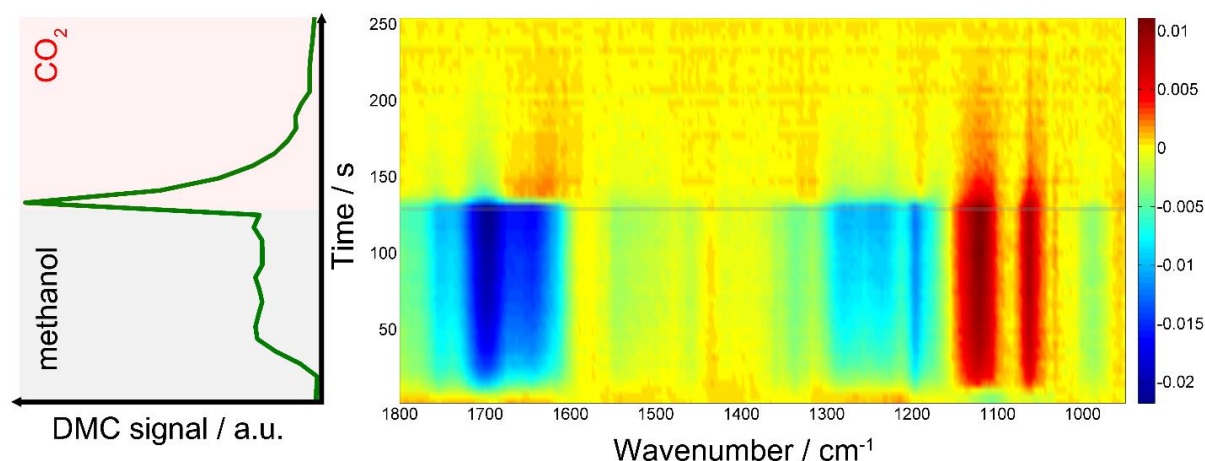


Figure 5.1 (left) MS signal of DMC ($m/z = 59$) and (right) time-resolved DRIFT spectra taken during methanol (the first half period) vs. CO₂ (the second half period) concentration perturbation experiment performed at 120 °C at 7 ml min⁻¹. The DRIFT spectra were calculated taking the last spectrum in the CO₂ atmosphere as background

To overcome this limitation, MCR analysis was employed to disentangle overlapping peaks into the spectra of “kinetically pure” components (i.e. surface species). Besides the spectral separation, it yielded conveniently the concentration profiles of the components. **Figure 5.2** shows the results of MCR analysis on the DRIFT spectra shown in **Figure 5.1**. The analysis found three kinetically-distinct components. Most strikingly, the analysis could separate the spectral component (**Figure 5.2**, green) with the concentration profile well-matching with that of DMC (**Figure 5.1**, left), which is indicative of surface species leading to DMC upon further transformation. The other two components show characteristic features of (i) methoxy species (**Figure 5.2**, black) and (ii) carbonate/bicarbonate species (**Figure 5.2**, red). The corresponding concentration profiles of these components (**Figure 5.2**, right) obviously reflect the atmosphere of the gas phase. The absorbance of the spectra appears with positive values because of the constraints employed (negative concentration was allowed), thus permitting more facile and direct interpretation of the disentangled component spectra.

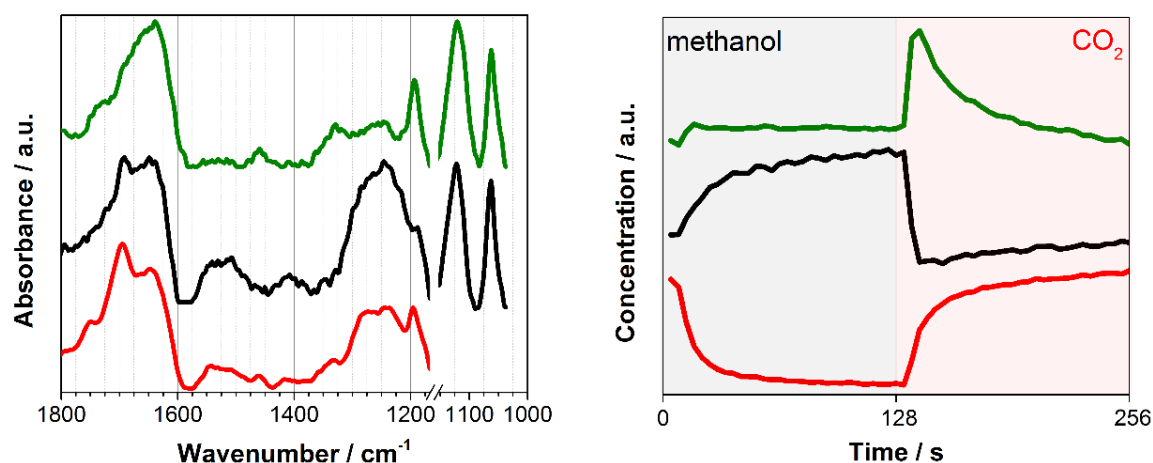


Figure 5.2 (*left*) Three components spectra and (*right*) the corresponding concentration profiles obtained by MCR analysis applied on the DRIFT spectra shown in **Figure 5.1** (the first half is methanol and the second half is CO₂ atmosphere). To ease the data analysis and improve component separation, MCR has been performed on two separate regions of methoxy (below 1170 cm⁻¹) and carbonates (above 1180 cm⁻¹). Both spectra and concentration profiles are normalized for clarity

In situ infrared and Raman studies reported by Tomishige, Bell and their co-workers over ZrO₂ materials suggested the formation of monomethyl carbonate (MMC, CH₃O-COO-Zr) as possible intermediate species through the reaction between methoxy species (CH₃O⁻) and CO₂ [37-39]. MMC further reacts with another molecule of methanol (methoxy) to afford DMC. Later, it was indicated that the reaction proceeds via the same intermediate (i.e. MMC) over CeO₂ catalysts [10, 16]. Besides, there are also reports supporting the existence of a different intermediate like carbomethoxide (CH₃OCO-Ce) species as suggested by Wang *et al.* [33]. The spectral characteristics of the captured intermediate (**Figure 5.2**, green) whose concentration profile resembles that of gas phase DMC generally show the mixed features of methoxy (1060 and 1120 cm⁻¹) and (bi)carbonates (e.g. 1200-1800 cm⁻¹), although they are somehow different especially in the region of 1200-1600 cm⁻¹ where the characteristic bands of MMC are expected to appear according to the literature [10, 20, 33, 40]. More precisely, Lavalley *et al.* assigned the two bands we observed at ca. 1330 and 1460 cm⁻¹ to a coupling between the bending mode of CH₃ and the stretching vibration of OCO [41]. This clearly indicates that the captured intermediate is MMC or species alike. The spectral features of the intermediate (**Figure 5.2**, green) in the methoxy region appear similarly to those of methoxy species (**Figure 5.2**, black). A closer look verifies that they are similar but there are noticeable differences especially in the band of terminal methoxy at ca. 1120 cm⁻¹, showing a broadening and a small shift towards lower vibrational frequency. This implies that the terminal methoxy has reacted or interacting with the CO₂ molecule trapped on the surface, resulting in the red shift. Also, it is interesting to note that the species responding to the gas-phase methanol concentration (**Figure 5.2**, black) show the spectral features of (bi)carbonates in the region

5 | Mechanistic insights

1200-1800 cm^{-1} . This is indicative of the formational correlation of methoxy species with specific surface (bi)carbonate species which are not replaced but uniquely generated by the formation of methoxy species. The dissociation of MeOH into MeO and H is expected to take place upon methanol adsorption over CeO_2 and this H may lead to more pronounced formation of bicarbonates from carbonates and the spectral feature of the methoxy species may reflect the accompanied formation of bicarbonate surface species since MCR cannot disentangle spectral components behaving kinetically identical.

The nature of the intermediate species was examined by means of the identical study with MCR analysis using ^{13}C -labeled CO_2 and ^{13}C -labeled methanol. **Figure 5.3** presents the component spectra whose concentration profile follows that of DMC formation (**Figure 5.2**, green) for the three cases (unlabeled, $^{13}\text{CH}_3\text{OH}$, and $^{13}\text{CO}_2$).

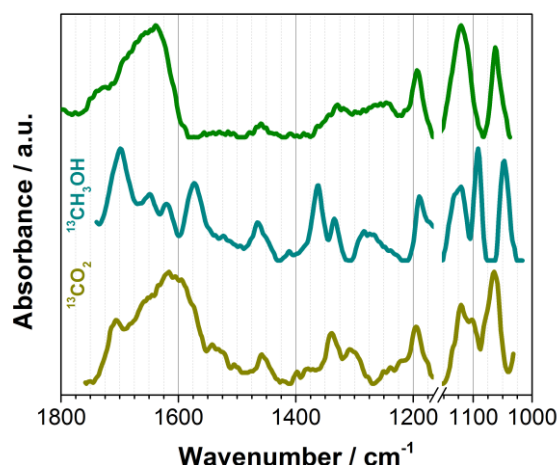


Figure 5.3 The component spectra of the identified intermediate leading to DMC formation for the three cases using unlabeled CO_2 and methanol (top, i.e. **Figure 5.2**, green), $^{13}\text{CH}_3\text{OH}$ (middle), and $^{13}\text{CO}_2$ (bottom) obtained by the MCR analysis

When ^{13}C -labeled methanol was used, in the region of methoxy bands (1020-1150 cm^{-1}) there were clear red-shifts of both terminal and bridged bands by ca. 30 and 10 cm^{-1} , respectively. According to a DFT calculation, about 25 cm^{-1} red-shift of C-O stretching is expected upon ^{13}C -labeling of methoxy carbon in MMC anion (see **Appendix E, Figure 7.6** for DFT results). This degree of shift is in good agreement for the terminal methoxy but not for the bridged one. This difference may originate from the more distorted state of the C-O bond, in other words a stronger influence of CeO_2 surface to the bond, in the methoxy group upon bridge adsorption over CeO_2 . Interestingly, with $^{13}\text{CH}_3\text{OH}$ the band at ca. 1120 cm^{-1} was unshifted. This indicates that the carbonate-like moiety of the intermediate may have an infrared-active vibration at that position, which is naturally unbiased upon methanol-carbon labeling. Tomishige *et al.* also related the presence of a band around 1110 cm^{-1} to the

existence of the MMC intermediate [10]. The experiment with $^{13}\text{CO}_2$ supports this view since the two band positions do not change obviously but there are bands arising at ca. 1080 and 1100 cm^{-1} , indicating that the carbonate-like moiety of the intermediate may have a band at the frequency close to the C-O stretching of the terminal methoxy.

There were also clear 30-50 cm^{-1} red-shifts of (bi)carbonate bands appearing at 1600-1800 cm^{-1} when $^{13}\text{CO}_2$ was used. This shift is in good agreement with the DFT calculation (ca. 50 cm^{-1}) where the carbon of the carbonate in MMC anion was labelled (see [Appendix E, Figure 7.6](#) for DFT results). The most drastic change was observed in the region of 1150-1800 cm^{-1} when $^{13}\text{CH}_3\text{OH}$ was used. Even the generally assigned carboxylate vibrations mentioned above (1600-1800 cm^{-1}) underwent great changes apparently with more distinct spectral features compared to the unlabeled case. This is a clear indication of a coupling of oxygen atoms of adsorbed CO_2 as (bi)carbonate with the carbon of methanol molecule present in methoxy.

Furthermore, under similar transient conditions we looked into the change in the oxidation state of Ce by XAS at Ce K and L3-edges and in associated structural changes by Raman spectroscopy. Under oxidation (O_2) and reduction (H_2) treatment at high temperature (350 $^\circ\text{C}$), the MCR analysis on the XAS and Raman data could clearly extract the redox features of CeO_2 (see [Appendix E, Figure 7.7 – 7.9](#)), whereas these redox features could not be observed at the reaction temperature of 100-150 $^\circ\text{C}$ which was obviously too low for the redox to take place as expected. Although we could not detect spectral changes in the bulk-sensitive XAS under the transient reaction conditions of MeOH vs. CO_2 flow, there was a clear change in the F_{2g} Raman active mode at ca. 460 cm^{-1} , corresponding to the symmetric breathing of O^{2-} atoms vibrations around the Ce^{4+} cations ([Figure 5.4](#)). The width and position of this band is known to be extremely sensitive to any structural disorder of the O-sublattice [42]. MCR analysis on the Raman data disentangled the two spectral components with contrasting concentration profiles: one increasing upon CO_2 exposure which is obviously assigned to the band associated with the Ce^{4+} state ([Figure 5.4](#), Component 1, red), and the other increasing with methanol with the band feature slightly red-shifted and broadened ([Figure 5.4](#), Component 2, black). These changes are in accordance with the reports on CeO_2 -based materials under reduction-oxidation cycles [43-45]. This subtle change took place on the surface of the material and therefore could not be measured by XAS. Likewise, the change was less obvious when a longer wavelength excitation laser (785 nm) was used in Raman since in this case we sample more bulk of the material (see [Appendix E, Figure 7.10](#)). Recently, Tomishige *et al.* reported the redox properties of CeO_2 catalysts in organic reactions (i.e. synthesis of imines from alcohols and amines) at temperature as low as 30 $^\circ\text{C}$ [46]. This

5 | Mechanistic insights

study further confirms that redox property of CeO_2 plays key roles in the catalytic cycle of the DMC synthesis from CO_2 and methanol.

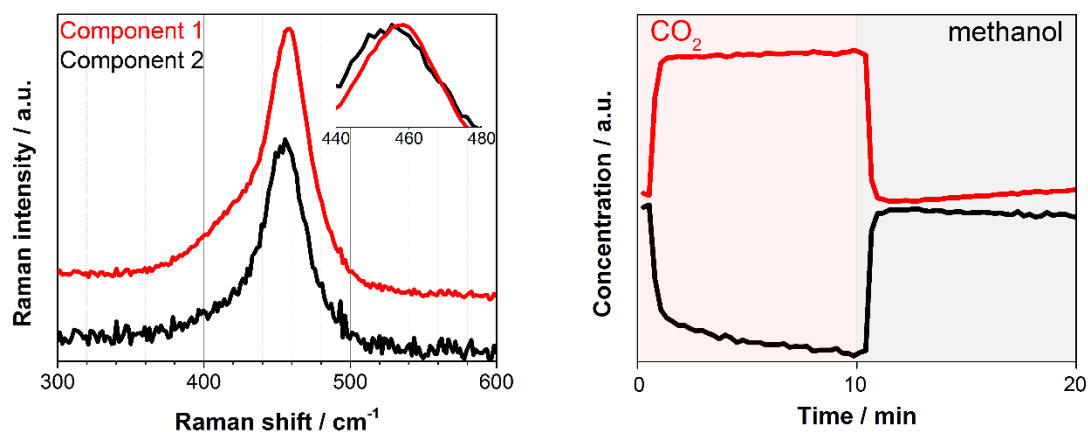


Figure 5.4 MCR applied for F_{2g} band of CeO_2 during DMC synthesis experiment (CO_2 vs. methanol) at 140°C . The Raman measurement was performed with a 532 nm laser (green). Both spectra (*left*) and concentration (*right*) profiles are normalized for clarity

5.4 Conclusions

In summary, the present study showed the involvement of CeO_2 redox properties in the gas phase DMC synthesis from CO_2 and methanol. While methanol acts as a reducing agent for CeO_2 , CO_2 behaves as an oxidizing agent. Furthermore, a boost in DMC production is observed when CO_2 is passed over methoxy covered surface accompanying the oxidation of CeO_2 . The surface intermediate species directly correlated with DMC formation was elucidated by *operando* DRIFTS with the aid of MCR analysis. It showed the feature of both methoxy and (bi)carbonates, in accordance with the reported structure of monodentate methyl carbonate (MMC). The isotopic labeling study indicated that the carbon in methyl/methoxy group of MMC strongly interacts with the CO bond of the carbonate moiety, implying that the methyl group may be delocalized around the carbonate (anion) even within the time-scale of IR spectroscopy, thus strongly coupling with the carbonate vibrations.

Bibliography

- [1] A.-A.G. Shaikh, S. Sivaram, *Chem. Rev.*, 96 (1996) 951–976.
- [2] T. Sakakura, J.-C. Choi, H. Yasuda, *Chem. Rev.*, 107 (2007) 2365–2387.
- [3] Y. Ono, *Appl. Catal. A-Gen.*, 155 (1997) 133–166.
- [4] M. Aresta, E. Quaranta, *ChemTech*, 27 (1997) 32-40.
- [5] N. Keller, G. Rebmann, V. Keller, *J. Mol. Catal. A-Chem.*, 317 (2010) 1-18.
- [6] D. Delledonne, F. Rivetti, U. Romano, *Appl. Catal. A-Gen.*, 221 (2001) 241–251.
- [7] M.A. Pacheco, C.L. Marshall, *Energ. Fuel.*, 11 (1997) 2–29.
- [8] I. Garcia-Herrero, R.M. Cuellar-Franca, V.M. Enríquez-Gutierrez, M. Alvarez-Guerra, A. Irabien, A. Azapagic, *ACS Sustain. Chem. Eng.*, 4 (2016) 2088–2097.
- [9] K. Tomishige, T. Sakaihorii, Y. Ikeda, K. Fujimoto, *Catal. Lett.*, 58 (1999) 225-229.
- [10] Y. Yoshida, Y. Arai, S. Kado, K. Kunimori, K. Tomishige, *Catal. Today*, 115 (2006) 95–101.
- [11] K. Tomishige, Y. Furusawa, Y. Ikeda, M. Asadullah, K. Fujimoto, *Catal. Lett.*, 76 (2001) 71-74.
- [12] K. Tomishige, *Curr. Top. Catal.*, 3 (2002) 81 - 101.
- [13] M.G. Cutrufello, I. Ferino, V. Solinas, A. Primavera, A. Trovarelli, A. Auroux, C. Picciau, *Phys. Chem. Chem. Phys.*, 1 (1999) 3369-3375.
- [14] A. Bansode, A. Urakawa, *ACS Catal.*, 4 (2014) 3877–3880.
- [15] M. Honda, M. Tamura, Y. Nakagawa, S. Sonehara, K. Suzuki, K.-i. Fujimoto, K. Tomishige, *ChemSusChem*, 6 (2013) 1341–1344.
- [16] M. Honda, M. Tamura, Y. Nakagawa, K. Nakao, K. Suzuki, K. Tomishige, *J. Catal.*, 318 (2014) 95–107.
- [17] D. Stoian, A. Bansode, F. Medina, A. Urakawa, *Catal. Today*, (2016) <http://dx.doi.org/10.1016/j.cattod.2016.1003.1038>.
- [18] S. Wada, K. Oka, K. Watanabe, Y. Izumi, *Front. Chem.*, 1 (2013) 1-8.
- [19] M. Aresta, A. Dibenedetto, C. Pastore, C. Cuocci, B. Aresta, S. Cometa, E.D. Giglio, *Catal. Today*, 137 (2008) 125–131.
- [20] M. Aresta, A. Dibenedetto, C. Pastore, A. Angelini, B. Aresta, I. Pápai, *J. Catal.*, 269 (2010) 44–52.
- [21] A. Trovarelli, *Comment. Inorg. Chem.*, 20 (1999) 263-284.
- [22] S.K. Meher, G.R. Rao, *ACS Catal.*, 2 (2012) 2795–2809.
- [23] H.C. Yao, Y.F.Y. Yao, *J. Catal.*, 86 (1984) 254-265.
- [24] A. Malik, A.d. Juan, R. Tauler, 40 Years of Chemometrics – From Bruce Kowalski to the Future, *ACS Symposium Series*, pp. 95-128.

5 | Mechanistic insights

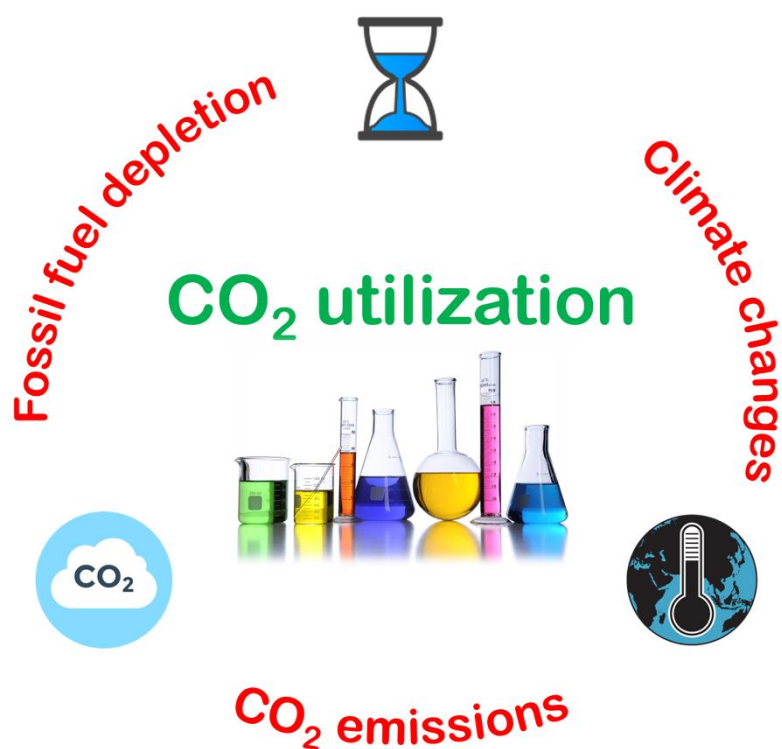
- [25] A. Voronov, A. Urakawa, W.v. Beek, N.E. Tsakoumis, H. Emerich, M. Rønning, *Anal. Chim. Acta*, 840 (2014) 20-27.
- [26] T. Hyakutake, W.v. Beek, A. Urakawa, *J. Mater. Chem. A*, 4 (2016) 6878-6885.
- [27] <http://www.esrf.eu/>, 2016, pp. SNBL workstation.
- [28] W.v. Beek, O.V. Safonova, G. Wiker, H. Emerich, *Phase Transit.*, 84 (2011) 726–732.
- [29] A. Urakawa, N. Maeda, A. Baiker, *Angew. Chem. Int. Edit.*, 47 (2008) 9256 –9259.
- [30] A.D. Becke, *J. Chem. Phys.*, 98 (1993) 5648–5652.
- [31] J.P. Perdew, Y. Wang, *Phys. Rev. B*, 45 (1992) 13244–13249.
- [32] M.J. Frisch, G.W. Trucks, H.B. Schlegel, G.E. Scuseria, M.A. Robb, J.R. Cheeseman, G. Scalmani, V. Barone, B. Mennucci, G.A. Petersson, H. Nakatsuji, M. Caricato, X. Li, H.P. Hratchian, A.F. Izmaylov, J. Bloino, G. Zheng, J.L. Sonnenberg, M. Hada, M. Ehara, K. Toyota, R. Fukuda, J. Hasegawa, M. Ishida, T. Nakajima, Y. Honda, O. Kitao, H. Nakai, T. Vreven, J. Montgomery, J. A., J.E. Peralta, F. Ogliaro, M. Bearpark, J.J. Heyd, E. Brothers, K.N. Kudin, V.N. Staroverov, R. Kobayashi, J. Normand, K. Raghavachari, A. Rendell, J.C. Burant, S.S. Iyengar, J. Tomasi, M. Cossi, N. Rega, J.M. Millam, M. Klene, J.E. Knox, J.B. Cross, V. Bakken, C. Adamo, J. Jaramillo, R. Gomperts, R.E. Stratmann, O. Yazyev, A.J. Austin, R. Cammi, C. Pomelli, J.W. Ochterski, R.L. Martin, K. Morokuma, V.G. Zakrzewski, G.A. Voth, P. Salvador, J.J. Dannenberg, S. Dapprich, A.D. Daniels, O. Farkas, J.B. Foresman, J.V. Ortiz, J. Cioslowski, D.J. Fox, *Gaussian 09, Revision A.02*, Gaussian, Inc., Wallingford CT, 2009.
- [33] L. Chen, S. Wang, J. Zhou, Y. Shen, Y. Zhao, X. Ma, *RSC Adv.*, 4 (2014) 30968-30975.
- [34] S.-Y. Zhao, S.-P. Wang, Y.-J. Zhao, X.-B. Ma, *Chinese Chem. Lett.*, (2016).
- [35] G.N. Vayssilov, M. Mihaylov, P.S. Petkov, K.I. Hadjiivanov, K.M. Neyman, *J. Phys. Chem. C*, 115 (2011) 23435–23454.
- [36] O. Pozdnyakova, D. Teschner, A. Wootsch, J. Kröhnert, B. Steinhauer, H. Sauer, L. Toth, F.C. Jentoft, A. Knop-Gericke, Z. Paál, R. Schlögl, *J. Catal.*, 237 (2006) 17–28.
- [37] K. Tomishige, Y. Ikeda, T. Sakaihorii, K. Fujimoto, *J. Catal.*, 192 (2000) 355–362.
- [38] S. Xie, A.T. Bell, *Catal. Lett.*, 70 (2000) 137-143.
- [39] K.T. Jung, A.T. Bell, *J. Catal.*, 204 (2001) 339–347.
- [40] J. Lamotte, V. Moravek, M. Bensitel, J.C. Lavalley, *React. Kinet. Catal. Lett.*, 36 (1988) 113-118.
- [41] M. Bensitel, V. Moravek, J. Lamotte, O. Saur, J.C. Lavalley, *Spectrochim. Acta A*, 43 (1987) 1487-1491.
- [42] W.Y. Hernández, O.H. Laguna, M.A. Centeno, J.A. Odriozola, *J. Solid State Chem.*, 184 (2011) 3014–3020.

- [43] M. Machida, T. Kawada, H. Fujii, S. Hinokuma, J. Phys. Chem. C, 119 (2015) 24932–24941.
- [44] L.E. Gomez, J.F. Munera, B.M. Sollier, E.E. Miro, A.V. Boix, Int. J. Hydrogen Energ., 41 (2016) 4993–5002.
- [45] S. Lorentzou, G. Karagiannakis, D. Dimitrakis, C. Pagkoura, A. Zygogianni, A.G. Konstandopoulos, Energy Procedia, 69 (2015) 1800 – 1809
- [46] M. Tamura, K. Tomishige, Angew. Chem. Int. Ed., 54 (2015) 864 –867.

5 | Mechanistic insights

6

Conclusions and Outlook



6 | Conclusions and Outlook

6.1 Summary of the thesis

The subject of this thesis was the continuous dimethyl carbonate (DMC) synthesis via direct carboxylation reaction of methanol (CH_3OH) with carbon dioxide (CO_2). The major challenge that comes together with this highly equilibrium limited process lies in the extremely low methanol conversion ($\leq 1\%$) and DMC yield values even under thermodynamically favorable high-pressure conditions. Consequently, a high-pressure laboratory scale microreactor setup (up to 300 bar) for the continuous catalytic transformation of CO_2 towards DMC was successfully designed and implemented, achieving the major task of the present research project. To overcome the thermodynamic limitations (endergonic process with $\Delta_r G^\ominus @ 298 \text{ K} = 26.21 \text{ kJ/mole} \rightarrow$ non-spontaneous under normal conditions of pressure and temperature), the use of an appropriate organic dehydrating agent was employed (2-cyanopyridine, 2-CP). It is mandatory to efficiently remove the water formed during the DMC production and shift the equilibrium on the product side. The known role of 2-CP as a dehydrating agent for a batch reaction system has been successfully employed in a continuous process. Moreover, the *in situ* dehydration presents a highly important practical aspect since the separation of a water-methanol-DMC ternary mixture is extremely difficult to realize at industrial scale. Particularly, the heating of the back-pressure regulator (BPR) with ensured proper functionality was vital, and a modification to the BPR was made to allow adequate heating at the position where the fluid passed through. To reach a good separation between the high boiling point compounds (originating from 2-CP) and the low boiling point ones (mostly methanol and DMC), the outlet of the BPR was connected to the in-house built hot trap-cold trap separation system. Only the products directly or indirectly originated from methanol above the trace level were quantified and discussed in the present study. The reaction product identification and analysis was carried out by a gas chromatograph (GC) equipped with a flame ionic detector (FID) coupled with a mass spectrometer (MS) from Bruker. The GC method for product separation was successfully developed.

The reactor setup was used for CO_2 valorization towards DMC. It is well known that very few metal oxides are catalytically active for the direct carbonate synthesis from alcohol and CO_2 (i.e. zirconia, ZrO_2 , CeO_2 , and ceria-zirconia mixed oxides/solid solutions). Despite offering good selectivity for DMC, in conditions without any dehydrating agents their activity is very poor. After an exhaustive screening of materials, conditions, and reactors design, throughout this project it was strengthened the idea that ceria (CeO_2) is one very special and unique material for this reaction. The ideal synergy between this rather abundant rare earth metal oxide and the organic dehydrating agent (2-CP) has proven extremely efficient under both batch and continuous operations. Especially, by implementing the protocol in a continuous flow system high DMC yield with a much shorter reaction time than in a batch

operation has been achieved. Under this approach, side-reactions involving the dehydrating agent and the hydrated products could not be avoided. Deactivation of the catalyst by the dehydrating agents or the corresponding derivatives is also a commonly encountered issue in this field. More than 50% methanol conversion drop was observed by using CeO_2 catalyst during ca. 10 days of time on stream (TOS). Importantly, Tomishige *et al.* (2013) have shown the recyclability of the dehydrating agent, a very significant observation in view of practical use, over $\text{Na}_2\text{O}/\text{SiO}_2$ catalyst.

First, the cause of the catalyst deactivation was deeply investigated. For that purpose, the common stainless steel (SS) reactors were replaced by optically transparent, fused quartz reactors. They were meant to allow visual and spectroscopic inspection of the catalyst under *operando* conditions. Initially, the verification of the quartz reactors (at temperatures ranging from 70 to 160 °C and pressure from 1 to 30 bar) afforded good functionality of the system and good reproducibility of the results obtained with SS reactors. Moreover, it has been demonstrated that there is an optimum condition (30 bar, 120 °C) to achieve high catalytic performance in terms of methanol conversion (X_{MeOH}) and DMC selectivity (S_{DMC}). The first striking observation while using the fused quartz reactors was related with the severe color change of the light yellowish CeO_2 catalyst which turns dark maroon within the first hours of the reaction. The color change of the catalyst could be correlated with the X_{MeOH} drop.

The great advantage of using optically transparent quartz reactors is that they are ideal to perform spectroscopic studies (e.g. Raman and UV-Vis spectroscopy). However, our attempts to run *operando* Raman (lasers with excitation wavelength at 532 and 785 nm) analysis failed due to strong fluorescence observed under the reaction conditions. This was most likely a consequence of the products originating from 2-CP. To disentangle the cause of CeO_2 deactivation, a combined *ex situ* ATR-IR and Raman approach was employed. Based on the Raman and IR studies (supported by DFT calculations), it was identified that 2-picolinamide (2-PA, and not coke formation as it was initially speculated) is the main source of catalyst deactivation by strongly binding to and thus poisoning the catalyst surface at increased time on stream. The space resolved spectroscopic results along the catalyst bed showed the existence of a gradient reflecting how much the catalyst was poisoned (more intense towards the inlet and less intense towards the outlet of the reactor) in very good agreement with the color gradient visually observed.

Most importantly from practical point of view, complete catalyst reactivation was achieved under mild conditions, just by using *in situ* methanol washing coupled with a moderate thermal treatment at 300 °C in air (in less than 1 h). Furthermore, the use of quartz reactors afforded the observation of the complete synergy between the solid catalyst, the liquid methanol and

6 | Conclusions and Outlook

2-CP mixture, and gaseous CO₂ – the reaction is taking place in both bulk and surface of CeO₂ catalyst. This would explain the higher conversion efficiency of the continuous system in comparison with the batch one, likely occurring due to a much better mixing of CO₂, methanol, and the dehydrating agent over the catalyst.

After addressing the catalyst deactivation issue, an even bigger challenge arose. For a catalyst to be industrially relevant there are many requirements that must be fulfilled. A successful catalyst should allow the reaction to proceed at a fast rate under conditions that are economically advantageous (i.e. low temperature and low pressure) and it must also be long lasting and selective. In this context, the effects of three types of promoters, namely Zr, precious metals (PMs; Rh, Ru, Pd), and rare earth metals (REMs; La, Gd, Pr), to CeO₂ on the long-term behavior of catalytic performance in continuous DMC synthesis from CO₂ and methanol in the presence of a dehydrating agent (2-CP) were investigated. Reactions were run under previously optimized conditions of 120 °C and 30 bar. Among the tested materials, 1 wt% REM-promoted catalysts, especially Gd-CeO₂ and Pr-CeO₂, exhibited outstanding catalyst stability while retaining the high catalytic performance of bare CeO₂. In the present study, Zr incorporation into CeO₂ as well as PMs promotion of CeO₂ showed rather poor catalytic results. Nevertheless, CeO₂-ZrO₂ solid solutions displayed high and stable S_{DMC}.

Unfortunately, the catalyst poisoning by 2-PA adsorption could not be completely prevented. However, the results of the visual, spectroscopic (*ex situ* ATR-IR and Raman) and TGA investigations of the pristine CeO₂ and 1 wt% REM promoted CeO₂ before and after a 30 h catalytic test clarified that there was a clear relationship between the amount of 2-PA adsorbed and the degree of catalyst deactivation. The better the catalyst, the less 2-PA adsorbed over its surface. Clearly, small amounts of REMs finely dispersed over CeO₂ promote the long term catalytic activity and stability. To better understand the origin of the promoter effects, they were thoroughly investigated by characterizing the textural properties, acidity-basicity, and reducibility of the catalyst materials. It was discovered that the right balance in basicity and acidity, especially at sufficiently high basicity/acidity ratio (>1) thus more basic nature, is essential to achieve excellent catalytic activity. It is confirmed that the pure CeO₂ has the right acidity-basicity balance that is retained for REM-promoted CeO₂ materials, while Zr and PM incorporation induced the reduction in basicity and this resulted in lower catalytic performance of these materials. Additionally, there are indications that correlate the catalyst deactivation with the basicity and the reducibility of the materials. When the basicity is lower and catalyst reducibility is higher (i.e. easier to create surface defects and increased surface oxygen mobility), there was a clear improvement in the catalyst stability. The enhanced surface redox properties of the REM-promoted catalysts, especially at 1 wt% Gd/Pr, may have resulted in reduced basicity and assist facile desorption of 2-PA (or directly

hindering 2-PA adsorption), thus improving the long-term stability. Nevertheless, deeper investigation is required to completely comprehend the implications of REMs over CeO₂.

Remarkably, the total cooperation between acidity, basicity and reducibility in the case of REM promoted CeO₂ led to great catalytic results. Compared to CeO₂, 1 wt% Pr-CeO₂ and 1 wt% Gd-CeO₂ exhibited 35% higher DMC yield after 150 h and 25% higher DMC yield after 100 h of time on stream, respectively. In the light of the previously mentioned reactivation protocol, this great enhancement in the catalyst stability by addition of REM promoters render the process much more attractive in practice to produce DMC from CO₂ and methanol.

To gain better insights into the reaction pathway, a mechanistic study of the gas phase direct DMC synthesis from CO₂ and methanol was conducted. This was achieved by using a combined *operando* approach (XAS/Raman/MS and DRIFTS/MS) coupled with the adequate chemometric method (multivariate curve resolution, MCR). It was the first attempt ever to capture by diffuse reflectance infrared Fourier transform spectroscopy (DRIFTS) the surface intermediate species leading to DMC formation and to elucidate the contribution of redox properties of CeO₂ by XAS and Raman spectroscopy under working, *operando*, conditions. At the same time, the product concentration was continuously followed by using mass spectrometry (MS). Transient techniques by periodical concentration perturbation were employed to highlight the signals due to reactive species and the change in the oxidation state of Ce in CeO₂. To overcome the common limitations arose from *in situ/operando* spectroscopic measurements, i.e. overcrowded spectra, overlapping peaks and impossibility to deconvolute the spectral contributions of different chemical species, MCR was utilized as a very powerful blind source and spectral separation method. It allowed disentangling overlapping spectral features into the spectra of kinetically pure components and the corresponding concentration profile without any *a priori* information or the need for external spectral libraries.

The surface intermediate species directly correlated with DMC formation was elucidated by *operando* DRIFTS with the aid of MCR analysis. It is formed by the reaction between pre-adsorbed methanol (i.e. as terminal methoxy species) and (bi)carbonates arising from CO₂ molecules. It showed the feature of both methoxy and (bi)carbonates, in accordance with the previously reported structure of monodentate methyl carbonate (MMC) intermediate. More importantly, the isotopic labeling experiments together with the DFT calculations indicated that the carbon in methyl/methoxy group of MMC strongly interacts with the CO bond of the carbonate moiety, implying that the methyl group may be delocalized around the carbonate (anion), thus strongly coupling with the carbonate vibrations.

CeO₂ is a very well-known acid-base catalyst. It is also a famous material for its oxygen storage/release capacity (OSC) due to swiftly switching between 4+ and 3+ oxidation states

6 | Conclusions and Outlook

($\text{Ce}^{4+} \leftrightarrow \text{Ce}^{3+}$) under proper reaction conditions. Traditionally, the partial reduction of CeO_2 is known to promote electron-donating type of catalysis. Up to date there were no clear proofs resulted from *in situ/operando* studies relating the redox properties of CeO_2 with the catalytic activity in the methanol carboxylation reaction. In the present study, it was discovered that despite running at moderate temperatures from 100 to 150 °C, CeO_2 shows clear and direct redox involvement in DMC synthesis. While methanol can act as a reducing agent for CeO_2 and inhibiting the DMC formation, CO_2 behaves as an oxidizing agent preventing the methanol oxidation and CeO_2 reduction. Importantly, the manifestation of the redox behavior covers only a small portion of the catalyst surface as it could be unraveled by *operando* Raman studies but not from XAS measurements. Furthermore, a boost in DMC production is observed at low CO_2 coverage, whereas this one rapidly goes to zero at higher coverage.

6.2 Open challenges and outlook

In the context of fossil fuel depletion and CO₂ accumulation in the atmosphere directly linked to the increasing global temperature of the earth and severe climate changes, this thesis dealt with the activation of CO₂, a thermodynamically stable and highly unreactive molecule, towards the production of organic carbonates (i.e. dimethyl carbonate). As already mentioned, dimethyl carbonate is a very good polar solvent for paints and coatings, methylating and carbonylating agent in organic chemistry synthesis, electrolytes in Li-ion batteries, and an appropriate substitute for methyl tert-butyl ether (MTBE) as a fuel additive owing to its very high oxygen content. Replacing old-fashioned and much more dangerous routes, such as phosgene (COCl₂) path or carbonylation (requiring CO / NO) reactions, with processes such as carboxylation of alcohols, alcoholysis of urea, and transesterification of cyclic carbonates for the synthesis of linear organic carbonates represents a great challenge for both academia and industry. Nonetheless, the direct carboxylation of alcohols has strong limitations due to the thermodynamics (the equilibrium concentration at 100–200 °C is around 1%) and to the water formation that may destroy the catalysts and shift the equilibrium on the reactants side. Implementing such technologies on a larger scale while using heterogeneous catalysts, which can be easily recovered, reactivated (if necessary), and reused is even a more difficult task. Now, the direct synthesis of DMC starting from methanol and carbon dioxide is less promising than the other CO₂-based routes due to its higher Gibbs free energy values and lower product yields. The results shown in this thesis are highly relevant as CO₂ mitigation strategy as well as to utilize the carbon which is found in CO₂ for the synthesis of valuable chemicals. Regardless of the spectacular improvement by the usage of 2-CP against other approaches (i.e. catalytic membrane reactors, CMR, other chemical or physical water traps, or high pressure-high temperature conditions), further research is still required for the regeneration reaction of 2-PA back to 2-CP. This is obvious since the recovery of 2-CP from 2-PA takes more than 400 hours over a Na₂O/SiO₂ catalyst to afford ca. 84% yield of 2-CP. Only if this reaction can be carried out on a large scale, the direct methanol carboxylation reaction could be a promising alternative for the continuous DMC synthesis.

Theoretically, there are many critical factors that have a huge impact on the non-reductive conversion of CO₂ into DMC, as it is the case for any other heterogeneously catalyzed reactions. To mention only a few of them, the catalyst material employed in the process and its physical-chemical properties (e.g. particle size, pore volume/size-distribution and structure, surface area, acidity and basicity, oxidation and reduction capabilities); the effect of the calcination temperature over the final material; different synthesis methods that can highly influence both the support and the support-metal interaction along with metal dispersion on the catalyst surface; reaction conditions (reactants ratio, reaction temperature, pressure, and

6 | Conclusions and Outlook

time, operation under batch or continuous approach). However, in practice all this extensive work in search for the best results (in terms of methanol conversion and DMC selectivity) has been narrowed down to the system composed CeO_2 and 2-CP, the only one capable of performing methanol carboxylation and 2-CP hydrolysis while providing high yields towards DMC.

One of the major challenges of this work, the important loss in the catalyst activity at higher time on stream due to strong 2-PA adsorption over CeO_2 surface has been addressed, and partially solved, by a simple and effective promotion of CeO_2 with rare earth metal elements (i.e. La, Gd, and Pr). A good catalyst must possess both high activity and long-term stability. Not to mention that its selectivity towards the desired product reflects its ability to directly convert the reactants along a specific reaction pathway. In the pursuit of bringing this process one step closer to being more relevant for the chemical industry of today and having acquired solid information regarding the fast and easy to get implemented reactivation protocol, we have been seeking for possible solutions/mechanisms to further improve the process. Preliminary results from the experiments carried out in our laboratories have shown that even after more than 100 h of time on stream, a small increase in the reaction temperature (from 120 to 140 °C) can recover the catalyst activity (DMC yield) via what we hypothesize it is easiness of 2-PA removal. On the other hand, decreasing the temperature to only 100 °C leads to a considerable decrease in the productivity of the reaction, as already reported for the case of pristine CeO_2 . **Figure 6.1** shows the catalytic results for two of the best materials tested so far (i.e. rare earth promoted CeO_2 , 5 and 1 wt% La, respectively).

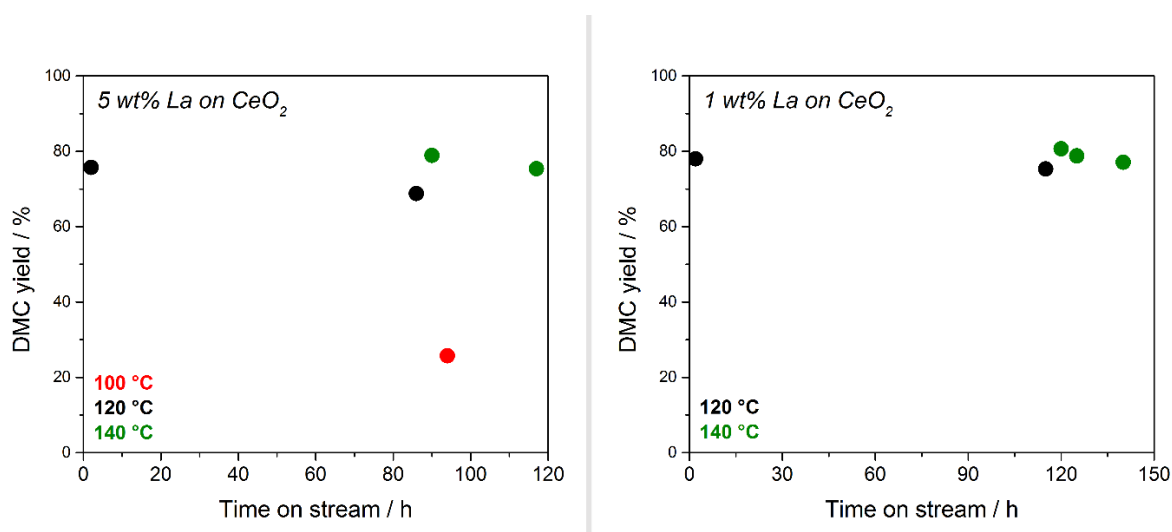


Figure 6.1. Long-term stability study on direct DMC synthesis from CO_2 and methanol in the presence of a dehydrating agent. Effect of reaction temperature at high time on stream for 5 (left) and 1 (right) wt% La promoted CeO_2 materials

Reactions have been run at 30 bar and 120 °C. It can be observed how, after ca. 100 h for the 5 wt% La and 120 h for 1 wt% La, respectively, an increase of 20 °C in the reaction temperature allowed complete recovery of the initial DMC yield. This has a huge importance in practice and further investigation should be performed. A deeper mechanistic understanding is desirable to completely clarify the involvement of 2-CP in the reaction mechanism, and to assess the exact effect/role of the rare-earth metal promoters in the catalytic process. And this brings us to our last contribution on the topic. Given the outstanding improvement made by doping the CeO₂ catalyst with rare earth metals, the rapid and reliable catalyst reactivation protocol and the catalytic results disclosed above, we came up with a new reactor design presented in **Figure 6.2**. The setup would, in principle, be capable of continuously producing DMC from CO₂ and methanol in the presence of a dehydrating agent (2-CP). It consists of 2-parallel reactors. While *Reactor 1* is running the methanol carboxylation reaction, the catalyst in the *Reactor 2* is subjected to regeneration protocol (under air). When the catalyst in the *Reactor 1* displays important decrease in activity, the process automatically switches from *Reactor 1* to *Reactor 2*, where reaction continues running, while the catalyst in the *Reactor 1* gets reactivated. The feasibility of such a design would require more attention as soon as proper 2-PA regeneration protocol back to 2-CP could be implemented.

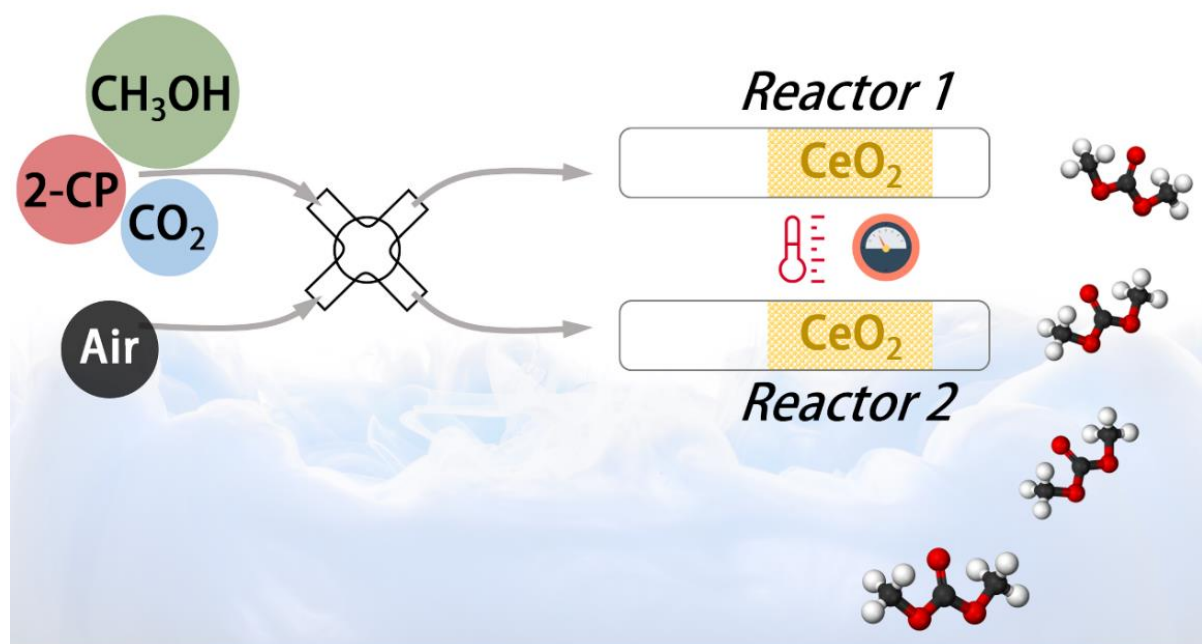


Figure 6.2. Proposed reactor scheme for continuous DMC synthesis from CO₂ and methanol in the presence of a dehydrating agent (2-CP). While reaction is carried out in the *Reactor 1*, regeneration of the catalyst (in a flow of air) is performed in the *Reactor 2* and vice-versa

6 | Conclusions and Outlook

This last chapter of the thesis summarizes the most important findings encountered throughout the project, i.e. continuous DMC synthesis from CO₂ and methanol. It presents a good way on how moderate pressure approach offers new opportunities in heterogeneous catalysis and investigation of reactions in a continuous manner using microreactors. Despite the difficulties, this research field is new and rapidly growing over the last couple of years. CO₂ mitigation strategies are the key for a better, greener, and safer future. Moreover, efficient use of this very abundant molecule (CO₂) to produce important and highly relevant chemical products (e.g. organic carbonates) is a vital part of the CO₂ abatement long-term plan.

7

Appendices



Appendix A Supplementary information Chapter 1

Full Mauna Loa CO₂ record

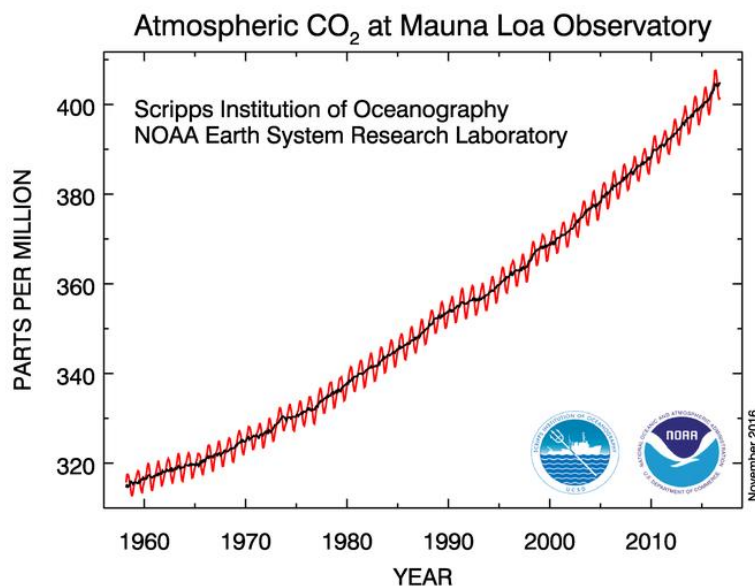


Figure 7.1 Monthly mean atmospheric carbon dioxide measurements at Mauna Loa Observatory, Hawaii. The red curve depicts the longest record of direct measurements of CO₂ in the atmosphere, whereas the black curve represents the seasonally corrected data. Image from <http://www.esrl.noaa.gov/gmd/ccgg/trends/full.html> (full reports and extra info at NOAA Earth System Research Laboratory, Global monitoring division)

Appendix B Supplementary information Chapter 2

High-pressure methanol carboxylation reactor setup

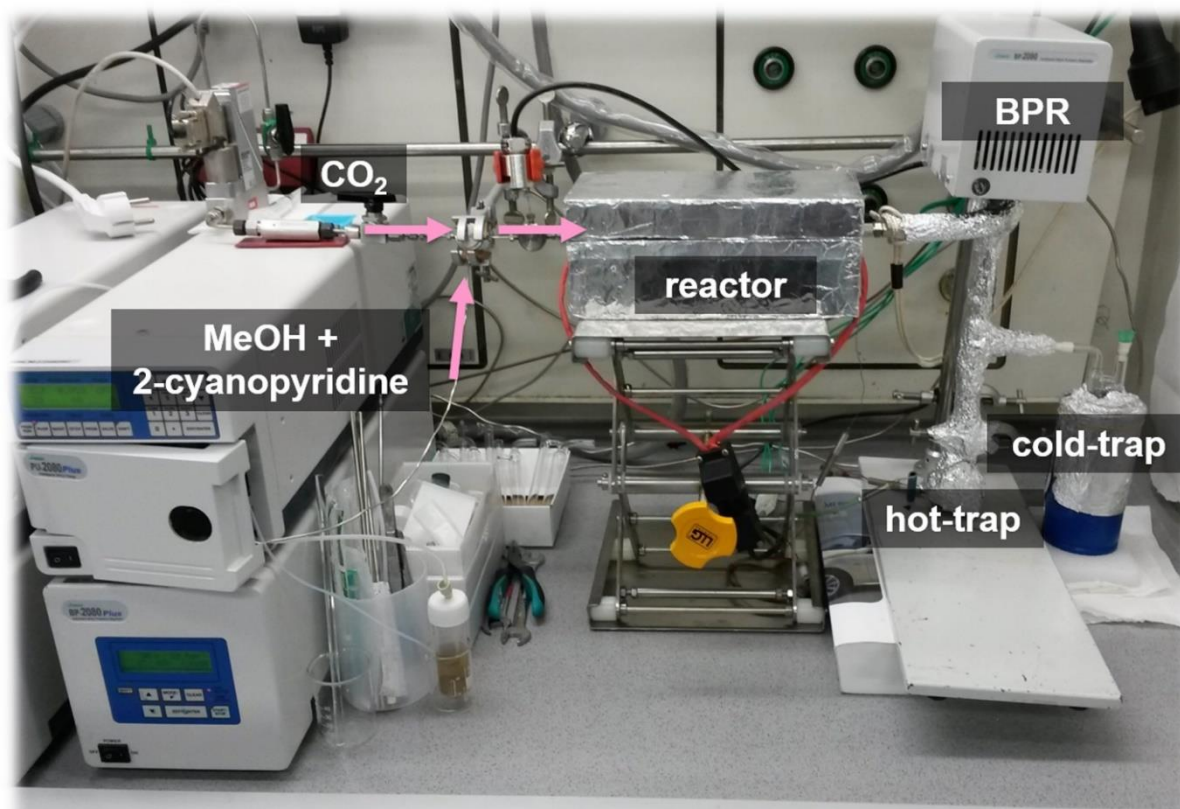


Figure 7.2 High-pressure in-house built methanol carboxylation reactor setup. CO₂ (gas) is fed to the reactor by means of a high-pressure mass flow controller (MFC) from Bronkhorst High-Tech B.V., whereas the liquid mixture (methanol and 2-cyanopyridine, 2-CP) using a HPLC pump (Jasco). A Jasco back pressure regulator (BPR) is used to hold the pressure in the reactor system. At the outlet of the BPR, the products are separating based on their boiling points (°C) via the home-made hot-trap and cold-trap separation system

Appendix C Supplementary information Chapter 3

Estimation of space time (adapted from Bansode and Urakawa, ACS Catalysis, 2014, 4 (11), pp 3877–3880)

The exact space time is a difficult parameter to evaluate because of the multiphase mixture and the dependence of its volume on temperature and pressure besides uncharacterized void space in the reactor. Nevertheless, the experimental space time was estimated with some assumptions, namely (i) the volume of the reaction mixture can be expressed by the simple sum of those of the fluid components (methanol, CO₂, 2-cyanopyridine), (ii) methanol and 2-cyanopyridine are not compressive and the density does neither vary with temperature nor with pressure, (iii) no volume change by the reaction, (iv) the gas and supercritical CO₂ density can be expressed by the Bender equation of state (*Fluid Phase Equilibria*, 45 (1989) 7).

With the experimental flow rates of 6 NmL min⁻¹ CO₂ and 10 μL min⁻¹ methanol+2-cyanopyridine, the catalyst bed length of 75 mm, reactor ID of 1.74 mm, and with an assumption of void fraction of the fixed bed to be 0.5, we can estimate the space time under the employed reaction conditions. As representative conditions, we calculated the total reactant flow rate and space time at 30 and 300 bar at 80 and 160 °C (**Table 7.1**).

Table 7.1 Space time estimation

Pressure / bar	Temperature / °C	Reactant flow rate / mL min ⁻¹	Space time / s
30	80	0.251	21
30	160	0.321	17
300	80	0.026	206
300	160	0.036	151

The volume of gaseous/supercritical phase can drastically reduce by the reaction. Hence, the actual space time would be higher than the values shown above. At high conversion, the effluent stream contains mainly DMC and 2-picolinamide, whose volume could be like those of methanol and 2-cyanopyridine mixture (10 μL/min).

By only assuming this flow rate and calculating the space time, one can estimate the maximum space time using our reactor system. The value is 534 s, nearly 9 min. Therefore, it can be concluded that the mean residence time of the reactants are rather small and can be in the order of 10 s to close to 10 min. These values are much smaller compared to the case

of batch operation (>10 h). This higher conversion efficiency of continuous system is likely due to the better mixing of CO₂, methanol, and the dehydrating agent over the catalyst because they may coexist or exist in proximity in continuous operation, whereas in batch operation methanol, the dehydrating agent, and the catalyst would stay in the liquid phase while CO₂ would be present in the gas/supercritical phase. Efficient dissolution and mass transfer of CO₂ into the liquid phase would be critical for better catalytic performance in batch operation.

Appendix D Supplementary information Chapter 4

X-ray diffraction and thermogravimetric analysis supplementary results

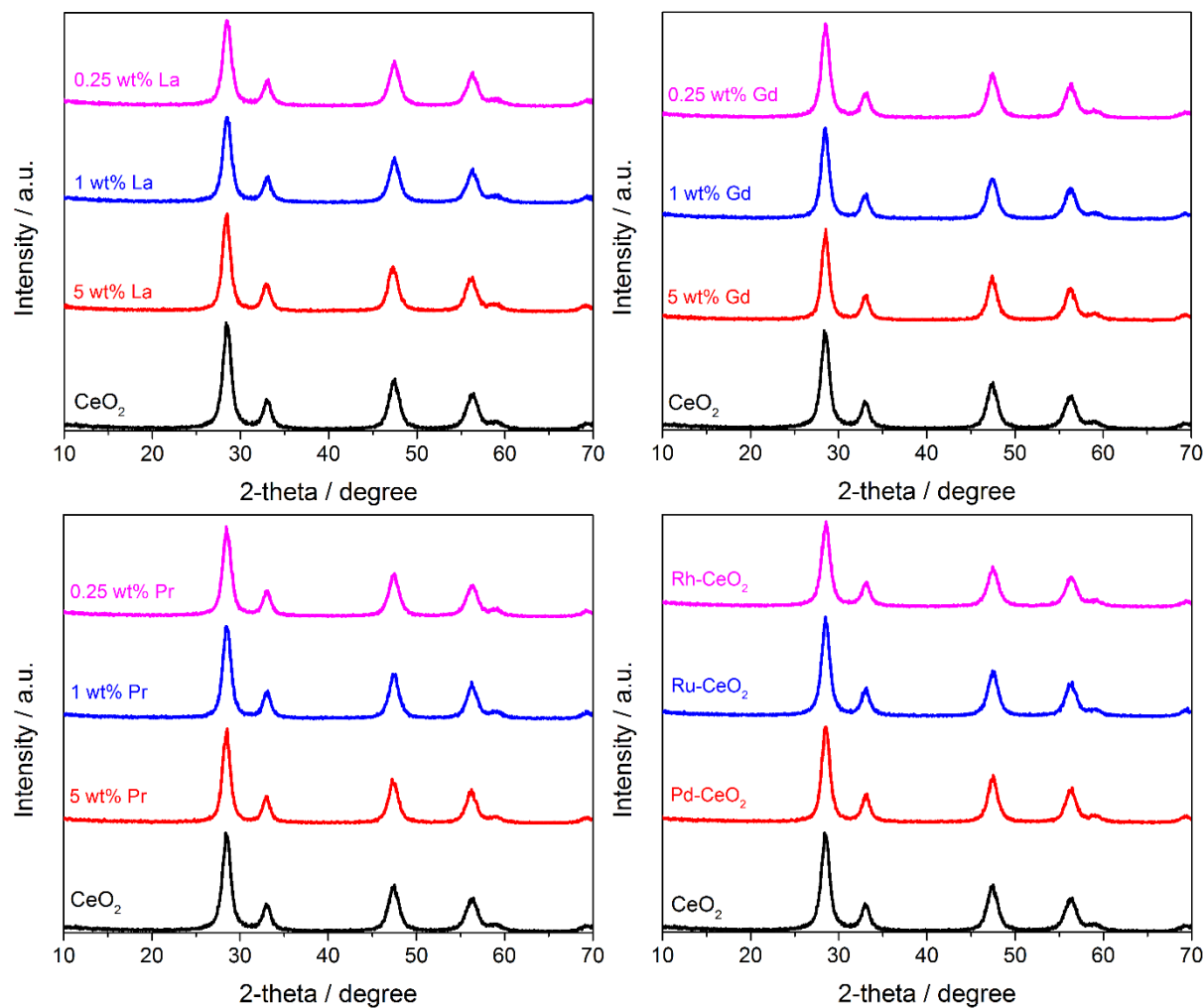


Figure 7.3 XRD patterns of the as-synthesized rare-earth metals (REMs, i.e. La, Gd, and Pr) promoted CeO₂ materials (0.25, 1, and 5 wt%, respectively) and precious metals (PMs) doped CeO₂ (i.e. 1 wt% Pd, Ru, and Rh, respectively)

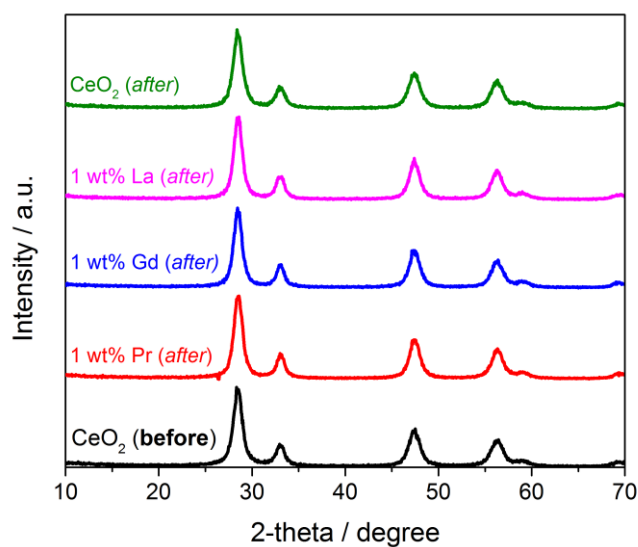


Figure 7.4 XRD patterns for pristine CeO_2 (green) and 1 wt% REM promoted CeO_2 (i.e. La in pink, Gd in blue, and Pr in red) after 30 h reaction time. No structural change in the crystallinity of the materials was detected (CeO_2 before the reaction in black)

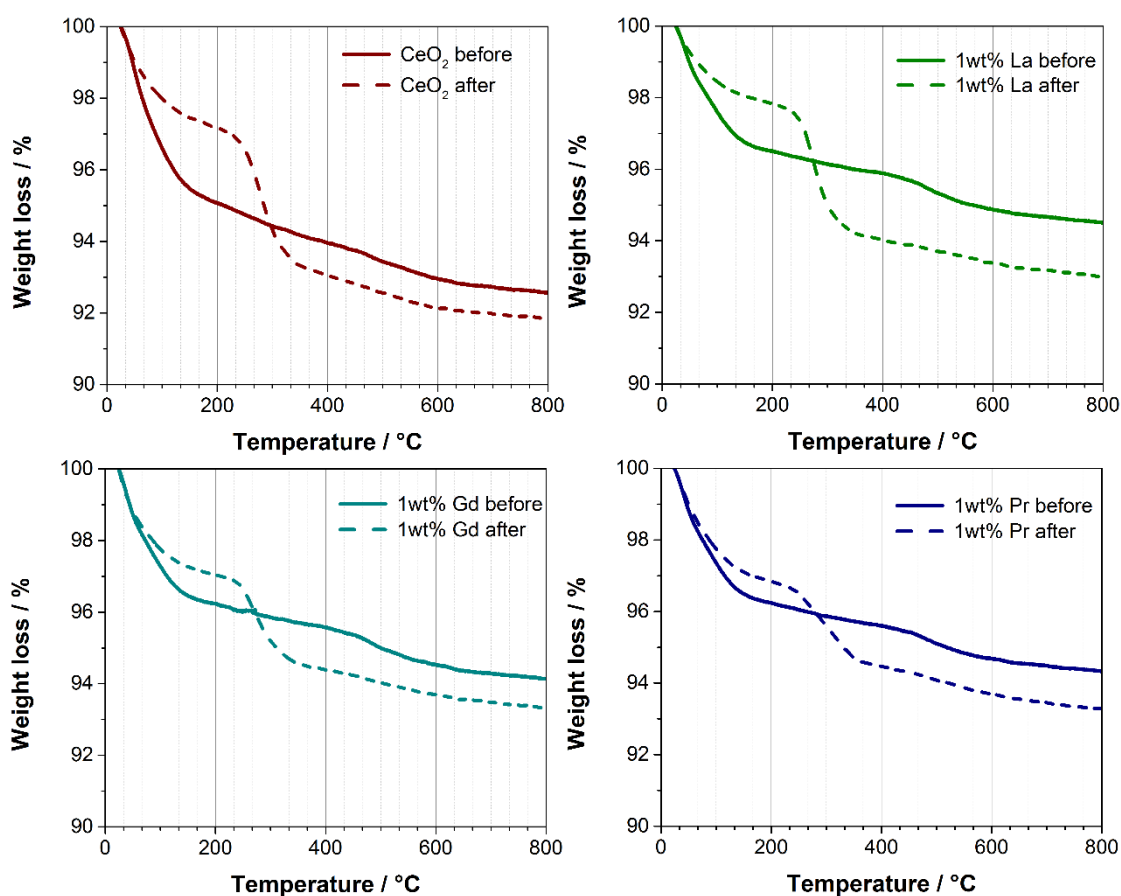


Figure 7.5 TGA profiles (weight loss vs. temperature) for CeO_2 and 1 wt% REM (i.e. La, Gd, and Pr) promoted CeO_2 before and after 30 h reaction time

Appendix E Supplementary information Chapter 5

Theoretical IR spectra calculation and *in situ* XAS/Raman results

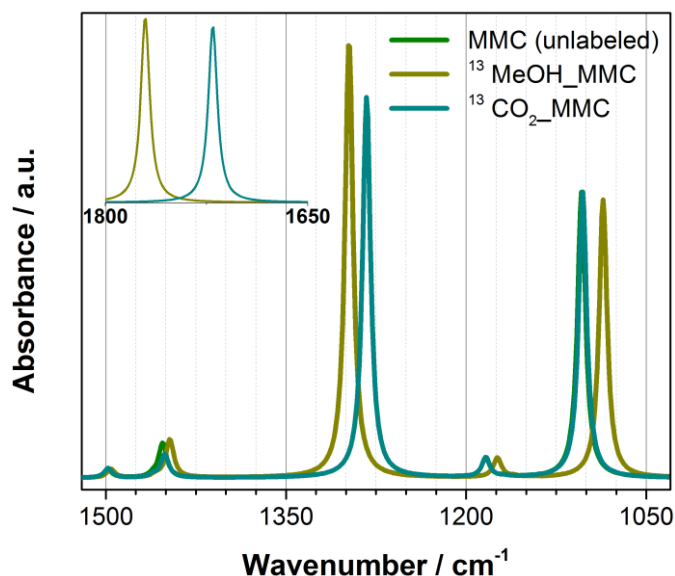


Figure 7.6 Direct DMC synthesis from CO₂ and methanol. Theoretical IR spectra of monomethyl carbonate anion (MMC) obtained by a DFT method (B3PW91/6-311++G(2d,2p)) without solvent effect. The image presents the 1800-1000 cm⁻¹ region for the three cases, namely (i) unlabeled, (ii) ¹³C-methanol, and (iii) ¹³C-CO₂

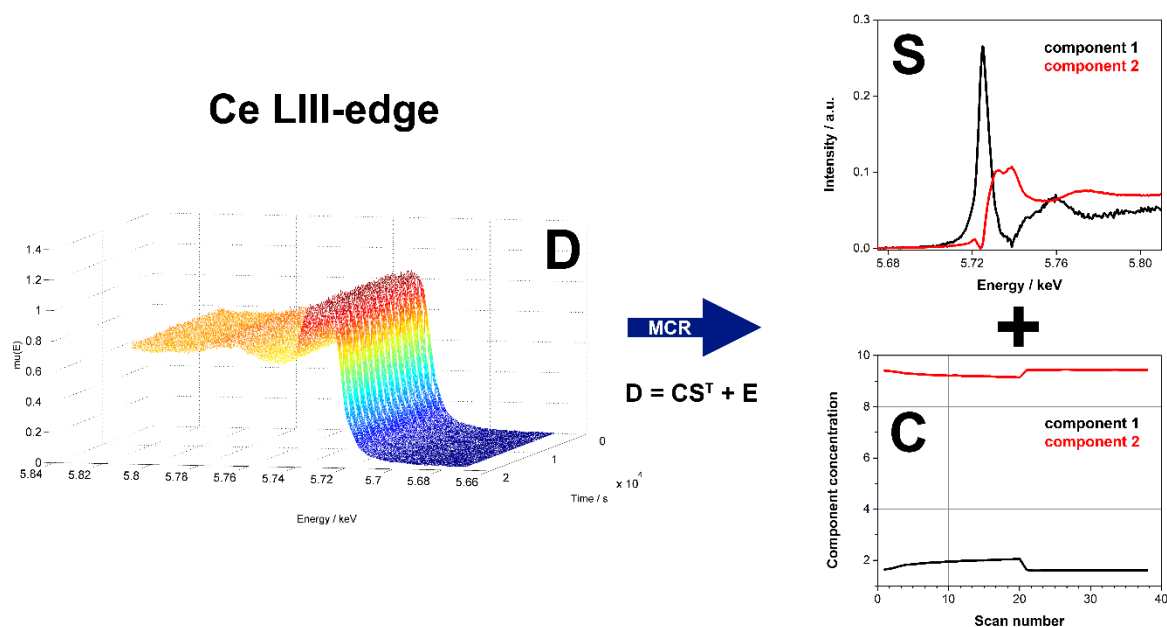


Figure 7.7 Ce L3-edge: H₂ vs. O₂ concentration perturbation experiment performed at 350 °C. MCR analysis has been applied to disentangle the two component spectra (upper panel, S)

and the corresponding concentration profiles (lower panel, C), respectively. **N.B.** Component 1 (black, Ce^{3+} under H_2) and component 2 (red, Ce^{4+} under O_2)

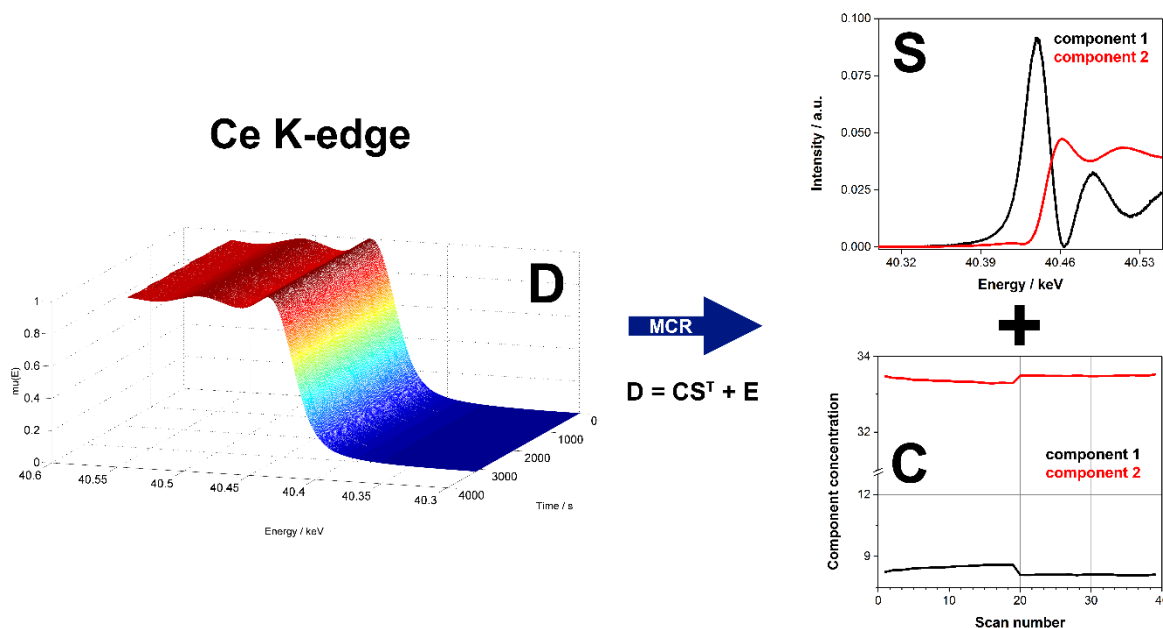


Figure 7.8 Ce K-edge: H_2 vs. O_2 concentration perturbation experiment performed at 350°C . MCR analysis has been applied to disentangle the two component spectra (upper panel, S) and the corresponding concentration profiles (lower panel, C), respectively. **N.B.** Component 1 (black, Ce^{3+} under H_2) and component 2 (red, Ce^{4+} under O_2)

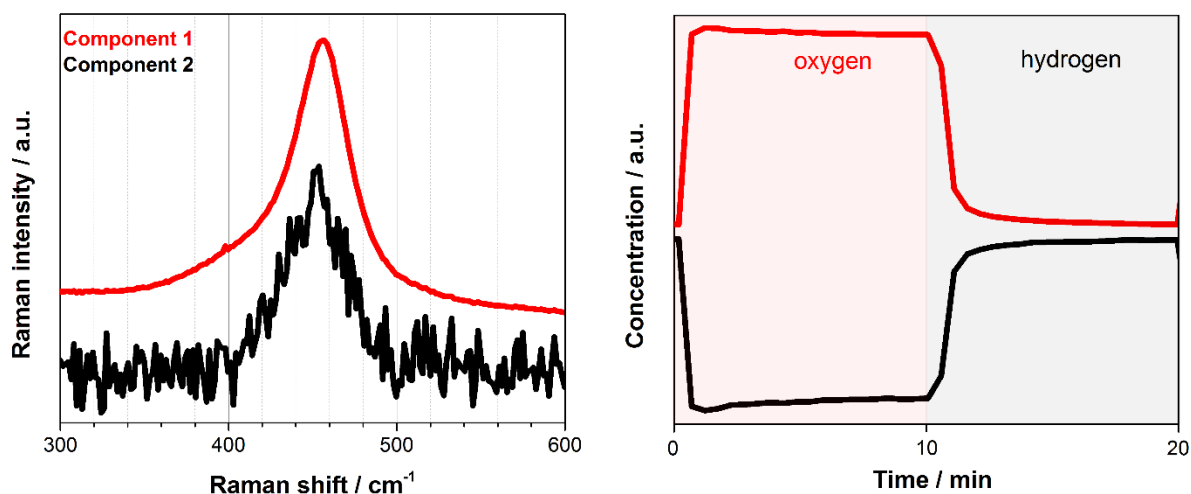


Figure 7.9 MCR applied on the region of F_{2g} band of CeO_2 . Raman spectra were collected for a H_2 vs. O_2 concentration perturbation experiment performed at 350°C . Raman measurements done with 532 nm laser (green) at SNBL, ESRF (Grenoble, France). Both

7 | Appendices

spectra (*left*) and concentration (*right*) profiles are normalized for clarity. **N.B.** Component 1 (red, Ce^{4+} under O_2) and component 2 (black, Ce^{3+} under H_2)

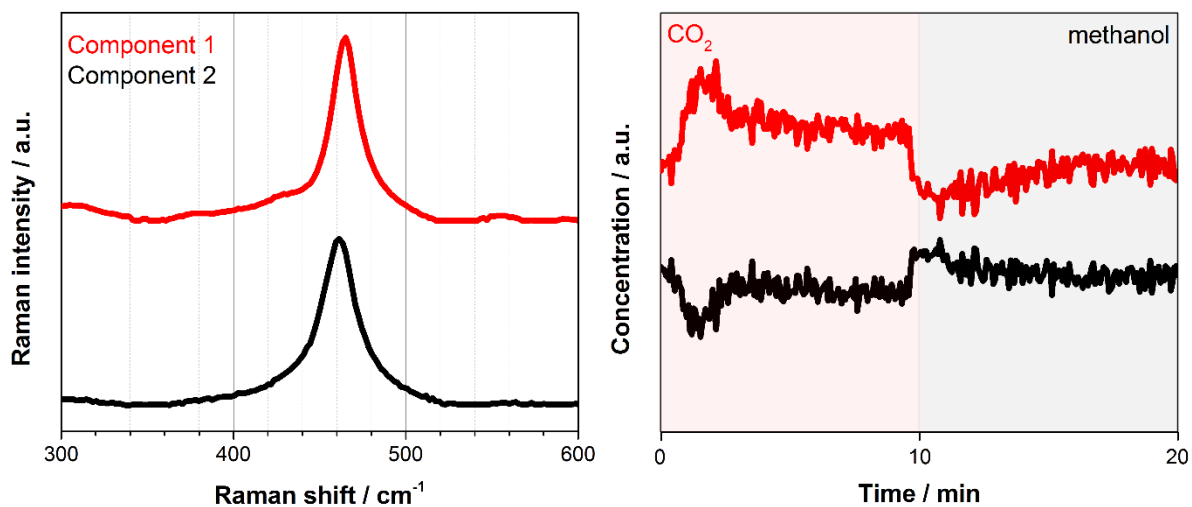


Figure 7.10 MCR applied on the region of F_{2g} band of CeO_2 . Raman spectra were collected during CO_2 vs. methanol concentration perturbation experiment performed at 120°C (DMC synthesis). Raman measurements done with 785 nm Raman laser (red). **N.B.** Component 1 (red, Ce^{4+} under CO_2) and component 2 (black, Ce^{3+} under methanol)

SHORTHAND AND GLOSSARY

$\Delta_r H^\ominus_{298K}$	Standard enthalpy of reaction
$\Delta_r G^\ominus_{298K}$	Gibbs free energy
2-CP	2-cyanopyridine
2-PA	2-picolinamide
AGGI	Annual Greenhouse Gas Index
Ar	Aryl ring
ATR-IR	Attenuated Total Reflectance Infrared Spectroscopy
BET	Brunauer–Emmett–Teller theory employed for the measurement of the specific surface area of a material ($\text{m}^2 \text{g}^{-1}$)
BJH	Barrett-Joyner-Halenda method employed for pore size (nm) and volume analysis ($\text{cm}^3 \text{g}^{-1}$)
BPR	Back pressure regulator
BV	Ball valve
CC	Channel-cut monochromator for diffraction experiments
CCS	Carbon Capture and Storage (sequestration)
CCU	Carbon Capture and Utilization (recycling)
CH_3X	Methyl halides
CMR	Catalytic membrane reactors
COP21/CMP11	United nations conference on climate change held in Paris, 2015
CV	Check Valve
DCC	Dicyclohexylcarbodiimide (dehydrating agent)
DCM	Double-crystal monochromator for XAFS measurements

Shorthand and glossary

DEC	Diethyl carbonate
DFT	Density functional theory
DMC	Dimethyl carbonate
DME	Dimethyl ether
DMP	2,2-dimethoxy propane
DMS	Dimethyl sulphate
DRIFTS	Diffuse Reflectance Infrared Fourier Transform Spectroscopy
DTGS	Deuterated triglycine sulfate (IR detector)
E_a	Activation energy. Term coined by the Swedish scientist Svante Arrhenius
EIA	U.S. Energy Information Administration (U.S. Federal Statistical System)
EPR	Electron Paramagnetic Resonance
ESRF	European Synchrotron Radiation Facility in Grenoble, France
EtOH	Ethanol
EXAFS	Extended X-Ray Absorption Fine Structure
F	Filter (reactor setup)
FID	Flame ionic detector (gas chromatography)
FT-IR	Fourier Transform Infrared Spectroscopy
GC	Gas chromatography (chromatograph)
GC-MS	Gas chromatography coupled with mass spectrometry
GHGs	A greenhouse gas is a gas that both absorbs and emits radiation commonly called thermal radiation or heat
GHSV	Gas hourly space velocity
GUI	Graphical user interface
HPLC pump	High pressure liquid chromatography pump

HTs	Hydrotalcites
ID	Inner diameter (reactors)
IEA	International Energy Agency (autonomous intergovernmental organization)
IPCC	Intergovernmental Panel on Climate Change – an international organism under the hood of United Nations
IR	Infrared Spectroscopy (vibrational spectroscopy) dealing with the infrared region of the electromagnetic spectrum
IS	Internal standard (GC chromatography)
LDHs	Layered double hydroxides
LINAC	Linear accelerator (synchrotron facility)
LN-MCT	Liquid-nitrogen-cooled mercury cadmium telluride (IR detector)
MCR-ALS	Multivariate Curve Resolution Alternating Least Square
Me-CBM	Methyl carbamate
Me-PCN	Methyl picolinate
Megatonne	A million tons, SI unit of mass (Mt)
MeOH	Methanol
MEK	Methyl ethyl ketone
MES	Modulation excitation spectroscopy
MFC	Mass flow controller
MMC	Monomethyl carbonate
MS	Mass spectrometry (or mass spectrometer)
MTBE	Methyl <i>tert</i> -butyl ether
MV	Mixing valve
NASA	National Aeronautics and Space Administration

Shorthand and glossary

NIRS	Near-Infrared Spectroscopy
NOAA	National Oceanic and Atmospheric Administration is a scientific agency within the United States Department of Commerce
NO_x	Generic term for NO and NO ₂
OCO-2	Orbiting Carbon Observatory-2
OD	Outer diameter (reactors)
Odiac	Open-source Data Inventory for Anthropogenic CO ₂
OECD	Organization for Economic Co-operation and Development (intergovernmental economic organization with 35 member countries, founded in 1961 to stimulate economic progress and world trade)
PC	Polycarbonates
PCBTF	<i>para</i> -chlorobenzotrifluoride
PCV	Pressure control valve
PEEK	Polyether ether ketone
PI	Pressure indicator
PID	A proportional–integral–derivative controller (PID controller) is a control loop feedback mechanism (controller) commonly used in industrial control systems
PMs	Precious metals
ppm	parts-per-million, 10 ⁻⁶
PSD	Phase-sensitive detection (mathematical model)
Py	Pyridyl ring
Raman	Raman spectroscopy technique named after Sir C. V. Raman
REMs	Rare earth metals
RF	Radiative forcing. Describes the change in energy in the atmosphere due to GHGs emissions
RPM	Rotations per minute

RT	Retention time (min) in GC
RVP	Reid vapor pressure is a common measure of the volatility of gasoline
S_{DMC}	DMC selectivity (%)
S/N	Signal-to-noise ratio
SI	International System of Units
SNBL	Swiss Norwegian Beam Line at ESRF
SS	Stainless steel
TAP	Temporal analysis of products
tBuAc	<i>tert</i> -butyl acetate
TCD	Thermal conductivity detector (gas chromatography)
TE-cooled detector	Thermoelectrically cooled detector (Raman)
TGA	Thermogravimetric analysis
TPD	Temperature programmed desorption (e.g. CO ₂ and NH ₃)
TPES	The world total primary energy supply. Expressed in million tons of oil equivalent (Mtoe); 1 Mtoe = 11.63 TWh (terawatt-hours)
TPR	Temperature programmed reduction (e.g. H ₂)
UNCCC	United Nations Climate Change Conference held in Paris, France
UNCED	United Nations Conference on Environment and Development held in Rio de Janeiro, Brazil
UNFCCC	United Nations Framework Convention on Climate Change
ULS	Ultrafast laser spectroscopy
VSO	V ₂ O ₅ -SiO ₂
WEC	The world total final energy consumption by resource. Expressed in million tons of oil equivalent (Mtoe); 1 Mtoe = 11.63 TWh (terawatt-hours)
3-WV	3-Way valve

Shorthand and glossary

X_{MeOH}	Methanol conversion (%)
XAFS	X-ray Absorption Fine Structure
XANES	X-ray Absorption Near Edge Structure
XAS	X-ray Absorption Spectroscopy
XPS	X-ray Photoelectron Spectroscopy
XRD	X-ray Powder Diffraction
ZnSe	Zinc Selenide (material used for IR windows)

LIST OF PUBLICATIONS

Journal publications

1 Improving the stability of CeO₂ catalyst in the continuous dimethyl carbonate synthesis from CO₂ and methanol with 2-cyanopyridine.

Dragos Stoian, Francesc Medina, and Atsushi Urakawa. Submitted manuscript (2016)

2 Catching the surface intermediate and elucidating the redox contribution of CeO₂ during dimethyl carbonate synthesis from CO₂ and methanol.

Dragos Stoian, Atul Bansode, Francesc Medina, Wouter van Beek, and Atsushi Urakawa. Submitted manuscript (2016)

3 Catalysis under microscope: Unraveling the mechanism of catalyst de- and re-activation in the continuous dimethyl carbonate synthesis from CO₂ and methanol in the presence of a dehydrating agent.

Dragos Stoian, Atul Bansode, Francesc Medina, and Atsushi Urakawa. *Catalysis Today*, (2016) at doi:10.1016/j.cattod.2016.03.038

4 Continuous DMC synthesis from CO₂ and methanol over a CeO₂ catalyst in a fixed bed reactor in the presence of a dehydrating agent.

Atul Bansode, Atsushi Urakawa. *ACS Catalysis*, 4 (2014) 3877. **Experimental contribution**

5 Boosted CO₂ reaction with methanol to yield dimethyl carbonate over Mg-Al hydrotalcite-silica lyogels.

Dragos Stoian, Elena Taboada, Jordi Llorca, Elies Molins, Francesc Medina, and Anna M. Segarra. *Chemical Communications*, 49 (2013) 5489

List of publications

Conference contributions

- 1** April **2016**, Carbon Dioxide Catalysis Conference, Albufeira (Algarve, Portugal)
– **poster** and **oral presentation**.

Catalytic active site and deactivation mechanism in continuous dimethyl carbonate (DMC) synthesis from CO₂ and methanol in the presence of a dehydrating agent.

Catalysis under microscope: Unraveling the mechanism of catalyst de- and re-activation in the continuous dimethyl carbonate synthesis from CO₂ and methanol in the presence of a dehydrating agent.

Dragos Stoian, Atul Bansode, Francesc Medina, and Atsushi Urakawa.

- 2** July **2015**, SECAT'15 – Catálisis, confluencia interdisciplinaria: modelos, catalizadores y reactores, Barcelona (Spain) – **poster presentation**.

Continuous DMC synthesis from CO₂ and methanol over ceria based catalysts: *Operando* inspection and mechanistic investigation.

Dragos Stoian, Atul Bansode, Francesc Medina, and Atsushi Urakawa.

- 3** June **2015**, Japan-Spain Joint Symposium on Heterogeneous Catalysis, Tarragona (Spain) – **poster presentation**.

Continuous DMC synthesis from CO₂ and methanol over ceria based catalysts: *Operando* inspection and mechanistic investigation.

Dragos Stoian, Atul Bansode, Francesc Medina, and Atsushi Urakawa.

- 4** September **2013**, XIth European Congress on Catalysis (EuropaCat), Lyon (France) – **poster** and **oral (flash) presentation**.

Design and synthesis of heterogeneous acid-basic catalysts for the valorization of CO₂: synthesis of dimethyl carbonate from CO₂ and methanol.

Dragos Stoian, Salwa Bougacha Ghorbel, Francesc Medina, and Anna M. Segarra.

5 September **2012**, Large-volume CO₂ Utilization: Enabling Technologies for Energy and Resource Efficiency 2nd Edition, Lyon (France) – **poster presentation**.

Novel phosphoric acid intercalated Mg-Al hydrotalcite like compounds for catalytic carboxylation reaction of methanol in a continuous system.

Dragos Stoian, Salwa Bougacha Ghorbel, Abdelhamid Ghorbel, Francisco Medina, and Anna M. Segarra.

List of publications

CURRICULUM VITAE

Personal information

Name	Dragoş Constantin Stoian
Date of birth	March 30th, 1985
Place of birth	Buzau, ROMANIA
Nationality	Romanian
Email	dragos.stoian.c@gmail.com / dragos.stoian@live.com

Education and training

October 2011 – Present PhD Chemical Engineering

University “Rovira i Virgili”, Chemical Engineering Department, Campus Sescelades
Av. Països Catalans no. 26, 43007 - Tarragona (Spain)

The Institute of Chemical Research of Catalonia (ICIQ), Av. Països Catalans no. 16,
43007 - Tarragona (Spain)

Under the supervision of Prof. Dr. Francesc Medina (University “Rovira i Virgili”) and
Prof. Dr. Atsushi Urakawa (ICIQ)

Part of a project dedicated to CO₂ utilization (i.e. Acción preparatoria para la
revalorización del CO₂. Agencia Española de Cooperación Internacional, Gobierno de
España – 2011-2013)

Research topics:

- Heterogeneous catalysis, CO₂ valorization, flow chemistry
- Reaction engineering, *in situ* / *operando* spectroscopic techniques

Grants:

- University “Rovira i Virgili” (URV) Scholarship

Curriculum Vitae

October 2009 – August 2011 Master Degree

“Politehnica” University of Bucharest – Faculty of Applied Chemistry and Material Science, “Polizu” Campus, no. 1-7, Polizu Street, Sector 1, Bucharest, 011061, (Romania)

Program: Pharmaceutical Products and Cosmetics

Subjects: Toxicology, Drugs, Enzymes, Pharmaceutical Technology, Natural Ingredients

Final evaluation: 95/100

October 2004 – June 2009 Engineering Degree

“Politehnica” University of Bucharest – Faculty of Engineering in Foreign Language – English Stream, no. 313, Splaiul Independentei, Bucharest, 060042 (Romania)

Program: Chemical Engineering

Subjects: Organic Chemistry, Inorganic Chemistry, Drugs, Analytical Chemistry, Chemical Engineering, Biochemistry, Organic Chemistry Technology

Final evaluation: 90/100

Work experience

January 2012 – June 2014 Teaching Assistant

University “Rovira i Virgili”, Chemical Engineering Department, Campus Sescelades

Av. Països Catalans no. 26, 43007 - Tarragona (Spain)

- Chemical engineering II laboratory (Laboratori d'Enginyeria Química)
- Unit operation laboratory (Laboratori Integrat d'Operacions Unitaries)
- Supervising and coordinating students and grading homework & projects

June 2008 - August 2011 Trainer IT

Avantaj Consulting SRL, no. 8-12, Sgt. Nutu Ion Street, Sector 5, Bucharest (Romania)

- Web Design – HTML, CSS, FLASH and ActionScript classes
- Supervising and coordinating students and grading homework & projects

March 2008 - August 2011 Research Assistant

Research Centre of Organic Chemistry “Costin D. Nenitescu” of Romanian Academy
no. 202B, Splaiul Independentei, Sector 6, 711441 Bucharest (Romania)

- Organic chemistry synthesis (and characterization) and NMR analysis

July 2007 - November 2007 Assistant marketing

K Tech Electronics-Ultra Pro Computers, Bucharest (Romania)

- Marketing department – web-design and online strategy

Seminars and courses

- 2015, Madrid (Spain) – New trends and challenges of the chemical processes in the 21st century (2nd edition)
- 2014, Tarragona (Spain) – Safe and Efficient Fluid Handling Systems – Swagelok Iberica
- 2013, Tarragona (Spain) – Training Course Micromeritics AUTOCHEM II 2920
- 2013, Jarandilla de la Vera (Spain) – The Physical and Chemical Characterization of the Surface of the Solids
- 2013, Barcelona (Spain) – Training on valves and fittings (Iberfluid Instruments)
- 2013, Tarragona (Spain) – Training Course UV-Visible JASCO V-630
- 2012, Tarragona (Spain) – Occupational First Aid Training, “Rovira i Virgili” University
- 2006-2009, Bucharest (Romania) - Psychological and Pedagogical Course, “Politehnica” University of Bucharest

Research projects

- 2014-2016. 2014SGR1640: Grupo consolidado MEtA - Materials engineering and their applications (Enginyeria dels materials i les seves aplicacions). AGAUR (Generalitat de Catalunya). IP: F. Medina
- 2014-2015 - EUIN2013-50984: AD-CO₂CHEM - Acción Europa investigación: Convirtiendo CO₂ en productos químicos (Converting CO₂ in chemical

Curriculum Vitae

products). Ministerio de Economía y Competitividad (Gobierno de España). IP:
A.M. Segarra

- 2005-2009. WP2 "Selection of objective green molecules and Solvsafe green alternatives for coatings" Program (FP6/2005-2009). E.U. Sixth Framework.

